

Flow phenomena in rocks: from continuum models to fractals, percolation, cellular automata, and simulated annealing

Muhammad Sahimi

Department of Chemical Engineering, University of Southern California, Los Angeles, California 90089-1211*
and HLRZ Supercomputer Center, c/o KFA Jülich, 52425 Jülich, Germany

In this paper, theoretical and experimental approaches to flow, hydrodynamic dispersion, and miscible and immiscible displacement processes in reservoir rocks are reviewed and discussed. Both macroscopically homogeneous and heterogeneous rocks are considered. The latter are characterized by large-scale spatial variations and correlations in their effective properties and include rocks that may be characterized by several distinct degrees of porosity, a well-known example of which is a fractured rock with *two* degrees of porosity—those of the pores and of the fractures. First, the diagenetic processes that give rise to the present reservoir rocks are discussed and a few geometrical models of such processes are described. Then, measurement and characterization of important properties, such as pore-size distribution, pore-space topology, and pore surface roughness, and morphological properties of fracture networks are discussed. It is shown that fractal and percolation concepts play important roles in the characterization of rocks, from the smallest length scale at the pore level to the largest length scales at the fracture and fault scales. Next, various structural models of homogeneous and heterogeneous rock are discussed, and theoretical and computer simulation approaches to flow, dispersion, and displacement in such systems are reviewed. Two different modeling approaches to these phenomena are compared. The first approach is based on the classical equations of transport supplemented with constitutive equations describing the transport and other important coefficients and parameters. These are called the *continuum models*. The second approach is based on network models of pore space and fractured rocks; it models the phenomena at the smallest scale, a pore or fracture, and then employs large-scale simulation and modern concepts of the statistical physics of disordered systems, such as scaling and universality, to obtain the macroscopic properties of the system. The fundamental roles of the interconnectivity of the rock and its wetting properties in dispersion and two-phase flows, and those of microscopic and macroscopic heterogeneities in miscible displacements are emphasized. Two important conceptual advances for modeling fractured rocks and studying flow phenomena in porous media are also discussed. The first, based on *cellular automata*, can in principle be used for computing macroscopic properties of flow phenomena in any porous medium, regardless of the complexity of its structure. The second, *simulated annealing*, borrowed from optimization processes and the statistical mechanics of spin glasses, is used for finding the optimum structure of a fractured reservoir that honors a limited amount of experimental data.

CONTENTS

I. Introduction	1395	D. Topological properties of porous media and their measurement	1417
A. Problems involving porous media	1395	E. Fractal, self-similar, and self-affine properties of porous media and their measurements	1420
B. Continuum versus discrete models of flow phenomena	1395	1. The box method	1420
II. Percolation Processes	1397	2. Adsorption methods	1420
A. Historical background	1397	3. Chord-length measurements	1421
B. Definitions and percolation thresholds	1397	a. Chord-length measurements on fracture surfaces	1421
C. Generation of percolation clusters on a network	1398	b. Chord-length measurements on thin sections	1423
D. Percolation quantities	1398	4. Correlation function method	1423
E. Universal scaling laws for percolation quantities	1399	5. Small-angle scattering methods	1425
F. Percolation in finite systems and finite-size scaling	1400	6. Spectral methods	1426
G. Percolation in random networks and in continua	1400	F. Fractal properties of heterogeneous and fractured rocks	1427
H. Fractal diffusion	1401	1. Diagenetic processes and formation of fractured rocks	1427
I. A note on the history of application of percolation theory to porous-media problems	1402	2. Morphological and fractal properties of fracture networks	1428
III. Rock Formation, Characterization, and Properties	1403	3. Fractal patterns in fault systems	1430
A. Diagenetic processes and the formation of rocks	1403	IV. Models of Reservoir Rocks	1430
B. Geometrical models of diagenetic processes	1404	A. Models of macroscopically homogeneous porous media	1430
C. Pore-space geometry and pore-size distribution and their measurement	1406	1. Spatially periodic models	1431
1. Mercury porosimetry and percolation	1407	2. Bethe lattice models	1432
2. Adsorption-desorption phenomena and percolation	1412	3. Network models	1432
3. Small-angle scattering method	1413	4. Modeling of pore surface roughness	1433
4. Nuclear magnetic resonance	1414	B. Models of heterogeneous porous media	1434
		1. Random hydraulic conductivity models	1435
		2. Fractal models	1435
		3. Multifractal models	1435
		C. Models of fractured rocks	1436

*Present and permanent address.

1. Multiporosity models	1436	G. Crossover from fractal to compact displacement at finite mobility ratios	1490
2. Network models of fractured rocks	1437	H. Miscible displacements in heterogeneous porous media	1491
3. Simulated annealing	1439		
V. Single-Phase Flow and Transport in Reservoir Rocks	1440		
A. Continuum models: Derivation of Darcy's law	1440	VIII. Two-Phase Flow and Immiscible Displacement Processes	1492
B. Calculation of the permeability and electrical conductivity of rocks	1442	A. Wettability and its measurement	1492
1. Exact results and rigorous bounds	1442	1. Contact-angle measurements	1493
2. Effective-medium approximations and derivation of Archie's law	1443	2. Amott method	1493
3. Position-space renormalization group and renormalized EMA	1447	3. U.S. Bureau of Mines method	1494
4. Field-theoretic and perturbation methods	1449	B. Dependence of dynamic contact angle and capillary pressure on capillary number	1494
5. Percolation methods	1450	C. The effect of surface roughness on contact angles	1495
6. Random-walk methods and network simulations	1453	D. Fluid distribution on fractal surfaces: Hypodiffusion versus hyperdiffusion	1495
7. Relation between permeability and electrical conductivity	1455	E. Effect of wettability on capillary pressure	1496
8. Relation between permeability and nuclear magnetic resonance	1456	F. Immiscible displacement processes	1498
9. Dynamic permeability	1457	1. Spontaneous imbibition	1499
VI. Hydrodynamic Dispersion	1457	2. Quasistatic imbibition	1499
A. The phenomenon of dispersion	1457	3. Imbibition at constant flow rates	1500
B. Mechanisms of dispersion processes	1458	4. Dynamic invasion at constant flow rates	1500
C. The convective-diffusion equation	1458	5. Displacement of blobs: Choke-off versus pinch-off	1500
D. Dispersion in a tube	1459	G. Models of two-phase flow and displacement	1501
E. Dispersion in spatially periodic media	1460	1. Continuum equations and relative permeabilities	1501
F. Models of dispersion in macroscopically homogeneous porous media	1460	2. Measurement of relative permeability	1502
1. Statistical-kinetic models	1461	3. The effect of wettability on relative permeability	1502
2. Fluid-mechanical models	1461	H. Percolation models of capillary-controlled two-phase flow and displacement	1503
3. Continuum models: Volume-averaging methods	1463	1. Random-percolation models	1503
4. Network models	1463	2. Random site-correlated bond percolation models	1505
G. Long-time tails: Dead-end pores versus disorder	1464	3. Invasion percolation	1505
H. Dispersion in short porous media	1465	4. Random percolation with trapping	1506
I. Dispersion in fractal porous media and percolation networks	1466	5. Crossover from fractal to compact displacement	1507
J. Dispersion in heterogeneous porous media	1469	6. Roughening and pinning of fluid interfaces: Dynamic scaling of rough surfaces	1508
1. Continuum models: Large-scale volume-averaging techniques	1469	7. Finite-size effects on capillary pressure and relative permeability: Devil's staircase	1510
2. Continuum models: Stochastic-spectral methods	1470	8. Immiscible displacements under the influence of gravity: Gradient percolation	1510
3. Monte Carlo methods	1472	9. A phase diagram for displacement processes	1511
4. Fractal models	1473	10. Scaling laws for relative permeability and dispersion coefficients	1512
K. Dispersion in fractured rocks	1474	11. Comparison of invasion and random-percolation models	1512
1. The double-porosity and related models	1474	I. Network models of immiscible displacements at finite capillary numbers	1512
2. Fracture network models	1474	J. Stability of immiscible displacements in porous media	1514
L. Dispersion in stratified porous media	1475	K. Two-phase flow in heterogeneous and stratified rock; continuum models and large-scale averaging	1515
VII. Miscible Displacement Processes	1475	L. Two-phase flow in fractured rocks	1518
A. Factors affecting miscible displacement processes	1476	IX. Advances in Computational Methods	1518
B. Viscous fingering	1477	A. Cellular automaton and lattice-gas simulation of fluid flow	1518
C. Miscible displacements in Hele-Shaw cells	1478	B. Cellular automata and lattice-gas simulation of single-phase flow in porous media	1519
D. Miscible displacements in porous media	1481	C. Cellular automaton and lattice-gas simulation of two-phase flow in porous media	1520
1. Continuum approaches to miscible displacements in porous media	1482		
2. Linear stability analysis of miscible displacements in porous media	1482	X. Conclusions	1521
E. Discrete models of miscible displacements	1484	Acknowledgments	1521
1. Diffusion-limited aggregation	1484	References	1522
2. The dielectric breakdown model	1486		
3. Gradient-governed growth model	1486		
4. The two-walker model	1487		
5. Probabilistic models that include the effect of dispersion	1487		
6. Deterministic models that include the effect of dispersion	1489		
F. Relation between miscible displacements and diffusion-limited aggregation	1489		

I. INTRODUCTION

A. Problems involving porous media

Flow, dispersion, and displacement processes in natural porous media or industrial synthetic porous matrices arise in many diverse fields of science and engineering, ranging from agricultural, biomedical, construction, ceramic, chemical, and petroleum engineering to food and soil sciences and powder metallurgy. Fifty percent or more of the original oil-in-place is left in a typical oil reservoir by traditional (primary and secondary) recovery techniques. This unrecovered oil is a large target for enhanced or tertiary oil recovery methods now being developed. However, oil recovery processes constitute only a small fraction of an enormous, and still rapidly growing, literature on porous media. In addition to oil recovery processes, the closely related areas of soil science and hydrology are perhaps the best-established topics. The study of groundwater flow and the restoration of aquifers that have been contaminated by various pollutants are important areas of research on porous-media problems. Classical research areas of chemical engineering that deal with porous media include filtration, centrifuging, drying, and multiphase flow in packed columns. Morrow (1991) gives a long and interesting list of problems involving porous media, a few of which are mentioned here. For the construction industry, transmission of water by building materials (bricks, concretes, etc.) is an important problem to consider when designing a new building. Wood is an interesting porous medium whose properties have been studied for a long time. Some of the phenomena involving wood include drying and impregnation by preservatives. Civil engineers have long studied asphalts as water-resistant binders for aggregates, protection of various types of porous materials from frost heave, and the properties of road beds and dams with respect to water retention. Some porous media whose pore-space morphology and wetting behavior are of physiological interest are skin, hair, feathers, teeth, and lungs. Other examples of porous media that are of widespread use are ceramics, pharmaceuticals, contact lenses, explosives, and catalysts.

In all of these phenomena one has to deal with the complex pore structure of the medium and how it affects the distribution, flow, or displacement of one or more fluids, or dispersion (i.e., mixing) of one fluid in another. Each process can, in itself, be very complex. For example, displacement of one fluid by another can be carried out by many different mechanisms, which may involve heat and mass transfer, thermodynamic phase behavior and phase change, and the interplay of various forces such as viscous, buoyancy, and capillary forces. If the solid matrix of the porous medium is deformable, its porous structure may change during flow or any other phenomenon. If the fluid is reactive, or if it carries solid particles of various shapes, sizes, and electrical charges, the pore structure of the medium may change due to the reaction of the fluid with the pore surface, or the physicochemical interaction between the particles and the

pore surface.

In this paper, we review and discuss various experimental, theoretical, and computer simulation approaches to flow, dispersion, and displacement processes in reservoir rocks. We do not consider other types of porous media, such as catalysts, woods, porous composite materials, etc., although most of our discussions are equally applicable to such systems. We discuss flow phenomena only in a *static* porous medium, i.e., a medium whose morphology does not change during a given process. Thus deformable porous media, as well as those whose morphology changes due to a chemical reaction or to physicochemical interactions between the pore surface and a fluid are not discussed here. The interested reader is referred to Sahimi *et al.* (1990) for a complete discussion of transport and reaction in porous media and the resulting changes in the structure of the media.

The outcome of any given phenomenon in reservoir rock depends on several length scales over which the porous medium may or may not be homogeneous. When there are inhomogeneities in the system that persist at different length scales, the overall behavior of the system is dependent on transport processes such as diffusion, conduction, and convection, the way the fluids distribute themselves in the medium, and the morphology of the system. Often, the morphology of the system plays a role that is more important than that of other influencing factors.

Two classes of disordered porous media are considered here. In the first class are porous media that are *microscopically disordered* but *macroscopically homogeneous*. Provided that they are large enough, such porous media are characterized by well-defined and unique pore-space properties, such as porosity and pore-size distribution, and size-independent transport properties such as diffusivity, conductivity, and permeability. We shall refer to such systems as homogeneous porous media. Porous media that are *macroscopically heterogeneous*, in the sense that there are large-scale spatial variations in their properties as one samples different regions of their pore space, are in the second class, and will be referred to as heterogeneous porous media. Multiporous media, i.e., those characterized by several distinct degrees of porosity, or several distinct families of transport path, are in this class of porous media. For example, a reservoir with large fractures and comparatively small pores is a well-known example of a *double-porosity* medium. The effective transport properties of such a reservoir are dominated by the fractures, whereas most of its porosity is provided by the pores. We shall show that, despite significant differences between homogeneous and heterogeneous media, there are several concepts and tools that can provide a unified approach to various phenomena in both types of rock.

B. Continuum versus discrete models of flow phenomena

The analysis of flow, dispersion, and displacement processes in rock has a long history in connection with the

production of oil from underground reservoirs. However, it is only in the past fifteen years that this analysis has been extended to include detailed structural properties of the media. These studies are quite diverse in the physical phenomena that they consider. In this review we shall classify the models for flow, dispersion, and displacement processes in reservoir rocks as *continuum models* and *discrete models*. Continuum models represent the classical engineering approach to describing materials of complex and irregular geometry, characterized by several length scales. The physical laws that govern fluid transport at the microscopic level are well understood, with the exception of ultramicroporous structures. Leaving aside that case, one could in principle write down differential equations for momentum, energy, and mass and the associated initial and boundary conditions at the fluid-solid interface. However, as the interface in typical rocks is very irregular, practical and economical techniques are not available for solving such boundary-value problems—even in the unlikely event that one knows the detailed morphology of the medium. Determination of the precise solid-fluid boundary in anything but the simplest rocks is, and will probably remain, a very difficult (if not impossible) task; the boundary (even if known) within which one would have to solve the equations of change would be so tortuous as to render the problem mathematically intractable. Moreover, even if the solution of the problem could be obtained in such great detail, it would contain much more information than would be useful in any practical sense. Thus it becomes essential to adopt a macroscopic description at a length scale much larger than the dimension of individual pores or fractures.

Macroscopic properties such as effective transport coefficients are defined as averages of the corresponding microscopic quantities (see, for example, Slattery, 1967, 1969; Whitaker, 1967). The averages must be taken over a volume V that is small enough compared to the volume of the system, but large enough for the equation of change to hold when applied to that volume. At every point in the medium one uses the smallest such volume and, thereby, generates macroscopic field variables obeying equations such as Darcy's law of flow or Fick's law of diffusion. The reasons for choosing the smallest suitable volume for averaging are to allow in the theory suprapore variations of the porous medium and to generate a theory capable of treating the usual macroscopic variations of effective properties. In this review we shall encounter several situations in which the conditions for the validity of such an averaging are not satisfied. Even when the averaging is theoretically sound, the prediction of macroscopic properties is often difficult because of the complex structure of rock. In any case, with empirical, approximate, or exact formulae for the transport coefficients and other effective properties, the results of a given phenomenon in a porous medium can be analyzed with the macroscopic theory.

Past theoretical attempts to derive macroscopic transport coefficients from the microstructure of the rock entailed a simplified representation of the pore space, often

as a bundle of capillary tubes (Scheidegger, 1974). In this model, the capillaries were initially treated as parallel and then, later, as randomly oriented. These models are relatively simple, easy to use, and sufficiently accurate, provided that the relevant parameters are determined experimentally and the interconnectivity of the pore space does not play a major role.

Having derived macroscopic equations and suitable effective transport properties, one has the classical description of the system as a continuum. We shall therefore refer to various models associated with this classical description as *continuum models*. These models have been widely applied because of their convenience and familiarity to the engineer. They do have some limitations, one of which was noted above in the discussion concerning scales and averaging. They are also not well suited for describing those phenomena in rock in which the connectivity of the pore space or a fluid phase plays a major role. Such models also break down if there are long-range correlations in the system.

The second class of models, the *discrete models*, are free of these limitations. These models have been advanced to describe phenomena at the microscopic level and have been extended in the last few years to describe various phenomena at the macroscopic level. Their main shortcoming, from a practical point of view, is the large computational effort required for a realistic discrete treatment of the system. They are particularly useful when the effect of the pore-space interconnectivity or long-range correlations is strong. The discrete models that we shall consider here are mostly based on a network representation of the rock. The original idea of network representation of a pore space is rather old (Owen, 1952; Fatt, 1956), but it was only in the early '80s that systematic and rigorous procedures were developed (Mohanty, 1981; Lin and Cohen, 1982) to map, in principle, any disordered rock onto an equivalent random network of bonds and sites. Once this mapping is complete, one can study a given phenomenon in porous media in great detail.

However, only in the past fifteen years have ideas from the statistical physics of disordered media been applied to flow, dispersion, and displacement processes in porous rocks. These concepts include percolation theory (Stauffer and Aharony, 1992; Sahimi, 1993b), the natural language for describing connectivity effects, diffusion-limited growth processes (Meakin, 1988), which describe fundamentally nonequilibrium growth processes, fractal concepts (Mandelbrot, 1982; Bunde and Havlin, 1991), which are the main tool for describing the self-similarity and self-affinity of the morphology of a system and the effect of long-range correlations, and universal scaling laws, which describe how and under what conditions the effective macroscopic properties of a system may be independent of its microscopic details. What we intend to do here is to review the relevant literature on the subject, define and discuss relevant ideas and techniques from the statistical physics of disordered media and their applications to the processes of interest in this paper, and review

the progress that has been made as a result of such applications. In particular, we emphasize the important effect of the connectivity of the pores or fractures of the system on the phenomena of interest and point out how scaling and fractal concepts provide powerful tools for describing flow, dispersion, and displacement processes in reservoir rocks.

This review is divided roughly into two parts. In the first part of the paper we discuss mainly those phenomena that involve one fluid and one fluid phase. Hence, in the next section we discuss the concepts of percolation theory as a prelude to describing various properties of porous and fractured rocks. We then review and discuss, in Sec. III, reservoir rock properties and characteristics and how they are measured, correlated, and interpreted. Models of porous media, both homogeneous and heterogeneous, and fractured rocks are discussed in Sec. IV. In Sec. V single-phase flow and transport in porous media are discussed. The second part of the paper starts with hydrodynamic dispersion processes, which are reviewed and discussed in Sec. VI. Next, we study miscible displacement processes and discuss in Sec. VII various models of such phenomena. In Sec. VIII, two-phase flow processes are introduced, and various forms of displacements and instabilities are discussed. Finally, Sec. IX contains a discussion of recent computational advances for the study of flow phenomena in reservoir rocks. In particular, we review and discuss cellular automata approaches to flow phenomena in porous media. The final version of this review was completed in December 1992.

II. PERCOLATION PROCESSES

In this section we discuss the ideas and concepts of percolation theory that we shall use in the rest of this review. As we shall show, such ideas and concepts are invaluable tools for understanding rock properties and transport therein.

A. Historical background

Percolation processes were first developed by Flory (1941) and Stockmayer (1943) to describe how small branching molecules react and form large macromolecules. This polymerization process may lead to gelation, i.e., to the formation of a network of monomers connected by chemical bonds, spanning the whole system. However, Flory and Stockmayer did not call their theory a percolation process; they also developed their theory of gelation for a special kind of network, namely, the Bethe network, an endlessly branching structure without any closed loops.

In the mathematical literature, percolation processes were introduced by Broadbent and Hammersley (1957). They originally dealt with the concept of the spread of a hypothetical fluid through a random medium. The terms fluid and medium were viewed as totally general: a fluid could be a liquid, vapor, heat flux, electric current, infec-

tion, solar system, and so on. The medium in which the fluid is carried could be the pore space of a rock, fluid phases of an interspersion, an array of trees, a distribution of permeable regions in an impermeable background, or the universe. Generally speaking, the spread of a fluid through a medium may involve some random elements. But one has to realize that the underlying mechanism of this randomness might be of two very different types. In one type, the randomness is dictated by the *fluid*: this is the classical *diffusion process*. In the other type, the randomness is imposed by the *medium*: this was the new situation that was considered by Broadbent and Hammersley (1957). They decided to call it a *percolation process*, since they thought that the spread of the fluid through the random medium resembled the flow of coffee in a percolator!

B. Definitions and percolation thresholds

We first discuss percolation processes on networks and lattices (discrete systems) and then briefly discuss them for continua. The classical percolation theory centers on two problems. In the *bond percolation problem*, the bonds of the network are either occupied (i.e., they are open to flow, diffusion, and reaction, they are conducting elements, etc.), randomly and independently of each other with probability p , or they are *vacant* (i.e., they are closed to flow or current or have been plugged, they are insulating elements, etc.), with probability $1-p$. For a large network, this assignment is equivalent to removing a fraction $1-p$ of all bonds at random. Two sites are called *connected* if there exists at least one path between them consisting solely of occupied bonds. As shown in Sec. III, in porous media applications sites are equivalent to pore bodies, while bonds are equivalent to pore throats. A set of connected sites bounded by vacant bonds is called a *cluster*. If the network is of very large extent and if p is sufficiently small, the size of any connected cluster is likely to be small. But if p is close to 1, the network should be entirely connected, apart from occasional small holes. At some well-defined value of p , there is a transition in the topological structure of the network; this value is called the *bond percolation threshold* p_{cb} . This is the largest fraction of occupied bonds below which there is no sample-spanning cluster of occupied bonds.

Similarly, a *site percolation problem* can be defined. In this case, sites of the network are occupied with probability p and vacant with probability $1-p$. Two nearest-neighbor sites are called connected if they are both occupied, and connected clusters on the network are again defined in the obvious way. As before, there is a site percolation threshold p_{cs} above which an infinite cluster of occupied sites spans the network. Note that the percolation phenomenon as defined above is a static process; that is, once a percolation cluster is generated, its configuration is in "equilibrium" and does not change with time. Dynamic percolation processes have also been

invented and will be briefly discussed below. It is always possible to convert a bond problem to a site problem on a different lattice and, therefore, in some sense site percolation problems are more fundamental. However, depending on the specific application of percolation theory to a problem of interest, many variants of the classical percolation processes have been developed. For example, one may think of a *correlated* percolation process in which whether a bond or site is occupied depends on its environment. The interested reader is referred to Stauffer, Coniglio, and Adam (1982) or to Sahimi (1993b) for a list of variants of the classical percolation problem and their applications.

The derivation of the exact values of p_{cb} and p_{cs} has been possible to date only for certain lattices related to the Bethe lattice and for a few two-dimensional lattices. For the Bethe lattice Fisher and Essam (1961) showed that

$$p_{cb} = p_{cs} = \frac{1}{Z - 1}, \quad (2.1)$$

where Z is the coordination number of the lattice. We compile the current estimates of p_{cb} and p_{cs} (and their exact values if they exist) for three common two-dimensional lattices in Table I, while the currently accepted values of p_{cb} and p_{cs} for four common three-dimensional lattices are compiled in Table II. Also shown in these tables is the product $B_c = Zp_{cb}$ and, as can be seen, this quantity is almost an invariant of percolation networks.

C. Generation of percolation clusters on a network

Generating a percolating lattice by randomly removing sites or bonds is not totally suitable for engineering applications, because in addition to the sample-spanning cluster, this method also generates isolated finite clusters. In most applications one works only with the sample-spanning cluster (or the process of interest starts with a single cluster) and, therefore, we must first delete all isolated clusters from the system. Alternatively (and more simply), we can use a different method due to Leath (1976) and Alexandrowicz (1980) that generates only the sample-spanning (or the largest) cluster. In this method one starts with a single occupied site, which is usually selected to be the center of the lattice. One then identifies the nearest-neighbor sites of the occupied site

TABLE I. Values of bond percolation threshold p_{cb} , site percolation threshold p_{cs} , and $B_c = Zp_{cb}$ for three common two-dimensional networks.

Network	Z	p_{cb}	B_c	p_{cs}
Honeycomb	3	$1 - 2 \sin(\pi/18) \approx 0.6527^a$	1.96	0.6962
Square	4	$1/2^a$	2	0.5927
Triangular	6	$2 \sin(\pi/18) \approx 0.3473^a$	2.08	$1/2^a$

^aExact result.

TABLE II. Numerical estimates of bond percolation threshold p_{cb} , site percolation threshold p_{cs} , and $B_c = Zp_{cb}$ for four common three-dimensional networks.

Network	Z	p_{cb}	B_c	p_{cs}
Diamond	4	0.3886	1.55	0.4299
Simple Cubic	6	0.2488	1.49	0.3116
BCC	8	0.1795	1.44	0.2464
FCC	12	0.119	1.43	0.199

and considers them occupied and adds them to the cluster if random numbers r , attributed to the sites, are less than the fixed value p . The perimeters (the nearest-neighbor empty sites) of these sites are found and the process of occupying the sites continues in the same way. If a selected perimeter site is not occupied, then it remains unoccupied forever. The generalization of this method for generating clusters of occupied bonds is obvious. Since the growth of the cluster can continue indefinitely, this can be considered as a sort of dynamic percolation.

An important task in computer simulations of percolating systems is to count the number of clusters of a given size. For example, during displacement of a fluid A by another immiscible fluid B we may need to know the number of islands or blobs of fluid A of a given size which are completely surrounded by B , which is equivalent to knowing the number of clusters of a given size within the context of a percolation model. An algorithm due to Hoshen and Kopelman (1976) can perform this task very efficiently. This algorithm is described in detail by Stauffer and Aharony (1992), who also give a computer program for counting the clusters.

D. Percolation quantities

In addition to the percolation thresholds, the connectivity of percolation clusters, and hence transport processes therein, are characterized by several other quantities. In this section we introduce and discuss these. Percolation quantities of interest are

(i) the *percolation probability* $P(p)$, which is the probability that, when the fraction of occupied (conducting) bonds is p , a given site belongs to the infinite (sample-spanning) cluster of occupied bonds;

(ii) the *accessible fraction* $X^A(p)$, which is that fraction of conducting bonds (or sites) belonging to the infinite cluster;

(iii) the *backbone fraction* $X^B(p)$, which is the fraction of conducting bonds in the infinite cluster with actually participate in conduction (or carry flow or current), since some of the bonds in the infinite cluster are dead-end and do not carry any current (flow), and therefore $X^A(p) \geq X^B(p)$;

(iv) the *correlation length* $\xi_p(p)$, which is the typical radius of the connected clusters for $p < p_c$ and the length scale over which the percolating network is macroscopically homogeneous for $p > p_c$. Thus, in any Monte Carlo

simulation of percolation processes, the linear size L of the network must be larger than ξ_p for the results to be independent of L ;

(v) the average number of clusters of size s (per lattice site) $n_s(p)$, which is an important quantity in some of the problems of interest here because it corresponds, for example, to the number of finite islands or blobs of fluids of a given size that are formed during the displacement of one fluid by another, if the displaced fluid is incompressible (see below);

(vi) the effective conductivity g_e , which is the conductivity of the network in which a fraction p of bonds (or sites) are conducting and the rest are insulating. In a similar way, the effective diffusivity D_e and hydrodynamic permeability k of the system can be defined. Figure 1 shows the typical behavior of some of these properties for a simple cubic network in site percolation. Also shown is $X^I(p)$, the fraction of isolated occupied sites, which attains its maximum at p_{cs} .

E. Universal scaling laws for percolation quantities

Similar to the behavior of various thermodynamic properties near a critical temperature, the behavior of many percolation quantities near the percolation threshold is insensitive to the lattice structure and to whether the percolation process is a site or a bond percolation problem. The quantitative statement of this apparent universality is that critical exponents, characterizing the nonanalytic structure at or near the percolation threshold of certain quantities, depend only on dimension d of the system. Even long-range, but finite, correlations do not change this universality.

Near the (site or bond) percolation threshold p_c , we

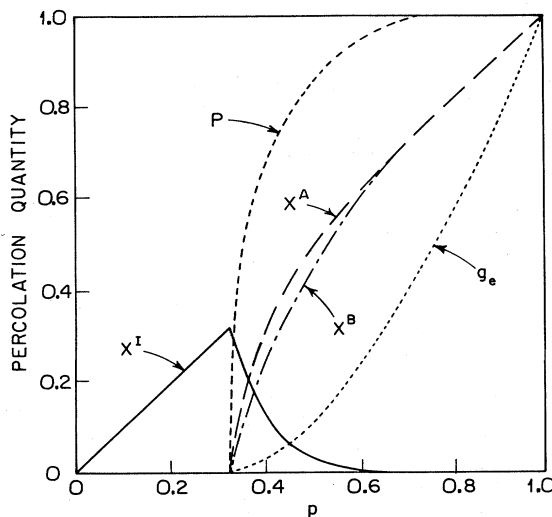


FIG. 1. Typical behavior of some percolation quantities as a function of p , the fraction of occupied sites in a simple cubic lattice.

have the following scaling laws:

$$P(p) \sim (p - p_c)^{\beta_p}, \quad (2.2)$$

$$X^A(p) \sim (p - p_c)^{\beta_p}, \quad (2.3)$$

$$X^B(p) \sim (p - p_c)^{\beta_B}, \quad (2.4)$$

$$\xi_p(p) \sim |p - p_c|^{-\nu}, \quad (2.5)$$

$$g_e(p) \sim (p - p_c)^\mu. \quad (2.6)$$

The scaling behavior of the effective diffusivity D_e is related to that of $g_e(p)$. According to Einstein's relation, $g_e \sim n_e D_e$, where n_e is the density of the electrons. Although a particle can diffuse on all clusters, only diffusion on the sample-spanning cluster contributes significantly to D_e (except at p_c ; see below), in which case, $n_e \sim X^A(p)$, i.e., $g_e(p) \sim X^A(p) D_e(p)$, and therefore

$$D_e(p) \sim (p - p_c)^{\mu - \beta_p}. \quad (2.7)$$

Similarly, we can write down a scaling law for the permeability k of a percolation network near p_c ,

$$k(p) \sim (p - p_c)^\epsilon. \quad (2.8)$$

For lattice models, $\epsilon = \mu$. However, for percolation in continua, ϵ can be significantly different from μ (see below).

For large clusters near p_c , $n_s(s)$ obeys the scaling law

$$n_s \sim s^{-\tau_p} f[(p - p_c)s^{\sigma_p}], \quad (2.9)$$

where τ_p and σ_p are two more universal critical exponents and $f(x)$ is a scaling function such that $f(0)$ is not singular. These exponents are not all independent. For example, one has $\tau_p = 2 + \beta_p \sigma_p$ and $\nu d = \beta_p + 1/\sigma_p$, and in fact knowledge of ν and another exponent is sufficient for determining most of the percolation exponents. The implied prefactors in Eqs. (2.2)–(2.9) do depend on the type of lattice and are not universal. If two phenomena are described by two different sets of critical exponents, the physical laws governing the two phenomena must be fundamentally different. Thus critical exponents can help one to distinguish between different classes of problems and the physical laws that govern them. As we shall see, some of the problems of interest here may not even belong to the universality class of random percolation. In Table III the values of the critical

TABLE III. Values of the critical exponents of percolation. The exponents at $d=2$ and for the Bethe lattice are exact. The values of μ for $d=2$ and 3 are numerical estimates.

Exponent	Bethe lattice		
	$d=2$	$d=3$	$(d \geq 6)$
β_p	5/36	0.41	1
β_B	0.47	1.05	2
τ_p	187/91	2.18	5/2
σ_p	36/91	0.45	1/2
ν	4/3	0.88	1/2
μ	1.3	2.0	3

exponents in two and three dimensions are compiled. For comparison, the mean-field values of the exponents, which are valid for $d \geq 6$, are also given.

As mentioned earlier, the correlation length ξ_p has the physical significance that for length scales L larger than ξ_p the system is macroscopically homogeneous. However, for length scales smaller than ξ_p , the system is *not* homogeneous, and the macroscopic properties of the system depend on L . In this regime, the sample-spanning cluster is statistically self-similar at all length scales less than ξ_p , and its mass M (its total number of bonds or sites) scales with ξ_p as

$$M \sim \xi_p^{D_p}, \quad (2.10)$$

where D_p is the fractal dimension of the cluster. However, D_p is not a totally new quantity and is given by

$$D_p = d - \frac{\beta_p}{\nu}, \quad (2.11)$$

so that $D_p(d=2)=91/148 \approx 1.9$ and $D_p(d=3) \approx 2.5$. Similarly, for $L < \xi_p$, the backbone is a fractal object and its fractal dimension D_{BB} is given by

$$D_{BB} = d - \frac{\beta_B}{\nu}. \quad (2.12)$$

The pore volume and pore surfaces of many reservoir rocks are also fractal, as will be discussed in the next section. Pfeifer and Avnir (1993), Avnir *et al.* (1985) and Katz and Thompson (1985) have demonstrated the relevance of fractals and fractal dimensions to heterogeneous surfaces and rocks. Note that if $L < \xi_p$ one should replace ξ_p in Eq. (2.10) by L . Note also that at $p=p_c$ the correlation length is infinite, so that then the sample-spanning cluster and its backbone are fractal objects at *any* length scale.

Once it is established that a system is a fractal, many classical laws of physics have to be significantly modified. For example, Fick's law of diffusion with a constant diffusivity is no longer appropriate for describing diffusion processes in fractal systems. Instead, the diffusion coefficient is a time- and length-dependent quantity; this is called *anomalous* (Gefen *et al.*, 1983) or *fractal* diffusion (Sahimi *et al.*, 1983b). Therefore, when interpreting experimental data, one has to make sure that one is not in the regime of anomalous diffusion; otherwise, the interpretation of the data in terms of a constant diffusivity may be seriously in error. This is discussed below.

F. Percolation in finite systems and finite-size scaling

So far we have restricted our attention to percolation processes in disordered systems of infinite extent. However, percolation in finite systems deserves discussion, since both in practical applications and in computer simulations one usually deals with a system of a finite extent. Fisher (1971) investigated the effect of the finite size

of a thermal system on its critical properties near the critical temperature and developed a theory for it, which is usually called finite-size scaling. His analysis can be adopted for percolation processes. In a finite system, as p_c is approached ξ_p eventually exceeds the linear size L of the network, in which case L becomes the dominant length scale of the system. Therefore, following the finite-size scaling theory of Fisher (1971), the variation of any property P_L of a system of size L is written as

$$P_L \sim L^{-\gamma} f(u), \quad (2.13)$$

where $f(u)$, which is a function of the variable $u = L^{1/\nu}(p - p_c) \sim (L/\xi_p)^{1/\nu}$, is a nonsingular function. If in the limit $L \rightarrow \infty$ one has a scaling law such as $P_\infty \sim (p - p_c)^\delta$, then one must have $\gamma = \delta/\nu$. Therefore the variations with L of $P_L(p)$ in a *finite network* at p_c can be used to obtain information about the quantities of interest for an *infinite network* near p_c . This method has been used successfully by many authors to obtain accurate estimates of quantities of interest from simulation of finite systems. The finite size of the network also causes a shift in the percolation threshold (Levinshtein *et al.*, 1976; Reynolds *et al.*, 1980),

$$p_c - p_c(L) \sim L^{-1/\nu}. \quad (2.14)$$

In this equation p_c is the percolation threshold of the infinite system, and $p_c(L)$ is an *effective* percolation threshold for a finite system of linear dimension L . However, we should note that even Eqs. (2.13) and (2.14) are valid for large values of L . In practice, very large systems cannot easily be simulated and, therefore, an equation such as (2.13) is modified to

$$P_L \sim L^{-\gamma} [a_1 + a_2 g_1(L) + a_2 g_2(L)], \quad (2.15)$$

where g_1 and g_2 are two *correction-to-scaling* terms that are particularly important for small and moderate values of L , and where the a 's are constant. For *transport properties*, $g_1 = (\ln L)^{-1}$ and $g_2 = L^{-1}$ often provide an accurate estimate of γ (Sahimi and Arbabi, 1991).

G. Percolation in random networks and in continua

Although percolation in regular networks has routinely been used for investigating transport in disordered systems, percolation in continua and in topologically random networks are also of great interest, since in most practical situations one has to deal with such systems. There are at least three ways of realizing a percolating continuum. In the first method, one has a random distribution of inclusions, such as circles, spheres, or ellipses, in an otherwise uniform system (Pike and Seager, 1974; Haan and Zwanzig, 1977; Gawlinski and Stanley, 1981; Elam *et al.*, 1984; Thorpe and Sen, 1985; Sen and Torquato, 1988; Sevik *et al.*, 1988; Torquato *et al.*, 1988; Xia and Thorpe 1988). In such systems percolation is defined either as the formation of a sample-spanning cluster of the paths between un-touching inclusions or as the

formation of a sample-spanning cluster of touching or overlapping inclusions. In the second method, one generates a percolating continuum by dividing the space into regular or random polyhedra (Winterfeld *et al.*, 1981), a fraction of which is conducting, while the rest of the polyhedra are insulating. Finally, in the third method, one distributes at random conducting sticks of a given aspect ratio, or plates of a given extent, and studies transport in such systems (Balberg *et al.*, 1983, 1984; Balberg and Binenbaum, 1983, 1985; Charlaix *et al.*, 1984, 1987a; Robinson, 1984a, 1984b), which are relevant to transport in fractured systems reviewed in this paper.

One of the most important discoveries for continuum percolation (Scher and Zallen, 1970) is that a critical occupied volume fraction ϕ_c , which is defined as

$$\phi_c = p_{cs} f_l , \quad (2.16)$$

where f_l is the filling factor of a lattice when each site of the lattice is occupied by a sphere in such a way that two nearest-neighbor impermeable spheres touch one another at one point, appears to be almost an invariant of the system, with a value of about 0.17 for three-dimensional systems. Shante and Kirkpatrick (1971) generalized this idea to permeable spheres and showed that the average number of bonds per sites B_c at p_c is related to ϕ_c by

$$\phi_c = 1 - \exp(-B_c/8) \quad (2.17)$$

and that the continuum B_c is the limiting value of $p_{cs}Z$ when $Z \rightarrow \infty$. It is clear from Table II that, in three dimensions, $B_c \approx 1.5$. It has been established (Haan and Zwanzig, 1977; Gawlinski and Stanley, 1981; Elam *et al.*, 1984; Balberg and Binenbaum, 1985) that the geometrical exponents, defined by Eqs. (2.2)–(2.5) and (2.9), are the same for lattice and continuous systems.

However, transport in percolating continua can be quite different from that in discrete networks. Consider, for example, the "Swiss cheese" model in which spherical inclusions are punched at random in an otherwise uniform system. If transport takes place through the channels between the nonoverlapping spheres, then the system can be mapped onto an equivalent problem on the edges of a Voronoi network (Kerstein, 1983), which is a random network. The Voronoi network was used by Jerauld *et al.* (Jerauld, Hatfield, *et al.*, 1984; Jerauld, Scriven, and Davis, 1984) to study transport in a random network. Its average coordination numbers are about 6 and 15.5 in two and three dimensions, respectively. Halperin *et al.* (1985) and Feng *et al.* (1987) used a scaling analysis and showed that the critical exponents μ_c and e_c , defined for the conductivity and permeability of this model, are quite different from μ and e defined above. In particular, they showed that, in a three-dimensional Swiss cheese system, $\mu_c \approx \mu + 1/2$ and $e_c \approx \mu + 5/2$, whereas for the two-dimensional system $\mu_c = \mu$ and $e_c \approx \mu + 3/2$.

The model in which the matrix is insulating, but the spherical inclusions are very good conductors, was employed by Batchelor and O'Brien (1977) to study trans-

port in granular porous media. This system can also be mapped onto an equivalent random network, which is in fact the dual of the Voronoi network. Jerauld *et al.* (Jerauld, Hatfield, *et al.*, 1984; Jerauld, Scriven, and Davis, 1984) showed that the geometrical critical exponents for such random networks are the same as those for regular networks. Moreover, they established that, as long as the average coordination number of a regular network and a topologically random one (for example, the two-dimensional Voronoi and triangular networks) are about the same, many transport properties of the two systems are, for all practical purposes, identical.

H. Fractal diffusion

The scaling law (2.7) is valid if the linear size L of a system is much larger than ξ_p . However, if $L \ll \xi_p$, then one has anomalous diffusion in which D_e is a time-dependent quantity. Since the mean-square displacement $\langle r^2(t) \rangle$ of a diffusant at time t is related to its effective diffusivity D_e through $\langle r^2(t) \rangle = 2dD_e t$, where d is the dimensionality of the system, the behavior of D_e can be inferred from that of $\langle r^2(t) \rangle$. If $r_s = [\langle r^2(t) \rangle]^{1/2} \ll \xi_p$, then

$$\langle r^2(t) \rangle \sim t^{2/d_w} , \quad (2.18)$$

where d_w is called the fractal dimension of the walk and, therefore, $D_e(t) \sim \langle r^2(t) \rangle / t \sim t^{2/d_w - 1} \rightarrow 0$, as $t \rightarrow \infty$. Equation (2.18) is the manifestation of what is called anomalous or fractal diffusion (Gefen *et al.*, 1983; Schimi *et al.*, 1983b). If diffusion takes place only on the sample-spanning cluster, then (Gefen *et al.*, 1983)

$$d_w = 2 + \frac{\mu - \beta_p}{\nu} , \quad (2.19)$$

whereas if diffusion takes place on *all* clusters one has

$$d_w = 2 \frac{2\nu + \mu - \beta_p}{2\nu - \beta_p} . \quad (2.20)$$

These results demonstrate clearly the significant role of a macroscopic length scale for homogeneity of a system (which, for percolating systems, is ξ_p). It is obvious that Eqs. (2.18)–(2.20) provide a means of estimating μ by random-walk simulations, and this has been exploited by several authors (see Pandey *et al.*, 1984, and Roman, 1990, and references therein). For pure diffusion in percolating systems and $r_s \ll \xi_p$, $d_w > 2$. However, in the presence of a drift, or random driving forces (for example, random velocity fields), one may encounter situations in which $d_w < 2$, i.e., one has *superdiffusion*. This phenomenon has been observed in hydrodynamic dispersion in geological systems and will be discussed later in this paper.

If a diffusion process is characterized by Eq. (2.18), then it *cannot* be described by the classical continuum equation of diffusion with a constant diffusivity. For this case, it has been proposed that the concentration C of the

diffusant (or the probability of finding it) at a point \mathbf{r} at time t is given by (Guyer, 1985; see also Harris and Aharony, 1987)

$$C(\mathbf{r}, t) \sim t^{-d_s/2} \exp[-(|\mathbf{r}|/t^{1/d_w})^{\nu_d}], \quad (2.21)$$

where $d_s = 2D_p/d_w$ and $\nu_d = d_w/(d_w - 1)$. Equation (2.21) is very different from a Gaussian distribution, the solution of the classical diffusion equation. Klafter *et al.* (1991) have argued that Eq. (2.21) is valid if $\xi = |\mathbf{r}|/t^{1/d_w} \gg 1$. However, if $\xi \ll 1$, then numerical simulations indicate that the following equation, proposed by O'Shaughnessy and Procaccia (1985), is approximately correct:

$$C(\mathbf{r}, t) \sim t^{-d_s/2} \exp(-|\mathbf{r}|^{d_w}/t). \quad (2.22)$$

Both Eqs. (2.21) and (2.22) are approximations, and the problem of the exact form of $C(\mathbf{r}, t)$ is still unsolved. For a complete discussion of this issue see Sahimi and Hughes (1993). Equation (2.18) also gives rise to a cross-over time t_{co} such that for $t \gg t_{co}$ the diffusion process is Gaussian, but for $t \ll t_{co}$ diffusion is described by Eqs. (2.18) and (2.21) [or Eq. (2.22)]. It is clear that $t_{co} \sim \xi_p^2/D_e$, and therefore

$$t_s \sim (p - p_c)^{-\mu - 2\nu + \beta_p}, \quad (2.23)$$

so that t_{co} diverges as p_c is approached. Many other aspects of fractal diffusion are reviewed by Havlin and Ben-Avraham (1987).

I. A note on the history of application of percolation theory to porous-media problems

Before closing this section, it may be interesting to give a brief review of the history of application of percolation theory to modeling of porous-media problems. Even before Broadbent and Hammersley (1957) discussed the application of percolation theory to flow in random media, Fatt (1956) had used two-dimensional networks to model two-phase flow in porous media, which is a percolation phenomenon (see Sec. VIII). But despite the fact that Broadbent and Hammersley expressed the hope that their theory would someday be used for solving some practical problems involving porous media, explicit use of percolation processes for describing flow phenomena in porous media gained popularity only in the 80s. Since "who was the first to use it" has been a matter of some contention and controversy, it may be interesting to review the history to see who said what and when, at least according to the published papers in the open literature.

To the best of this author's knowledge, Torelli and Scheidegger (1972) were the first to recognize the usefulness of percolation theory for modeling flow and dispersion phenomena in porous media. These authors were interested in hydrodynamic dispersion in porous media (see

Sec. VI) and pointed out that percolation theory, if appropriately modified and applied, might provide some useful insights into the behavior of the phenomenon. However, they did not actually use percolation and, in fact, they did not even report any results in their paper.

Melrose and Brandner (1974) suggested that the entrapment of oil in reservoir rocks is similar to percolation processes and proposed that an approach based on percolation might yield deeper insight into the problem. Again, these authors did not actually calculate anything using their idea. Davis *et al.* (1975), who studied transport processes in composite media, remarked at the end of their paper that, "Although, to our knowledge, no quantitative work has been done on the subject, we believe that two-phase oil-water flow in oil fields is a percolation process in which the connectivity of each phase determines the relative permeability of that phase." But these authors also did not report any result.

Larson (1977) and Larson, Scriven, and Davis (1977) suggested that percolation theory might be useful for describing entrapment of one fluid phase by another in porous media. To demonstrate the usefulness of their idea, they calculated the percolation cluster-size distribution for various coordination numbers and made a qualitative comparison between the results and relevant experimental data (see Sec. VIII). Almost simultaneously, Chatzis and Dullien (1977) published a paper in which they calculated several percolation properties for various two- and three-dimensional networks and pointed out how they might be used for simulating two-phase flow in porous media. They compared their predictions with the measured capillary pressure curves. This will be discussed in the next section.

Shortly after these two papers, de Gennes and Guyon (1978) also suggested that two-phase flow problems in porous media might belong to the class of percolation processes. They used visualization of mercury porosimetry (see Sec. III) as an example and proposed methods of using percolation concepts for modeling this phenomenon and other processes in porous media. They also pointed out how permeability and cluster-size distribution in porous media may be calculated using percolation.

Finally, two papers in 1980 further established the applicability of percolation for modeling of two-phase flow in porous media. Lenormand and Bories (1980) proposed a percolation model, now popularly known as invasion percolation (see Sec. VIII), for modeling a drainage process, i.e., a process in which a nonwetting fluid displaces a wetting fluid from a porous medium. Golden (1980) discussed the application of percolation theory for studying two-phase flow and the hysteresis (history-dependent) phenomena that are routinely observed in many two-phase flow problems in porous media (see Sec. VIII).

After the publication of these original papers, there was an explosion of new ideas and methods for the modeling of porous-media problems using percolation theory. We shall review these concepts and methods in the appropriate sections of this paper.

III. ROCK FORMATION, CHARACTERIZATION, AND PROPERTIES

Before we discuss rock characterization, it may be useful to review the processes that give rise to its present structure. These are *diagenetic processes*, and what follows is a brief description of them.

A. Diagenetic processes and the formation of rocks

In order to understand reservoir rock properties, one has to have an understanding of the diagenetic processes that lead to the formation of rocks. Reservoir rock formation starts with deposition of sediments and is followed by compaction and alteration processes that can cause drastic changes in the morphology of the reservoir. Consider, for example, sandstones, which are assemblages of discrete grains with a wide variety of chemical compounds and mixtures. If the environment around the sandstone changes, the grains start to react and produce new compounds. The mechanical properties of the grains also change. The chemical and physical changes in the sand after its deposition constitute diagenetic processes. The main features of diagenetic processes are (i) mechanical deformation of grains; (ii) solution of grain minerals; (iii) alteration of grains; and (iv) precipitation of pore-filling minerals, cements, and other materials. These features have a key influence on the volume of the content of the reservoir because they control the porosity of the rock.

Immediately after deposition diagenesis starts; it continues during burial and uplift of the rock until outcrop weathering reduces it again to sediment. These changes produce an end product with specific diagenetic features, whose nature depends on the initial mineralogical composition of the system and also on the composition of the surrounding basin-fill sediments. Given a system with a particular mineralogical composition, its diagenetic history depends on several factors, including time-dependent exposures to varying temperatures and pressures and the chemistry of the pore fluid. All of these factors constitute the *historical* aspects of a reservoir and affect its quality. Therefore the ability of reservoir rocks to produce, say, oil, is closely related to their diagenetic history. If appropriate relations between diagenesis and petrophysical properties of reservoir rocks can be found, one can use such relations in the analysis of reservoirs to predict their potential for producing oil or any other material that they may contain.

Porosity of reservoir rocks, i.e., the volume fraction of their open space, has either a *primary* or a *secondary* origin. Primary porosity is due to the original pore space of the sediment, whereas secondary porosity is due to the fact that unstable grains or cements have undergone chemical and physical changes through reaction with the formation water and have partially or entirely passed into the solution. Therefore, if the pore space is restored through dissolution of authigenic minerals, then the original porosity that had been protected from precipitation

by deposition of minerals is converted into secondary porosity. According to Schmidt and McDonald (1979), solution pores provide more than half of all the pore space in many sedimentary rocks. The significance of secondary porosity in carbonate rocks has been recognized for a long time, but the importance of secondary porosity in sandstones has only recently been appreciated (Hayes, 1979).

As discussed by Schmidt and McDonald (1979), there are five classes of secondary porosity in sandstones, defined according to their origin: (i) fracturing; (ii) shrinkage, (iii) dissolution of sedimentary grains and matrix; (iv) dissolution of authigenic pore-filling cement; and (v) dissolution of authigenic replacive minerals. Five different kinds of pores can contain secondary porosity, namely, (i) intergranular pores; (ii) oversized pores; (iii) moldic pores; (iv) intraconstituent pores; and (v) open fractures. Of these, fractures are distinctly different from the other four types of pores and therefore are discussed separately in this paper. The existence of secondary porosity can sometimes even be recognized with the naked eye. Other indications of the occurrence of secondary porosity include oversized or elongated pores, corroded and fractured grains, and several others.

The diagenetic processes discussed above lead to distinct morphologies for reservoir rocks. Pores can take on essentially any shape or size, and they can also be highly interconnected. Patsoules and Cripps (1983) used scanning electron microscopy (SEM) to study rock and obtained information about the shapes, sizes, and connectivity of the pores and the roughness of their surface. They reported that their rock, which was upper cretaceous chalk from East Yorkshire and the North Sea, contained highly interconnected pores. Some of the ring-shaped pores of the chalk were connected to at least 25–30 other pores. These pores remain connected even when the porosity of the system is very low, and therefore one important effect of the diagenetic process is to keep the pore space highly interconnected. As discussed above, rock formation involves compaction and alteration processes. During these alteration processes complex phenomena such as nucleation on the surface of the pores and mineral crystal growth take place. These are time-dependent phenomena, which reduce the porosity and permeability of the rock. If the permeability of the medium is reduced, the flow rate also decreases, which means that the rate of nucleation of mineral crystals increases. However, the crystals cannot grow indefinitely because they are limited by the growth rate at the time they are nucleated. Moreover, the growth of new mineral crystals inhibits that of the older ones. Thus there is competition between nucleation of new mineral crystals and the growth of the older crystals, which determines the distribution of the crystal sizes.

Since diagenetic processes are similar for many different rocks, and since there appear to be many similarities between the geometries of various rocks, one may hope that many fundamental elements of pore formation processes are *universal*, independent of many microscopic

properties of rocks. If so, one may be able to develop a general model of pore formation and growth processes that can explain, at a fundamental level, many features of various rocks. If such a model can be developed, its generality may be comparable to that of diffusion-limited aggregation (DLA) models, first proposed by Witten and Sander (1981, 1983), which are the prototype models of nonequilibrium growth processes. Indeed, Fowler *et al.* (1989), who studied igneous rocks formed from lava of the Archaean era, which usually contain disequilibrium-tortured crystals characterized by spherulitic, branching, or dendritic morphologies, found that over a finite range of length scales some of the disequilibrium textures are scale invariant (have a fractal structure) and can be described by a variant of the DLA model.

B. Geometrical models of diagenetic processes

How can we model diagenetic processes? A study of the literature shows that there are essentially two approaches to this problem. The first approach, which we call *chemical modeling*, relies on the continuum equations of transport and reaction. It ignores the morphology of the pore space and its time variations and attempts to characterize the process by *average* macroscopic properties. The details of the kinetics of the surface reactions are usually included in the model, which contains several parameters, e.g., the diffusivity of each species, which has to be estimated independently or measured experimentally. This approach has been developed by several authors (Palciauskas and Domenico, 1976; Wood and Surham, 1979; Wood and Hewett, 1982; Walsh *et al.*, 1984; Lichtner *et al.*, 1986; Novak *et al.*, 1989). Since this approach is essentially the continuum solution to transport and reaction in a dynamic porous medium, we shall not review or discuss it here, but refer the interested reader to Sahimi *et al.* (1990).

The second approach, in which the details of reaction kinetics and mass transfer are ignored, is what we call *geometrical modeling*. The diagenetic process is modeled by starting from a model of unconsolidated pore space and making several simple assumptions about the rate of change of grains and pores. This approach can take into account the effects of connectivity and percolation of pores and grains. Two such models for granular media, such as sandstones, are those due to Wong *et al.* (1984) and Roberts and Schwartz (1985).

In the model of Wong *et al.* (1984) one starts with a random resistor network on a simple cubic lattice. Each resistor R_i represents a cylindrical fluid-filled tube with radius r_i . To mimic the consolidation process and the reduction in the porosity and permeability of the system during the diagenetic process, a tube is selected at random and its radius is reduced by a fixed factor x

$$r_i \rightarrow xr_i , \quad (3.1)$$

where $0 < x < 1$. Of course, this simple model cannot really simulate the effect of deposition of irregularly

shaped particles in an irregularly shaped pore, or that of thin lubricating films of fluid which, if present, inhibit grain contact. However, the model has two attractive features, namely, (i) that it preserves for any $x > 0$ the network connectivity, even when the porosity has almost vanished; and (ii) that the amount of change in the pore radius r_i at any step of the simulation (time) depends on the value of r_i at that time. Wong *et al.* (1984) used this model qualitatively to explain empirical laws such as Archie's law and the Kozeny equation for permeability of a porous medium. These will be discussed later in this paper. Note that the limit $x=0$ approaches a percolation process.

The second geometrical model for diagenesis of granular media is due to Roberts and Schwartz (1985); it was studied further by Schwartz and Kimminau (1987). In this model, one starts with a dense pack of spherical grains of random radii R . The coordinates of the centers of the spheres follow the Bernal distribution (Bernal, 1960; Bernal *et al.*, 1970; Alben *et al.*, 1976); see Fig. 2(a). The radii of the particles are then allowed to increase simultaneously, as a result of which the system's porosity and permeability decrease. In the region where the spheres overlap, the grains are truncated; see Fig. 2(b). This can be continued to yield a series of porous media with various values of permeability and porosity; see Fig. 2(c). The percolation threshold (the critical porosity) of the system is $\phi_c = 0.03 \pm 0.004$, shown in Fig. 2(d). Given that the initial porosity of the system with the Bernal distribution is 0.364, this algorithm generates models of porous media whose porosities span more than one order of magnitude. They also resemble natural

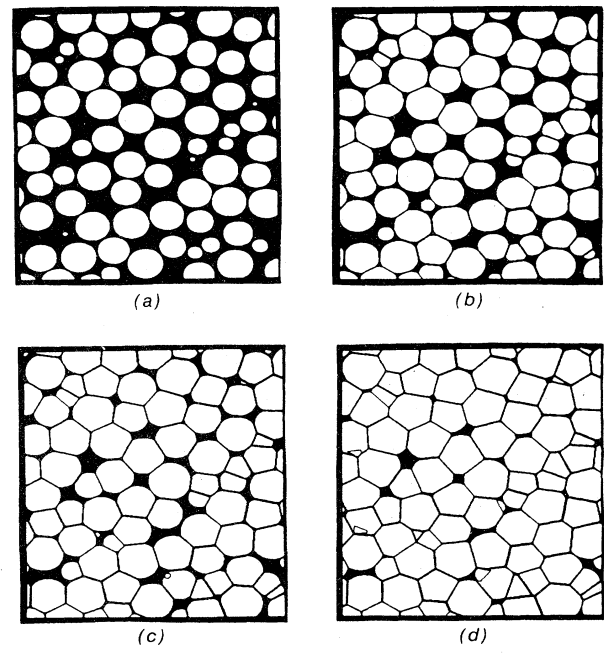


FIG. 2. Four stages of the development of the grain-consolidation model of Roberts and Schwartz (1985).

sandstones, an example of which is shown in Fig. 3. Because the porosity of sandstones and similar rocks is usually less than 0.4, this algorithm provides a reasonable model of the diagenetic process. Schwartz *et al.* (1989a) also considered a model in which the initial grains were not spherical, in order to simulate anisotropic or layered media.

Two points are worth mentioning here. First, if instead of the Bernal distribution one starts with a simple cubic lattice in which spherical grains of unit radius are placed at its nodes and follow the same algorithm, then the percolation threshold or the critical porosity of the system is 0.349, which is close to that of the random sphere packing. If one starts with a body-centered-cubic lattice of spheres, then one obtains $\phi_c \approx 0.0055$, one order of magnitude smaller than what can be achieved with the Bernal distribution. This indicates the relative flexibility of the model for obtaining the desired porosities. Secondly, the sedimentation and diagenetic processes that give rise to many sedimentary rocks such as sandstones tend to favor a distribution of particles that are roughly equal in size (Pittman, 1984). In this region, the algorithm of Roberts and Schwartz (1985) is much more efficient than one in which the porosity is reduced by adding additional spheres with smaller and smaller radii to progressively fill the pore space of the original packing. To obtain a comparable porosity range by this method, one has to use spheres whose radii vary over many orders of magnitude, but the final configuration would bear little resemblance to most naturally occurring porous materials.

The two algorithms described above have been useful in developing a unified framework for the description of many properties of granular media such as sandstones. Such porous media possess pore or solid phases that have many simplifying characteristics. However, other porous media, e.g., carbonate rocks (such as those of Iran), are more complex and their pore and solid phase geometries

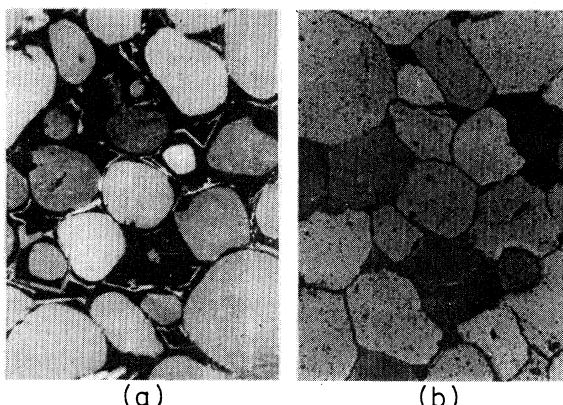


FIG. 3. Heavily cemented Devonian sandstone from Illinois observed (a) with cathodoluminescence to show the original round sand grains, and (b) with ordinary light to show the angular forms of the grains after cementing, for which the grain-consolidation model of Fig. 2 is intended (from Roberts and Schwartz, 1985).

are not as simple as those of granular porous media such as sandstones. The major differences between carbonate and sandstone reservoirs, as discussed by Pittman (1984), are (i) mineralogy; (ii) origin of grains; (iii) size and shape of grains; and (iv) influence of early diagenesis on carbonate rocks. For example, most minerals in carbonate rocks are relatively soluble carbonate materials, whereas sandstone's grains originate through erosion of existing rocks with transportation of the minerals by fluid flow to site of deposition, as discussed above. The grains in carbonate rocks pack more loosely than those in sandstones, and they are usually large with shapes like twigs, rods, and flakes. The pores of carbonate rocks tend to be sheetlike, rather than cylindrical or tubelike. Early diagenesis had a much stronger effect on carbonates than on sandstones. It is, therefore, clear that carbonate rocks have a more complex heterogeneous pore system than sandstones. The diagenesis of carbonate rocks such as crystalline dolomite usually starts with a high-porosity packing of CaCO_3 grains (Wardlaw, 1976; Blatt *et al.*, 1980). The initial grain sizes are in the range 1–10 μm . Nucleation at random sites of $\text{CaMg}(\text{CaCO}_3)_2$ rhombohedral crystals starts the dolomitization process. These centers are usually at the surface of the CaCO_3 grains and, after several million years, grow into grains whose sizes are of order of tens of microns. Gradually, CaCO_3 is replaced by $\text{CaMg}(\text{CaO}_3)_2$, where Mg ions come from the brine that saturates the pore space. This replacement introduces intercrystalline porosity, while at the same time the original porosity is decreased by compaction and cementation processes similar to those during diagenesis of sandstones. At the end of diagenesis, the solid matrix is made of random $\text{CaMg}(\text{CaO}_3)_2$ "rhombs," with a broad pore-size distribution.

To model this process, Crossley, Schwartz, and Banavar (1991) proposed the following model. One starts with a three-dimensional random number array $I_0(x, y, z)$, distributed uniformly over (0, 1). This initial "configuration" is then smoothed by convolving with a kernel $\text{Kr}(x, y, z|w)$ with a correlation length w :

$$I(x, y, z) = \int_{-\infty}^{\infty} \int_{-\infty}^{\infty} \int_{-\infty}^{\infty} \text{Kr}(x - x', y - y', z - z'|w) \times I_0(x', y', z') dx' dy' dz'. \quad (3.2)$$

To generate a pore structure similar to those in carbonate rocks, Crossley *et al.* (1991) showed that the Gaussian distribution

$$\text{Kr}(x, y, z|w) \sim \exp[-(x^2 + y^2 + z^2)/w^2] \quad (3.3)$$

leads to pore structures similar to those in crystalline dolomites. After $I(x, y, z)$ is obtained, it is binarized by setting a threshold to distinguish between pore and solid phase voxels. The size of the pores is controlled by w . A pore can be rendered with higher resolution if w increases. This process is much more time consuming than that used for generating a model of sandstones described

above. Figure 4 shows a comparison between a thin-section optical photo of crystalline dolomite and an image of it generated by the above algorithm. Note that the Gaussian convolution described above mimics the disordered nucleation and growth of $\text{CaMg}(\text{CaCO}_3)_2$ rhombs. The critical porosity for this system was found to be about 0.1.

We have now completed our review and discussion of diagenetic processes. At the end of these processes one obtains the present porous media, whose morphological properties are now discussed.

C. Pore-space geometry and pore-size distribution and their measurement

In this section, we review and discuss geometrical properties of reservoir rocks. The geometry of rock describes the shapes and sizes of its pores or fractures. Various experimental methods are used for measuring such properties. However, the interpretation of the data is not straightforward and requires proper modeling. Thus we also review and discuss the models that have been developed for interpreting such data.

In a porous medium consisting of particles, the spaces between the particles are called voids, whereas if the particles themselves are porous, then the void spaces in the particles are called pores. Careful examination of natural

porous media reveals that what are usually referred to as pores can in fact be divided into two groups. In the first group are *pore bodies*, where most of the porosity resides, while in the second group are *pore throats*, which are the channels that connect the pore bodies. One usually assigns *effective radii* to pore bodies and throats, which in reality are nothing but the radii of spheres that have the same volume. Thus pore bodies and pore throats are defined in terms of approximate maxima and minima of the largest-inscribed-sphere radius. In a network representation of the pore space, the pore bodies are represented by the sites or nodes of the network, and the pore throats are represented by its bonds. All of the volume of a pore body can be assigned to the corresponding node; alternatively it can be apportioned among the network bonds, which is what is done in most network modeling of transport processes in porous media. Dullien (1979) discussed in great detail various definitions of the effective sizes that one can assign to pore bodies and pore throats.

The pore-size distribution is defined as follows: It is the *probability density function* that gives the distribution of pore volume by an effective or characteristic pore size. Even this definition is somewhat vague because, if the pores could be separated, then each pore could be assigned an effective size, in which case the pore-size distribution would become analogous to the particle-size dis-

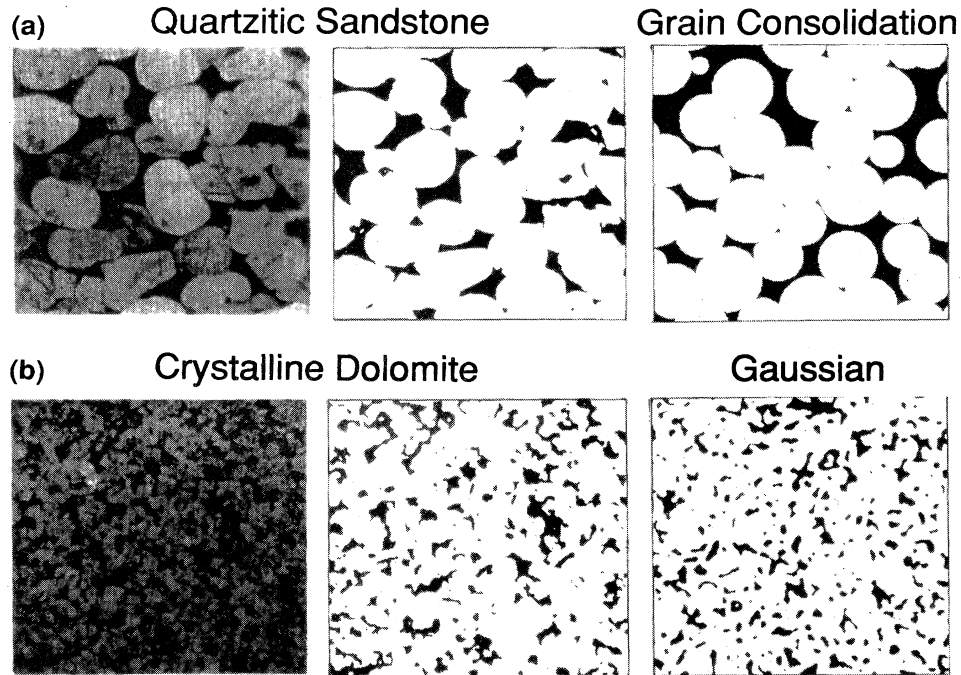


FIG. 4. Comparison of the models and the actual porous media. (a) Left-hand and middle panel show a thin-section optical photo and the corresponding binary (pore=black, grain=white) representation. Right-hand panel shows a section based on the consolidation of densely packed spherical grains. The model porosity has been adjusted to equal that of the sandstone. (b) Left-hand and middle panels are the same as those in (a), except that they are for a crystalline dolomite. Right-hand panel shows a single plane from a Gaussian smoothed 3d model. The model porosity has been adjusted to equal that of the dolomite section (from Crossley *et al.*, 1991).

tribution. But, because the pores are interconnected, the volume that one assigns to a pore can be dependent upon both the experimental method and the model of pore space that one employs to interpret the data. Four methods of measuring pore-size distribution are mercury porosimetry, adsorption-desorption experiments, small-angle scattering (SAS), and nuclear magnetic relaxation methods. The first two methods have been used extensively, while the latter two are newer and seem to be more accurate.

1. Mercury porosimetry and percolation

In this method, the porous medium is evacuated and immersed in mercury. The pressure is then increased and the volume of mercury injected into the porous medium is measured as a function of the applied pressure. The pressure is usually increased either incrementally or continuously. Larger and larger pressures are needed to penetrate progressively smaller pores. Very high pressures can even damage the internal structure of the medium, but we ignore them here. The pressure is then lowered back to atmospheric pressure, as a result of which the mercury is retracted from the pores. During this process there is a characteristic shift, or hysteresis, between the injection and retraction curves. There is also some mercury that stays in the medium. Typical injection and retraction curves are shown in Fig. 5. This technique was first developed by Ritter and Drake (1945) and has remained popular ever since. It is usually used for pores between 3 nm and 100 μm .

A precise apparatus for measuring mercury injection curves is described by Thompson *et al.* (Thompson, Katz, and Krohn, 1987; Thompson, Katz, and Rashke, 1987). It consists of four components; (i) a mercury reservoir positioned on an elevator raised by a stepper-motor-driven screw; (ii) a sample holder on a pan balance connected to the reservoir by stainless steel tubing; (iii)

stainless steel electrodes located on the top and bottom of the cylindrical sample; and (iv) electronics for measurement of the ac resistance, the temperature, and the atmospheric pressure. The experiment is automated by computer control. Before injection is started, the pore space is evacuated to a pressure of 10^{-3} Pa. During measurement, the elevator height is changed by typically 0.1–10 mm and the sample weight is monitored until equilibrium is reached. The typical experimental sensitivities are 10^{-5} cm³ for volume, 0.5 Pa for pressure, and $0.1 \mu\Omega$ for resistance, which result in resolutions of better than 1 part in 10^4 for all parameters of interest. A typical experiment consists of 30 000 observations taken at 3-sec. intervals.

While mercury porosimetry is a relatively straightforward experiment, the interpretation of the data is not simple. The data are usually interpreted using an equation due to Washburn (1921)

$$P_c = \frac{2\sigma_{mv}}{r} \cos(\theta + \varphi), \quad (3.4)$$

where P_c is the applied pressure, often called the capillary pressure, σ_{mv} the interfacial tension between mercury and the vacuum, θ the contact angle between mercury and the surface of the pores, and φ the wall inclination angle at which the pore radius is r , with $r_t \leq r \leq r_b$, where r_t and r_b are the pore throat and the pore body radii, respectively. Equation (3.4) results from a capillary force balance on a cylindrical tube. Up until 1977, the interpretation of porosimetry was based on modeling of the pore space as a bundle of nonintersecting capillary tubes.

Leverett (1941) defined a reduced capillary pressure function, which is usually used for correlating data and is defined by

$$J = \frac{P_c}{\sigma_{mv} \cos \theta} \left[\frac{k}{\phi} \right]^{1/2}. \quad (3.5)$$

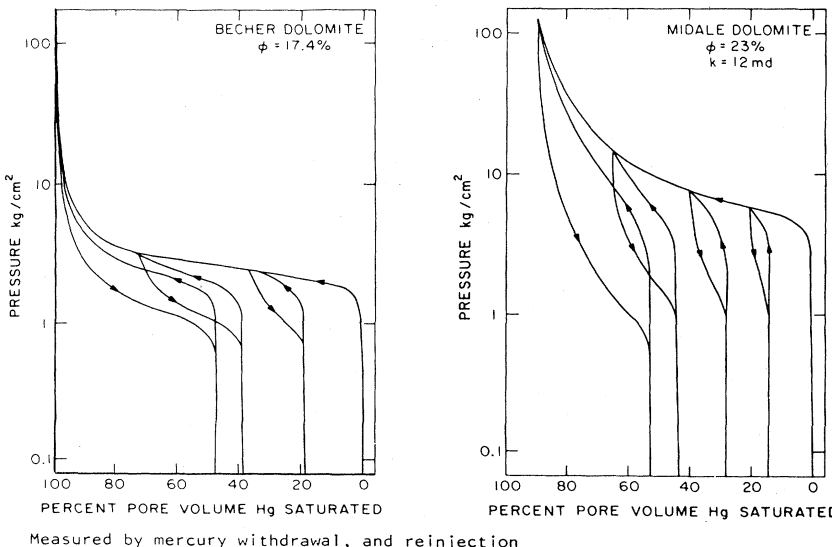


FIG. 5. Typical mercury porosimetry curves (from Larson and Morrow, 1981).

This function was named the Leverett J function by Rose and Bruce (1949). It has been found that the J function is successful in correlating capillary pressure data originating from a specific lithologic type within the same formation, but it is not of general applicability. The reason for this lack of generality is perhaps that $(k/\phi)^{1/2}$ is not an adequate scale factor for taking into account the individual differences between pore structures of various porous media. Capillary pressure curves have been reported by a large number of authors, a long list of which is given by Dullien (1979).

As Fig. 5 indicates, there is hysteresis between the injection and retraction curves. At the end of retraction, mercury can be reinjected into the medium and a second injection curve can be obtained. In some cases the hysteresis depends on the *history* of the system or the way the experiment has been carried out. Thus in some cases hysteresis can be eliminated by performing the experiment very slowly, while in other cases it *cannot* be eliminated. This type of hysteresis was called *permanent hysteresis* by Everett (1967).

Although we are discussing capillary pressure curves for mercury porosimetry, the phenomenon is more general and is used for characterizing any two-phase flow system. In general, if a nonwetting fluid (in this case mercury), one for which the contact angle is larger than 105° , is to displace a perfectly wetting fluid, one for which the contact angle is nearly zero, it must overcome a capillary pressure at the pore throat,

$$P_c = P_n - P_w = 2 \frac{\sigma_{nw}}{r_t}, \quad (3.6)$$

where P_n and P_w are the pressures in the nonwetting and wetting phases, respectively, and σ_{nw} is the interfacial tension between the phases. Similarly, for the wetting phase to displace the nonwetting phase in the pore segment, the capillary pressure must be

$$P_c = 2 \frac{\sigma_{nw}}{r_b}. \quad (3.7)$$

Thus in general capillary pressure curves depend on the contact angles, and their shapes can therefore be characteristic of the wettability of the pore space. This will be discussed in Sec. VIII, where we review two-phase flow and wettability in porous media.

Although the effect of pore-space interconnectivity on mercury porosimetry, or more generally, the capillary pressure curves for any two-phase flow problem in porous media, had been appreciated for a long time, it was only relatively recently that the connection between this phenomenon and percolation was recognized and appreciated. Chatzis and Dullien (1977), Larson (1977), de Gennes and Guyon (1978), Larson and Morrow (1981) and Wall and Brown (1981) were among the first to recognize the possibility of developing a percolation model for mercury porosimetry and capillary pressure phenomena in porous media. Androutsopoulos and Mann (1979) used two-dimensional networks of intercon-

nected pores to model these phenomena, although they did not mention percolation explicitly. All of these authors recognized that a bundle of nonintersecting capillary tubes is inadequate for interpreting mercury porosimetry data. Interconnectivity of the pores greatly affects the injection and retraction processes. Meyer (1953) had already recognized this effect 40 years ago when he stated that, "There may, for example, be large pores which one would expect to fill at a low pressure, which have no connection with the mercury except through smaller pores. The effect of these ink-bottle pores is to assign too small a portion of the pore space to the large pores and too large a part to the small pores, if the mercury injection data is taken at its face value."

As discussed by Larson and Morrow (1981) and Wall and Brown (1981), pores that are close to the external surface of a porous medium can be reached more easily than those in the middle of the medium, since if a pore in the interior of the medium is to be penetrated by the mercury, a connection with the external surface via the penetrated pore bodies and pore throats has to be established. If this effect is not taken into account, one obtains a wrong pore-size distribution. This was nicely demonstrated by Dullien and Dhawan (1975), who compared pore-size distributions obtained by photomicrographic techniques with those inferred from mercury porosimetry data interpreted with the above assumptions. Of course, one way of decreasing the effect of interior pores is to use thin or small samples. This also reduces the measurement time. However, before this is done, one has to establish that the pore-size distribution obtained with small or thin samples is in fact representative of the actual and much larger porous medium. Larson and Morrow (1981) developed a model that could take into account the effect of sample size.

Once one recognizes the importance of interconnectivity and pore accessibility, then the application of percolation concepts to mercury porosimetry seems natural. Many authors have used such concepts to calculate the capillary pressure curves of porous media (Larson and Morrow, 1981; Wall and Brown, 1981; Conner *et al.*, 1984, 1988; Conner and Lane, 1984; Neimark, 1984a; Chatzis and Dullien, 1985; Heiba, 1985; Lane *et al.*, 1986; Ramakrishnan and Wasan, 1986). Some recognized that, although mercury porosimetry is a percolation process, there are certain differences between this process and the random percolation described in Sec. II (see, for example, Lane *et al.*, 1986). Some used two-dimensional networks, which are actually not suitable for simulating mercury porosimetry, since this is a two-phase flow problem, and no two-dimensional bicontinuous structure exists, while others (for example, Larson and Morrow, 1981) represented the pore space with a Bethe lattice to take advantage of the analytical expressions for the percolation properties of Bethe lattices derived by Fisher and Essam (1961). Tsakiroglou and Payatakes (1990) developed a more general three-dimensional network simulator in which percolation was not explicitly used.

Before describing a percolation model of mercury porosimetry, let us first mention a few earlier works which, although they did not use the terminology of percolation theory explicitly, were more or less percolation models and hence took into account the effect of pore interconnectivity. The earliest work appears to be that of Ksenzhek (1963), who used a cubic lattice of pores to investigate the penetration of a porous medium by a nonwetting liquid. The pores were assumed to be capillary tubes of a given radius. The pore radii were distributed according to a probability density function. By making a few simplifying assumptions, Ksenzhek derived several formulae for various quantities of interest. In particular, a quantity essentially equivalent to the percolation probability was calculated and its dependence on the network size was investigated. Topp (1971) noticed that, in the early theories of hysteresis phenomena developed by Everett (1954) and others, only the shapes of the pores determined the shapes of the curves and the sequence by which pores are filled by the penetrating fluid, whereas in reality both pore geometry and the *state of neighboring pores* should be important. This is also what Meyer (1953) had stated 18 years earlier, but the significance of Topp's work is that he developed integral convolutions of the pore-size distribution and a quantity that is essentially equivalent to the accessibility function of percolation discussed above. Like Ksenzhek (1963), Topp made several simplifying assumptions, but it seems that he clearly recognized the significance of *both* the pore-size distribution and the pore-space accessibility. Pis'men (1972) developed elegant integral expressions describing capillary equilibrium, which included the effects of branching of bifurcating pores and pore distribution. Finally, Chatzis and Dullien (1977) used percolation concepts to calculate capillary pressure curves, and Androutsopoulos and Mann (1979) used network simulations, without mentioning percolation, to achieve the same end. Complete details of the work of Chatzis and Dullien (1977) is given in their 1985 paper.

Let us now use percolation concepts and describe a simple model for mercury porosimetry. We should first note that a percolation model for describing any two-phase flow phenomenon in porous media is appropriate if the capillary pressure across a meniscus separating the two fluids (e.g., Hg and the vacuum) is greater than any other pressure difference in the problem, e.g., that due to buoyancy. The second condition is that frictional losses due to viscosity must be small compared to the capillary work. If we define a capillary number Ca by

$$Ca = \frac{\eta v}{\sigma_{mv}}, \quad (3.8)$$

where v is the average fluid velocity and η the average viscosity, then one must have $Ca \ll 1$ in order to fulfill this criterion.

The porous medium is represented by a three-dimensional network in which each site represents a pore

body and each bond represents a pore throat. For now, we ignore the size of the pore bodies and consider a "pore-size distribution" $f(r)$ for the pore throats. For simplicity, we ignore the inclination angle φ in Eq. (3.4). The penetration of the pore space by mercury is the same as the invasion of the pore space by a nonwetting fluid, for which the contact angle θ is *larger* than 90° . During this process and the reverse process of withdrawal or retraction, the subdistributions of the pore space, accessible to and occupied by mercury, are different. Consequently the "pore-size distribution" of the subset of pore space occupied by mercury differs from the overall pore-size distribution. Thus during injection of mercury into the pore space, the fraction of pores that are *allowed* to receive it is (Heiba *et al.*, 1982, 1992)

$$X_i(r_{\min}) = \int_{r_{\min}}^{\infty} f(r) dr, \quad (3.9)$$

where r_{\min} is the minimum pore radius into which Hg can penetrate. The fraction of those pores that are accessible to and thus occupied by the mercury is $X^A(X_i)$, where X^A is the percolation accessibility function defined above. Therefore the distribution $f_i(r)$ of the pore radii that are occupied by the mercury is (Heiba *et al.*, 1982, 1992)

$$f_i(r) = \begin{cases} f(r)/X^A, & r \geq r_{\min}, \\ 0, & r < r_{\min}. \end{cases} \quad (3.10)$$

At each stage of the process, the corresponding capillary pressure can be calculated from Eq. (3.4). The idea behind Eqs. (3.9) and (3.10) is that, during injection of the mercury, the *largest* pores will be occupied [which can be understood by examining Eq. (3.4)].

Consider now the retraction process during which the mercury is expelled from the pore space. During this process, as the pressure is lowered the mercury is first expelled from the *smallest* pores [see Eq. (3.4)]. The *allowed* fraction of such pores is (Heiba *et al.*, 1982, 1992)

$$X_r = \int_0^{r_0} f(r) dr + \left[1 - \frac{X^A(X_{i,t})}{X_{i,t}} \right] \int_{r_0}^{\infty} f(r) dr, \quad (3.11)$$

where r_0 is the radius of the pore at a given capillary pressure P_c such that the mercury is expelled from all pores for which $r \leq r_0$, $X_{i,t} = X_i(r_{\min,t})$, and $r_{\min,t}$ is the pore radius at the end of the injection process. The first term on the right side of Eq. (3.11) is clearly the fraction of pores from which the mercury is expelled, if at the end of injection there were no pores that were accessible to it. However, at the end of injection a fraction $1 - X^A(X_{i,t})/X_{i,t}$ of the pores could not be reached by the mercury and, consequently, the second term on the right side of Eq. (3.11) is the fraction of pores that were not invaded by the mercury at the end of injection. Hence the size distribution of the pores from which Hg is expelled is given by (Heiba *et al.*, 1982, 1992)

$$f_r(r) = \begin{cases} \frac{f(r)}{X_r} \left[1 - \frac{X^A(X_{i,t})}{X_{i,t}} \right], & r > r_0, \\ \frac{f(r)}{X_r} \left\{ 1 - \frac{X^A(X_{i,t})}{X_{i,t}} \left[1 - \frac{X^A(X_r)}{X_r} \right] \right\}, & r_{\min,t} < r < r_0, \\ \frac{f(r)}{X_r}, & r < r_{\min,t}. \end{cases} \quad (3.12)$$

It is essential to specify clearly all of the assumptions that are made in order to arrive at these formulae. (i) The pore space is infinitely large. (ii) The entire process can be described by random bond percolation. (iii) Entrapment of Hg in isolated clusters is ignored. The first assumption is essential if we are to use the results for percolation on infinitely large lattices. However, finite-size scaling, discussed in Sec. II, allows one to investigate systematically the effect of sample size. For the Bethe lattice, the accessible fraction X^A can be calculated analytically for a given lattice size, which is why this lattice was used by some authors.

The second assumption is not, strictly speaking, correct. While it is true that the injection process is controlled by the radii of the pore throats and therefore can be considered as a bond percolation process [see Eq. (3.6)], the same is not true about the inverse process of retraction. This process is controlled by the sizes of the pore bodies [see Eq. (3.7)], and therefore retraction is a sort of site percolation process. Therefore a correct modeling of mercury porosimetry should involve a mixture of bond and site percolation, with size distributions for both pore bodies and pore throats, whereas the above formulae are derived assuming a size distribution for the pore throats and ignoring that of the pore bodies. The assumption that the entire process is a classical random percolation phenomenon is also, strictly speaking, not correct, since in practice the pore space is invaded by the

mercury from its external surface, and therefore the phenomenon is an *invasion percolation* process, which is discussed in Sec. VIII. However, as discussed there, the error caused by this assumption is often small and can be neglected. Finally, although the third assumption is not completely correct, the resulting error is not large. Although one has to consider a percolation problem in which trapping of clusters of one kind is allowed, if they are completely surrounded by clusters of another kind, a problem that was first studied by Sahimi (1985) and Sahimi and Tsotsis (1985) in the context of catalytic pore-plugging, computer simulations (Dias and Wilkinson, 1986) showed that, for three-dimensional networks, the effect of trapping is so small that it can be neglected.

Despite such assumptions, shortcomings, and criticism, the above percolation picture has been relatively successful in describing mercury porosimetry. Figure 6 shows the predicted capillary pressure-saturation curves (saturation of a phase is the volume fraction of the pore space occupied by that phase) if one uses a Bethe lattice of coordination number $Z=4$ and $f(r)=2r \exp(-r^2)$. If we compare this figure with Fig. 5, which is the measured capillary pressure curve for Becher dolomite with a porosity of 17.4%, we see that all of the main features of the experimental results are reproduced by the percolation model, even though the pore-space model (the Bethe lattice) or the pore-size distribution may not seem very realistic. The reason for this apparent success is that per-

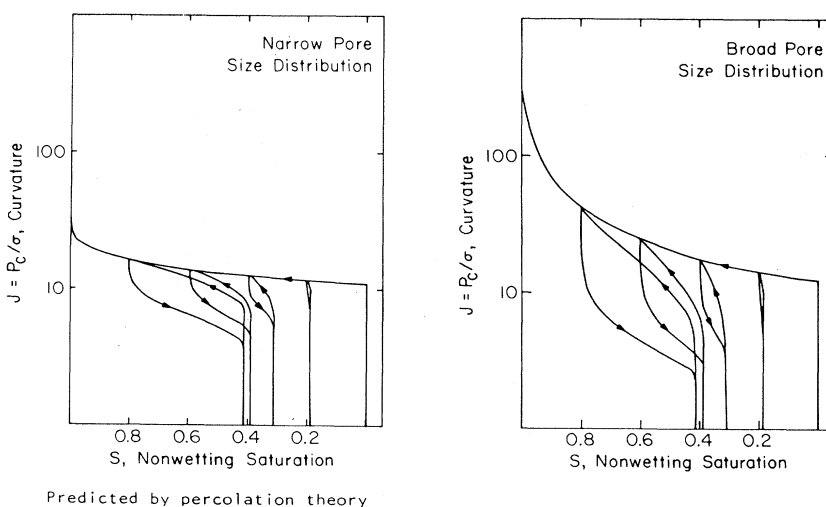


FIG. 6. Typical mercury porosimetry curves as predicted by random-percolation theory (from Larson and Morrow, 1981).

colation effects, which to a large extent control the process, have been taken into account, and the pore-size distribution that was used mimics that of the porous medium (which is presumably a unimodal pore-size distribution with a maximum). Note that in both Figs. 5 and 6 we show the injection and retraction curves, as well as the reinjection and retraction curves, which start at the end of the first retraction and second injection, respectively.

What is the effect of sample size on capillary pressure curves? The main effect is increased accessibility of pore space, which causes reduction in the sharpness of the injection-curve knee. Injection curves for unconsolidated packings indicate rather strong dependence on sample thickness for systems up to about 10 particle diameters or about 30 pore-throat diameters. For thicker media, the dependence is relatively weak, and if the thickness exceeds 20 particle diameters, no appreciable sample size can be detected. Figure 7 shows the effect of sample size based on the percolation model (Larson and Morrow, 1981).

How can we extract a pore-size distribution from the mercury porosimetry data? Consider, for example, the injection process during which the mercury saturation S_{Hg} is given by

$$S_{\text{Hg}} = \frac{X^A(X_i)}{X_i} \frac{\int_{r_{\min}}^{\infty} f_i(r) V_p(r) dr}{\int_0^{\infty} f(r) V_p(r) dr}, \quad (3.13)$$

where $V_p(r)$ is the volume of the pore throat of radius r . As the first step of extracting the pore-size distribution, a functional form for $V_p(r)$ and hence a pore shape have to be assumed. Next, one has to calculate the accessibility function of the pore space, which means that either the average coordination number \bar{Z} of the pore space has to be known from measurements (or it has to be assumed),

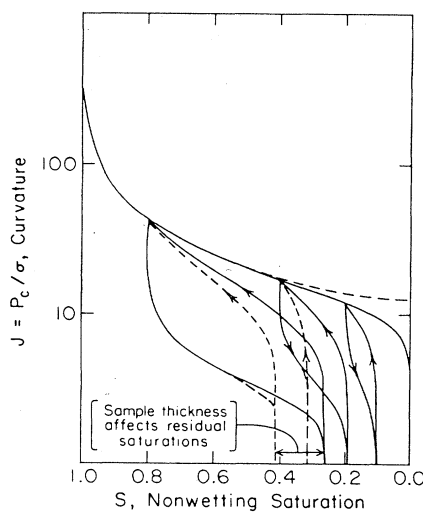


FIG. 7. Effect of sample size on capillary pressure curves, as predicted by random-percolation theory [from Larson and Morrow (1981)].

or it must be treated as an adjustable parameter of the system in order to fit the percolation model to the data. Later in this section we discuss how a combination of a percolation model and adsorption-desorption isotherms in porous media can be used for estimating \bar{Z} . Alternatively, \bar{Z} may be estimated from serial sectioning of the porous sample. Both S_{Hg} and P_c (from which r_{\min} is calculated) are measurable quantities. Thus, assuming an $f(r)$ as an initial guess, Eq. (3.13) is iterated many times until a satisfactory $f(r)$ can be found. Normally, a particular form of $f(r)$, with one or two adjustable parameters, is assumed and the parameters are varied until a satisfactory fit is found. However, note that since for $p < p_c$, $X^A = 0$, one cannot obtain the complete pore-size distribution: no information about the largest pores penetrated by the mercury can be obtained. On the other hand, if we use the measurements during the retraction process, we obtain information about the size distribution of the pore bodies, but this information is again not complete. One way of resolving this difficulty is to do the measurements in small samples, so that the effective percolation threshold is small and, as a result, more information can become available. Care should, however, be taken to ensure that the small sample is representative of the true porous medium.

At this point, we should mention the dissenting view of Thompson *et al.* (Thompson, Katz, and Krohn, 1987; Thompson, Katz, and Rashke, 1987) regarding a percolation picture for mercury porosimetry. These authors made high-precision measurements of mercury injection into three sandstones and a sintered glass-bead pack, and measured mercury pressure and volume as well as the sample resistivity. They found that the pore-by-pore filling process gives rise to a stepwise resistance curve with a power-law step distribution covering several orders of magnitude; this is shown in Fig. 8. They also found that the steps are irreversible, that the exponent in the power-law distribution depends on the ratio of gravitational to capillary forces, and that the results are consistent with a percolation picture of mercury geometry, but they stated that, "the mercury injection involves hysteretic volume changes of first-order character." They

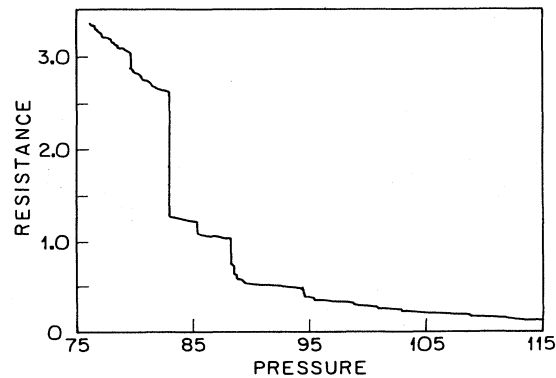


FIG. 8. Resistance of a porous medium during mercury porosimetry (from Thompson, Katz, and Rashke, 1987b).

further stated, "We conclude that percolation concepts can be applied to the *mercury geometry* but the injection process itself is not second order and should not be modeled by...percolation transitions." They drew these conclusions based on Fig. 8. However, this behavior is mainly a finite-size effect, which would disappear as larger and larger samples were used, so that in the limit of large systems the resistivity curve would become smooth, typical of second-order phase transitions. We shall return to this point in Sec. VIII, where we discuss two-phase flow in porous media.

2. Adsorption-desorption phenomena and percolation

Another method of determining the pore-size distribution of a porous medium is using adsorption-desorption isotherm data (Barrett *et al.*, 1951). Normally, liquid nitrogen is used in such an experiment, although in principle one can also use gases. Let us consider first nitrogen adsorption in a single pore. During the adsorption experiment the pressure is increased, as a result of which an adsorbed film of nitrogen forms on the pore walls, whose thickness increases with increasing pressure. At condensation pressure P_{co} the pore is filled with a (liquidlike) condensed phase which results in a step increase in the adsorption isotherm. The condensation pressure is given by the Kelvin equation, which, for a pore of radius r , is given by

$$\frac{P_{co}}{P_0} = \exp[-2\sigma_{lv} V_L / (RTr)], \quad (3.14)$$

in which P_0 is the saturation pressure, σ_{lv} the liquid-vapor surface tension, R the gas constant, T the temperature, and V_L the molar volume of the liquid. Thus, using Eq. (3.14), for any value of P_{co}/P_0 the adsorption process can be uniquely parametrized by an effective radius, which from here on we denote by r_a . Hence adsorption or desorption processes correspond to an increase or decrease, respectively, in r_a . During adsorption, all pores are equally accessible, vapor condenses in all pores of size $r > r_a$, and the liquid nitrogen fills the pores. For $r < r_a$, the first-order phase transition disappears and the pores fill rapidly and continuously with nitrogen. Thus, during this process, often called *primary adsorption*, connectivity of the pores plays no role. All that matters is the effective size of the pores.

Consider now the primary desorption process. At the beginning, as the pressure is reduced, the desorption isotherm does not retrace that of adsorption but, as in mercury porosimetry, forms a hysteresis loop before rejoining the adsorption isotherm. However, unlike the primary adsorption process, here the geometry and interconnectivity of a pore do matter. A pore with an effective radius r is allowed to desorb (to contain vapor) if $r > r_a$ and if it has access to either the bulk vapor, in primary desorption, or the isolated vapor pockets, in secondary desorption, which occurs after the secondary ad-

sorption. Typical adsorption-desorption isotherms are shown in Fig. 9. The International Union of Pure and Applied Chemistry (IUPAC) has classified the various hysteresis loops that can be observed experimentally as types H1, H2, H3, and H4, shown in Fig. 10. According to the report of Sing *et al.* (1985) to IUPAC, at least for types H1, H2, and H3 the connectivity plays an important role.

As in the injection stages of mercury porosimetry,

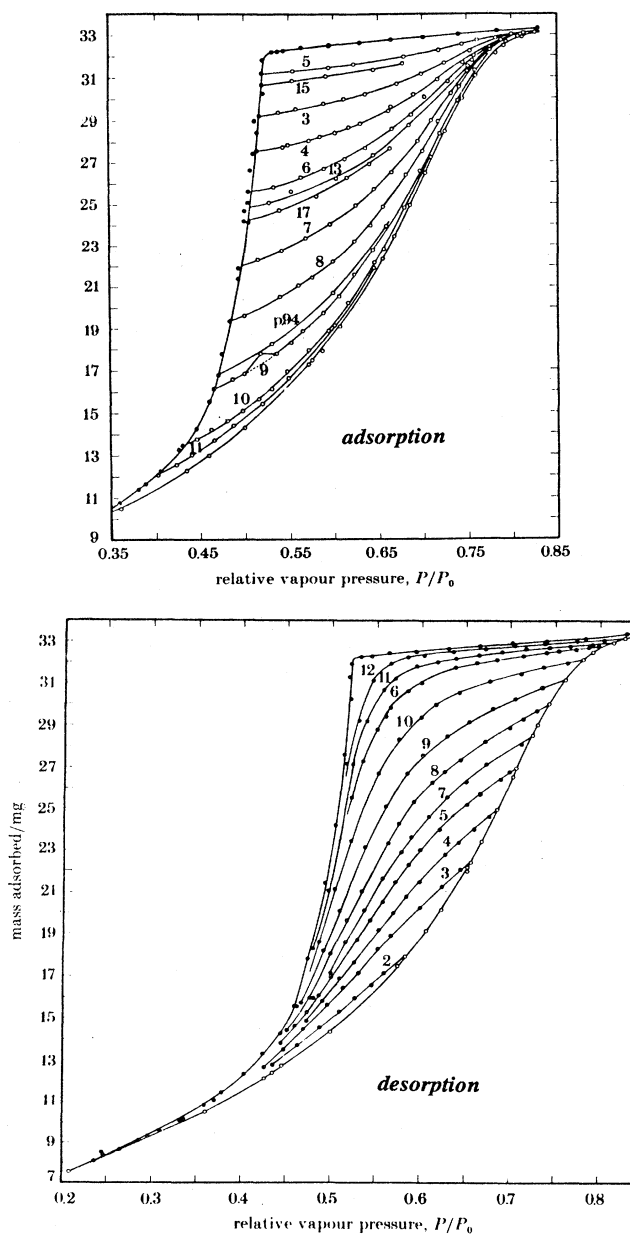


FIG. 9. Typical absorption-desorption isotherms in porous media. In both figures various curves correspond, from top to bottom, to primary adsorption (desorption), secondary adsorption (desorption), and so on. Numbers refer to the experiment number (from Mason, 1988).

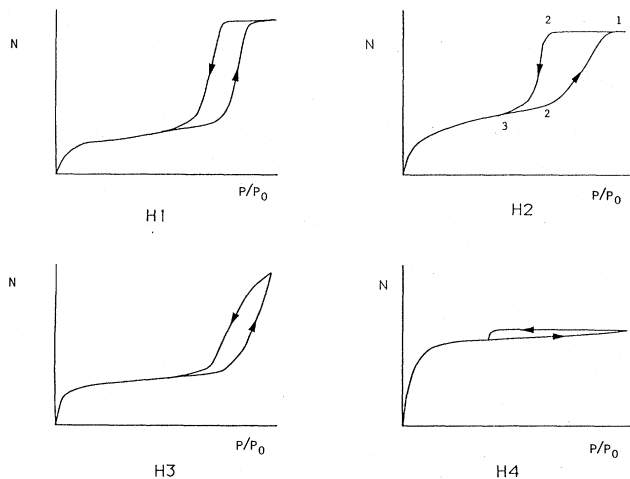


FIG. 10. Various types of hysteresis curves that can occur during adsorption (upper curve)- desorption (lower curve) phenomena.

desorption is controlled by pore throats. Thus, if $f_{pt}(r)$ is the size distribution of the pore throats, since desorption starts at the percolation threshold at which a sample-spanning cluster of pore throats containing vapor is formed, the onset of primary desorption is defined in terms of a radius r_i such that

$$\int_{r_i}^{\infty} f_{pt}(r)dr = p_{cb}, \quad (3.15)$$

because the left-hand side is simply the fraction of pore throats with effective radii larger than r_i . On the other hand, adsorption is controlled by the pore bodies. Now, if $V_{pb}(r)$ is the volume of a pore body and $f_{pb}(r)$ its size distribution, then it is clear that, since percolation and connectivity play no role during the primary adsorption, the saturation S_{LA} of the liquid during adsorption is given by

$$S_{LA} = 1 - \frac{\int_{r_a}^{\infty} f_{pb}(r)V_{pb}(r)dr}{\int_0^{\infty} f_{pb}(r)V_{pb}(r)dr}. \quad (3.16)$$

Note the similarity between Eqs. (3.13) and (3.16).

Primary desorption begins at the end of primary adsorption. During this process, a pore filled with liquid vaporizes if $r > r_a$ and if it is accessible to a sample-spanning vapor phase. Thus the fraction of pore bodies or throats that are actually occupied by the vapor is given by

$$X_j = X_j^A, \quad j = pb, pt, \quad (3.17)$$

where X_j^A is the percolation accessibility function defined earlier. The size distribution of the liquid-filled pores is simply given by

$$f_{Lj}(r) = \begin{cases} f_j(r)/(1-X_j), & r < r_a, \\ f_j(r)(1-X_j/p_j)/(1-X_j), & r > r_a, \quad j = pb, pt \end{cases} \quad (3.18)$$

where the quantity p_j , given by

$$p_j = \int_{r_a}^{\infty} f_j(r)dr, \quad j = pb, pt, \quad (3.19)$$

is simply the fraction of pore bodies or pore throats that have a radius greater than r_a . The corresponding liquid saturation during desorption is

$$S_{LD} = (1 - X_{pb}) \frac{\int_0^{\infty} f_{L,pb}(r)V_{pb}(r)dr}{\int_0^{\infty} f_{pb}(r)V_{pb}(r)dr}. \quad (3.20)$$

We emphasize again the similarities between these equations and those for mercury porosimetry. It is clear that Eqs. (3.18) and (3.20) provide a method of determining $f_{pb}(r)$. We have to assume a functional form for $V_{pb}(r)$, and have *a priori* knowledge of the average coordinate number \bar{Z} of the porous medium so that the accessibility function X_j^A can be determined. It is of course the desorption process which is sensitive to the morphology of the pore space, and if we ignore pore bodies and attribute everything to the pore throats, then the above equations can be used for obtaining a pore-size distribution for the pore space. Note that if we assign effective sizes to both pore bodies and pore throats, then since the effective radii of all pore throats connected to the same pore body must be smaller than that of the pore body itself, the size distributions of the pore bodies and pore throats must obey certain restrictions (Parlar and Yortsos, 1989). The same is true for mercury porosimetry. Moreover, the accessibility function X_j^A for the general case of a mixed problem of pore bodies and pore throats (mixed site and bond percolation) is different from that of random site or bond percolation discussed above.

The above picture of desorption was exploited by several authors to extract information on the pore-size distribution of porous media (Wall and Brown, 1981; Mason, 1982, 1983, 1988; Neimak, 1984b; Zhdanov *et al.*, 1987; Parlar and Yortsos, 1988, 1989). Mason, and Parlar and Yortsos used Bethe lattices to take advantage of the analytical expressions for the accessibility function. Zhdanov *et al.* (1987) assumed that the radius of any pore body is greater than all pore throats in order to simplify the problem. Wall and Brown (1981) used Monte Carlo calculations and a simple cubic network of pore bodies and pore throats. Finally, Parlar and Yortsos (1988, 1989) also investigated the effect of heterogeneous nucleation on adsorption-desorption processes in porous media.

3. Small-angle scattering method

Mercury porosimetry is applicable in the range 3 nm to 100 μm and is of limited accuracy in the small-pore-size range. Adsorption-desorption methods can provide pore-size distributions in the range 1–60 nm. However, as we discussed above, the isotherms show hysteresis, and it is not guaranteed that a pore-size distribution calculated from primary desorption will agree with that obtained

from the secondary adsorption. Moreover, in both mercury porosimetry and adsorption-desorption methods one needs to have some information on the connectivity or the average coordination number of the pore space. In this subsection we discuss a method that appears to be free of such limitations. The method is based on SAS methods, either small-angle x-ray scattering (SAXS), or small-angle neutron scattering (SANS).

The basic idea is as follows. One measures the scattering intensity $I(q)$, where q is the scattering vector given by

$$q = 4\pi\lambda^{-1}\sin(\theta_s/2), \quad (3.21)$$

where λ is the wavelength of the radiation scattered by the sample through an angle θ_s . One then assumes a pore shape, e.g., a sphere, a cylinder, or a sheetlike structure. Suppose that the effective size of a pore (e.g., its radius) is r with a number density n_p . Then, according to Vonk (1976), one has

$$I(q) = \bar{\rho}^2 \sum_{i=1}^n n_p V_p^2 |S_F(qr)|^2, \quad (3.22)$$

where V_p is the volume of a pore of effective radius r . Here $\bar{\rho}$ is the difference in scattering amplitude densities between the solid matrix and the pore space, and $S_F(qr)$ is a *form factor* which depends on the shape of the pores. For pores of any shape, one must have $S_F \sim 1$ as $q \rightarrow 0$, and $S_F \rightarrow 0$ as q becomes sufficiently large. Thus one measures $I(q)$, assumes a pore shape, fits the measurements to Eq. (3.22), and calculates n_p by a constrained least-squares fitting procedure.

Using this idea and SAXS and SANS, Hall *et al.* (1986) measured the pore-size distributions of eight different rocks. Three of them were fractured rocks, while two of them were sandstone. Figure 11 shows their typical results, obtained with SANS and compared with the results obtained with mercury porosimetry and adsorption-desorption isotherms. The rock studied was a shale outcrop from Eastern Kentucky with very low porosity (about 4%). In general, the pore-size distributions obtained by scattering methods tend to agree with

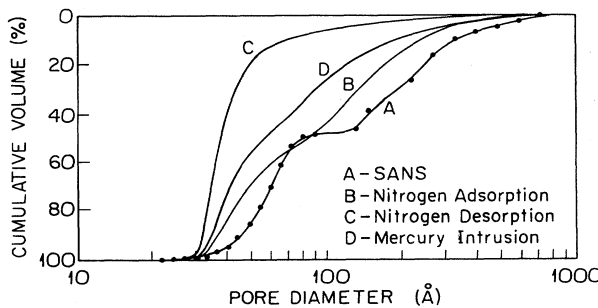


FIG. 11. Comparison of cumulative pore-size distribution of an oil shale, obtained by small-angle neutron scattering, with those obtained by adsorption-desorption and mercury porosimetry (from Hall *et al.*, 1986).

those yielded by secondary adsorption isotherms. Note that adsorption and desorption isotherms show significant hysteresis, resulting in significantly different cumulative pore volumes, and that mercury porosimetry results are in between adsorption and desorption results. This figure also reveals a basic dilemma for anyone who wishes to measure the pore-size distribution of a given rock: What method should one use and when? How can one know *a priori* which method of measuring the pore-size distribution yields the most accurate and realistic results? There are questions that, despite their significance, have not yet found definitive answers. While both mercury porosimetry and adsorption-desorption methods suffer from the fact that *a priori* knowledge of the connectivity of the pore space and pore shapes is essential to their success, and while it is also true that these methods cannot yield the complete pore-size distribution of the pore space, unless thin samples are used, the scattering method, as described by Eq. (3.22), also has its own shortcomings. First of all, it contains the unknown shape factor S_F , the specification of which requires specifying the pore shape, and secondly, even if the pore shape is specified, the resulting pore-size distribution appears to be sensitive to the pore shape. The conclusion is that all of the above methods of determining the pore-size distribution have their own strengths and weaknesses. It is the opinion of the author that, at present, scattering and adsorption methods seem to be more reliable, although the range of pore sizes that can be detected by the former method seems to be broader than that of the latter method.

4. Nuclear magnetic resonance

Application of nuclear magnetic resonance (NMR) for determining the pore-size distribution of a rock seems to have been pioneered by Cohen and Mendelson (1982). We should, however, mention the work of Brownstein and Tarr (1979), who used the method to study proton-spin relaxation in water in biological cells, and delineated the separate influences of diffusion and surface relaxativity (see below). In this method, the porous medium is first saturated with a suitable fluid such as water. An appropriate pulse is then applied and the magnetization relaxation with time is measured. Magnetization relaxation is caused by the interaction of the solid surface of the pores with the fluid near the surface, as well as with that in the bulk. Therefore the relaxation rate can provide direct information about the surface-to-volume ratio and, hence, an effective pore size. If the porous medium is characterized by a pore-size distribution, and if there are regions of the pore space that are separated by more than one diffusion length (by which the molecules move in the pore space), then such regions can be distinguished in the relaxation data. If the pore space of the medium is too complex, NMR relaxation may not be able to reveal all of its complexities. Moreover, if the ratio of signal to noise is finite, then extracting a pore-size distribution

may be too difficult. Despite these difficulties, NMR relaxation has been used for probing the pore space of various rocks and other porous media and obtaining their pore-size distributions. Let us now describe how the NMR data are analyzed for determining the pore-size distribution. To do this, we follow Cohen and Mendelson (1982) and Schmidt *et al.* (1986).

One assumes that each pore contains two kinds of fluid. One is a layer of thickness d , adsorbed on the pore surface with relaxation time t_a , and the other is the fluid in the bulk away from the surface with relaxation time t_b . In the presence of a fluid applied from the surface, t_a is shorter than t_b because the applied field hinders the diffusion of the fluid. The ratio t_a/t_b depends on the nature of the adsorbent and the surface geometry. NMR relaxation, together with diffusion, acts to smooth any spatial gradient in the magnetization which exists between the adsorbed and bulk fluids, as well as between fluids in adjacent pores. The governing equation for the magnetization M is

$$\frac{\partial M_z}{\partial t} = \gamma_p (\mathbf{M} \times \mathbf{H})_z - \frac{M_z - M_\infty}{T_1} + D_e \frac{\partial^2 M_z}{\partial z^2}, \quad (3.23)$$

where \mathbf{H} is the magnetic field, γ_p the proton gyromagnetic ratio, D_e the diffusivity, T_1 some relaxation time, and M_∞ the equilibrium magnetization.

In a pore of effective radius r , the magnetic field gradients between the surface and the bulk are smoothed by diffusion in a time

$$t_d = \left[\frac{r^2}{6D_e} \right] \left[\frac{S_p l}{V_p} \right], \quad (3.24)$$

where S_p and V_p are the surface and pore volumes, respectively. Each pore is characterized by a relaxation time t_p . If $t_d < t_p$, then one will observe an averaged signal for that pore. However, if $t_d > t_p$, one will observe a complex signal because of the spatial inhomogeneities. Thus there is a critical pore radius r_c such that if $r < r_c$ one will observe an averaged signal, whereas for $r > r_c$ one will obtain a complex or multicomponent signal. Therefore, for pores with $r < r_c$, the average relaxation time t_{av} is given by

$$\frac{1}{t_{av}} = \frac{1 - S_p l / V_p}{t_b} + \frac{S_p l / V_p}{t_a}, \quad (3.25)$$

and by measuring t_{av} for a given pore one can obtain S_p / V_p .

So far we have discussed only diffusion within a pore. One should also consider diffusion between the pores, which depends on the distance L_p between them. For rocks of spherical pores of radius r , this is given by $L_p \sim r\phi^{-1/3}$, where ϕ is the porosity. If diffusion between pores totally dominates the rock response, only one relaxation time is observed for the entire rock. Normally, however, diffusion between pores is not significant, and the porous medium behaves as a collection of isolated

pores. In this situation, each pore has its own relaxation time, which depends on its surface-to-volume ratio. Thus, if one groups pores of the same effective radius together, one can write

$$M_z(t) = M_\infty + (M_0 - M_\infty) \int_{\omega_{\min}}^{\omega_{\max}} P(\omega) e^{-\omega t} d\omega, \quad (3.26)$$

where $\omega = T_1^{-1}$ is the frequency of relaxation and $P(\omega)$ the fraction of fluid that resides in pores with relaxation frequency ω . Equation (3.26) can be rewritten as

$$M_z(t) = M_\infty - \int_{\omega_{\min}}^{\omega_{\max}} P_1(\omega) e^{-\omega t} d\omega, \quad (3.27)$$

where $P_1(\omega) = (M_\infty - M_0)P_\omega$. Because one measures $M_z(t)$ at various discrete times τ_j ($j=1, 2, \dots, N$), Eq. (3.27) is written in a discretized form

$$M_z(\tau_j) = M_\infty - \sum_{\omega_i=\omega_{\min}}^{\omega_{\max}} e^{-\omega_i \tau_j} P_1(\omega_i). \quad (3.28)$$

Note that $P(\omega)$ is normalized, and therefore $\sum_{\omega_i=\omega_{\min}}^{\omega_{\max}} P(\omega_i) = 1$. Equation (3.28) is then solved for $m+2$ unknowns and N data points, where the interval $(\omega_{\min}, \omega_{\max})$ has been divided into m subintervals of length $\Delta\omega = (\omega_{\max} - \omega_{\min})/m$. If $N \geq m+2$, then Eq. (3.28) is used to calculate S_p / V_p for pores with frequency ω_i . If a pore shape is assumed, the effective size of the pore can then be calculated.

This method is based on the assumption that diffusion between pores is not important and hence the pores can be treated independently. Cohen and Mendelson (1982) and Mendelson (1982) discussed the conditions under which this assumption is valid for an NMR experiment. One geometrical requirement for the validity of this assumption is that the pore throats be relatively narrow, because then diffusion between pores will be severely restricted. For some porous media this assumption is valid, while for some others it is not. In the latter case, one can still obtain a pore-size distribution, but the effective sizes that are obtained are only rough estimates of the true values. Since a pore shape has to be assumed anyway, which is an approximation in itself, the calculated pore-size distribution will be based on two approximations. Latour *et al.* (1992) presented some data on the temperature dependence of decay of the spectra as evidence for the concept of isolated or uncoupled pores. McCall *et al.* (1991) actually implemented the method of Cohen and Mendelson (1982) and showed how the spectrum of decay narrows as the diffusivity increases. Mendelson (1986) extended the above analysis to a fractal pore space.

The NMR method was used by Schmidt *et al.* (1986), Lipsicas *et al.* (1986), and Bilardo *et al.* (1991) for measuring the pore-size distributions of various sandstones. Schmidt *et al.* (1986) compared their results with those obtained by mercury porosimetry and showed that the NMR technique is more sensitive to the pore structure and can also reveal a bimodal pore-size distribution, if there is one. Note that, while mercury porosimetry

and adsorption-desorption methods depend critically on the interconnectivity of the pore space (and hence on percolation concepts), NMR and SAS methods are independent of this effect and thus are more flexible and presumably more accurate.

Given the pore-size distribution of a reservoir rock, what can we learn from it? Pittman (1984) gives a detailed discussion of various forms of pore-size distributions and the kind of information that one can deduce from them. For example, Fig. 12(a) shows the measured pore-size distribution for Nugget sandstone, which is the major reservoir in the overthrust play of Utah and Wyoming. A mercury injection test shows that the Nugget sandstone has large pore apertures, because the mercury entry point is approximately $50 \mu\text{m}$. Figure 12(b) shows the pore-size distribution for Baker dolomite, a carbonate rock with intercrystalline porosity. The mercury injection curve shows that the entry point of the mercury is about $11 \mu\text{m}$, with well-sorted apertures be-

tween 4 and $11 \mu\text{m}$. The fact that the curve has a hump means that the pore system is bimodal. The effective radii of the micropores are between 0.25 and $1 \mu\text{m}$. The total porosity of the sample was about 20%, of which 12.5% was contributed by the macropores. Figure 12(c) presents the pore-size distribution for Tuscarora sandstone of Appalachian provenance. The total porosity of the system is about 10%. The pores are poorly connected, resulting in a low permeability. The mercury injection curve is indicative of the presence of small pore apertures. It also indicates that only 58% of the pores are penetrated by mercury at the end of the injection process. The aperture of the largest pores is only about $1 \mu\text{m}$. Finally, Fig. 12(d) shows the pore-size distribution for the Drum limestone of Kansas, which is a carbonate reservoir. This reservoir contains oolites, peloids, and skeletal grains, which are seen in the figure. The pore system is very heterogeneous. The mercury injection curve for this limestone shows a wide range in sizes with

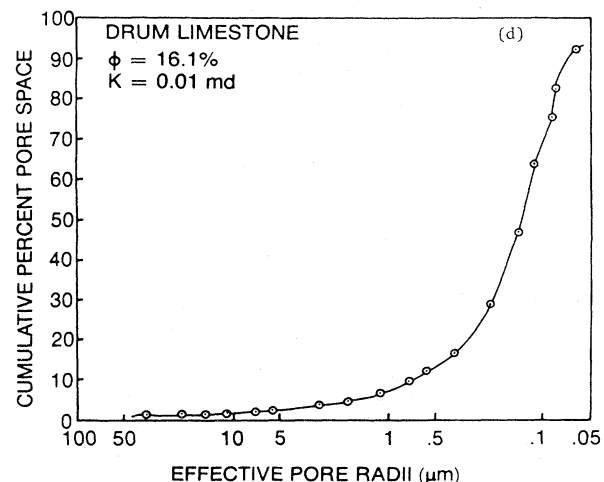
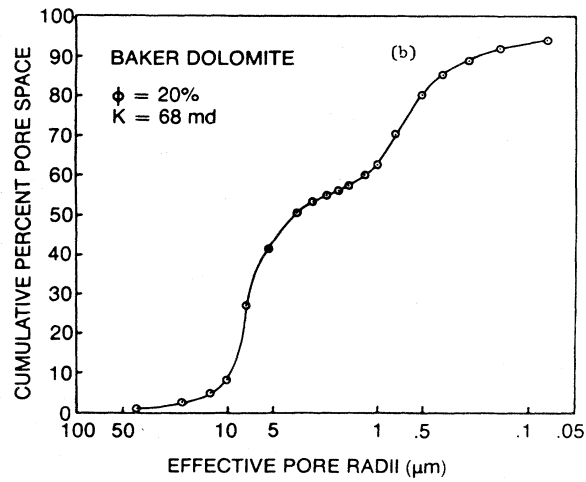
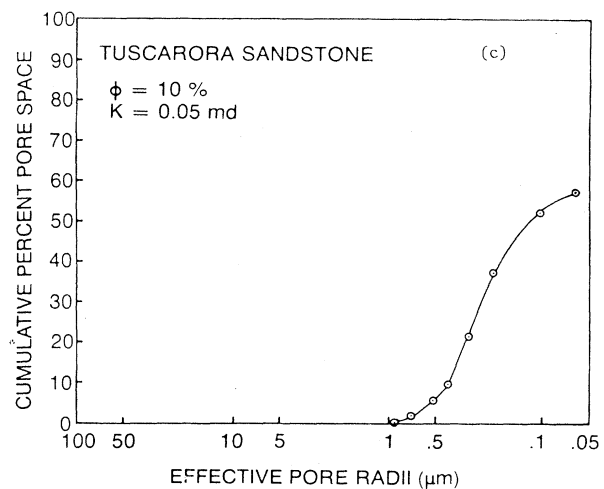
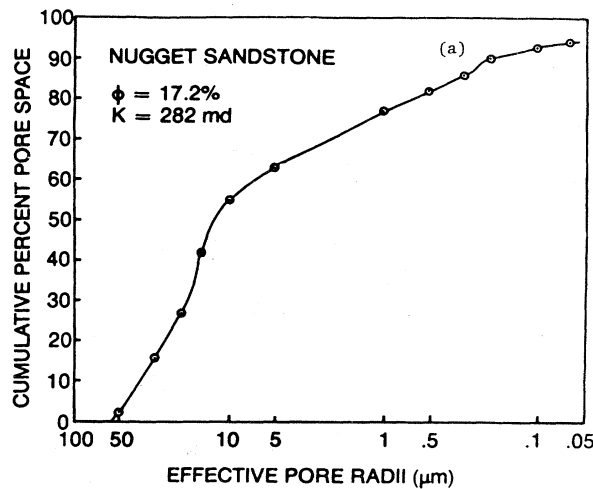


FIG. 12. Pore-size distribution of various rocks. Insets show the properties of the rocks (from Pittman, 1984).

only a few percent of large pores whose apertures exceed $5 \mu\text{m}$. More than 85% of the pore apertures are less than $0.5 \mu\text{m}$. As a result, the permeability of the system is very low. The above comparison between sandstones and carbonate rocks shows clearly the major differences between the two types of reservoirs. It also shows how the measured pore-size distribution, no matter how incomplete it may be, can shed light on the pore structure of reservoir rocks and thus explains why mercury porosimetry and the resulting pore-size distribution, even when vaguely defined, have always been of great interest.

D. Topological properties of porous media and their measurement

Any reservoir rock consists of a pore space and a solid matrix. Parts of the pore space may be isolated and inaccessible from the external surface of the reservoir, whereas the solid matrix is mostly connected and accessible. The solid matrix and the pore space are separated by a pore wall, which is essentially an oriented surface. One of the simplest concepts for characterizing the topology of a rock is the coordination number Z , which is loosely defined as the number of pore throats that meet at a given point or pore body of the medium. For regular pore structures, such as cubic arrays of spheres, it is easy to determine Z , whereas for an irregular pore space estimating \bar{Z} is usually difficult and often ambiguous. One has to define an average coordination number \bar{Z} , and this average value has to be taken over a large enough sample. For microscopically disordered, macroscopically homogeneous media, \bar{Z} is independent of sample size. Moreover, topological properties of porous media are invariant under any deformation of the pore space and solid matrix.

How can we determine the average coordination number and other topological properties of a porous medium? Stereology (Underwood, 1970) and serial sectioning (Pathak *et al.*, 1982; Lin and Hamasaki, 1983; Koplik *et al.*, 1984; Yanuka *et al.*, 1984; Lin *et al.*, 1986; Kwiecien *et al.*, 1989) have been used in the past to deduce the three-dimensional structure of porous media. In particular, Kwiecien *et al.* (1989) developed computer programs that take data, analyze them, and generate a computer image of a porous medium and its various properties, such as pore-body and pore-throat size distribution and the average coordination number. However, neither of these methods is used routinely at present. More popular are indirect methods by which only *statistical* information about the structure of the system is obtained. Some of the indirect methods are NMR, porosimetry, and sorption experiments, already discussed, which may yield parts or all of the pore-size distribution, and if the true average coordination number of the pore space is treated as an adjustable parameter, it can also simultaneously be estimated with the pore-size distribution. Mason (1988) and Seaton (1991) developed a direct method for estimating the average coordination number

of a pore space, which is based on the percolation model of adsorption-desorption phenomena discussed above. In what follows, we describe Seaton's method and comment briefly on Mason's technique, which is closely related to Seaton's.

Seaton's method is based on finite-size scaling analysis, discussed in Sec. II, according to which we can write

$$X^A(p) = L^{-\beta_p/\nu} f[(p - p_c)L^{1/\nu}] . \quad (3.29)$$

Equation (3.29) can be rewritten as

$$\bar{Z}X^A(p) = L^{-\beta_p/\nu} f[(\bar{Z}p - B_c)L^{1/\nu}] , \quad (3.30)$$

using $B_c = \bar{Z}p_{cb}$. Accurate values of $X^A(p)$ were obtained by Kirkpatrick (1979) for a simple cubic network for various sizes L , and can be shown to follow Eq. (3.30).

Consider now, as an example, the H2 loop in Fig. 10. The desorption curve has three segments indicated by 1, 2, and 3 in the figure. In the 1–2 interval, the isotherm is almost linear and occurs because of decompression of the liquid nitrogen in the pores. In the corresponding percolation network, p , the fraction of open pores (i.e., those in which the nitrogen pressure is below the condensation pressure), increases, but X^A is still zero because a sample-spanning cluster of open pores has not yet been formed. At point 2, the network reaches its p_c , a sample-spanning cluster of open pores is formed, and the metastable liquid nitrogen in the pores of the cluster vaporizes. If one decreases pressure further, the number of pores containing metastable nitrogen and the number of pores whose nitrogen has vaporized both increase. At point 3, almost all the pores in which the nitrogen pressure is below their condensation pressure can also vaporize, and therefore $X^A \approx p$. Note that in a finite percolation network one has a *smeared out* percolation, in which the discontinuity in the desorption isotherm causes a rapid increase in the slope and can even be detected in practice. A similar analysis can be used for interpreting the H1 loop.

Thus Seaton's method consists of two steps: (i) $X^A(p)$ is determined from the adsorption-desorption data; and (ii) \bar{Z} and L are determined by fitting Eq. (3.30) to $X^A(p)$. At this point, as in the other methods, it is necessary to assume a relation between pore radius and length. For example, one may assume that the length and the radius of a pore are uncorrelated. Note that $X^A(p)/p$, which is the ratio of the number of pores in the percolation cluster and the number of pores below their condensation pressures, can also be written as N_p/N_b , where N_b is the number of moles of nitrogen which would desorb if all the pores containing nitrogen below its condensation pressure had access to the vapor phase, and N_p is the number of moles of nitrogen which actually have desorbed at that pressure. Now, if N_A is the number of moles of nitrogen present in the pores at a given pressure during the adsorption experiment, N_D the number of moles of nitrogen present in the pores at that pressure during the desorption experiment, and N_F the number of

moles of nitrogen which would have been present in the pores at that pressure during the desorption experiment if no nitrogen had vaporized from the pores which contain nitrogen below its condensation pressure, then it is clear that $N_p = N_F - N_D$, and $N_b = N_F - N_A$, and therefore

$$\frac{X^A(p)}{p} = \frac{N_F - N_D}{N_F - N_A}, \quad (3.31)$$

so that $X^A(p)/p$ is written in terms of measurable quantities. The final step is to determine p , so that $X^A(p)$ can be calculated from Eq. (3.31). But this is straightforward, because if $f(r)$ is the normalized distribution of pore numbers of pore radius r , then for a given pressure P_g one has [cf. Eq. (3.19)]

$$p = \int_r^\infty f(x) dx, \quad (3.32)$$

where r is the pore radius in which nitrogen condenses at P_g . Therefore, given the pore-size distribution $f(r)$ determined from mercury porosimetry, desorption isotherms, or any other method, p and hence $X^A(p)$ can be determined.

Conceptually, Mason's method (1988) has many similarities with Seaton's. However, Mason (1988) adopts the Bethe lattice as the network model of the pore space, and although this enables him to write down several analytical formulae for his theoretical adsorption-desorption isotherms, it is not clear how his estimate of \bar{Z} can be related to the average connectivity of the pore space, since a Bethe lattice is not expected to be a reasonable model of any pore space. However, one can establish an approximate relation between his \bar{Z} and that of an equivalent three-dimensional network. Since for three-dimensional networks one has (Shante and Kirkpatrick, 1971; see Table II)

$$p_{cb} \simeq \frac{1.5}{\bar{Z}} \quad (3.33)$$

and because for a Bethe lattice of coordination number Z_b , $p_{cb} = (Z_b - 1)^{-1}$ [see Eq. (2.1)], then if we fix p_{cb} on a Bethe lattice and its "equivalent" three-dimensional network, we find a relation between \bar{Z} and Z_b

$$\bar{Z} = \frac{3}{2}(Z_b - 1), \quad (3.34)$$

so that the average coordination number of the actual porous medium will be larger than what Mason's method predicts. For large values of Z_b , the difference between \bar{Z} and Z_b can become significant.

A more precise method of characterizing the connectivity of a pore space relies on Betti numbers. These numbers were discussed by Barrett and Yust (1970) for metallurgical systems, and by Lin and Cohen (1982) and Pathak *et al.* (1982) for porous rocks. A fundamental theorem of topology (see, for example, Alexandroff, 1961) states that two structures are topologically equivalent if and only if their Betti numbers are *all* equal. For a given structure one can define many Betti numbers, and their

precise definition requires considerable knowledge of topology. According to Barrett and Yust (1970), "The n th Betti number β_n of a complex . . . (is) . . . the maximum number of homologically independent n -cycles," which is a quite complex statement! For our present purpose though, we need only the first three Betti numbers. The zeroth Betti number β_0 is the number of isolated clusters in a structure. In other words, β_0 is the number of separate components that make a structure. For example, the grain space of a single, finite sandstone has $\beta_0 = 1$. Thus $\beta_0 > 1$ may indicate that the structure contains isolated porosity. The first Betti number β_1 is the number of holes through a structure, or the maximum number of nonintersecting closed curves that can be drawn on the surface of the structure *without separating it*. It is given by $\beta_1 = E - N_V + 1$, where E is the number of edges and N_V the number of vertices (sites) of the network equivalent of the pore space. For example, if a torus is cut along a closed curve, the resulting solid can be deformed into a cylinder, whereas if the cylinder is cut along a closed curve, it separates into two disconnected clusters. Thus the first Betti number of the torus is one, whereas that of the cylinder is zero.

The notion of the *genus* of a surface is also used for characterizing the topology of a complex system. Also called *holeyness*, the genus G and the first Betti number are equal, for graphs lying on surfaces in complexes. One can use a genus per unit volume G_V by normalizing it over the volume over which it is measured. For large systems $\beta_1 \simeq E - N_V$, and therefore $G_V = \beta_1 / N_V = (E / N_V) - 1$. Note that for graphs or a network equivalent of a porous medium, G_V is half of the coordination number, but the notion of genus and genus per unit volume are more general than the coordination number. It is clear that the first Betti number or genus is also a measure of multiplicity of independent paths in a structure.

Finally, the second Betti number β_2 is a measure of the sidedness of a structure. For example, a Möbius strip shown in Fig. 13(a) is one-sided, because if a normal vec-

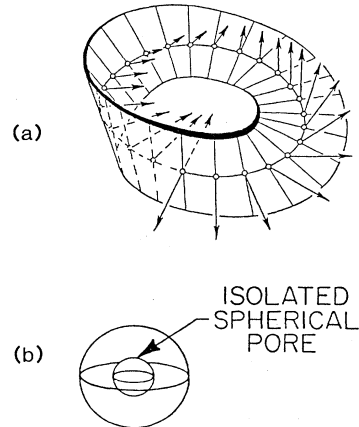


FIG. 13. Sidedness of (a) a Möbius strip, which is a one-sided surface, and (b) a hollow sphere, which has two boundary surfaces, one inside the other (from Pathak *et al.*, 1982).

tor pointing to one side is moved around the strip, it is pointing to the opposite side when it returns to the point it started from. By the same reasoning, a hollow sphere shown in Fig. 13(b) is two sided, and a solid structure containing n isolated pores is n sided.

These Betti numbers can be defined for both the solid matrix, β_0^s , β_1^s , and β_2^s , and for the pore space β_0^p , β_1^p , and β_2^p . However, a duality theorem relates these numbers as

$$\beta_0^p = 1 + \beta_2^s, \quad (3.35)$$

$$\beta_1^p = \beta_1^s = G, \quad (3.36)$$

$$\beta_2^s = 1 + \beta_2^p, \quad (3.37)$$

and therefore

$$\beta_0^p + \beta_2^p = \beta_0^s + \beta_2^s, \quad (3.38)$$

which means that the topologies of pore space and solid matrix are conjugate, and one need measure only one of them. For a microscopically disordered rock, the Betti numbers have to be averaged over a large enough sample. Although, as mentioned above, one may also use topological measures per unit volume, these measurements suffer from the disadvantage that they depend on the unit chosen for volume. For example, a heavily consolidated rock with many large, irregular grains that have many contacts with one another may have the same genus per unit volume as a lightly consolidated rock that consists of small, well-rounded grains with few grain-to-grain contacts.

Topology and geometric shapes are related through the Gauss-Bonnett theorem (see, for example, Kreyszig, 1959). The local Gaussian curvature of a surface κ_G is given by $\kappa_G = \kappa_1 \kappa_2$, where κ_1 and κ_2 are the local principal curvatures of the surface. κ_G is negative if the surface is saddle shaped and positive if the surface is convex or concave. One defines the integral Gaussian curvature $\langle \kappa_G \rangle$ by

$$\langle \kappa_G \rangle = \int_s \kappa ds. \quad (3.39)$$

According to the Gauss-Bonnett theorem, one has

$$\langle \kappa_G \rangle = 4\pi(1 - G_V). \quad (3.40)$$

Reservoir rocks are highly porous and have high genus. They also have large negative $\langle \kappa_G \rangle$. Therefore they must be riddled with the pore wall areas that are saddle shaped.

These topological quantities were measured by Pathak *et al.* (1982) for artificial porous media. They sintered three different copper powders: (i) spherically shaped grains in the range 30–90 microns; (ii) electrolytically prepared grains of less regular shape in the range 30–90 microns; and (iii) electrolytically prepared grains in the size range 250–300 microns. The sintering process parallels, in many important aspects, the diagenesis of sedimentary rocks described above. By using cold compression of spherical grains, Pathak *et al.* also prepared polyhedral-shaped particles. Using serial sec-

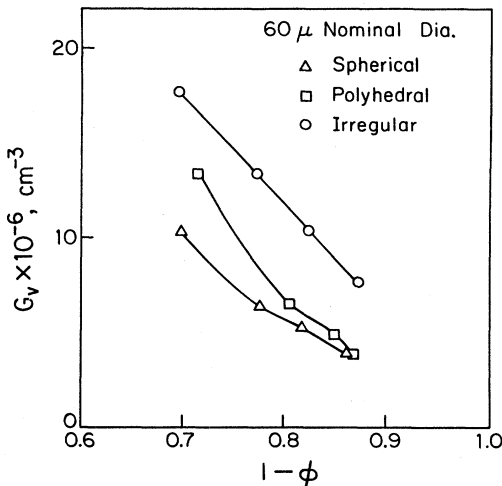


FIG. 14. Genus per unit volume G_V of sintered copper cores as a function of porosity ϕ (from Pathak *et al.*, 1982).

tioning, they measured the genus per unit volume G_V and surface area per unit volume \bar{S}_V of their porous media. Figure 14 shows how G_V varies with the porosity ϕ for the three different porous media, while Fig. 15 presents the variations of \bar{S}_V with ϕ . As Fig. 14 indicates, with increasing sintering the initial rough surface and edges of the original powders are smoothed out; the surface areas per unit volume no longer depend on the original shape and show a universal dependence on ϕ .

Lin and Cohen (1982) studied six different Berea sandstones and measured by serial sectioning and image analysis several of their topological properties. Only for the main pore subsystem β_1 was measured: its minimum was 91, whereas its maximum was found to be 280, while β_0 was measured to be about 23, indicating large amounts of isolated porosity. Also measured were the number of contacts per pore section, which had a broad distribution. The connectivity of the pore or grain system of Berea was found to be lower than the connectivities of

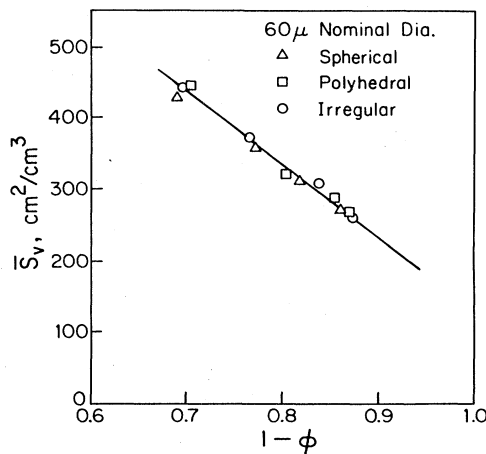


FIG. 15. Surface area per unit volume \bar{S}_V of sintered copper cores as a function of porosity ϕ (from Pathak *et al.*, 1982).

regular monosized sphere packs with similar porosities and the same mean grain diameter.

To summarize, all of these studies indicate that for sandstones an average coordination number between 4 and 8 is a reasonable estimate (Lin and Cohen, 1982; Ko-plik *et al.*, 1984; Yanuka *et al.*, 1984).

E. Fractal, self-similar, and self-affine properties of porous media and their measurements

In the last section we reviewed and discussed the pore-size distribution and connectivity of reservoir rocks. The average coordination number of a sedimentary rock can vary anywhere from 4 or 5 to 15. Many other types of porous media, e.g., catalyst particles, coals, and membranes can also have an average coordination number roughly in the same range. Therefore what distinguishes a reservoir rock from other types of porous media is its geometry, that is, the shapes and sizes of its pores and its possible fractal properties. In the last several years, fractal properties of reservoir rocks have attracted considerable attention, and many theoretical, computer simulation, and experimental studies have been undertaken in an attempt to understand them. These properties can be of geochemical (diagenetic) or geomechanical (fracture) origin. Thompson, Katz, and Krohn (1987), and Thompson (1991) have presented lucid discussions of some of the fractal and self-similar properties of porous media. In this section, we discuss and review some of these issues and attempt to address questions and issues that were not discussed by them. We follow Thompson *et al.*, first reviewing the methods of measuring fractal properties of reservoir rocks and then discussing the implications of the results. There are six basic methods of measuring fractal properties: the box method, adsorption studies, chord-length measurements, correlation function measurements, small-angle scattering, and spectral methods.

1. The box method

To characterize a fractal set, one must estimate the fractal dimension D . The simplest method of measuring D is the so-called *box counting* method, which can be described as follows. The fractal set is completely covered by non-overlapping spheres (in a general sense) of Euclidean size δ_E . The number $N(\delta_E)$ of such spheres required is then plotted and the following relation is used, in the limit $\delta_E \rightarrow 0$:

$$N(\delta_E) \sim \delta_E^{-D}. \quad (3.41)$$

Equation (3.41) may be valid over only a finite range of scales, above, below, or between certain cutoffs. In various applications, one may use percolation clusters, diffusion-limited aggregates, etc. to model the pore space or a certain transport process therein. Many such structures possess multifractal properties that necessitate consideration of an *infinite* family of dimensions, the sim-

plest of which is the above fractal dimension. We offer an illustration below; the interested reader is referred to Stanley and Meakin (1988) for a more detailed discussion. We consider the partition of a given object or set, which may not necessarily be fractal, into N cells of size δ_E , and take a measure, for example, in terms of the probability $p_i(\delta_E)$ that cell i of the partition has a certain property. We then define the general moments $M(\delta_E, q)$,

$$M(\delta_E, q) = \sum_{m=1}^N p_m^q(\delta_E), \quad (3.42)$$

and recognize the special cases $q=0$ and $q=1$ as corresponding to the box counting method and to the conservation of mass, respectively, in which case we have $M(\delta_E, 0) = N \sim \delta_E^{-D}$ and $M(\delta_E, 1) = 1 \sim \delta_E^0$. Therefore one expects the general scaling law

$$M(\delta_E, q) \sim \delta_E^{-\tau_f(q)}. \quad (3.43)$$

Knowledge of $\tau_f(q)$ for $-\infty < q < +\infty$, which can be interpreted as a generalized fractal dimension (hence the name multifractal), allows the calculation of all moments and therefore the complete statistical characterization of the system. For example, $D = \tau_f(0)$ is the largest fractal dimension, while the limits $q \ll -1$ and $q \gg 1$ yield information about the regions where a given property has low and high probabilities, respectively. Geometrically speaking, a multifractal object is a fractal system in which, if broken into many pieces, each piece is also a fractal whose fractal dimension is *not* the same as that of the whole set. Various phenomena in turbulence have been shown to possess multifractal properties (Meneveau and Sreenivasan, 1987). For our purpose, the most important systems with multifractal properties are diffusion-limited aggregates, which are used for the modeling of viscous fingers, as discussed in Sec. VII. By contrast, simple self-similar fractals have the property that

$$\tau_f(q) = (1-q)D. \quad (3.44)$$

2. Adsorption methods

In a pioneering work, Avnir *et al.* (1983) measured, using gas adsorption methods, pore surface properties at the nanometer scale. The monomolecular coverage n , e.g., moles/adsorbent weight, for various species of different molecular weight, and hence different surface coverage per site σ_s , was found to satisfy the relation

$$n \sim \delta_E^{-D_s} \sim \sigma_s^{-D_s/2}. \quad (3.45)$$

Under the assumption that surface coverage per site σ_s is uniquely determined by the adsorbed gas species, we recognize D_s in Eq. (3.45) as the fractal dimension obtained with the box method discussed above, and therefore it may be seen as the *surface fractal dimension* of the pores. Surface fractal dimensions almost up to 3 were obtained for various surfaces. Avnir *et al.* (1983, 1985)

extended the range well beyond molecular sizes by studying adsorption properties of fractal surfaces in larger particles and by considering their scaling with the Euclidean particle size R_p . In contrast to Eq. (3.45), a single species was used. The following equation is then expected to hold:

$$n \sim R_p^{D_s - 3}, \quad (3.46)$$

if we assume that the surface area is proportional to $R_p^{D_s}$ and that the particle weight varies with the volume as R_p^3 . In order to measure D_s , one sieves the system under study into several fractions. For each fraction the apparent monolayer value n is determined by any convenient method, e.g., adsorption from solution. If D_s is very close to 3, which is indicative of very wiggly porous material, then n becomes independent of R_p . One can also express Eq. (3.46) in terms of an *apparent* surface area S_{app} ,

$$S_{\text{app}} = N n \sigma_s \sim R_p^{D_s - 3}, \quad (3.47)$$

where N is Avogadro's number. The range of self-similar and fractal behavior can also be found with this method. If a fractal dimension D_s is found from the measurements of monolayer values of sieved fractions of particle diameter from R_{\min} to R_{\max} , with a probe molecule of cross-sectional area σ_0 , then $\sigma_{\max} = \sigma_0 (R_{\max}/R_{\min})^2$, and the range of self-similarity is

$$\sigma_0 \leq \sigma_s \leq \sigma_{\max}. \quad (3.48)$$

It is clear that, in order to get maximum information on the molecular size geometry of the surface, one should select σ_0 to be as small as possible. This is the case in practice, since nitrogen or argon is usually used. Note that σ_0 dictates the finest resolution in probing a surface and therefore, if a large σ_0 is used, self-similarity below σ_0 can only be speculated.

The measurements of Avnir *et al.* (1983, 1985) revealed interesting results. Six carbonate rocks were found to have fractal pore surface with $2.16 \leq D_s \leq 2.97$, seven types of soils with $2.19 \leq D_s \leq 2.99$, and a number of crushed rocks from nuclear test sites with fractal dimensions in the range $2.7 \leq D_s \leq 3$. These results will be compared with those obtained by other methods in the subsections that follow.

Adsorption methods are *not* free of limitations or potential problems. If, as discussed by de Gennes (1985), chemical disorder on the pore surface is important, or if molecular conformation and orientation are functions of the structure of the pore surface, then adsorption methods can yield estimates of D_s that are biased. Moreover, if D_s is close to 3, which is indicative of a very rough surface, some parts of the surface can shadow neighboring surfaces. This leads to incomplete adsorption and a lower bound to D_s , rather than its true value. However, while such problems may be important when one studies porous media such as catalysts and coal particles, they do not seem important as far as reservoir rocks

are concerned, since for them adsorption methods have yielded estimates of D_s that are in general agreement with those obtained by other methods. Aside from these issues, one major shortcoming of adsorption methods is that the size range of the adsorbates is very narrow, usually from 0.2 to 1 nm. One could use probes with high molecular weights, but this can involve problems of conformation and orientation of the molecules, as mentioned above.

3. Chord-length measurements

There are two basic methods of measuring chord lengths, namely, on fracture surfaces and on thin sections. A description of each method follows.

a. Chord-length measurements on fracture surfaces

This method was described in the papers of Krohn and Thompson (1986) and Krohn (1988a), which we summarize. At the outset, however, we should mention that these authors do not distinguish between a fractal pore surface (fractal dimensionality D_s) and a fractal pore space (fractal dimensionality D). In fact, Katz and Thompson (1985) argued that for sandstones $D_s = D$. This will be discussed below. One counts features in a large number of horizontal lines (e.g., a hundred or more) across a digitized image of a fracture surface (see Fig. 16). The counting is then repeated for a number of magnifications and locations. One starts by selecting a highly structured location on the surface and digitizing the images at several different magnifications. A con-

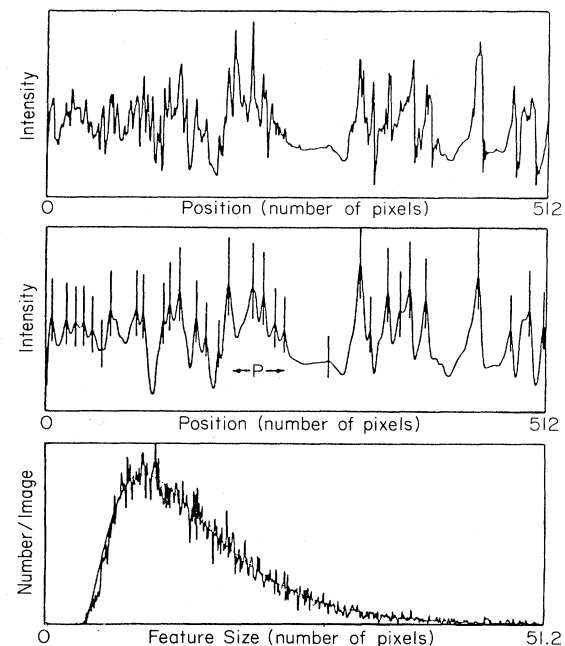


FIG. 16. The size distribution of surface features of a sandstone (from Krohn and Thompson, 1986).

stant resolution for feature detection is then set using a digital low-pass filter. Features sizes, defined as the distance between local maxima, are then measured. This generates a histogram, which is linearized and placed on a log-log plot. That this can be done is because the probability of detecting a feature at each magnification is known. The effects of various factors on the construction of the histograms and the resulting plots were thoroughly investigated by Krohn and Thompson (1986) and Krohn (1988a). For example, they showed that the same fractal measures are obtained whether one uses an analog or a digital filter, that the results are independent of the filter frequencies, and that signal-to-noise ratios do not have any important effect on the result. One sets an amplitude threshold to make sure that features that correspond to noise are not counted. This threshold sets a cutoff for the resolution, which sets a limit to the high frequencies that are counted. However, to ensure a constant frequency cutoff, the threshold must be set as a fraction of the signal size at each magnification. The signal size is measured by counting the features using a constant threshold and measuring the average amplitude difference between neighboring minima and maxima for features of a size less than the cutoff of the filter. The amplitude is usually measured for features with sizes between 15/512 and 20/512 of the field of view.

This technique does not depend on the delineation of the pore or grain space. This is an automatic method, which statistically measures structural features using scanning electron microscopy (SEM) images of the surface. A change in contrast in the secondary electron intensity of the SEM that results in a local maximum in intensity is defined as the edge of a feature. The technique makes it possible to decide whether features of a given size dominate the geometry of the pore space. Ehrlich *et al.* (1980) and Orford and Whalley (1983) also used SEM measurements of grain roughness to analyze the results in terms of fractal concepts. However, they measured the roughness of individual grains by analyzing the outline of the grains in a grain mount, whereas fracture surface technique measures the pore-gain interface without isolating individual grains. As a result, while the fracture surface technique yields a single fractal dimension for all lengths, the fractal analysis of Orford and Whalley (1983) does not.

The next step is to analyze the feature distribution. For fractal behavior, the number of features counted per centimeter $N_{cm}(l)$ for features of size l can be expressed as

$$N_{cm}(l) \sim l^{2-D}, \quad (3.49)$$

where $l_1 \leq l \leq l_2$, and l_1 and l_2 are the limits of fractal behavior. For $l > l_2$ the samples are homogeneous and $D=3$, which is the case if the geometrical features appear only as statistically random noise. Because all measurements are made from images, one expresses the feature sizes in terms of pixels, where a pixel is 1/512 of the image. One obtains a sequence of intensities $I(J)$ for

representing the digitized data, where J is a pixel ranging from 1 to 512. If one edge of a feature is at J_1 and the other is at J_2 then the feature size l is $J_2 - J_1$. For each image the width in centimeters of the field of view is $12/Ma$, where Ma is the magnification. Therefore

$$N_{cm}(l) = a(12l/512Ma)^{2-D}. \quad (3.50)$$

However, the true number of features counted, $N(l)$, is written as

$$N(l) = N_{cm}(l)P_f(l)R(l), \quad (3.51)$$

where P_f is the probability of finding a feature and $R(l)$ is the distance in centimeters over which the features are counted. The digital filter sets $P_f(l)$, which can be determined by performing the Fourier transform of the impulse response and expressing the amplitude as a function of R . The probability of resolving a feature is directly dependent on the amplitude of the filter and equals 1 at the largest feature sizes. This probability is set to zero for $l < l_0$, where the amplitude of the filter becomes less than the signal-to-noise threshold, in order to simulate the amplitude threshold for the removal of the noise. The final expression for $N(l)$ is

$$N(l) = a(12l/512Ma)^{2-D}P_f(l)(12/Ma)[1 - F(l-1)], \quad (3.52)$$

where $F(l-1)$ is the fraction of the field of view occupied by features of size less than l ,

$$F(l-1) = \frac{1}{512} \sum_{i=1}^{l-1} iN(i), \quad (3.53)$$

and $N(i)$ is the number of features of size i . Thus the model contains two adjustable parameters, namely, the prefactor a and the fractal dimension D .

The chord lengths that are measured by this technique could represent either pore-surface structure or fracture surface structure. The method does have the drawback that the fracturing process may introduce unwanted structures. Thus one has to make sure that a section of the surface is measured and not a projection. Figure 17

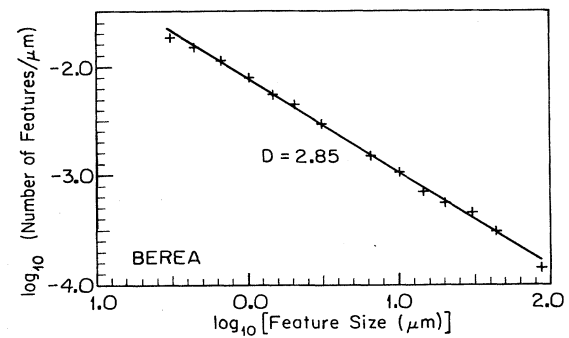


FIG. 17. Typical fractal plot for Berea sandstone, which yields a fractal dimension $D=2.85$ (from Krohn and Thompson, 1986).

shows typical results for Berea sandstone with a porosity of about 20%. For this sample, it was found that $D \approx 2.85$ and $l_2 > 32 \mu\text{m}$. In general, after examining a dozen sandstones, it was found that D is *not* universal and is in the range $2.55 < D < 2.85$.

b. Chord-length measurements on thin sections

This method is not as accurate as the fracture surface technique and was essentially developed to provide data that are complementary to those obtained with the fracture surface method. However, it also has its own advantages. For example, it can be used for measuring the amount of porosity and its distribution, which may or may not be fractal. But let us first discuss the method itself by following Krohn (1988a) and summarizing her work.

In this method one digitizes SEM images and delineates the pore space whenever the intensity is less than a set gray level. Usually, the edge of a feature appears bright on SEM images. If one examines the gray-level histograms of images, one finds that the distribution of grains always appears to be brighter than the pore distribution. The gray level for pore fill is between those of grains and pores, and therefore it is important to measure the pores within the pore fill. Once the SEM images are digitized, chord lengths are measured from the interception of horizontal lines with the surface of pores. Using a logarithmic bin size, one constructs a histogram of the number of chords whose lengths are in a given range. The results are not dependent on the specific choice of gray level, so long as the method is consistent from magnification to magnification.

Typical results are shown in Fig. 18 for Coconino sandstone, which has a porosity of about 10%. The measured fractal dimension is about 2.75, which is close to that of Berea sandstone. The results with thin sections generally agree with those obtained with the fracture surface technique. Note that from both methods one can obtain estimates for l_2 , the upper limit of fractal

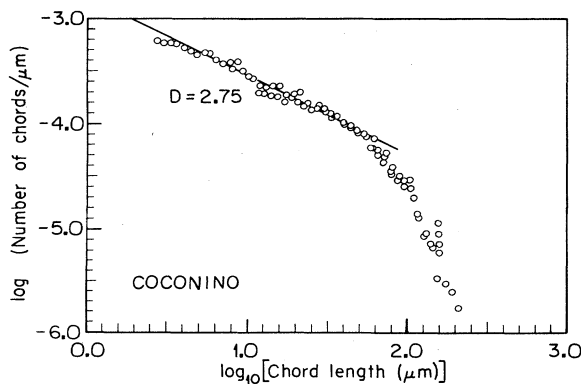


FIG. 18. Typical fractal plot for Coconino sandstone with a fractal dimension $D=2.75$. Also seen are the upper and lower limits of fractal behavior (from Krohn, 1988a).

behavior. The chord-length methods do not contain any information on the correlation functions, and therefore the results obtained with these two methods are *not* unambiguous evidence for fractal behavior (see below).

The linear intersection of the pore space that one uses in chord-length measurements on thin sections can be used for characterizing the pore space. For example, one can measure a pore volume distribution, which is defined as the porosity associated with each chord length and can be expressed as

$$\phi(L)=N_C(l)l(\Delta l)^2, \quad (3.54)$$

where $N_C(l)$ is the number of chords per unit volume of length l and $(\Delta l)^2$ is the cross-sectional area associated with each chord, which is equal to one pixel. To obtain $N_C(l)$ one counts the chord lengths on the thin section and assumes that the thin section is representative of the core. Figure 19 shows the pore volume distribution for Coconino sandstone. It is clear that most pores are in the fractal regime, but there are also some that are not. Thus there are generally two types of behavior for sandstones, Euclidean and fractal, and the pore volume of the rock may include any amount of the two types of porosity. There is almost no sedimentary rock that does not have any fractal component. The fractal component is the result of diagenetic processes discussed above which deposit clays on the surface of the grains, making it rough. In a second paper, Krohn (1988b) measured the fractal properties of carbonate rocks and shales and found qualitatively the same behavior as that of sandstones. The only case for which fractal behavior was not observed was Arkansas stone, which is a recrystallized quartz sandstone that is almost pure quartz with single-crystal grains that have well-defined crystal faces. Note that Krohn's results are consistent with those of Avnir *et al.* (1983, 1985) discussed above.

4. Correlation function method

Measuring fractal properties of a given system in terms of correlation functions is the most unambiguous method

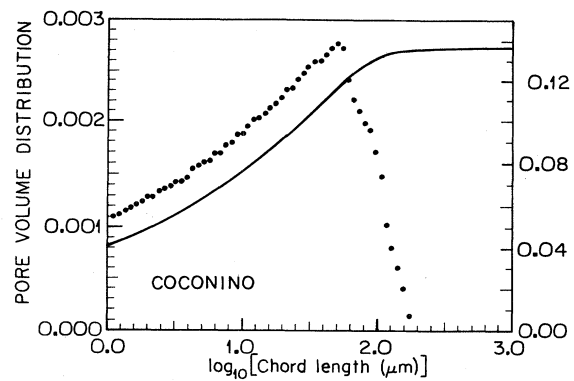


FIG. 19. Pore volume distribution for Coconino sandstone. L_2 is the upper limit for fractal behavior (from Krohn, 1988a).

of establishing whether a system is fractal or not. In this method one measures the density-density autocorrelation function at a distance $r = |\mathbf{r}|$,

$$C(r) \sim \sum_{\mathbf{r}'} s(\mathbf{r}')s(\mathbf{r} + \mathbf{r}'). \quad (3.55)$$

The origin of the coordination system is in the pore space $s(r)=1$, if a given point at a distance r from the origin belongs to the pore space, and $s(r)=0$ otherwise. Thus the geometrical meaning of $C(r)$ is the probability of finding a given point at a distance r in the pore space. For large values of r we must have $C(r) \sim r^{D-d}$, for a d -dimensional system, and therefore D can be estimated. Fara and Scheidegger (1961) were the first to use such statistical properties for characterizing porous media. Their method consisted of the following elements. One draws an arbitrary line through a porous medium. Points on this line are defined by giving them an arc length κ from an arbitrarily selected origin. Certain values of κ correspond to the pore space, while other values represent the solid matrix. A function $f(\kappa)$ is then defined such that $f=1$ if the line at κ passes through the pore space, and $f=-1$ if the line at κ passes through the matrix. It is easy to see that $\langle f \rangle = 2\phi - 1$, where ϕ is the porosity of the medium, $\langle f^n \rangle = \langle f \rangle$ if n is odd, and $\langle f^n \rangle = 1$ if n is even. One then carries out a spectral analysis of f by calculating its Fourier transform, from which some information about the structure of the pore space and the solid matrix can be obtained. These basic ideas were later used by others for obtaining the fractal properties of porous media (see below).

Berryman and Blair (1986) investigated the statistical properties of the function $s(\mathbf{r})$ used in Eq. (3.55). If we define the following quantities

$$S_1 = \langle s(\mathbf{r}) \rangle, \quad (3.56)$$

$$S_2(\mathbf{r}_1, \mathbf{r}_2) = \langle s(\mathbf{r} + \mathbf{r}_1)s(\mathbf{r} + \mathbf{r}_2) \rangle, \quad (3.57)$$

$$S_3(\mathbf{r}_1, \mathbf{r}_2, \mathbf{r}_3) = \langle s(\mathbf{r} + \mathbf{r}_1)s(\mathbf{r} + \mathbf{r}_2)s(\mathbf{r} + \mathbf{r}_3) \rangle, \quad (3.58)$$

then because two points lie along one line and three points lie in a plane, these quantities can be measured by using images of cross sections of the porous medium. If one assumes that the porous medium is macroscopically homogeneous and isotropic, then it is easy to show that $S_2(\mathbf{r}_1, \mathbf{r}_2) = S_2(\mathbf{r}_2 - \mathbf{r}_1) = S_2(|\mathbf{r}_2 - \mathbf{r}_1|)$. Moreover,

$$S_1 = S_2(0) = \phi, \quad (3.59)$$

$$\lim_{r \rightarrow \infty} S_2(r) = \phi^2, \quad (3.60)$$

$$S'_2(0) = -\bar{S}_V/4, \quad (3.61)$$

where \bar{S}_V is the specific internal surface area per unit volume, discussed above. Equation (3.61) was actually first derived by Debye *et al.* (1957).

The next step is to obtain images of the porous medium in order to analyze them. The standard method consists of the following steps (Berryman and Blair, 1986). Samples of the porous medium are saturated with a low-

viscosity epoxy, from which petrographic thin sections are prepared, which are then polished. A scanning electron microscope is used in backscatter mode for viewing the thin sections and producing high-contrast images of the pore space and the solid matrix. Various magnifications of the images are produced and are digitized with a raster scanning digitizer. The resulting digital images are then stored on arrays of given sizes. They are then processed using digital image-processing techniques. Then an image of zeros and ones that closely approximate the matrix and pore space of the working image is created, from which various correlation functions are calculated.

Katz and Thompson (1985) used an optical technique to measure the correlation functions. In their method, backscattered micrographs of polished thin sections are photographically enhanced to produce a binary image. Two identical negatives are made on 35-mm film format and are placed in an optical microscope to measure the transmitted light through both films. The transmitted intensity is measured. The correlation function $C(r)$ is calculated as the transmitted intensity as a function of the distance one film is translated relative to the other. Because of polishing, resolution is limited. The polishing is usually done by a $1/4\text{-}\mu\text{m}$ abrasive that leaves scratches of $1\text{ }\mu\text{m}$ dimension on the surface of the thin section.

Figure 20 shows the results for a Price River sandstone from Utah (Thompson, Katz, and Krohn, 1987). The plot has been made on a log-log scale in order to reveal the possible fractal behavior. On such a plot, the deviations from a straight line reveal the limits l_1 and l_2 of fractal behavior. The porosity of this sandstone is very low, and it has been highly altered by the diagenetic processes discussed above, so much so that the original sedimentary sandstone grains are difficult to recognize. If the alterations by the diagenetic process are not very severe, then the pore space may not be a fractal, and only the pore surface may have fractal properties. In such a case, the correlation function has a complex structure, even on a log-log plot. In some cases, the pore space is

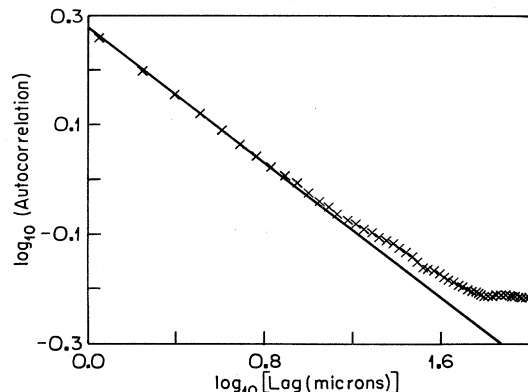


FIG. 20. Autocorrelation function for Price River sandstone from Utah. The upper limit of fractal behavior is clearly seen (from Thompson, Katz, and Krohn, 1987).

fractal, but a variety of complicating factors make the shape of the correlation function look complex. For example, Coconino sandstone has a fractal pore space, but it is *anisotropic*. As a result, even the log-log plot of its correlation function is not a straight line, and chord-length measurements are a better way of revealing its fractal properties (Figs. 18 and 19). Another complicating factor is the presence of pores that are not connected or are separated by more than a distance l_2 . Such pores are uncorrelated and their presence can complicate correlation function measurements. In such cases, even the appearance of straight lines on a log-log plot of correlation functions is *not* unambiguous evidence for fractal behavior of the pore space. Thus, although methods that use thin sections of the porous medium can yield important information about the structure of a porous medium, they also have their limitations.

5. Small-angle scattering methods

As already mentioned, SAS methods have been used to obtain pore-size distributions of shaly rocks (Hall *et al.*, 1986). In this section we outline how SAS methods can be used to study fractal properties of a pore space and its pore surface. These methods provide a measure of fractal behavior at length scales between 0.5 and 50 mm. Suppose that $C(\mathbf{r})$ is the density-density autocorrelation function at point \mathbf{r} . Then the observed scattering density $I(\mathbf{q})$ is given by the Fourier transform of $C(\mathbf{r})$

$$I(\mathbf{q}) = \int_0^\infty C(\mathbf{r}) \exp(i\mathbf{q} \cdot \mathbf{r}) d^3 r, \quad (3.62)$$

where \mathbf{q} is the scattering vector whose magnitude is given by Eq. (3.21). For a scattering experiment, $C(\mathbf{r})$ refers to spatial variations in scattering amplitude per unit volume, rather than physical density. For a porous medium with sufficiently low porosity, it is not unreasonable to assume that, to a good approximation, there will be no interference scattering, and therefore the total scattering intensity $I_t(q)$ is the sum of the scattering from all pores. For an isotropic medium, $C(\mathbf{r})=C(r)$, where $r=|\mathbf{r}|$, and Eq. (3.62) becomes

$$I(q) = \int_0^\infty 4\pi r^2 \frac{\sin(qr)}{qr} C(r) dr. \quad (3.63)$$

As we already discussed for fractal objects, the correlation function for a three-dimensional system is given by $C(r) \sim r^{D-3}$. Substitution of this into Eq. (3.63) yields

$$I(q) \sim q^{-D} \Gamma(D-1) \sin[(D-1)\pi/2], \quad (3.64)$$

where Γ is the gamma function. Both light scattering and small-angle x-ray scattering from silica aggregation clusters confirmed this q^{-D} dependence of I on q (Schaefer *et al.*, 1984). As already discussed, in real systems the range of scale invariance and fractal behavior may be limited by lower and upper cutoffs l_1 and l_2 . Finite size of a system can also limit this behavior. Under such conditions, the assumption of scattering by individ-

ual pores may break down and lead to interference scattering. To remedy this situation, Sinha *et al.* (1984) introduced into $C(r)$ an exponentially decaying term, incorporating a correlation length ξ_s , which reflects this upper limit, namely,

$$C(r) \sim r^{D-3} \exp(-r/\xi_s), \quad (3.65)$$

which, when used in Eq. (3.63), yields

$$\begin{aligned} I(q) &\sim q^{-1} \Gamma(D-1) \xi_s^{D-1} \sin[(D-1)\tan^{-1}(q\xi_s)] \\ &\times [1 + (q\xi_s)^2]^{(1-D)/2}. \end{aligned} \quad (3.66)$$

This form of $I(q)$ was also confirmed by Sinha *et al.* (1984) for silica particle aggregates. Note that in the limit $\xi_s \rightarrow \infty$ we recover Eq. (3.64), and for small values of $q\xi_s$ and $D=3$ (homogeneous systems) we recover

$$I(q) \sim 8\pi\xi_s^2 [1 + (q\xi_s)^2]^{-1}, \quad (3.67)$$

which is the classical result of Debye *et al.* (1957).

If r is small, i.e., scattering at larger values of q but still within the small-angle approximation, then the scattering reflects the nature of the boundaries between the pores and their surfaces. Thus the pore surface may have a fractal structure with a fractal dimension D_s discussed above. The surface fractal dimension D_s may or may not be the same as the fractal dimension D of the pore space itself. One may also have a nonfractal object with a fractal surface and vice versa. Bale and Schmidt (1984) showed that for rough surfaces described by a fractal dimension $D_s > 2$, the correlation function takes on the form

$$C(r) \sim 1 - ar^{3-D_s}, \quad (3.68)$$

in which $a = n_0[4\phi(1-\phi)V]^{-1}$, where V is the sample volume, ϕ the porosity, and n_0 a nonuniversal constant having the dimensions of area, which becomes the pore surface area if it is smooth and nonfractal. Substitution of Eq. (3.68) into (3.63) gives

$$I(q) \sim q^{D_s-6} \Gamma(5-D_s) \sin[(D_s-1)\pi/2], \quad (3.69)$$

which reduces to $I(q) \sim q^{-4}$, the classical result of Porod (1951) for smooth surfaces for which $D_s=2$, which is valid for the *shortest* length scales. Bale and Schmidt (1984) were able to confirm this for pores in lignites and subbituminous coals using small-angle x-ray scattering. If both the pore space and the pore surface are fractal and $D \neq D_s$, it is not difficult to show that

$$I(q) \sim q^{D_s-2D}. \quad (3.70)$$

Therefore one has a crossover from q^{-D} dependence to q^{D_s-2D} dependence to q^{D_s-6} dependence. The crossover between q^{-D} and q^{D_s-6} occurs at a value of ξ_s such that $q \sim \xi_s^{-1}$. If D_s is close to 3, as is found for some shaly rocks (Mildner *et al.*, 1986), the crossover between the q^{-D} and q^{D_s-6} regimes may be difficult to discern. Finally, if the correlation function is not isotropic, but only

possesses rotational symmetry around a unique axis, one obtains a scattering law that has an elliptically symmetric dependence on the azimuthal orientation of \mathbf{q} . This elliptical dependence can be removed by averaging the scattering law in terms of a reduced scattering vector. The SAS methods encounter difficulty at the smallest length scales. It is difficult to find, in SAS data, fractal rock data which span one order of magnitude in length scale.

Wong *et al.* (1986) used small-angle neutron scattering to study 26 different rocks, of which 12 were sandstones, 4 shales, 4 limestones, and 6 dolomites. Of the 16 sandstones and shales, 15 were found to have a *fractal pore surface* but *not* a fractal pore volume with $2.25 \leq D_s \leq 2.9$. The largest value was found for a Coconino sandstone, consistent with Krohn's (1988a) result mentioned above (Fig. 18). The lowest value was found for a Fountainebleau sandstone. It was found in SEM images of Coconino sandstone that the quartz grains are covered by clay, which results in a convoluted surface and a high value of D_s . On the other hand, the SEM images of Fountainebleau sandstone showed that the quartz grains were very clean. Thus, as discussed above, diagenetic processes give rise to highly convoluted surfaces and large values of D_s . The fact that the data of Wong *et al.* (1986) indicated that $D_s \neq D$ for many samples is significant in view of the proposal by Katz and Thompson (1985) that $D_s = D$.

Wong *et al.* (1986) also found that the carbonate rocks they studied had quite different behavior than that of their sandstones and shale rocks. The carbonate rocks they studied were quite "clean," showing almost no trace of clays and therefore no diagenetic alteration. The scattering intensity indicated a q^{-4} behavior for $q \leq 0.02 \text{ \AA}^{-1}$, indicating a smooth surface. What is the reason for this? As argued by Wong *et al.* (1986) and discussed earlier in this paper, the formation process of carbonate rocks is similar to conventional crystal growth, in which carbonates can dissolve in water and reprecipitate later. The roughness of the surface would be determined by the competition between thermal fluctuations and the surface tension if the water is clean. This phenomenon would then be similar to the roughening of domain walls in the Ising model, for which it is known that above a certain roughening transition the width of the interface w grows with the length scale r as $w \sim (\ln r)^2$, which means that the roughness grows so slowly that a fractal structure may be hard to detect. Even if the water does contain impurities, the phenomenon would be similar to the roughening transition in a random-field or random-bond Ising model, for which the same law of growth at very low roughening transition temperature is predicted. Note that the results of Wong *et al.* (1986) for carbonate rocks are not inconsistent with those of Krohn (1988b), who found a *fractal pore volume* for such rocks, although in her data analysis she does not seem to distinguish between a fractal pore surface and fractal pore volume. The reason for this apparent fractality of the pore volume of carbonates is that their grain-size distribution is broad and this, together with their packing, can lead to

a fractal pore volume.

We should mention two other studies of reservoir rocks and their fractal properties. Lucido *et al.* (1988) used small-angle neutron scattering on 18 different volcanic rocks and concluded that: (i) the pore volumes of these rocks were *not* fractal; and (ii) it was not possible to determine from their data whether the pore surfaces were fractal. Hansen and Skjeltorp (1988) used the box method discussed above and studied sandstones from $0.5\text{--}200 \mu\text{m}$. They found that $D \approx 2.7 \pm 0.05$ and $D_s \approx 2.56 \pm 0.07$, almost consistent, to within the estimated errors, with the equality of D and D_s .

We should also mention a proposal by Katz and Thompson (1985) regarding estimation of the porosity of fractal porous media. These authors proposed that

$$\phi = c(l_1/l_2)^{3-D}, \quad (3.71)$$

where c is a constant of order unity and l_1 and l_2 are the lower and upper limits of fractal behavior. The predictions of this equation seem to agree well with the measured values, indicating the usefulness of fractal properties for estimating morphological properties of porous rocks. This agreement also supports their proposal that $D_s = D$, at least for the rocks that they studied. Finally, Pfeifer *et al.* (1984) proposed that the total volume V of pores of diameter $\geq 2r$ obeys

$$-\frac{dV}{dr} \sim r^{2-D_s} \quad (3.72)$$

from which a pore-size distribution can be determined.

6. Spectral methods

This method was proposed by Voss (1985) and was further discussed by Hough (1989). The method is applicable to *self-affine* rather than self-similar fractals, such as pore surfaces and pore volumes that we have discussed so far. Strictly speaking, a self-affine fractal distribution describes phenomena that are continuous but not differentiable and correlated over several length scales. Mandelbrot (1983, 1985) introduced the concept of self-affine fractals for describing systems that have different scaling properties parallel and perpendicular to the surface. In these systems there is some kind of anisotropy, which may have been caused by an external force such as gravity. Such anisotropies are usually seen in large-scale geological systems. The basic idea, discussed below, is similar to the work of Fara and Scheidegger (1961), namely, using spectral analysis to obtain information about the structure of a porous medium.

A function $z(t)$ has a Fourier transform $\hat{z}(\omega, T)$ in the interval $0 < t < T$ given by

$$\hat{z}(\omega, T) = \frac{1}{T} \int_0^T z(t) \exp(2\pi i \omega t) dt \quad (3.73)$$

and a spectral density $S(\omega)$,

$$S(\omega) = T |\hat{z}(\omega, T)|^2 \quad \text{as } T \rightarrow \infty. \quad (3.74)$$

For a self-affine fractal one has

$$S(\omega) \sim \omega^{-\beta_f}. \quad (3.75)$$

One defines a two-point autocorrelation function given by

$$C(\tau) = \langle z(t)z(t+\tau) \rangle^2 - \langle z(t) \rangle^2, \quad (3.76)$$

which is somewhat similar to $S_2(\mathbf{r}_1, \mathbf{r}_2)$ defined by Eq. (3.57). In the case of a random, stationary process, $C(\tau)$ is related to $S(\omega)$ through the Wiener-Khintchine relation

$$C(\tau) = \int_0^\infty S(\omega) \cos(2\pi\omega\tau) d\omega. \quad (3.77)$$

Equation (3.77) can be extended to nonstationary processes. Then for a self-affine fractal Eqs. (3.75) and (3.77) yield

$$C(\tau) \sim \tau^{\beta_f - 1}. \quad (3.78)$$

On the other hand, $C(\tau)$ is related to the mean-square increments $M_i(\tau)$ of the function $z(t)$ by

$$M_i(\tau) = \langle |z(t+\tau) - z(t)|^2 \rangle = 2(\langle z^2 \rangle - \langle z \rangle^2) - 2C(\tau). \quad (3.79)$$

If the fractal dimension of a two-dimensional profile is D , then Eq. (3.79) is used to relate β_f to D . The result is

$$D = \frac{1}{2}(5 - \beta_f), \quad 1 < \beta_f < 3. \quad (3.80)$$

Hough (1989) discussed the mathematically rigorous conditions under which Eq. (3.80) can be derived. If $\beta_f > 3$, D sticks to $D=1$ and does not change. In this case the self-affine fractal distribution is differentiable. Instead of using Eq. (3.73), which is a one-dimensional Fourier transform, one can also perform a two-dimensional Fourier transform and obtain the fractal dimension of two-dimensional topography. In this case $2 < D < 3$, as opposed to the first case, for which $1 < D < 2$.

The moments of $S(\omega)$ are also useful to study. The n th moment is given by

$$m_n = \int_{\omega_0}^\infty \omega^n S(\omega) d\omega, \quad (3.81)$$

where ω_0 corresponds to the profile length λ_0 . In practice, the upper limit of the integral is a cutoff corresponding to a wavelength of twice the sample interval (the so-called Nyquist cutoff). For a self-affine fractal, Eqs. (3.73) and (3.76) yield $m_0 = a\lambda_0^{2(2-D)}$, where a is a constant. Since m_0 is nothing but the variance of heights of the profile, this equation relates the fractal dimension to this variance, which is an important property of the profile.

Huang and Turcotte (1989) applied this method to the topography of Arizona, using seven points per kilometer, and obtained maps of fractal dimension and roughness amplitude. For two-dimensional Fourier spectral analyses, the mean value of the fractal dimension was found to be $D \approx 2.09$, and the corresponding value for one-dimensional analyses was $D \approx 1.52$. Mandelbrot (1983)

concluded that fractal dimensions in the range $D \approx 2.1-2.2$ produce the most realistic topography. Huang and Turcotte (1989) also showed that maps of roughness amplitudes can provide valuable information on geological processes. Brown and Scholz (1985) used a similar technique to study the topography of various rock surfaces up to wavelengths of nearly 1 m. The estimated fractal dimensions varied between 1 and 1.7. The fact that the fractal dimension was found to vary with the wavelength means that these surfaces are not self-similar or self-affine on all length scales.

F. Fractal properties of heterogeneous and fractured rocks

So far our discussion has been limited to porous media. However, macroscopically heterogeneous porous media in which there are large-scale spatial variations of the properties of the system are also of considerable importance, since in practical applications, such as field-scale displacement of oil by a displacing fluid, or groundwater flow, one has to deal with such reservoirs. A complete review of the properties of such reservoirs is well beyond the scope of this paper. The interested reader is referred to Haldorsen *et al.* (1988) and Lake and Carroll (1986) for a fuller exposition of this important subject. Here, we restrict our attention to a few issues that are pertinent to this paper, namely, connectivity, morphological and fractal properties of macroscopically heterogeneous systems, and, in particular, fractured rocks.

Two types of large-scale heterogeneities that are of interest to us and that do interfere with the movements of fluids in reservoirs are fractures or faults. The effect of such heterogeneities is so severe that many of the smaller-scale heterogeneities, such as those at the pore or laboratory scales, may seem "simple" by comparison.

1. Diagenetic processes and formation of fractured rocks

The presence of fractures, natural or man-made, is crucial to the economics of oil recovery from underground reservoirs. Likewise, the presence of fractures is very important to the development of groundwater resources. In both cases, fractures provide high permeability patterns for fluid flow in reservoirs that are otherwise of very low permeabilities and porosities and would not be able to produce at high rates. Despite the obvious significance of fractures, the field of characterization of fractured rocks is not as well-developed as that of porous media which do not contain fractures, discussed above. The existence of a heterogeneous framework of reservoir rock interpenetrated by a network of fractures poses a difficult setting for the estimation of recoverable hydrocarbons and the implementation of improved recovery methods.

We have already discussed diagenetic processes for sandstones and carbonate rocks. Such porous media do not usually contain large fractures. On the other hand, many fractured reservoirs, such as Monterey sediments

in California, were originally complex mixtures of primary biogeneous components, finely disseminated organic matter, fine terrigenous sediment, and authigenic minerals formed during early diagenesis (Isaacs, 1984). As discussed above, the accepted mechanism for diagenesis relies on a dissolution-precipitation sequence. An additional and important feature of diagenetic origin is the extensive lamination of the rock. Rich spatial patterns of alternating layers of high and low porosity (delineating low and high extents of diagenesis, respectively) are prevalent in many fractured reservoirs over many length scales ranging from millimeter to tens of millimeters. This spatial microlamination and layering is an integral aspect of fractured rock formation and represents a significant obstacle to reservoir characterization. Various theories have been advanced to explain such phenomena, based on cyclic sedimentation triggered by climatic events. This traditional approach should be contrasted to more modern theories (see, for example, Fenney *et al.*, 1983) that attribute the laminations to self-organization, driven by the competition between nonlinear reaction and diffusion.

The sedimentologic, tectonic, and diagenetic histories of such fractured formations are complex, making results from conventional measurements difficult to interpret. It is well known that many formations have had complex biodegradation, maturation, and migration histories. Depositional environments could also influence the primary composition of the sediment as well as diagenesis and the development of reservoir-related properties such as brittleness and dolomitization. Sedimentary cycles on scales from millimeters to meters are common throughout many such fractured formations. These cycles appear to record important fluctuations in environmental conditions, such as oxygen levels, and may also serve as indicators of depositional environments. Diverse rock compositions have also been observed in fractured reservoirs. Silica phase transformation and dolomitization can lead to the production of fractured reservoirs characterized by a wide range of physical properties. Production data from many fractured reservoirs indicate that high productivities must be associated with fractures. Fracture porosities are generally considered low, usually in the range 1–6 %, whereas the pore porosity is usually larger than 10%.

2. Morphological and fractal properties of fracture networks

Although the intensity of fracturing in some reservoirs has been correlated with rock type and layer thickness, very few attempts have been made to map fracture networks systematically in order to quantify the hydraulic characteristics of the individual fractures and of the network as a whole, or to understand the orientation, temporal development, or spatial extent of individual fracture zones in terms of the local tectonic and geological history. One such attempt was carried out by the U.S. Geological Survey as part of the effort to characterize the

geologic and hydrologic framework at Yucca Mountain, Nevada (Barton and Larsen, 1985; Barton *et al.*, 1987; summarized in Barton and Hsieh, 1989). The site was evaluated by the U.S. Department of Energy as a potential underground repository for high-level radioactive waste. Barton and Larsen (1985) developed the *pavement method* of clearing a subplanar surface and mapping the fracture surface in order to measure its connectivity, trace length, density, and fractal scaling in addition to orientation, surface roughness, and aperture. Each of these parameters is important in predicting the hydraulic characteristics of the network and in working out the history of its development in relation to the regional tectonics. An example of one of their mapped pavements is given in Fig. 21. We now briefly discuss the important parameters for characterizing a fracture network.

Fracture surface roughness is important in reservoir modeling because it controls the aperture variation and therefore channeling of flow between the fracture walls. It also controls the closure of fractures under lithostatic stress (Brown and Scholz, 1985) and can be important in working out the temporal development of the fracture network by identifying fractures with a common mechanical and temporal origin.

Fracture aperture is the crucial parameter that determines permeability; the volumetric flow rate through a fracture is a function of its aperture cubed. For rough fractures, the dependence is more sensitive, depending on powers of the aperture as high as six. Although apertures measured at the surface may be wider than those at depth, due to unloading, an approximate measurement may still be useful. For example, no correlation was observed between fracture trace length and aperture in the Yucca Mountain pavements. Fractures in a network thus appear to have different characteristics from isolated fractures, where the aperture is expected to correlate with fracture length. However, it was found that the frequency of inverse aperture y , when plotted against the in-

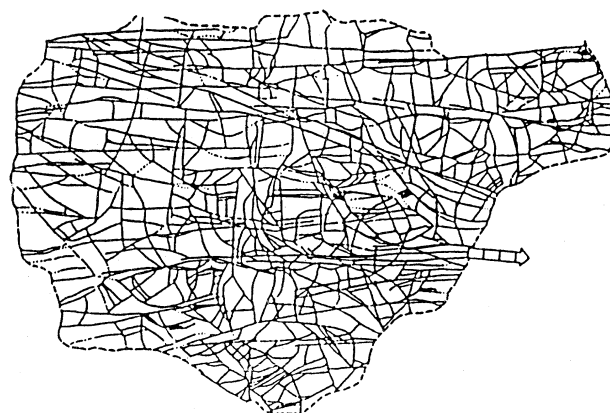


FIG. 21. Mapped pavements for Yucca Mountain in Nevada (from Barton and Larsen, 1985).

verse aperture, follows a power law, a strong indication of self-similar and fractal behavior.

Fracture trace lengths for Yucca Mountain were also best fit with a power law of the form $y = ax^b$, where y is the frequency, x is the trace length, and a and b are constants.

Fracture density and spatial geometry are both important parameters in reservoir modeling. The areal fracture density is defined as the sum of fracture trace lengths per unit area. For an isotropic fracture network this is also the fracture area per unit volume.

Fracture connectivity of a network, similar to the coordination number of a pore space, has an important effect on its permeability.

The most significant observation of the Yucca Mountain study was that the fractured pavements have a fractal geometry and are scale independent. The importance of this result is that it is possible to represent the distribution of fractures ranging from 20 cm to 20 m by a single parameter, the fractal dimension D defined as

$$D = \log(N_l) / \log(1/l), \quad (3.82)$$

where N_l is the number of fractures of length l . Using the box counting method described above, fractal dimensions at Yucca Mountain were found to be in the range 1.6–1.7. This is the same range of fractal dimensions found over a wider range of scales in fault gouges by Sammis *et al.* (1985), who proposed a simple physical reason why materials fractured in shear zones evolve toward self-similarity with a fractal dimension of 1.6. It is possible that the mechanisms which produce fractal gouges are also responsible for fractal fracture networks (which may be viewed as poorly developed gouges).

A similar study was undertaken for the Geysers geothermal field in northeast California (Sahimi, Robertson, and Sammis, 1993). This field, from which heat is extracted for generating electrical power, covers an area of more than 35 000 acres and is one of the most significant geothermal fields in the world. The heterogeneous nature of the reservoir, its fracture network, and *nonsedimentary* rock distinguish it from ordinary sandstone reservoirs (Stockton *et al.*, 1984). While the fractures are the main conduits for fluid transport through the reservoirs, tight rocks containing very small pores between the major fractures contain more than 90% of the fluid reserves. The fractures of the reservoir can be detected during drilling, since they produce a sudden and measurable increase in steam pressure. The average spacing between steam-producing fractures is of the order 100–500 ft.

Using the box counting method, Sahimi *et al.* (1993) determined the fractal dimension of the fracture patterns for this reservoir. A typical fracture map for this field is shown in Fig. 22. They found that, over a length scale varying by more than one order of magnitude, the fracture pattern is fractal and its fractal dimension is about 1.9, which is the same as that of two-dimensional percolation (see Sec. II). They also argued that, at large length scales, the fracture network must have the struc-

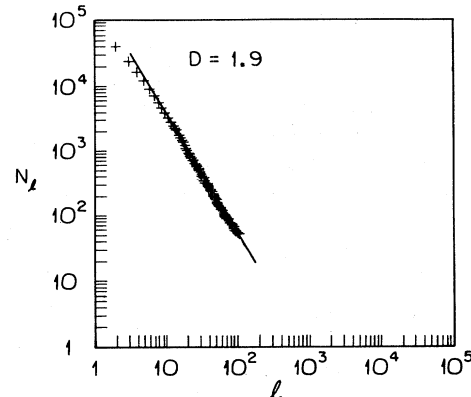


FIG. 22. Fractal plot of surface fracture pattern of the Geysers field in Northern California (from Sahimi *et al.*, 1993).

ture of percolation clusters and developed a model for nucleation and formation of fracture networks, based on the earlier model of Sahimi and Goddard (1986), which seems to support their view.

Nolen-Hoeksema and Gordon (1987) studied the fracture patterns in Stockbridge dolomite marble. This marble is from Unit "A" of the Stockbridge formation (near Canaan, Connecticut) and is a white, high-quality, dolomite marble whose average grain size is about 0.3 mm. Its properties are isotropic and there is no discernable texture or fabric. The fracture pattern in this rock is very branched and appears to be a highly interconnected network. Chelidze and Gueguen (1990) analyzed the fracture pattern in this rock and showed that the three-dimensional fracture network is a fractal object with a fractal dimensionality of about 2.5, essentially the same as that of percolation clusters. Finally, the distribution of contact areas in single, natural fractures in quartz monzonite (Stripa granite) was measured by Nolte *et al.* (1989) and was found to be fractal, with a fractal dimensionality of about 2.

In many cases, fracture networks are products of fragmentation processes. Rocks are fragmented by joints and weathering. Explosives are often used to fragment rocks. Another mechanism for fragmenting a porous medium is dissolving it in a reactant (e.g., an acid). Large fractures can form in all cases. If the fragmentation process can give rise to a fractal fragment-size distribution, then the fractures formed may also be expected to be fractal objects, and this has been found to be so in many cases. Turcotte (1986) analyzed the size distribution of rocks that had been impacted by an explosion, basalt rocks that had been impacted by polycarbonate projectiles, and many other systems, and showed that the number n_m of fragments of mass m scales with m as

$$n_m \sim m^{-\tau}, \quad (3.83)$$

where τ was found to be about 0.85. Since $D = 3\tau$ can be interpreted as a fractal dimension, his results imply a fractal dimension of about 2.5. Note that Eq. (3.83) is

similar to the cluster-size distribution for percolation clusters, Eq. (2.9). Likewise, Poulton *et al.* (1990) found that the length and spacing of discontinuities in rock masses follow power laws, typical of fractal systems. Finally, Sahimi (1991) showed how fractal fragment-size distribution and fracture pattern can arise as a result of the consumption of a porous medium by a reactant.

If it is established that a fracture network is in fact a fractal object, then it may be possible to model it starting from a single generator, which is the fundamental building block from which a fractal pattern or network is generated. However, as for all natural fractal patterns, the task of deducing a generator for a particular fractal fracture network is not easy. An interesting method for deducing a fractal generator is the iterated function system developed by Barnsley and Demko (1985), which systematically deduces a fractal generator for a given fractal object. With this scheme, one may be able to generate fractal fracture patterns that not only look "realistic," but have transport properties that mimic those of fracture networks in real rocks. On the other hand, if large-scale fracture networks do have the structure of percolation clusters, as claimed by Sahimi *et al.* (1993), then the task of modeling such fracture networks becomes much simpler.

3. Fractal patterns in fault systems

In simulation of fluid transport and displacement processes in a reservoir, it is usually assumed that the entire system is stratified and continuous. However, the presence of faults severely undermines this assumption because faults are usually created when two strata or layers move with respect to each other, as a result of some mechanical process, and the interface between the two displaced layers is what constitutes a fault. So, in some sense, faults are similar to fractures, and one often finds large faults in almost any kind of reservoir. However, unlike fractures, which can be created by a variety of processes, ranging from diagenetic to mechanical, faults are usually manifestations of tectonic processes that reservoirs experienced in the past. Moreover, unlike fractures, which usually provide large permeability zones and facilitate transport of fluids in reservoir rocks, faults may or may not do so. Sometimes they hinder fluid transport in the reservoir, because nonintersecting faults can compartmentalize reservoirs and isolate large portions of them. They can also interfere with fluid flow in the reservoir. On the other hand, faults are generally recognized as the largest-scale heterogeneities of any reservoir, and therefore they can be easily detected.

Tchalenko (1970), who studied the structure of shear deformation zones over many length scales, observed that over many orders of magnitude in length scale, ranging from millimeters to hundreds of meters, shear deformation zones are similar. This strongly suggests that fault patterns are fractal objects. Others (Andrews, 1980; Aki, 1981; G. C. P. King, 1984) have also suggested that fault

patterns are fractal systems. Okubo and Aki (1987) and Aviles *et al.* (1987) analyzed maps of the San Andreas fault system in California and obtained fractal dimensions for fault surfaces varying from 1.1 to 1.4. For a more complete description of faults and their fractal properties the interested reader is directed to the excellent paper of Haldorsen *et al.* (1988), in which a detailed description of fault systems and their realistic modeling can be found. For more application of fractals to geochemical systems, see Scholz and Mandelbrot (1989).

Our description of the morphological properties of sedimentary and other types of reservoir rocks is now complete. The accumulated experimental data and their interpretation in terms of fractals leave no doubt that reservoir rock heterogeneities, from the smallest scales (grains, pores, and pore surfaces), to the largest (fractures and faults), give rise to fractal properties. Why should rocks have fractal properties? This is not a completely resolved issue, but there is no doubt that diagenetic processes play an important role. As Cohen (1987) wondered, "why did sintering not occur and destroy the structure of sedimentary rock?" This is also not completely clear yet. However, we should be happy that sintering did not occur, since if it did, we could not have porous media that allow fluid flow at extremely low porosities, we would not have large oil and gas reservoirs, and we would not have oil and gas industries as we know them today. The same thing is true about groundwater flow. What is important to remember, however, is that any realistic modeling of fluid transport and displacement processes in reservoir rocks, which is the ultimate goal of any study of reservoirs, has to take into account such fractal properties.

IV. MODELS OF RESERVOIR ROCKS

Now that we have learned about various properties of reservoir rocks, the natural question that comes to mind is: How do we model reservoir rocks? Any realistic modeling of flow phenomena in reservoir rock has to include, as the first ingredient, a realistic model of the rock itself. In this section we review and discuss various models, first of porous media and then of fractured rocks.

A. Models of macroscopically homogeneous porous media

Pore-space models are needed for evaluating the transport coefficients and other important dynamical properties of porous media. The simplest of such properties are perhaps the permeability k and electrical conductivity σ . One major goal of modeling a pore space has always been to predict such properties, given some geometrical properties of the pore space. The simplest property of a pore space is its porosity ϕ , and therefore for many years an obvious goal was to find a relationship between ϕ and k , whose existence had seemed so obvious that in the early literature on flow of oil through reservoirs no distinction

had been made between k and ϕ ; it had been assumed that they are proportional. Later on, many empirical correlations between k and ϕ were suggested, perhaps the best-known of which was that of Rose (1945), who proposed that $k \sim \phi^m$, where m' is some undetermined constant. This relation is similar to the famous Archie's law (Archie, 1942) for the electrical conductivity of a fluid-saturated porous medium, which states that

$$\sigma = \sigma_f \phi^m, \quad (4.1)$$

where σ_f is the fluid conductivity. However, it must be clear to everyone that there *cannot* be any general relationship between k and ϕ , because one can have two porous media with the same ϕ but very different k . This obvious example prompted Cloud (1941) to conclude that "there is no sensible relation between porosity and permeability." Thus it became plain that one has to develop a model of the pore space before trying to estimate its permeability and transport coefficients. Over the years, many models of porous media have been developed, most of which have been motivated by a certain phenomenon, and often the model could be used to study that particular phenomenon and predict some of its properties. However, these models were not general enough to be useful for studying other problems, and they often contained parameters that either were defined very vaguely or had no physical meaning whatsoever, and their sole purpose was to make the models' predictions agree with experimental data. Scheidegger (1974) and Van Brakel (1975) give lucid discussions of such models. In what follows, we describe various models of porous media.

1. Spatially periodic models

These models have been described and discussed by Nitsche and Brenner (1989), whose paper we follow. In this class of model the pore space is represented by a periodic structure, the unit cell of which can be a capillary periodic network or some other geometrical element. A spatially periodic model is also characterized by an associated lattice that contains the translational symmetries of the porous medium for which the model is intended. Because of its periodic structure, the lattice is of infinite extent and is generated from any one lattice point by discrete displacements of the form $\mathbf{R} = i_1 \mathbf{e}_1 + i_2 \mathbf{e}_2 + i_3 \mathbf{e}_3$, where $\mathbf{I} = (i_1, i_2, i_3)$ is a triplet of integers and $\{\mathbf{e}_1, \mathbf{e}_2, \mathbf{e}_3\}$ is a triad of basic lattice vectors. This triad is *not* unique because, by applying any unimodular 3×3 matrix whose entries are integer to the basis $\{\mathbf{e}_1, \mathbf{e}_2, \mathbf{e}_3\}$ one can obtain another equally valid basis. The microscopic length scale of the lattice l_m is defined as $l_m = \max[d_{\min}(\mathbf{r})]$, where $d_{\min}(\mathbf{r})$ is the distance between \mathbf{r} and the nearest lattice points. For example, for a cubic lattice of size a , $l_m = (3^{1/2}/2)a$.

The simplest spatially periodic lattice model consists of a two-dimensional array of circular cylinders. Despite its simplicity, no rigorous results for transport in this model

were obtained until Sangani and Acrivos (1982a) used square and hexagonal arrays of circular cylinders, calculated the permeability of the system, and discussed their results in the context of heat transfer in porous media. Later, Larson and Higdon (1987) considered flow in the same lattices in both the axial and transverse directions. Hasimoto (1959) obtained the first results for three-dimensional lattices of spheres in the limit of small sphere concentrations. The first results for the full range of sphere concentrations were obtained by Zick and Homsky (1982) and by Sangani and Acrivos (1982b).

The analysis of transport processes in such models is a relatively simple problem, when numerical or analytical calculations are confined to a unit cell. In principle, the unit cell can have an arbitrary shape, but if one were to analyze a disordered unit cell with arbitrary inclusion shapes, the analysis would be no easier than that of other models of porous media discussed below. In a sense, spatially periodic models represent a sort of mean-field approximation to the true disordered system because they attempt to mimic the properties of the system in some average way. In some cases, the predicted effective properties come close to those of some real disordered media. For example, Ryan *et al.* (1980) showed that the predicted effective reaction rate of a spatially periodic model provides a useful estimate for some highly unconsolidated porous media such as packed beds. Many years ago, Philip (1957) stated that, "The particular case of flow through a cubical lattice of uniform spheres... appears capable of providing information on permeability-geometry relations." This statement turns out to be true in the case of the systems studied by Hasimoto (1959), Zick and Homsky (1982), and Sangani and Acrivos (1982b). Lahbabi and Chang (1985) studied high-Reynolds-number flow through cubic arrays of spheres and the transition to turbulence and found agreement between their predictions and *some* experimental data. Brenner (1980), Carbonell and Whitaker (1983), and Eidsath *et al.* (1983) studied hydrodynamic dispersion in spatially periodic models and found agreement between some of their results and the experimental data of Gunn and Pryce (1969). However, the main reason for the agreement between the predictions and the experimental data in all of these studies is that the geometry of the models used closely resembles that of the experimental systems. For example, Gunn and Pryce (1969) performed their dispersion experiments in a spatially periodic porous medium. Nitsche and Brenner (1989, p. 244) argue that, "while any given model of sample porous rock cannot generally be expected to possess perfect geometrical order, this does not mean that a spatially periodic model is not useful for understanding the fundamentals of a penetrant fluid flow through its interstices." Nonetheless, the usefulness of such models for predicting the effective transport properties of real disordered porous media of the type we are interested in in this paper is very limited. For example, the transverse dispersion coefficient calculated by Eidsath *et al.* (1983) differed by *two orders of magnitude* from the data for

disordered porous media. Nitsche and Brenner (1989) provide an extensive list of references for spatially periodic models; the interested reader should consult this paper.

What are the main shortcomings of spatially periodic models of porous media? Three major shortcomings limit the usefulness of such models. The first is the fact that regular arrays of spheres are limited to relatively low maximum concentrations of spheres, which are significantly *below* the solid volume fraction of many real porous media that are of interest here. The second is the fact that flow in regular lattices of isolated spheres occurs *around* the spheres instead of flow *through* narrow pores found in real porous media of interest here. Finally, such models may be useful for *unconsolidated* porous media in which [cf. Ryan *et al.* (1980)] the solid phase is *not* a sample-spanning percolation cluster, whereas in consolidated porous media, such as sandstones, both the solid and the fluid phases are macroscopically connected (at least in single-phase flow). This effect may not be very important for estimating the absolute permeability of the porous medium if the heterogeneities are not broadly distributed, but it is important for other transport phenomena in porous media, such as two-phase flow, hydrodynamic dispersion, etc., and even for single-phase flow when the medium is highly disordered. For example, in heat transfer in porous media, the effect of heat conduction through the solid matrix is important, and obviously heat conduction through a sample-spanning solid matrix is completely different from that in isolated solid inclusions.

To extend such spatially periodic models to consolidated porous media, Larson and Higdon (1989) made a simple extension. They started from a regular lattice of spheres, but then allowed the sphere radii to increase beyond the point of touching in order to form overlapping spheres. Obviously, the solid fraction of this model can be anywhere between the original fraction, before the growth of the spheres is started, and unity. Using different lattices results in different pore shapes and sizes. This model is similar to the grain consolidation model of Roberts and Schwartz (1985) except that, as discussed earlier, Roberts and Schwartz (1985) mostly used a random distribution of spheres, whereas Larson and Higdon (1989) used only a regular lattice as the starting point. The advantage of this model is that it is amenable to certain analytical and semianalytical calculations and, at the same time, it mimics certain features of consolidated porous media (see Sec. V).

2. Bethe lattice models

Next to spatially periodic models of porous media are branching network models. These are nothing but Bethe lattices of a given coordination number that have been used routinely in the statistical mechanics literature to investigate critical phenomena in the mean-field approximation. As far as their applicability to modeling porous

media is concerned, branching networks suffer from two major shortcomings. First, although they contain interconnected bonds that can mimic the interconnectivity of a pore space, they lack closed loops of bonds, which are a major element of the topology of any real pore space. Second, for a Bethe lattice of coordination number Z , the ratio of the number of sites on the external surface of the network to the total number of sites is $(Z - 2)/(Z - 1)$ (Ziman, 1979), which takes on finite values for any $Z \neq 2$, whereas for large three-dimensional networks this ratio is essentially zero. Thus surface effects may strongly affect any property of a Bethe lattice, which sometimes lead to anomalous phenomena such as those discussed by Hughes and Sahimi (1982), who investigated diffusion processes on Bethe lattices.

Liao and Scheidegger (1969) and Torelli and Scheidegger (1972) were the first to use Bethe lattices for modeling transport in porous media. These authors studied hydrodynamic dispersion in a porous medium, modeled by a Bethe lattice of a given coordination number. In particular, Torelli and Scheidegger showed that such a model is fairly successful in predicting the flow-velocity dependence of the longitudinal dispersion coefficient (see Sec. VI). Others have also used Bethe lattices to model transport and reactions in porous catalysts (Sahimi *et al.*, 1990).

3. Network models

The fact that fluid paths in a porous medium may branch and, later on, join one another is intuitively clear. This prompted many people to think of a network model of pore space in which the bonds represent in some sense the pore throats, or the narrow channels, that connect sites which represent the pore bodies. To each bond is assigned an effective radius, which can be selected from a probability density function or an experimentally measured pore-size distribution (see Sec. III). In principle, the bonds do not have to be cylindrical. They can represent sheetlike pores (as in carbonate rocks) or have converging-diverging segments. Normally, however, one chooses a configuration for which a given transport process can be solved analytically, and this is the reason why cylindrical pores have been used in most of such network modelings. Most authors also ignore sites and assign no volumes to them, although there have been several papers in which this assumption has been relaxed. These papers will be discussed later in the context of the problems that they investigated.

Although the idea of using a network to represent the pore space is intuitively clear and has been used for a long time, it was only about a decade ago that Mohanty (1981) and Lin and Cohen (1982) provided a firm mathematical foundation to such modeling approaches. In particular, Mohanty (1981) developed the procedure for deriving a network model for a given pore space. The network that results from such a mapping has a random topology whose local coordination number varies in

space. Over sixty years ago, Bjerrum and Manegold (1927) used a random network, made of randomly distributed points in space, connected to one another by cylindrical tubes, to study transport in porous media, although the computational limits of their time severely limited their ability to do any extensive computations. Extensive and analytical calculations with such models were first carried out by de Josselin de Jong (1958) and Saffman (1959) in the context of hydrodynamic dispersion in porous media, which will be discussed in Sec. VI. As already mentioned, computer simulations of Jerauld *et al.* (Jerauld, Hatfield, Scriven, and Davis, 1984; Jerauld, Scriven, and Davis, 1984) showed that, as long as the average coordination number of a random network is very close or equal to the coordination number of a regular network, the effective transport properties of the two networks are essentially identical.

The network models just described are "mathematical models," which are usually used in computer simulations of flow phenomena in porous media. Another class of models are "physical network models," which are man-made and transparent networks of pore bodies and pore throats. These models have been developed for flow visualization studies and have been particularly useful for gaining a deeper understanding of displacement of one fluid by another. The first of such models was constructed by Chatenever and Calhoun (1952), who made bead packs from single layers of glass and Lucite beads. They used this model to study immiscible displacement with oil and brine. Mattax and Kyte (1961) made the first etched glass network to study displacement processes in porous media, and Davis and Jones (1968) improved significantly their technique for construction of etched glass networks by introducing photoetching techniques. Finally, Bonnet and Lenormand (1977) developed a resin technique for controlling the geometry of the network. Currently, etched glass and molded resin are used for constructing most of the physical networks. Lenormand (1990) and Buckley (1991) reviewed various techniques of constructing such physical networks and discussed the results of flow studies using such micromodels.

4. Modeling of pore surface roughness

As discussed in the previous section, in most reservoir rocks the interface between the rock and the pores is very rough. It is covered by features or overhangs which often give rise to a fractal surface. For some phenomena occurring in porous media the presence of such overhangs and the fractal nature of the surface have very little effect and can be ignored, while some other phenomena are affected strongly by them. Examples include flow of fines (small, solid, and electrically-charged colloidal particles) and deep-bed filtration in porous media, and the distribution of a wetting phase on the pore surface of a porous medium. How can we modify a network model to include the effect of a rough or fractal pore surface? Three approaches have been proposed that are in

essence similar, but their details are different. These models are as follows.

The first model that we discuss is due to Sahimi and Imdakm (1991) and Imdakm and Sahimi (1991). In their model, the pore space is represented by a three-dimensional network of cylindrical tubes. However, the surface of the cylindrical pores is not smooth, but covered by protrusions, overhangs, or features of distributed heights h . Sahimi and Imdakm showed that such features have a crucial effect on the flow of fines in porous media and filtration processes. The inclusion of such overhangs in the model resulted in good agreement between the predicted and measured quantities of interest, whereas their exclusion resulted in unphysical results.

The second model is due to Katz and Trugman (1988) and is intended for proper modeling of distribution of a wetting fluid over the rough surface of a pore. In their model, the rough surface is represented by a triangular network in which an independent random number v_j , representing the height of the vertex, is assigned to the j th vertex of the network, which is distributed according to a continuous and bounded distribution. Bonds between the vertices lie along creases or folds in the surface. Now consider the angle α formed by the two triangular faces defining the crease, where α is defined in terms of the plane perpendicular to the crease. If $\alpha < 180^\circ$, then the crease is defined to be a (+) crease; otherwise it is a (-) one. The (+) and (-) creases reverse roles when one considers the back side of the surface, and therefore there are equal numbers of (+) and (-) creases. The relative heights of four vertices that define the parallelogram enclosing a bond dictate whether the bond is a (+) or a (-) crease.

Consider now the distribution of a strongly wetting fluid (contact angle $\simeq 0$) on a rough surface. The roughness of the surface provides channels capable of retaining the fluid up to very high capillary pressures. Thus, in the context of Katz and Trugman's model, the wetting fluid occupies only the (+) creases because they are the energetically favorable states. If one assumes that the (+) creases are strongly conducting, then the hydraulic conductivity of the network of the wetting fluid can be calculated. Because the state of a given crease depends on its neighbors, the question of whether the (+) creases that make the conducting phase form a percolating network is one of a correlated percolation. The correlation is of course short range, but it usually decreases the percolation threshold of the networks. If the correlation range increases, then the percolation threshold can decrease to small values, so that the network of (+) creases can be conducting down to very small values of fraction of (+) creases, consistent with experimental observations (Dullien *et al.*, 1986) that a strongly wetting fluid can retain its macroscopic network structure down to very small values of its saturation. If the contact angle is finite, the problem becomes more complex and the model of rough surfaces described above has to be modified.

The last model is due to Schwartz, Sen, and Johnson

(1989), who were interested in the effect of pore surface roughness on electrolytic conduction. A two-dimensional model was used in which the pore surface roughness was created by one of two methods. In the first method, the roughness was generated by a random walk. An example of the generated roughness is shown in Fig. 23(a). Here the interface between the pore and the matrix is a self-affine fractal curve. In the second method, the interface is a triadic Koch curve. As is well known, the Koch curve can be iterated repeatedly to increase the roughness of the interface. An example is shown in Fig. 23(b), where the interface after the third iteration is presented. Although, unlike the first method, the Koch curve is a self-similar fractal, the qualitative aspects of the two interfaces are similar. Of course, both are idealized models of a rough interface between a pore and the matrix, but they can capture some features of such interfaces.

Before closing this subsection, let us mention a few of the pioneering works that used network models to study transport phenomena in porous media. We already mentioned Bjerrum and Manegold's work. Benner *et al.* (1943) introduced a pore doublet model, which was in

fact a hexagonal network of channels through which fluid transport could take place. The same model was also used by Rose and Witherspoon (1956). But, due to the computational limitations of their times, no extensive calculations were carried out and the two papers received very little attention. Owen (1952) used a cubic network of bonds and sites to investigate the origin of Archie's law, Eq. (4.1). In this work, which was very sophisticated for its time, the nodes of the network represented pore bodies to which a volume was assigned. The bonds were narrow channels, representing pore throats and connecting pore bodies, to which no significant volume was assigned. Owen (1952) calculated the tortuosity factor for such a network and showed that it is affected strongly by the structure of the network.

The first application of network models to modeling two-phase flow in porous media was pioneered by Fatt (1956). He used various two-dimensional networks of bonds representing the pore throats. The radii of the bonds were selected from a probability density function, representing the pore-size distribution of the medium. No volume was assigned to the nodes. The length of each bond was assumed to be proportional to the inverse of its radius. Using this model and an analogy between laminar flow in tubes and Ohm's law of electrical currents, Fatt investigated the flow of two immiscible fluids in porous media and calculated the relative permeability to each fluid phase, i.e., the permeability of the sample-spanning cluster of bonds filled with a fluid, divided by the overall permeability of the network. He showed that, consistent with experimental data, the relative permeability to each phase effectively vanished at a *finite* value of the phase saturation, which, in the language of percolation theory, means that the relative permeabilities vanish at a nonzero percolation threshold. Later, Rose (1957) and Dodd and Kiel (1959) used such network models to study immiscible displacement processes in porous media. We have already mentioned the work of Ksenzhek (1963), who used a network model to predict capillary pressure curves for porous media. Thus, although in the condensed-matter literature two seminal papers of Kirkpatrick (1971, 1973) are generally credited with popularizing the use of resistor networks for investigating transport and percolation in disordered systems, the above pioneering works had already used such models to study transport processes in disordered porous media.

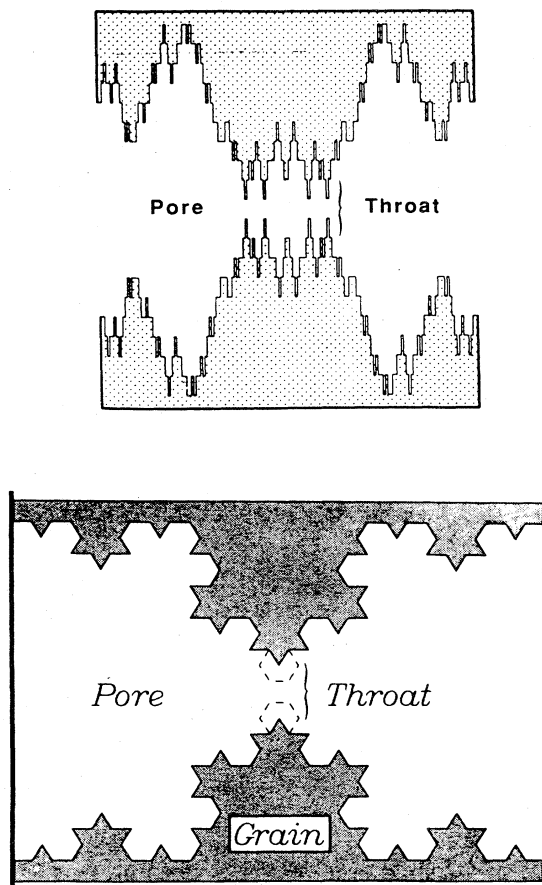


FIG. 23. Rough fractal surfaces generated by a random walk (top), and a Koch curve after the third iteration (bottom) (from Schwartz, Sen, and Johnson, 1989).

B. Models of heterogeneous porous media

So far, we have discussed models of porous media which, on a large enough scale, are macroscopically homogeneous. As a result, the effective transport properties of the system are independent of its size. We now discuss various models of porous media that are macroscopically heterogeneous, i.e., models in which there are large-scale spatial variations of the effective transport

properties of the system. There are three basic approaches to this problem, which are discussed below.

1. Random hydraulic conductivity models

In this approach the reservoir is represented by a rectangular region (or any other shape if desired). The region itself is divided into many smaller rectangular blocks, which are supposed to represent a portion of the reservoir that is homogeneous on the scale of the block's size. To each block a randomly selected hydraulic conductivity is assigned. This type of model was pioneered by Warren and Skiba (1964) and Heller (1972). In both studies it was assumed that there is no correlation between the conductivities of various blocks. Schwartz (1977) modified this model by inserting blocks of lower conductivities in an otherwise homogeneous two-dimensional region. One can also accommodate a non-random spatial structure by controlling the density and mode of aggregation of the inserted blocks or inclusions. In principle, the blocks do not have to be rectangular, but nonrectangular blocks cause a lot of difficulties for numerical computations of quantities of interest.

Smith and Freeze (1979) and Smith and Schwartz (1980, 1981a, 1981b) modified this basic model by including correlations between the blocks' hydraulic conductivities, which are expected to exist in real reservoirs and porous media. In their model, it is assumed that the spatial variations of hydraulic conductivities are described by a statistically homogeneous stochastic process. The spatial structure of the conductivity field is represented by a first-order nearest-neighbor stochastic process model. It is assumed that the hydraulic conductivity k_b of the blocks is log-normally distributed. If $Y = \log k_b$, then the first-order nearest-neighbor stochastic process implies that Y_{ij} , the random variable for the block with coordinates i and j , is given by

$$Y_{ij} = \alpha_x(Y_{i-1,j} + Y_{i+1,j}) + \alpha_z(Y_{i,j-1} + Y_{i,j+1}) + \epsilon_{ij}, \quad (4.2)$$

where α_x and α_z are autoregressive parameters expressing the degree of spatial dependence of Y_{ij} on its two neighboring values in the x and z directions, respectively, and ϵ_{ij} is a normal random variable uncorrelated with other ϵ_{ij} 's. If $\alpha_x = \alpha_z$, then the medium has a statistically isotropic covariance structure. Otherwise, the medium has an anisotropic structure and the covariance between conductivity values is dependent upon orientation. The random variables ϵ_{ij} are distributed according to a normal distribution with a zero mean and a given variance.

2. Fractal models

The models of Smith and Freeze (1979) and Smith and Schwartz (1980, 1981a, 1981b) with a short-range correlation were significantly generalized by Hewett (1986), who argued that permeability distribution and porosity

logs of heterogeneous reservoirs obey fractal statistics, and therefore there are infinitely-long-range correlations between the permeabilities of various regions of a reservoir, rather than the short-range correlation that was considered by Smith, Freeze, and Schwartz. More precisely, Hewett (1986) proposed that porosity logs and permeability distributions are fractional Gaussian noise (fGn) and fractional Brownian motion (fBm), respectively. Consider a stationary stochastic process $B_H(x)$ with the properties

$$\langle B_H(x) - B_H(x_0) \rangle = 0, \quad (4.3)$$

$$\langle [B_H(x) - B_H(x_0)]^2 \rangle \sim |x - x_0|^{2H}, \quad (4.4)$$

where $0 < H < 1$ is called the Hurst exponent. This is called an fBm (Mandelbrot and van Ness, 1968). The fBm is statistically self affine, and its trace has a fractal dimension $2 - H$. Its spectral density $S(\omega)$ takes the large-frequency asymptote [see Eq. (3.75)]

$$S(\omega) \sim \omega^{-(2H+1)}. \quad (4.5)$$

If we define a correlation function $C(x)$ by

$$C(x) = \frac{\langle -B_H(-x)B_H(x) \rangle}{\langle B_H(x)^2 \rangle}, \quad (4.6)$$

then fBm has the remarkable property that

$$C(x) = 2^{2H-1} - 1, \quad (4.7)$$

i.e., $C(x)$ is independent of x . Thus fBm displays persistence ($C > 0$), i.e., a trend at x (e.g., a high or low value of permeability) is likely to be followed by a similar trend at $x + \Delta x$, when $H > 1/2$, whereas one has antipersistence ($C < 0$) when $H < 1/2$. Equations (4.3)–(4.5) can be easily generalized for a d -dimensional system [see, for example, Feder (1988)]. For a given value of H , fGn has a different spectral density than fBm, namely, $S(\omega) \sim \omega^{-(2H-1)}$, and, roughly speaking, corresponds to the "derivative" of the trace of fBm. For example, for $H = 1/2$, fBm reduces to regular Brownian motion, and the corresponding fGn becomes a white noise. Based on an analysis of extensive data for the permeability and porosity of typical reservoirs, Hewett (1986) argued that vertical porosity logs are samples of fGn, while the lateral distribution of these properties follows fBm, although with the same H . His analysis also indicated that $H > 1/2$, indicating long-range positive correlations. Using an fBm and an fGn, Hewett generated permeability and porosity distributions and used them in the simulation of fluid transport in heterogeneous media, as will be discussed in Sec. VI.

3. Multifractal models

These models were introduced by Meakin (1987) and Lenormand *et al.* (1990). Consider a two-dimensional system, such as a square grid, and a probability p , which can be related at the end of the construction of a model

to a measure such as permeability or porosity and is distributed uniformly in the interval $(1-a, 1+a)$, with $0 \leq a \leq 1$. In the first step of constructing the model, a value p_{11} is selected at random and is given to all the pixels of the initial square. The first dichotomy is then carried out to make four squares of size $2^{n-1} \times 2^{n-1}$, and four values p_{21}, p_{22}, p_{23} , and p_{24} are selected at random and attributed to each of the four squares. The same process is repeated n times. At the end of the process, each pixel is characterized by n values of the probability p . A new measure P is now defined, which is the product of the n random values of p . Figure 24 shows the various stages of such a construction. The main property of this process is that it introduces correlations between pixels at all scales and thus induces a memory. A lower cutoff can also be introduced into this model by considering m dichotomy steps, where $m < n$, and n is the dimension of the pattern. One first makes $2^{n-m} \times 2^{n-m}$ independent multifractal patterns of size m_0 , and then computes $2^{n-m} \times 2^{n-m}$ independent products $p_{m+1} \times p_{m+2} \times \dots \times p_n$. The pixel values of each multifractal are then multiplied by these products in order to obtain products of order n . An example is shown in Fig. 25 with $m=4$ and $n=7$. This procedure can be further generalized to anisotropic systems by considering two probabilities p_x and p_y (or p_x, p_y , and p_z for three-dimensional systems) for x and y axes, distributing p_x and p_y uniformly in $(1-a_x, 1+a_x)$ and $(1-a_y, 1+a_y)$, and identifying p by the product $p_x \times p_y$.

For simulating flow in a porous medium, the measure p can be thought of as the effective radius or permeability

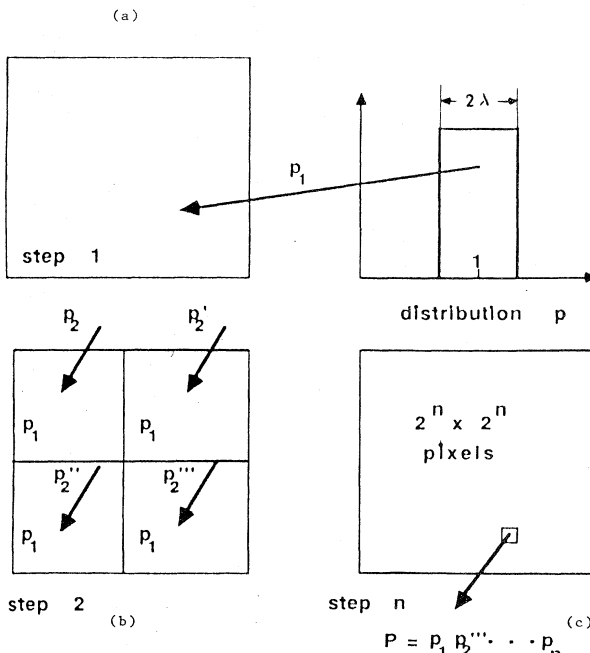


FIG. 24. The iterative process of constructing a multifractal model (from Lenormand *et al.*, 1990).

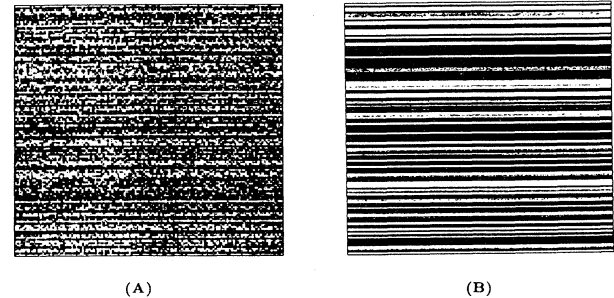


FIG. 25. (A) Isotropic and (B) anisotropic multifractal patterns (from Lenormand *et al.*, 1990).

of a pore. Given a pattern and a pore radius (or permeability) distribution, flow and displacement processes in a porous medium can be investigated. Lenormand *et al.* (1990) conducted such simulations and showed that their results were in good agreement with their experimental data obtained by CT scanning during gas injection in layered and heterogeneous Berea sandstones.

C. Models of fractured rocks

A study of the literature indicates that there have been three classes of models of fractured rocks. The first is the classical multiporosity model, which was proposed in the early 1960s. The second class consists of network models of fractured rocks, which are in essence extensions of network models of porous media. The last model is based on simulated annealing concepts. A brief description of each is now given.

1. Multiporosity models

Some of the earliest papers on modeling fractured reservoirs are those of Barenblatt *et al.* (1960), Warren and Root (1963), and Odeh (1965). Barenblatt *et al.* introduced what is popularly known as the *double-porosity model*. In this model, the reservoir is represented by a regular, fully connected fracture network (representing one degree of porosity), which is embedded in a porous matrix (representing the other degree of porosity). The matrix is assumed not to be interconnected, so that fluid flow occurs only through the fracture network. More sophisticated variations of this model were developed by Kazemi (1969) and Kazemi *et al.* (1976). Closmann (1975) and Abdassah and Ershaghi (1986) extended this model by including *three* degrees of porosity. Their model was motivated by investigation of the structure of fracture networks of carbonate reservoirs and the observations of actual well tests in such reservoirs indicating anomalous behavior that could not be explained by the double-porosity model. However, although multiporosity models may be appropriate for studying fluid flow in a *uniform* set of fractures, they are not suitable for modeling fracture networks of natural rocks because, as dis-

cussed in Sec. III, such networks have been shown to have fractal characteristics over certain length scales or they have incomplete connectivity, so that multiporosity models are not adequate for representing them. Moreover, these models contain too many adjustable parameters, often with no clear physical meaning, to be taken seriously for fundamental studies of flow phenomena in fractured reservoirs.

2. Network models of fractured rocks

The idea that a fractured rock can be represented by a network of interconnected and finite fractures is intuitively clear and appealing and thus has a relatively long history. Parsons (1966) and Caldwell (1972) appear to be the first to have used such an approach. They used electrical analog models to study flow through a network of fractures. In particular, Parsons (1966) used square and triangular networks of resistors in which each bond (or resistor) represented a finite fracture. However, his model had the drawback that the current in each resistor was assumed to be proportional to the width of the conductor, whereas flow rate in a fracture is proportional to the third or even higher power of the fracture's aperture (Tsang and Witherspoon, 1981). Snow (1969) used a three-dimensional model in which fractures were idealized as infinitely long and parallel ducts. As such, his model was in the same spirit as the bundle of parallel capillary tubes.

Over the past decade many authors have developed two- or three-dimensional models of fractured reservoirs in the form of networks of fractures of finite extent. In the two-dimensional models (Dienes, 1980; Long *et al.*, 1982; Englman *et al.*, 1983; Charlaix *et al.*, 1984; Endo *et al.*, 1984; Robinson, 1984a,b; Long and Witherspoon, 1985; Ross, 1986; Charlaix, Guyon, and Roux, 1987; Charlaix, Hulin, and Plona, 1987; Long and Billaux, 1987; Gueguen and Dienes, 1989; Hestir and Long, 1990) fractures are represented by one-dimensional finite line segments. These fracture networks are similar to two-dimensional networks of pores already discussed. These models can even be a reasonable representation of a three-dimensional system if most of the hydraulic conductivity is in the intersections between fractures, or if fluid flow is channelized in the fractures. In the three-dimensional models, the fractures are represented either by discs of finite radius (Long *et al.*, 1985; Andersson and Dverstorp, 1987; Charlaix, Guyon, and Roux, 1987; Billaux *et al.*, 1989; Piggott and Elsworth, 1989) or by flat planes of finite dimensions (Wilke *et al.*, 1985). There is experimental evidence that three-dimensional fractures are either roughly elliptical or disc-shaped (Pollard, 1976).

In the two-dimensional models, one distributes the fractures at random in a plane. One of the simplest models is the Poisson model, which was first used by Long *et al.* (1982). In this model, in a square block of size $L \times L$ one chooses x and y coordinates for a specified

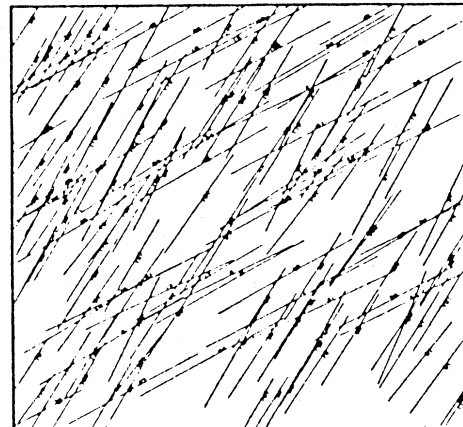


FIG. 26. An example of a two-dimensional fracture network in which fractures are represented by line segments.

number of line or fracture centers from a uniform distribution in $(0, L)$. Once the coordinates of the centers of the lines are selected, the orientation of the lines is also selected from a given distribution. Then the lines are assigned randomly selected lengths and hydraulic conductances. If the fractures cross the boundary of the system, they are truncated, but no truncation is done inside the $L \times L$ box. Figure 26 shows a typical network obtained by this method. These models are practically identical with the percolation networks of sticks studied by Balberg *et al.* (1983, 1984) and Balberg and Binenbaum (1983, 1985) that were mentioned in the discussion of continuum percolation. In particular, Balberg and Binenbaum (1983) studied two-dimensional anisotropic systems of conducting sticks, which may be more realistic models for two-dimensional fractured reservoirs, since such systems are usually anisotropic. Moreover, Balberg *et al.* (1984) considered a three-dimensional fracture network in which the fractures were finite cylinders of length L and radius r , at studied the dependence of the percolation threshold of the system on the aspect ratio L/r and on the macroscopic anisotropy of the system.

One major difference between fracture networks and percolation networks is as follows. In a percolation network, an upper bound to all properties is the case in which p , the fraction of conducting bonds, is unity. All quantities of interest are normalized against the $p=1$ case. On the other hand, for random fracture networks, there is theoretically no end to the degree of fracturing. If we add one more fracture to the network, its permeability or hydraulic conductivity increases *ad infinitum*. Thus one cannot determine how "filled" a fracture network is, and there is no analog of the $p=1$ case in percolation networks. As Hestir and Long (1990) pointed out, one can study systems in which λ_l , the average frequency of fractures intersecting a sample line, is held constant. Since any fracture network can be rescaled to a given constant λ_l if it is held fixed, the permeability of the network is maximum when all fractures are infinitely long, which is the system that Snow (1969) studied.

Thus, if λ_l is held fixed, Snow's analytical results for the permeability of a fracture network is equivalent to the $p=1$ case for percolation networks.

The next question is how to relate the parameters of fracture networks to those of percolation networks such as p and \bar{Z} , the average coordination number of the network. Robinson (1984b) and Charlaix, Guyon, and Roux (1987) used the average number of intersections per fracture ξ as the measure of the connectivity. Suppose now that the average fracture length is \bar{l} , the orientation distribution is $g(\theta)$, and the density of fracture centers is λ_A . It is easy to show that $\lambda_l = \bar{l}\lambda_A$, and

$$\xi = \lambda_l \bar{l} H(\theta), \quad (4.8)$$

where $H(\theta)$ is defined by

$$H(\theta) = \int_0^\pi \int_0^\pi \sin|\theta - \theta_0| g(\theta) g(\theta_0) d\theta d\theta_0. \quad (4.9)$$

For example, if the fracture orientation is uniformly distributed, $g(\theta) = 1/\pi$ and $H(\theta) = 2/\pi$. Now, for every ξ there is a $p_f(\xi)$, which is the analog of p for percolation networks. For example, in the fracture network of Engelman *et al.* (1983) one has $p_f(\xi) = 1 - \exp(-\xi)$. Therefore a critical value of ξ , ξ_c , can also be defined, and thus all the results of percolation theory discussed in Sec. II can be written in terms of ξ , if we replace p everywhere with $p_f(\xi) = 1 - \exp(-\xi)$. As a second example, consider Robinson's (1984a, 1984b) model that was analyzed by Hestir and Long (1990). In this model, $p_f(\xi)$ is the average fraction of a fracture that is available for flow. Now, consider a fracture of length l with $n(l)$ intersections. If the fracture length is constant, then $n(l)$ will be a Poisson process. The average fraction of a fracture available for flow, i.e., the fraction between the two end sites separated by l , is $[n(l)-1]/[n(l)+1]$. Therefore, if P_n is the probability that $n(l)=n$, one simply has $P_n = \xi^n e^{-\xi}/n!$ and

$$p_f(\xi) = \sum_{n=2}^{\infty} \frac{n-1}{n+1} P_n = \left[1 + \frac{2}{\xi} \right] (1 + e^{-\xi}) - \frac{4}{\xi}. \quad (4.10)$$

Again, all standard results of percolation can now be written down for Robinson's model by replacing p everywhere with p_f . Hestir and Long (1990) worked out several other examples relating p_f (or p) to ξ . They also considered the case in which the fracture lengths were not constant, but were distributed according to a given distribution. The goal of Hestir and Long (1990) was to use the effective-medium approximation (EMA; see Sec. V) and the scaling theory of conductivity near p_c [see Eq. (2.6)] to predict the hydraulic conductivity of fracture networks, and in order to do that one has to relate p (or p_f) to ξ . We should mention that, for two-dimensional fracture networks of constant length, Robinson (1984b) found that the percolation threshold, i.e., the average number of fractures intersecting a given fracture, is about 3.1.

Long and Billaux (1987) developed a two-dimensional

network model of fractures by incorporating field data into the model. The network was generated subregion by subregion, where the properties of each subregion were predicted through geostatistics. The region in which the data were collected was divided into statistically homogeneous subregions. The fractures were divided into five sets based on their tectonic history. It was observed that in each set fractures were spaced close together and had similar orientations. This information was incorporated into the network model. Another piece of information that was used in the simulation was the aperture distribution. The criterion for accepting a model was its ability to reproduce the measured permeability of the subregion. After all subregions were created, they were joined together to create the entire region. When the model was applied to Fanay-Augères, a uranium mine in France, it was found that macroscopically the region was barely connected. Only 0.1% of the fractures contributed to the permeability of the system. This implied that (i) the system had the structure of a percolation network and was extremely close to its p_c ; and (ii) the fracture network was a fractal object over the scale of the observation. Both of these findings support the ideas of Sahimi *et al.* (1993) discussed in the previous section. These results also appear to be typical of many fractured rocks and indicate the significance of percolation concepts to the modeling of such systems. Indeed, the relevance of such concepts to the modeling of fractured rocks was the chief reason for including these systems in this review.

The applicability of two-dimensional networks of fractures to the modeling of natural fractured rocks is limited. One main reason for this is that a two-dimensional model cannot realistically describe the fracture network connectivity, because fractures that do not connect in a planar cut may connect in the third dimension. Moreover, whenever two-dimensional data have been used with a three-dimensional model, it has been found that one has a nonuniqueness problem in the sense that many three-dimensional models can account for the same two-dimensional data. However, despite their significance, three-dimensional models have received less attention than their two-dimensional counterparts, perhaps because of the complex computations that are involved.

Charlaix *et al.* (1984) argued that, at the percolation threshold of a three-dimensional fracture network made of flat disks of radius r with a density of λ_A of disks per unit volume, one must have

$$\lambda_A r^3 \sim 0.15 - 0.3. \quad (4.11)$$

Note that r^3 represents the volume of a disk. For polydisperse disks one must replace r^3 with $\pi^2 \langle r^2 \rangle \langle r \rangle$ in Eq. (4.11), which is nothing but $\langle \text{surface} \rangle \langle \text{perimeter} \rangle / 2$, where $\langle \rangle$ represents the average of the quantity. These predictions were confirmed by Charlaix (1986) using Monte Carlo simulations. Robinson (1984b) found that, for three-dimensional networks of planar fractures, the number of intersections per plane is about 2. Wilke *et al.* (1985) considered percolation in

networks of planar fractures and showed that the geometrical critical exponents of percolation in their model are the same as those of random percolation (see Sec. II). Madden (1983) represented a three-dimensional fracture network by a cubic tessellation of elementary cubes and studied the connectivity properties of the network using renormalization-group theory (see Sec. V).

The above studies were concerned with the connectivity properties of idealized three-dimensional fracture networks. There have been a few papers in which three-dimensional models were employed in order to simulate the hydraulic behavior of a given field and match the measured data. Billaux *et al.* (1989) extended the model of Long and Billaux (1987), discussed above, to three dimensions. The fractures were represented as disks placed randomly in space. The diameter of each disc was selected independently from a probability distribution, which was assumed to be log-normal. To locate the fractures in the space, a point process called the *parent-daughter process* was used. In this method one starts from a Poisson process and places a cloud of points (or daughters) around each Poisson point (called a parent or seed). The number of points in each cloud is a Poisson random variable, and each point is placed in a given cloud independently of all other points. The motivation for doing this is the fact that experimental data indicate that fractures of real rocks often occur in swarms. Figure 27 shows a typical swarm of disklike fractures. As in the case of the two-dimensional model (Long and Billaux, 1987), the fractures were divided into five different sets. The orientation of the discs in each set was characterized as a fluctuation about the mean orientation for the set. This fluctuation had a spatial structure that could be simulated with geostatistics. After each set was generated, a model of a given fractured field was created by putting together all of the sets. By means of this model, the hydraulic and transport properties of the fractured rock were simulated. In work somewhat similar to that of Billaux *et al.*

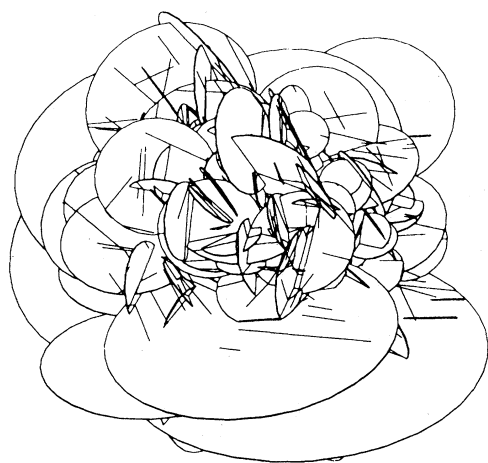


FIG. 27. A three-dimensional network of disklike fractures (from Billaux *et al.*, 1989).

(1989), Dverstorp and Andersson (1989) used a three-dimensional network of disklike fractures and showed that the model can be calibrated by one set of data and then be used to predict and match another set of data.

3. Simulated annealing

The simulated annealing approach recently developed by Long *et al.* (1991) appears to be a promising way to construct models of fractured rocks. In the last subsection, we discussed the models that were developed by Long and Billaux (1987), Billaux *et al.* (1989), and Dverstorp and Andersson (1989). There is a basic problem with these models that may limit, at least in some cases, their usefulness. This is the fact that, although there may be a large number of fractures in a given rock or field, usually only an extremely small fraction of the fractures contribute to the fluid flow. That is, most of such fractured rocks are at or near their percolation threshold, have fractal properties, and therefore cannot be treated with the classical methods of analysis. To overcome this difficulty, Long *et al.* (1991) developed a simulated annealing method. Such methods were originally developed by Kirkpatrick *et al.* (1983) for optimization processes, using a connection between such problems and the statistical mechanics of spin glasses.

In the work of Long *et al.* (1991) rock is represented by a three-dimensional network of finite fractures. Then simulated annealing is used to find an appropriate pattern of connected fractures, given some experimental information about rock. The most important issue to be resolved is to find how the fractures are connected, so that the transport behavior of the fracture network can mimic that of the actual system and honor the data. Given a problem, simulated annealing can be used if one has (i) a set of possible configurations of the system; (ii) a model for systematically changing the configuration; (iii) an "energy" function, in analogy with the work of Kirkpatrick *et al.* (1983), to minimize; and (iv) an annealing schedule of changing a temperature-like variable, so that the system can reach its minimum.

For fluid flow in fractured rock, requirement (i) is obvious: it is a network of fractures in which some of the fractures allow fluid flow to take place (they are "on") and some are closed to the transport process (they are "off"). Suppose $\{C\}$ denotes the set of all possible configurations of on and off fractures (note that such networks are similar to percolation networks of open and closed bonds discussed in Sec. II). The next requirement is a method according to which a given configuration is changed. Suppose that one assigns a probability function for randomly selecting a fracture. Then, if the selected fracture is on, it is turned off and vice versa. This generates a new configuration of the fracture network. One now defines the "neighborhood" N_C of C as the set of all configurations that are very close to C (in the language of Long *et al.*, they are one step away from C). Annealing the system means picking a configuration from N_C and

comparing it with C . In order to make the comparison precise, one needs to define an “energy” E , the third ingredient of simulated annealing. Long *et al.* (1991) defined E as

$$E = \sum_j |f(\mathbf{O}_j) - f(\mathbf{S}_j)|^{m_a}, \quad (4.12)$$

where \mathbf{O}_j and \mathbf{S}_j are vectors of *observed* and *simulated* responses, respectively, m_a is a constant, and $f(x)$ a real monotonic function. The measurements could be hydrological, geophysical, or geological. A probability distribution of the configurations was assumed to be expressible as a Gibbs distribution,

$$P(C) = a \exp[-E(C)/T], \quad (4.13)$$

where a is the renormalization constant (which is very

$$P\{C \rightarrow C' | C\} = \begin{cases} 0, & C' \notin N_C \\ P(C'|C) \times 1, & C' \in N_C, E(C') - E(C) \leq 0, \text{ and } C \neq C' \\ P(C'|C) \exp\{[E(C) - E(C')]/T\}, & C' \in N_C, E(C') - E(C) > 0, \text{ and } C \neq C' \end{cases} \quad (4.14)$$

The final ingredient of the model is a schedule for lowering the temperature as annealing progresses. This means that, as annealing continues, one is less likely to keep those configurations that increase E . The temperature schedule that Long *et al.* (1991) used was *ad hoc* but effective and was actually suggested by Press *et al.* (1986), who proposed that the temperature be changed after a number of configuration iterations sufficient to produce a fixed number of acceptable changes. At the end of each iteration i , the temperature T_i is decreased using a geometric series,

$$T_{i+1} = T_i R_i^i, \quad (4.15)$$

where $0 < R_i < 1$. Thus one need only select the initial temperature. This is selected such that it is of the same order of magnitude as the energy difference between the first two configurations, so that the energy difference between successive configurations remains (most of the time) between zero and 1.

What does one do if, for example, quantitative information, such as the range of possible responses, is available, but there are no actual measurements? For example, suppose one wants to predict the flow rate q at a point in the system far from a point at which a measurement was done, and one has the information that the flow rates were observed to be between a and b , $q \in [a, b]$. In this case, each time a configuration is changed, the following steps are also taken: (i) the new point is added to the configuration and q is calculated at that point; (ii) a new energy function E' is calculated such that $E'=0$, if the calculated q is in $[a, b]$, $E'=(q-a)^{m_a}$, if $q < a$, and $E'=(q-b)^{m_a}$ if $q > b$; (iii) if $E(C') + E'(C') < E(C) + E'(C)$, then C' is kept. Otherwise, the usual annealing

difficult to estimate, because one must know the energy of *all* configurations, which is impossible), and T is a “temperature” or a temperature-like variable to be defined below.

Because $P(C)$ is a Gibbs distribution, C , the current configuration, can be modeled as a Markov random field, which means that the transition probability for moving from C to C' depends only on C and C' and not on the previous configurations from the set $\{C\}$. Thus the transition probability can change from configuration to configuration, but it does not depend on the previous configurations that were examined. Therefore, given C and N_C , the transition probability for moving from C to C' (given our current configuration C) is equal to the probability that we select C' times the probability that the system would make the transition to a given configuration C' . Therefore

probability is used to keep or reject C' ; and (iv) finally, the new point is removed and the process is continued. This completes the simulated annealing method for selecting a configuration of a network of fractures that can mimic important features of a given rock and reproduce some of its measured properties. Long *et al.* (1991) showed that even if the initial configuration is a completely connected network of open (or “on”) fractures, the final configuration is usually a percolation network (although they did not mention percolation) that is “barely connected” (i.e., is very close to its percolation threshold).

V. SINGLE-PHASE FLOW AND TRANSPORT IN RESERVOIR ROCKS

In this section we review and discuss single-phase flow and transport in reservoir rocks. We focus on low-Reynolds-number flow, where Darcy’s law is applicable. We first give a theoretical derivation of Darcy’s law. We then review and discuss various methods of estimating permeability and the electrical conductivity of fluid-saturated rocks, and any possible relationship between them. Of course, as a result of Einstein’s relation, the electrical conductivity is proportional to the effective diffusivity D_e of the system.

A. Continuum models: Derivation of Darcy’s law

Darcy’s law is expressed as

$$\langle \mathbf{v} \rangle = -\frac{k}{\eta} (\nabla P - \rho \mathbf{g}), \quad (5.1)$$

where $\langle \mathbf{v} \rangle$, η , and ρ are, respectively, the average velocity, viscosity, and density of the fluid, k is the permeability, P the pressure, and \mathbf{g} the gravity vector. Many authors have given various derivations of Eq. (5.1) (Bear, 1972; Gray and O'Neil, 1976; Neumann, 1977; Keller, 1980; Tartar, 1980; Larson, 1981; Whitaker, 1986a; Rubinstein and Torquato, 1989). The one-dimensional version of Eq. (5.1) was discovered empirically by Darcy in 1856. However, it is the extension of Darcy's law to more than one dimension which is of practical importance. In this subsection, we present a summary of Whitaker's (1986a) derivation of Eq. (5.1), which is based on the method of volume averaging developed by him and his co-workers. This will also show us how continuum models of transport in porous media, of which Whitaker's method is perhaps the best known, are formulated.

The porous medium under consideration is shown in Fig. 28. The macroscopic length scale of the system is L , while the averaging volume is V . Other characteristic length scales of the system are l_β and l_σ , the characteristic length scales of the fluid and solid phases, respectively. The boundary value problem that one has to solve is expressed by the continuity and momentum equations,

$$\nabla \cdot \mathbf{v}_\beta = 0, \quad (5.2)$$

$$-\nabla P_\beta + \rho_\beta \mathbf{g} + \eta_\beta \nabla^2 \mathbf{v}_\beta = 0. \quad (5.3)$$

The interfacial area between the fluid and solid phases is $S_{\beta\sigma}$, and thus one boundary condition is that $\mathbf{v}_\beta = 0$ on $S_{\beta\sigma}$, the so-called *no-slip* boundary condition. As the second boundary condition one may specify \mathbf{v}_β on the entrance and exit surfaces of the porous medium. One can now use the spatial averaging theorem (Anderson and Jackson, 1967; Marle, 1967; Slattery, 1967; Whitaker, 1967), which states that, for any quantity ψ_β associated with the β (fluid) phase, one has

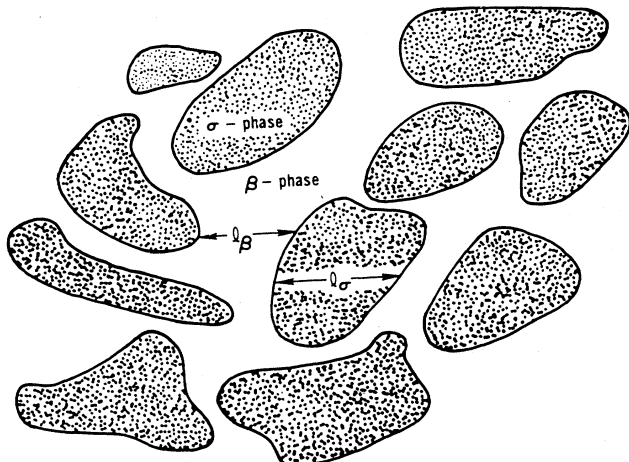


FIG. 28. The model of porous medium used in the volume averaging method (from Whitaker, 1986a).

$$\langle \nabla \psi_\beta \rangle = \nabla \langle \psi_\beta \rangle + \frac{1}{V} \int_{A_{\beta\sigma}} \mathbf{n}_{\beta\sigma} \psi_\beta d\mathbf{A}, \quad (5.4)$$

where $A_{\beta\sigma}$ is the interfacial area contained between the averaging volumes and $\mathbf{n}_{\beta\sigma}$ the unit outwardly directed normal vector for the β phase. Note that the averaging in Eq. (5.4) is over V . One can also define an average over phase volume, called the *intrinsic phase average*,

$$\langle \psi_\beta \rangle^\beta = \frac{1}{V_\beta} \int_{V_\beta} \psi_\beta dV, \quad (5.5)$$

where V_β is the volume of the β phase within V . Equation (5.4) and the no-slip boundary condition imply that $\nabla \cdot \langle \mathbf{v}_\beta \rangle = 0$, whereas if we use the averaging defined by Eq. (5.5) we obtain $\nabla \cdot \langle \mathbf{v}_\beta \rangle^\beta = -\epsilon_\beta^{-1} \nabla \epsilon_\beta \cdot \langle \mathbf{v}_\beta \rangle^\beta$, where ϵ_β is the volume fraction of the β phase (or the porosity of the porous medium). On the other hand, when we use Eq. (5.4) in the Stokes' equation, Eq. (5.3), yields

$$-\nabla \langle P_\beta \rangle - \frac{1}{V} \int_{A_{\beta\sigma}} \mathbf{n}_{\beta\sigma} P_\beta d\mathbf{A} + \epsilon_\beta \rho_\beta \mathbf{g} + \eta_\beta \langle \nabla \cdot \nabla \mathbf{v}_\beta \rangle = 0. \quad (5.6)$$

If we use the obvious relation $\langle P_\beta \rangle = \epsilon_\beta \langle P_\beta \rangle^\beta$, the decompositions $P_\beta = \langle P_\beta \rangle^\beta + \tilde{P}_\beta$ and $\mathbf{v}_\beta = \langle \mathbf{v}_\beta \rangle^\beta + \tilde{\mathbf{v}}_\beta$, and the relation

$$\frac{1}{V} \int_{A_{\beta\sigma}} \mathbf{n}_{\beta\sigma} d\mathbf{A} = -\nabla \epsilon_\beta,$$

which can be obtained from Eq. (5.4) using $\psi_\beta = 1$, then after some tedious manipulations and repeated applications of Eqs. (5.4) and (5.5), Eq. (5.6) finally becomes

$$-\nabla \langle P_\beta \rangle^\beta + \rho_\beta \mathbf{g} - \frac{1}{V_\beta} \int_{A_{\beta\sigma}} \mathbf{n}_{\beta\sigma} \tilde{P}_\beta d\mathbf{A} + \frac{\eta_\beta}{V_\beta} \int_{A_{\beta\sigma}} \mathbf{n}_{\beta\sigma} \cdot \nabla \tilde{\mathbf{v}}_\beta d\mathbf{A} = 0, \quad (5.7)$$

where several terms have been detected because their contributions are negligible; see Whitaker (1986a). We now need to develop governing equations for \tilde{P}_β and $\tilde{\mathbf{v}}_\beta$. This is done by substituting the above decompositions into Eqs. (5.2) and (5.3) to obtain

$$-\nabla \tilde{P}_\beta + \eta_\beta \nabla^2 \tilde{\mathbf{v}}_\beta = -(-\nabla \langle P_\beta \rangle^\beta + \rho_\beta \mathbf{g} + \eta_\beta \nabla^2 \langle \mathbf{v}_\beta \rangle^\beta), \quad (5.8)$$

$$\nabla \cdot \tilde{\mathbf{v}}_\beta = -\nabla \cdot \langle \mathbf{v}_\beta \rangle^\beta, \quad (5.9)$$

with the boundary conditions that $\tilde{\mathbf{v}}_\beta = -\langle \mathbf{v}_\beta \rangle^\beta$ on $S_{\beta\sigma}$ (since $\mathbf{v}_\beta = 0$ there) and with specified $\tilde{\mathbf{v}}_\beta$ on the entrance and exit surfaces of the system. Since all terms on the left-hand side of Eq. (5.8) are of the order of $\langle \mathbf{v}_\beta \rangle^\beta / l_\beta$, whereas those on the right-hand side are of the order of $\langle \mathbf{v}_\beta \rangle^\beta / L$, the right-hand side can be safely neglected (since $l_\beta \ll L$) and Eq. (5.9) becomes $\nabla \cdot \tilde{\mathbf{v}}_\beta = 0$. Then, use of the averaging expressed by Eq. (5.5) in Eq. (5.8) yields

$$\begin{aligned} \frac{1}{V_\beta} \int_{V_\beta} (-\nabla \tilde{P}_\beta + \eta_\beta \nabla^2 \tilde{\mathbf{v}}_\beta) dV \\ = -(-\nabla \langle P_\beta \rangle^\beta + \rho_\beta \mathbf{g} + \eta_\beta \nabla^2 \langle \mathbf{v}_\beta \rangle^\beta), \end{aligned} \quad (5.10)$$

which, when compared with Eq. (5.8), yields

$$-\nabla \tilde{P}_\beta + \eta_\beta \nabla^2 \tilde{\mathbf{v}}_\beta = \frac{1}{V_\beta} \int (-\nabla \tilde{P}_\beta + \eta_\beta \nabla^2 \tilde{\mathbf{v}}_\beta) dV . \quad (5.11)$$

We now search for a solution of the form

$$\tilde{\mathbf{v}}_\beta = \mathbf{B} \cdot \langle \mathbf{v}_\beta \rangle^\beta + \psi , \quad (5.12)$$

$$\tilde{P}_\beta = \eta_\beta \mathbf{b} \cdot \langle \mathbf{v}_\beta \rangle^\beta + \eta_\beta \zeta , \quad (5.13)$$

where ψ and ζ are arbitrary functions, which means that \mathbf{B} and \mathbf{b} can be specified in any way one wishes. Whitaker (1986a) goes on to show that ψ and ζ can be ignored altogether. Thus, if we use Eqs. (5.12) and (5.13) in Eq. (5.7), defining a tensor \mathbf{T} by

$$\mathbf{T} = -\frac{1}{V_\beta} \int_{A_{\beta\sigma}} \mathbf{n}_{\beta\sigma} \cdot (\nabla \mathbf{B} - \mathbf{I}\mathbf{b}) dA , \quad (5.14)$$

where \mathbf{I} is the identity tensor, and letting $\mathbf{K} = \epsilon_\beta \mathbf{T}^{-1}$, Eq. (5.7) becomes

$$\langle \mathbf{v}_\beta \rangle = \frac{\mathbf{K}}{\eta_\beta} (\nabla \langle P_\beta \rangle^\beta - \rho_\beta \mathbf{g}) , \quad (5.15)$$

which is Darcy's law, where \mathbf{K} is the permeability tensor. For isotropic porous media, Eq. (5.15) reduces to Eq. (5.1).

B. Calculation of the permeability and electrical conductivity of rocks

The above derivation of Darcy's law allows one, in principle, to calculate the permeability tensor \mathbf{K} , if the unknown functions \mathbf{B} and \mathbf{b} can be calculated. In practice, however, one can never find an exact solution for \mathbf{B} or \mathbf{b} , except for some model porous media whose structures are simple enough to allow exact analytical expressions for \mathbf{B} or \mathbf{b} to be found. In this subsection we review and discuss various methods for estimating permeability and the electrical conductivity of fluid-saturated rocks. Some of these methods are applicable to determining both the permeability and the electrical conductivity, while others are applicable only to one or the other.

1. Exact results and rigorous bounds

Before reviewing exact results, we should define precisely what we mean by exact. There are currently no exact results for the permeability and conductivity of porous media with an arbitrary microstructure. Therefore, when we refer to exact results or rigorous upper and lower bounds, we mean the results that can be obtained for a given morphology of the pore space.

Most of the exact results for the permeability of porous media are for periodic arrays of spherical particles of radius r , which are placed at the nodes of a regular lattice such as a simple cubic lattice. These models are idealizations of unconsolidated porous media and, as already discussed, can capture some of their features. Hasimoto (1959) was the first to treat slow fluid flow through a cu-

bic array of spheres. He derived the periodic fundamental solution to the Stokes equation. He then expanded the velocity profile in terms of the fundamental solution and obtained an expression for k , valid for dilute arrays of spheres. Sangani and Acrivos (1982b) modified and extended Hasimoto's work and obtained expressions for the permeability of all three types of cubic lattices of spheres. If c is the volume fraction of the spheres, then their result for a simple cubic lattice of spheres is given by

$$\frac{k_s}{k} = 1 - 1.7601c^{1/3} + c - 1.5593c^2 + 3.9799c^{8/3} - 3.0734c^{10/3} + O(c^{11/3}) , \quad (5.16)$$

where $k_s = 2r^2/(9c)$ is the Stokes permeability. Sangani and Acrivos (1982b) also presented the numerical coefficients in the above expansions for bcc and fcc lattices and two-dimensional square and hexagonal lattices of parallel cylinders. These expansions are convergent for $0 < c/c_{\max} < 0.85$, where c_{\max} is the maximum volume fraction of the spheres for a given packing and $c_{\max} = \pi/6$, $3^{1/2}\pi/8$, and $2^{1/2}\pi/6$ for simple cubic, bcc, and fcc lattices, respectively.

Zick and Homsy (1982) also considered the same problem and obtained the solutions for the cubic family of lattices, but used a different method from that of Sangani and Acrivos. Instead of trying to solve the Stokes equation directly, they reduced the set of partial differential equations to a set of Fredholm's integral equations of the first kind. Like Sangani and Acrivos (1982b), Zick and Homsy (1982) used Hasimoto's fundamental solutions. The kernel of the integrals in Zick and Homsy's method was a three-dimensional Fourier series which is difficult to evaluate. However, their method had its advantages. The unknown in their method was the surface stress vector, and therefore the domain of the problem was the two-dimensional surface of a sphere, as opposed to the three-dimensional domain of the original problem in terms of the velocity and pressure. The number of unknowns was three, the components of the surface stress vector, one less than the number of unknowns in the original problem, which were the three velocity components and the pressure. Zick and Homsy (1982) used a Galerkin method in which the unknown, say, $f(\mathbf{x})$, was expressed in terms of a linear combination of some basis functions $\psi_i(\mathbf{x})$,

$$f(\mathbf{x}) = \sum_{i=1}^{\infty} a_i \psi_i(\mathbf{x}) . \quad (5.17)$$

The unknowns are now the a_i 's. In practice, the above infinite sum is truncated after a few terms. One possible set of basis functions is $\psi_i(\mathbf{x}) = x^p y^q z^s$, where p , q , and s are integer or zero. For the present problem the coefficient a_1 is nonzero only if p , q , and s are even, a_2 is nonzero only if p and q are odd and s is even, a_3 is nonzero if p and s are odd and q is even, and so on. Such properties greatly facilitated the determination of a_i 's,

and were exploited by Zick and Homsy (1982). Their numerical solutions for various cubic lattices agreed with the expansions of Sangani and Acrivos (1982b).

Larson and Higdon (1989) considered the case in which the spheres in the cubic packing were allowed to grow, as already described above. For this case, Larson and Higdon expressed the velocity and pressure field in terms of harmonic expansions in spherical coordinates, as described by Happel and Brenner (1983). In this method, one writes

$$P = \sum_{n=-\infty}^{\infty} p_n, \quad (5.18)$$

$$\mathbf{v} = \sum_{n=-\infty}^{\infty} [\nabla \times (\mathbf{r} \chi_n) + \nabla \psi_n + \alpha_n r^2 \nabla p_n + \beta_n r p_n], \quad (5.19)$$

where $\alpha_n = (n+3)/2(n+1)(2n+3)\eta$; $\beta_n = n/(n+1)(2n+3)\eta$; and p_n , χ_n , and ψ_n are solid spherical harmonics, which are written in terms of the associated Legendre functions in the form $r^n P_n^m(\cos\theta) \exp(im\phi)$, where P_n^m is the Legendre function. These expressions are used in the continuity and Stokes equations, the geometry of the packing is specified, and the numerical solution of the problem is obtained. For high concentrations of the spheres an analytical asymptotic expression was also derived by Larson and Higdon.

The above results are in some sense exact because, as can be seen, one expresses the quantities of interest in terms of expansions and infinite series, every term of which can, in principle, be calculated. However, they are only applicable to periodic arrays of spheres and in all cases, except for the work of Larson and Higdon (1989), might be relevant only to unconsolidated porous media. Childress (1972), Howells (1974), and Hinch (1977) considered flow through a random array of spheres and obtained an asymptotic expression for the permeability of the system for low values of c . Hinch's (1977) results can be summarized by the equation

$$\frac{k_s}{k} = 1 + \frac{3}{\sqrt{2}} c^{1/2} + \frac{135}{64} c \log c + 16.456c \dots \quad (5.20)$$

Actually, Hinch's result contained a few numerical errors, which were corrected by Kim and Russel (1985), who also derived a few higher-order terms of the above expansion. Finally, Adler and Brenner (1984a, 1984b, 1984c) studied a variety of transport processes in spatially periodic capillary networks.

There are also a variety of rigorous results for the conductivity of a model random medium, which is usually a two-component mixture of spheres (or another relatively simple geometry such as ellipses or cylinders) of conductivity σ_s and the matrix (the channels between the spheres) in which the spheres are embedded, whose conductivity is σ_m . The system can have a periodic structure or a more complex configuration. Various methods have been used to determine, rigorously, the conductivity

of the system as a function of σ_s/σ_m (see Bonnecaze and Brady, 1990, and Torquato, 1991, for extensive lists of references). For our problem, if we assume that the matrix is where fluid flow takes place and the spheres represent the solid matrix of the medium, we would be interested in the limit $\sigma_s/\sigma_m = 0$. However, almost none of these results is applicable to this case, and none can provide an accurate estimate of the conductivity of the fluid-saturated porous medium.

Another set of rigorous results is obtained when, instead of trying to solve the problem completely and exactly, one obtains upper and lower bounds to the properties of interest. Prager (1962) and Weissberg and Prager (1962, 1970) pioneered this approach for calculating upper and lower bounds to k . [Note that Berryman and Milton (1985) corrected an error in the original results of Weissberg and Prager.] They proposed that variational bounds on k , which depends upon certain distribution functions that statistically characterize the medium, may be used for estimating k (or, more precisely, upper and lower bounds to k) for a wide range of sphere volume fractions c . Weissberg and Prager (1962, 1970) evaluated these bounds for a model in which the centers of the spheres are distributed at random, the so-called *fully-penetrable-sphere model*, or the Swiss cheese model. Torquato and Beasley (1987) considered the general case in which the spheres have an arbitrary degree of impenetrability, characterized by a parameter λ_{im} , where $\lambda_{im}=0$ corresponds to the fully penetrable model, whereas $\lambda_{im}=1$ represents the case of completely impenetrable spheres. This parameter also affects the percolation threshold c_p of the particle (sphere) phase. One has $c_p=0.3$ and 0.64 for $\lambda_{im}=0$ and 1 , respectively. Torquato and Beasley (1987) derived useful upper and lower bounds for the permeability of the system as a function of λ_{im} . In a later paper, Torquato and Lu (1990) derived upper and lower bounds for a polydisperse system of spherical particles. It should be mentioned that, in all cases that have been discussed so far, the Kozeny-Carman empirical formula

$$\frac{k_s}{k} = \frac{10c}{(1-c)^3} \quad (5.21)$$

(recall that $1-c=\phi$ is the porosity) falls within 15% of the results for at least one of the three types of periodic packings if $c > 0.5$, and in the case of the random-sphere model it is relatively close to the lower bound. One interesting result of Torquato and Beasley (1987) was that the bounds which incorporate a certain level of statistical information on the medium are *not* always necessarily sharper than bounds which involve less information.

Consider now a problem in which fluid particle, initially distributed uniformly in the pore space, are allowed to diffuse randomly towards the pore surface, but are removed as soon as they reach the surface (as a result of, for example, a reaction). The average lifetime for the

particles is given by

$$t_l = \frac{\delta^2}{D_e} , \quad (5.22)$$

where D_e is the effective diffusivity of the particles and δ is a characteristic measure of pore size relevant to the diffusion-limited interface reaction. Thus δ is a length defined by a physical problem and does not have a purely geometrical interpretation. Torquato (1990) proved that

$$k \leq k_r = \phi D_e t_l = \phi \delta^2 , \quad (5.23)$$

where k_r is the effective reaction rate constant and ϕ the porosity of the medium. Although this establishes an interesting connection between k and reaction properties of a porous medium, the upper bound provided by this relation is usually weak, so that its practical usefulness is limited; see Kostek *et al.* (1992) for a discussion of this.

Similar to permeability, various upper and lower bounds have also been derived for the electrical conductivity of a two-component mixture of particles and the matrix. As in the case of exact results, we are interested in the limit $\sigma_s/\sigma_m=0$. However, this is precisely the limit in which such bounds lose their usefulness, although using a very small value of σ_s/σ_m might provide a useful, order-of-magnitude estimate for the conductivity of a fluid-saturated medium; see Torquato (1991) for a review of this subject. The main problem with many such exact or rigorous bounds is that they are not very useful for the highly disordered porous media (some with fractal properties) that are of interest here. For example, rigorous upper and lower bounds are not useful if the porous medium is close to its percolation threshold. In fact, no bound can predict the existence of a nontrivial (i.e., not zero or unity) percolation threshold.

2. Effective-medium approximations and derivation of Archie's law

Effective-medium approximation (EMA) is a phenomenological method for determining the effective properties of a disordered medium, in which the medium is replaced with a hypothetical homogeneous one with unknown physical constants. There are two approaches for implementing this idea. The Maxwell-Garnett (1904) approach is applicable to the case in which isolated inclusions are embedded in a continuous matrix consisting of a single phase; the effective properties of the system are derived by placing a sphere (or an ellipse) of the effective medium in this matrix. This is usually called the average t -matrix, or non-self-consistent approximation. In the second approach, developed by Bruggeman (1935), each inhomogeneity is embedded in the effective medium itself, the unknown properties of which are determined in such a way that the volume average over all inhomogeneities yields no extra fields in the medium. Thus EMA is an ingenious way of transforming a many-body problem into a one-body problem. Bruggeman's EMA was rederived independently by Landauer (1952)

[see Landauer (1978) for a history of EMAs]. In Bruggeman's original theory, the shape of the inhomogeneity was assumed to be spherical. Stroud (1975) showed that the conductivity of the spherical inclusions need not be isotropic, but can be tensorial. Hori and Yonezawa (1977), Thorpe and Sen (1985), and Xia and Thorpe (1988) extended these ideas to the case in which inclusions are ellipses of a given aspect ratio.

Kirkpatrick (1971, 1973) showed how Bruggeman's EMA can be generalized to resistor networks. He showed that for a regular network of coordination number Z the EMA predicts that

$$\int h(g_p) \frac{g_p - g_e}{g_p + (\gamma^{-1} - 1)g_e} dg_p = 0 , \quad (5.24)$$

where $\gamma=2/Z$, $h(g_p)$ is the distribution of the pore (bond) conductance g_p , and g_e is the effective conductance of the system. The same equation was derived by Bruggeman and Landauer with $\gamma^{-1}=d$ for a d -dimensional continuous system with spherical inclusions. Using Eq. (5.24), we can calculate the permeability and conductivity σ of a porous medium. Consider an effective-medium network where each bond or pore has a conductance g_e . We fix the pressures at two opposite faces of the network so as to produce an average pressure gradient $\langle \nabla P \rangle$. The total fluid flux q crossing any plane perpendicular to $\langle \nabla P \rangle$ is the sum of the individual fluxes in the bonds intersecting the plane. Each pore flux is the pressure difference across it times g_e/η . If we approximate the local pressure difference as the projection of the average pressure gradient along the bond length l , we find

$$q = \sum \frac{g_e}{\eta} \langle \nabla P \rangle \cdot l . \quad (5.25)$$

If we divide q by the area S of the plane, we obtain an average velocity which, when compared with Darcy's law, yields an estimate of the permeability

$$k = g_e \left(\frac{1}{S} \sum l \cdot \mathbf{n} \right) , \quad (5.26)$$

where \mathbf{n} is a unit vector along the pressure gradient. But, if the medium is statistically homogeneous and isotropic, any unit vector can be used. Equation (5.26) shows clearly why, for random pore networks, k and g_e obey the same scaling law near p_c . In a similar way, the electrical conductivity σ of a fluid-saturated network can be calculated.

It should be pointed out that, in this kind of approach, the pressure drop in a pore body is neglected and it is assumed that all of the pressure drop occurs in the pore throats (or bonds) of the network. Koplik (1982) treated the case in which the pressure drops in both pore bodies and throats are taken into account. The analysis in this case is complex and will be ignored here. So long as pore bodies are large and compact and pore throats are long and narrow, the above approximation is valid.

An important test for any theory of transport in

porous media is its ability to predict the percolation threshold of the system. Despite its simplicity and lack of detailed information about the microstructure of the porous medium in its structure, the EMA can predict the existence of a nontrivial p_c . It is easy to show that the EMA predicts that $p_{cb} = 2/Z$, for the bond percolation threshold of a network. This prediction is accurate for two-dimensional networks, but not so for three-dimensional ones (see Tables I and II). The EMA also predicts that the critical exponents for the conductivity and permeability of the system near p_c are equal to 1 in all dimensions, which is a wrong result (see Table III). In general, as Koplik (1981) showed, the EMA is very accurate if the system is not close to its p_c , regardless of the structure of $h(g_p)$. Its predictions are also more accurate for two-dimensional networks than for three-dimensional ones. The performance of the EMA near p_c can be improved systematically (Blackman, 1976; Turban, 1978; Ahmed and Blackman, 1979; Sheng, 1980; Sahimi, 1984). For example, a cluster of several bonds with random conductances can be embedded in the effective-medium network, instead of a single bond as in Kirkpatrick's EMA, and the average of the resulting potential fluctuations in the effective medium is set to zero in order to calculate the effective conductance. The most accurate results are obtained with those clusters that preserve the symmetry of the network. Erdős and Haley (1976) showed how different averaging schemes can affect the performance of the EMA and suggested an averaging scheme that would improve the EMA's performance.

Equation (5.24) represents an EMA for steady-state transport. One can develop an EMA for transient transport (Odagaki and Lax, 1981; Webman, 1981; Sahimi, Hughes *et al.*, 1983b) and for the case in which there is a first-order chemical reaction (Sahimi, 1988b). Moreover, EMA has also been extended to anisotropic networks (Bernasconi, 1974), which can be used for calculating permeabilities of fracture networks that are usually anisotropic (Harris, 1990), to site percolation in random networks (Watson and Leath, 1974; Butcher, 1975; Bernasconi and Wiesmann, 1976; Joy and Strieder, 1978, 1979; Sahimi, Scrivan, and Davis, 1984), and has been modified to include the effect of a short-range correlation (Hori and Yonezawa, 1977; Hilfer, 1991a).

Koplik *et al.* (1984) analyzed in detail a Massilon sandstone, used a serial sectioning method to determine an equivalent random network to its pore space, and, using this information, employed Eq. (5.24) to calculate the permeability and conductivity of the pore space. They found that the predicted k 's differ from the data by about one order of magnitude, while the predicted σ 's differ by a factor of about 2. They attributed the difference to the fact that most sedimentary rocks, like the Massilon sandstone that they considered, are highly heterogeneous and anisotropic, properties that are not taken into account by Eq. (5.24). Doyen (1988) analyzed transport properties of Fontainebleau sandstones and used Eq. (5.24) to predict them; he found that their k and σ could be predicted to

within a factor of 3 by Eq. (5.24).

As already discussed in Sec. IV, a useful empiricism for sedimentary rocks is Archie's law, Eq. (4.1). The exponent m has been found to vary anywhere between 1.3 and 4, depending upon consolidation and other factors. Archie's law has been found to hold even for igneous rocks (Brace *et al.*, 1968; Brace and Orange, 1968). However, it may take a more complex form for clayey or shaly rocks because, e.g., the clays, which are capable of ion exchange, can complicate conduction mechanisms. Note that Archie's law implies that the fluid phase remains connected at all saturations, i.e., its percolation threshold is zero.

There have been many attempts to derive Archie's law in order to understand its origin. Here, we briefly review these works since most of them used a variation of the EMA. Sen (1981, 1984), Sen *et al.* (1981), Mendelson and Cohen (1982), and Yonezawa and Cohen (1983) showed that a modification of the EMA can be used to derive Archie's law. This version of the EMA was called a *self-similar* EMA because of the assumption that a rock grain is coated with a fluid that includes coated rock grains, the coating at each level consisting of other coated grains. First consider the standard EMA, Eq. (5.24). Since the electrical conductivity σ and the effective conductance g_e are, aside from a numerical coefficient, equal, one replaces in Eq. (5.24) g_p and g_e with σ_p and σ , respectively. With a binary distribution, $h(\sigma_p) = p\delta(\sigma_p - \sigma_f) + (1-p)\delta(\sigma_p - \sigma_r)$, Eq. (5.24) becomes

$$\sigma = \frac{-A \pm [A^2 + 4(\gamma^{-1}-1)\sigma_f\sigma_r]^{1/2}}{2(\gamma^{-1}-1)}, \quad (5.27)$$

where

$$A = [\sigma_f - (\gamma^{-1}-1)\sigma_r, -\gamma^{-1}(\sigma_f - \sigma_r)p].$$

Equation (5.27) has two solutions, but only one of them is physically meaningful. In the limits $p \rightarrow 0$ and $p \rightarrow 1$, we get

$$\sigma_{(1)} = \sigma_f \left[1 + (1-p)\gamma^{-1} \frac{\sigma_r - \sigma_f}{\sigma_r + (\gamma^{-1}-1)\sigma_f} \right], \quad (5.28)$$

$$\sigma_{(2)} = \sigma_r \left[1 + p\gamma^{-1} \frac{\sigma_f - \sigma_r}{\sigma_f + (\gamma^{-1}-1)\sigma_r} \right]. \quad (5.29)$$

The basic idea behind the self-similar EMA is as follows. One starts from the pure fluid system, replaces a small portion of it by pieces of rock step by step, and applies the EMA at each step. Assume that $\sigma^{(i)}$ is the conductivity of the mixture at a given step i , and replace a small volume Δq_i of the medium by grains of rock. Equation (5.24) yields

$$\begin{aligned} & \frac{\sigma^{(i)} - \sigma^{(i+1)}}{\sigma^{(i)} + (\gamma^{-1}-1)\sigma^{(i+1)}} (1 - \Delta q_i) \\ & + \frac{\sigma_r - \sigma^{(i+1)}}{\sigma_r + (\gamma^{-1}-1)\sigma^{(i+1)}} \Delta q_i = 0, \end{aligned} \quad (5.30)$$

where σ_r is the rock conductivity. If Δq_i is small enough, we obtain from Eq. (5.30)

$$\sigma^{(i+1)} = \sigma^{(i)} \left[1 + \gamma^{-1} \frac{\sigma_r - \sigma^{(i)}}{\sigma_r + (\gamma^{-1} - 1)\sigma^{(i)}} \Delta q_i \right]. \quad (5.31)$$

Note that by denoting the volume fraction of the fluid at the i th stage by p_i we have, $\Delta p_i q_i = p_i - p_{i+1}$. If we use Eq. (5.31) repeatedly, we obtain for the case of $\sigma_r = 0$

$$\sigma^{(n+1)} = \sum_{i=1}^n \left[1 + \frac{\gamma^{-1}}{\gamma^{-1} - 1} \frac{p_{i+1} - p_i}{p_i} \right] \sigma^{(0)}, \quad (5.32)$$

where $\sigma^{(0)} = \sigma_f$ and $p_0 = 1$ (where $p_0 = 1$ corresponds to pure fluid, the system we started with). If we take the limit $\Delta q_i \rightarrow 0$, then Eq. (5.32) becomes a differential equation,

$$\frac{d\sigma^{(i)}}{\sigma^{(i)}} = - \frac{dp_i}{p_i} \frac{\sigma_f - \sigma^{(i)}}{\sigma_f + (\gamma^{-1} - 1)\sigma^{(i)}} \gamma^{-1}, \quad (5.33)$$

which, after integrating and using the boundary condition $\sigma^{(i)} = \sigma_f$ for $p_i = 1$, yields

$$\sigma = \sigma_f p^m,$$

with

$$m = \frac{\gamma^{-1}}{\gamma^{-1} - 1}. \quad (5.34)$$

Thus, if we interpret p as the porosity of the medium, the EMA produces Archie's law. Equation (5.34) also shows that, consistent with experimental data, m is not universal but depends on the connectivity of the system.

What is the geometrical interpretation of this result? For a network model of a pore space, Yonezawa and Cohen (1983) presented a nice interpretation, which can be summarized as follows. At the i th stage every bond has the conductivity $\sigma^{(i)}$; one replaces a small fraction Δq_i of the bonds by a resistor with conductivity σ_r , and then uses the EMA to estimate the conductivity of the new system. This is equivalent to putting a resistor parallel to the original one on each bond. The conductivity $\sigma^{(ia)}$ of an added resistor should be

$$\sigma^{(ia)} = \gamma^{-1} \sigma^{(i)} \frac{\sigma_2 - \sigma^{(i)}}{\sigma_2 + (\gamma^{-1} - 1)\sigma^{(i)}} \Delta q_i, \quad (5.35)$$

if the original resistor belongs to the host medium; otherwise it is given by Eq. (5.31). The implication is that, even when $\sigma_r = 0$, the application of the EMA at each stage makes the link between the nodes conducting because of adding a parallel conducting resistor, and thus there is always a sample-spanning cluster of conducting bonds. Translating this for the rock-fluid system, it implies that this procedure guarantees the continuity of the fluid phase and the granularity of the rock grains. Note that in the original derivation of Sen *et al.* (1981) m was found to be 3/2, which corresponds to $d=3$ in the continuous EMA [or $Z=6$ in the discrete EMA, Eq. (5.24)], which corresponds to spherical grains. For nonspherical

particles $m > 3/2$, but under certain circumstances one can even have $m < 3/2$. Mendelson and Cohen (1982) give $m = \sum_i (1 - L_i)^{-1}/3$, where L_i 's are the depolarization factors and $\sum_i L_i = 1$. Bussian (1983) generalized the self-similar EMA to include finite rock conductivity σ_r , and fitted the resulting formula to the data, treating m and σ_r as adjustable parameters. He found $m \geq 3/2$ in almost all cases he considered, and argued that this is because clay gives a finite value to σ_r . Since clay particles are usually flat, they increase m (Mendelson and Cohen, 1982).

One major drawback of the above derivation of Archie's law is that it pertains only to a microstructure whose solid component is disjoint. This difficulty was circumvented by Sheng (1990), who generalized the self-similar EMA to a *three-component* system consisting of fluid, solid, and *cement material*. Component one, the starting phase, is composed of a mixture of fluid and cement material. Sheng (1990) showed that the self-similar EMA with three components reproduces Archie's law with $m = (5 - 3L)/[3(1 - L^2)]$, where L is the depolarization coefficient of the grains, but with the added feature that the solid grains also remain connected.

Although the self-similar EMA is successful in providing a derivation of Archie's law, its use for understanding the properties of rocks is not without conceptual difficulty. Generally speaking, rocks have porosities less than 40%. This is far from the dilute limit in which the assumptions of the models can be justified [recall that Eqs. (5.28)–(5.31) are valid only in the dilute limit]. If the porosity is low, then the grains are in close contact with one another and the interaction between them is important. Such interactions cannot be taken into account correctly by the EMA. In fact, Milton (1984) showed that self-similar EMA accounts for the interactions correctly only in the special case in which grains of any given size are surrounded by much smaller grains, and grains of the same size are far separated from each other. This is hardly the case in natural rocks. Moreover, rocks with very similar grains can have very different values of m , and rocks with very dissimilar grains can have very similar values of m . These cannot be explained with a self-similar EMA. Hilfer (1991b) presented an alternative derivation of Archie's law based on the percolation model. However, his result, $m = 1 + \mu$, where μ is the conductivity exponent, indicates that m is universal, in contradiction with the data.

Wong *et al.* (1984) showed that their shrinking-tube model, discussed in Sec. III, can reproduce Archie's law such that m would depend on the skewedness of the pore-size distribution. Their experiments with fused-glass beads and real rocks indicated that m is larger in porous media with a wider fluctuation of pore sizes, which their model also correctly predicted. Moreover, they showed that their model predicts that k is related to the porosity by

$$k \sim \phi^m, \quad (5.36)$$

where $m'=2m$. Equation (5.36) is consistent with the empirical Kozeny-Carman correlation, Eq. (5.21). Thus Wong *et al.*'s model allows a unified derivation of two well-established and widely used empirical laws. Note that if, for example, $m=3$, we obtain $m'=6$, consistent with experimental observations (Wyllie and Rose, 1950; Timur, 1968) that, if k is to be related to ϕ by a power law, the exponent has to be large.

We should mention here the work of Hori and Yonezawa (1977), who developed a cumulant expansion method for determining transport properties of disordered media. Their method is more accurate than the EMA for three-dimensional media, while the EMA is a better approximation for two-dimensional systems. In particular, the bond percolation threshold is predicted by the cumulant expansion to be

$$p_{cb} = 1 - \exp(-2/Z), \quad (5.37)$$

so that, for example, for the simple cubic network, Eq. (5.37) yields, $p_{cb} \approx 0.283$, which should be compared with the EMA's prediction, $p_{cb} = 1/3$ and the accepted value $p_{cb} \approx 0.249$ (Table II). This more accurate prediction is due to the fact that near p_c clustering, correlations, and fluctuations play an essential role, and while the EMA completely neglects such effects, the cumulant expansion can, to some extent, take them into account.

Finally, it should be mentioned that, as long as one represents a fractured rock by a network of channel- or disk-shaped features, the EMA can be used for estimating its permeability. In fact, Hestir and Long (1990) used the EMA for estimating the conductivity of two-dimensional fracture networks.

3. Position-space renormalization group and renormalized EMA

The main assumption behind any EMA is that fluctuations in the potential field are small. However, if the fluctuations are large, as in a fractal porous medium or one that is near its p_c or a macroscopically heterogeneous medium in which there is a broad distribution of permeabilities, the EMA breaks down and loses its accuracy. In such cases, a position-space renormalization-group (PSRG) method is more appropriate because this method first performs a certain amount of averaging and takes into account the properties of the pre-averaged medium. It can also predict nonanalytic scaling laws for transport properties near p_c , which is a distinct advantage over the EMA, which always predicts a linear relation for such properties. We describe the PSRG method for a random-network model of pore space. Its generalizations to other more complex systems will be clear.

Consider, for example, a square or a cubic network in which each bond is conducting with probability p . The idea in any PSRG method is that, since our network is so large that we cannot calculate its properties exactly, we partition it into $b \times b$ or $b \times b \times b$ cells, where b is the number of bonds in any direction, and calculate their

properties, which are hopefully representative of the properties of the original network. The shape of the cell can be selected arbitrarily, but it should be chosen in such a way that it preserves, as much as possible, the properties of the network. For example, an important topological property of a square network is that it is *self-dual*. The dual of a two-dimensional network is obtained by connecting the centers of the neighboring polygons that constitute the network. For example, if we connect the centers of the hexagons in a hexagonal network, we obtain a triangular network. Thus these networks are the dual of each other. However, if we connect the centers of the squares in a square network, we again obtain a square network, and thus this network is self-dual. This self-duality plays an important role in the percolation properties of a square network, and thus it is desirable to partition the network into self-dual cells. Figure 29(a) shows an example of such $b=2$ cells for square and cubic networks, where the two-dimensional cell is self-dual.

The next step in a PSRG method is to replace each cell with one bond in each principal direction. If in the original network each bond is conducting with probability p , then the bonds that replace the cells would be conducting with probability $p' = R(p)$; this is also shown in Fig. 29(a). $R(p)$ is called the *renormalization-group transformation* and is the *sum* of the probabilities of *all* conducting configurations of the renormalization-group cell. It is obtained as follows. Since we are interested in percolation and transport in our network, and since the renormalization-group cell is supposed to represent our network, we solve the percolation and transport problem in each cell by applying a fixed potential difference across the cell in a given direction. For example, as far as percolation and transport are concerned, the 2×2 cell of Fig. 29(a) is equivalent to the circuit shown in Fig. 29(b), usually called the Wheatstone bridge. Thus for this cell we need only deal with five bonds, and for the $2 \times 2 \times 2$ cell we can construct an equivalent 12-bond circuit, shown in Fig. 29(b). To obtain $R(p)$, we find all conducting configurations of such circuits, with some bonds conducting and some insulating (missing). Thus for the 2×2 cell we obtain

$$p' = R(p) = p^5 + 5p^4q + 8p^3q^2 + 2p^2q^3, \quad (5.38)$$

where $q = 1 - p$. It is easy to see how this equation is obtained: There is only one conducting cell configuration with all five bonds conducting (probability p^5), five conducting configurations with four bonds conducting and one bond insulating (probability $5p^4q$), and so on.

As discussed in Sec. II, the sample-spanning cluster at p_c is self-similar. This means that the renormalization-group transformation should remain invariant at p_c . The same thing should be true at $p=1$ and $p=0$, because under any transformation full and empty networks should be transformed to full and empty networks again. The points $p=0$, 1, and p_c are called the *fixed points* of the transformation. Since the renormalization-group transformation should not change anything at these points,

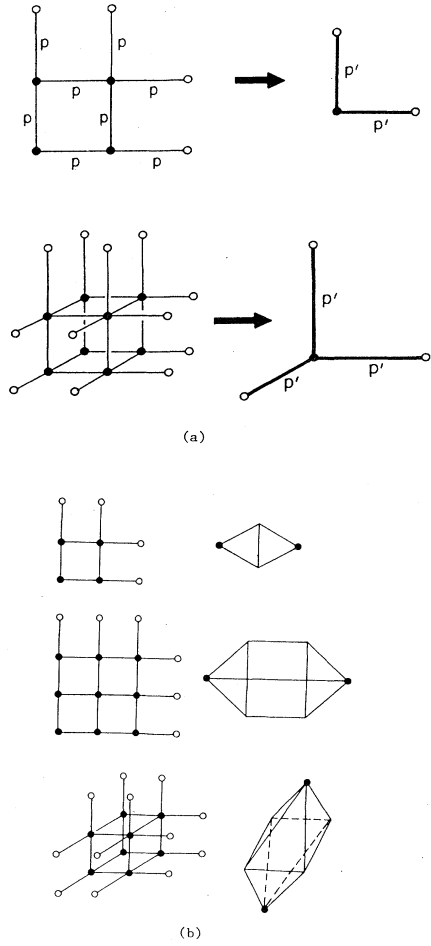


FIG. 29. (a) Transformation of renormalization-group cells in two and three dimensions. (b) The equivalent circuits for various two- and three-dimensional renormalization-group cells.

the implication is that at the fixed points the probability of having a conducting bond in the cell (p) and of having a bond in the renormalized cell [$p' = R(p)$] should be the same. Thus the fixed points should be the solution of the polynomial equation

$$p = R(p), \quad (5.39)$$

and indeed this equation usually has three roots, $p=0$, $p=1$, and $p=p^*$, where p^* is the renormalization-group transformation prediction for p_c . For the renormalization-group cells of Fig. 29 we obtain $p^*=1/2$ for both 2×2 and 3×3 cells, which is an exact result (see Table II). In fact, it can be shown (Bernasconi, 1978) that the renormalization-group transformation for such cells for any b predicts $p_c=1/2$. For the $2\times 2\times 2$ cell we obtain $p^*\simeq 0.208$, which should be compared with the numerical estimate $p_c\simeq 0.249$. The correlation length exponent ν_p is estimated from

$$\nu_p = \frac{\ln b}{\ln \lambda_p}, \quad (5.40)$$

where $\lambda_p = dR(p)/dp$, evaluated at $p=p^*$. Thus for the 2×2 and 3×3 cells we obtain $\nu_p\simeq 1.43$ and 1.38 , respectively, which should be compared with the exact value $\nu_p=4/3$. For the $2\times 2\times 2$ cell we obtain $\nu_p\simeq 1.03$, which should be compared with the numerical estimate $\nu_p\simeq 0.88$. We now discuss the PSRG approach for calculating the conductivity of a random network.

In the PSRG approach for calculating the conductivity of a random network, one starts with a probability distribution $h_0(g_p)$ for the bond conductances of the renormalization-group cell and replaces it with a new distribution $h_1(g_p)$, the probability distribution for the conductance of the renormalized bond, which is calculated by determining the equivalent conductance of the renormalization-group cell. Thus one obtains a recursion relation relating $h_1(g_p)$ to $h_0(g_p)$:

$$h_1(g_p) = \int h_0(g_1)dg_1 h_0(g_2)dg_2 \cdots h_0(g_n)dg_n \delta(g_p - g'), \quad (5.41)$$

where g_1, \dots, g_n are the conductances of the n bonds of the cell and g' is the equivalent conductance of the cell. For example, for the five-bond cell of Fig. 29, one has

$$g' = \frac{g_1(g_2g_3 + g_2g_4 + g_3g_4) + g_5(g_1 + g_2)(g_3 + g_4)}{(g_1 + g_4)(g_2 + g_3) + g_5(g_1 + g_2 + g_3 + g_4)}. \quad (5.42)$$

For example, it is easy to show that if

$$h_0(g_p) = (1-p)\delta(g_p) + p\delta(g_p - g_0), \quad (5.43)$$

then for the renormalization-group cell of Fig. 29, Eq. (5.41) will yield

$$\begin{aligned} h_1(g_p) &= [1 - R(p)]\delta(g_p) + 2p^3q^2\delta(g_p - \frac{1}{3}g_0) \\ &\quad + 2p^2(1+2p)q^2\delta(g_p - \frac{1}{2}g_0) \\ &\quad + 4p^3q\delta(g_p - \frac{3}{5}g_0) + p^4\delta(g_p - g_0), \end{aligned} \quad (5.44)$$

which is already more complex than Eq. (5.43). One iterates Eq. (5.41) to obtain a new distribution $h_2(g_p)$ by substituting $h_1(g_p)$ into the right-hand side of Eq. (5.41). The iteration process continues until a distribution $h_\infty(g_p)$ is obtained, the shape of which does not change under further iterations. This is the *fixed-point* distribution, and the conductance of the original network is simply an average of this distribution. However, it is difficult to iterate Eq. (5.41) analytically many times. The common practice is to replace the distribution after iteration i by an “optimized” distribution $h_i^o(g_p)$, which can mimic closely the properties of $h_i(g_p)$. The optimized $h_i^o(g_p)$ is usually taken to have the form

$$h_i^o(g_p) = [1 - R(p)]\delta(g_p) + R(p)\delta[g_p - g^o(p)], \quad (5.45)$$

where $g^o(p)$ is an “optimized” conductance. Various approximate schemes have been proposed in the past for determining $g^o(p)$, e.g., $g^o(p)$ is taken to be the arithmetic, or geometric or harmonic average of $h_i(g_p)$. Once

$g^o(p)$ is calculated, Eq. (5.41) is iterated again, a new distribution $h_2(g_p)$ and its optimized form $h_2^o(g_p)$ are determined, and so on. In practice, after a few iterations even a broad $h_o(g_p)$ may converge quickly to a stable distribution whose shape does not change under further rescaling, in which case $\lambda_c h_{n+1}(\lambda_c g_p) \approx h_n(g_p)$, where λ_c is a constant, and $\mu = v \ln \lambda_c / \ln b$, which in the case of the 2×2 RG cell of Fig. 29 yields $\mu \approx 1.32$, in excellent agreement with the accepted value $\mu \approx 1.3$ (see Table III).

This method can be used for estimating the permeability of a microscopically disordered porous medium modeled by a random network. The PSRG method for calculating the effective permeability of macroscopically heterogeneous media is similar to the above procedure. In this case one partitions the system into cells of equal sizes, each one of which is assigned an equivalent permeability, selected from its distribution. Then, as in the above procedure, a renormalized permeability distribution is constructed using Eq. (5.41) and a renormalization-group cell. A Monte Carlo sampling is used to select the permeability of each cell from the joint probability distribution of the cells' permeabilities. The sampling and the iteration process are continued until a satisfactory representation of the permeability distribution is obtained. King (1989) used this method for calculating the permeability of macroscopically heterogeneous porous media.

In the condensed-matter literature, Young and Stinchcombe (1975) were the first to use PSRG methods for calculating percolation properties of random networks. Stinchcombe and Watson (1976) were the first to use these methods for calculating the electrical conductivity of percolation networks. However, in a simultaneous and little noted paper, Madden (1976) used the same ideas for calculating transport properties of porous media modeled by random networks, although he did not call his method a renormalization approach. Many authors have proposed variants of PSRG methods for calculating both geometrical and transport properties of percolation networks and other disordered systems (Straley, 1977a; Payandeh, 1980; Reynolds *et al.*, 1980; Tsallis *et al.*, 1983; Sahimi *et al.*, 1984; Sahimi, 1988a). Stanley *et al.* (1982) and Family (1984) reviewed most of the literature on this subject.

PSRG methods are usually very accurate for two-dimensional systems and are flexible enough to be used for anisotropic and time-dependent systems, although the treatment of the latter case is considerably more complex. However, they have two drawbacks for three-dimensional systems. The first is that the results for a percolating network with *any* type of $b=2$ cell are not accurate. For example, a three-dimensional version of the renormalization group cell of Fig. 29 yields $\mu \approx 2.2$ for the cubic network, which is in considerable error (Table III). Moreover, in the treatment of the conductivity problem, even after the first iteration of Eq. (5.41), the renormalized conductance distribution $h_1(g_p)$ is very complex; if we start with distribution (5.43), $h_1(g_p)$ will

have *seventy-three* components of the form $\delta(g_p - a_i)$, $i=1-73$. Hence analytical calculation of $h_2(g_p)$ is practically impossible. The second drawback is that even for a $b=3$ cell, the renormalization-group transformation cannot be calculated analytically, because the number of possible configurations is of the order of 3×10^{11} . Thus one has to resort to a Monte Carlo renormalization-group method (Reynolds *et al.*, 1980), which is not any simpler than the simple Monte Carlo method itself.

In order to circumvent these difficulties for three-dimensional networks, Sahimi *et al.* (Sahimi, Hughes, *et al.*, 1983a; Sahimi, Scriven, and Davis, 1984) proposed a new method that combines the EMA and PSRG methods and is called the renormalized effective-medium approximation (REMA). The idea is that the effective-medium approximation is very accurate away from p_c . When we rescale a cell, the renormalized cell is farther away from p_c than the original cell (because its correlation length is reduced by a factor $1/b$). One may therefore use an EMA with the renormalized cell (or network) instead of the original network. That is, the pore conductance distribution that one uses in Eq. (5.24) should be $h_1(g_p)$ instead of $h_0(g_p)$. This renormalized effective-medium approximation markedly improves the accuracy of the results. For example, with the three-dimensional renormalization-group cell of Fig. 29, one obtains $p_{cb}^* \approx 0.265$, which is only 7% larger than the accepted value $p_{cb} \approx 0.249$ for the cubic network (see Table II). In general, if $R(p)$ is the renormalization-group transformation, REMA predicts that p_{cb} is the root of $R(p_{cb}) = 2/Z$ (instead of $p_{cb} = 2/Z$, which is the EMA prediction, and $R(p_{cb}) = p_{cb}$, which is the PSRG's estimate). Using REMA, Sahimi *et al.* (1983a, 1984) and Sahimi (1988a) obtained very accurate predictions of transport properties of various two- and three-dimensional networks.

Finally, it should be pointed out that, as long as a fractured rock is represented by a network of fractures, PSRG methods can be used for estimating its effective properties. Even if a fractured rock is represented by a random continuum of disks or ellipses, the EMA and PSRG methods can still be used; see Hori and Yonezawa (1977) and Gawlinski and Redner (1983) for the development of EMA and PSRG methods for continuum models.

4. Field-theoretic and perturbation methods

It has long been recognized that disorder is equivalent to a field. Thus field-theoretic methods can provide a means of estimating transport properties of disordered media. This fact has been exploited in the condensed-matter literature for a long time. However, its use for flow phenomena in porous media is relatively new and has been attempted only recently. P. R. King (1987a) was the first to develop a field-theoretic approach to estimating the permeability of macroscopically heterogeneous porous media.

For single-phase steady flow, Darcy's law together

with the equation of continuity yield

$$\nabla \cdot k \nabla P = 0, \quad (5.46)$$

where gravity has been neglected. Without loss of generality, the permeability can be taken to be isotropic, since the permeability tensor \mathbf{K} [see Eq. (5.15)] is real and symmetric and therefore can be diagonalized by using normal coordinates, which may be rescaled to ensure that it is isotropic. We may define a Green function G for Eq. (5.44) by

$$\nabla_r \cdot k(\mathbf{r}) \nabla G(\mathbf{r}, \mathbf{r}') = \delta(\mathbf{r} - \mathbf{r}'). \quad (5.47)$$

If we use the Neumann condition of constant flux and the Green theorem, we obtain

$$P(\mathbf{r}) = \mathbf{v} \cdot \int G(\mathbf{r}, \mathbf{r}') d\mathbf{S}'. \quad (5.48)$$

Suppose that we have a homogeneous porous medium with permeability k_0 . For this system the Green function is given by

$$k_0 \nabla_r^2 G_0(\mathbf{r}, \mathbf{r}') = \delta(\mathbf{r} - \mathbf{r}'). \quad (5.49)$$

Thus if we write $k(\mathbf{r}) = k_0 + \epsilon(\mathbf{r})$, where $\epsilon(\mathbf{r})$ is the perturbation, we obtain

$$k_0 \nabla^2 G = \delta(\mathbf{r} - \mathbf{r}') - \nabla \cdot \epsilon \nabla G. \quad (5.50)$$

We now recognize that G_0 is the inverse of the operator $k_0 \nabla^2$ and exploit this to rewrite Eq. (5.50) as an integral equation,

$$G(\mathbf{r}, \mathbf{r}') = G_0(\mathbf{r}, \mathbf{r}') - \int G_0(\mathbf{r}, \mathbf{r}'') k_0 \nabla_{r''} \cdot \epsilon(\mathbf{r}'') G(\mathbf{r}'', \mathbf{r}'') d\mathbf{r}''. \quad (5.51)$$

If we take the Fourier transform of Eq. (5.51), we obtain

$$G(\mathbf{i}, \mathbf{j}) = G_0(\mathbf{i}) \delta(\mathbf{i} + \mathbf{j}) + G_0(\mathbf{i}) \int M(\mathbf{i}; \mathbf{l}, \mathbf{m}) \epsilon(\mathbf{l}) G(\mathbf{m}, \mathbf{i}) d\mathbf{l} d\mathbf{m}, \quad (5.52)$$

where

$$M(\mathbf{i}; \mathbf{l}, \mathbf{m}) = k_0[(\mathbf{l} + \mathbf{m}) \cdot \mathbf{m}] \delta(\mathbf{l} + \mathbf{m} - \mathbf{i}). \quad (5.53)$$

This provides an iterative scheme by which a perturbation expansion for the Green function may be developed. Such expansions can be truncated at any order and have been tried by several authors (see, for example, Gutjahr *et al.*, 1978, and references therein). However, what one is interested in is not the permeability itself but its average. Hence one has to average the perturbation series, as was done by King (1987a). If one is to average the n th term of Eq. (5.51), one needs to know the n th moment of $\epsilon(\mathbf{r})$. Since polarization diagrams (of the  type) are absent in King's perturbation expansion, his field theory is equivalent to a zero-state Potts model. Having calculated the average Green function, one can estimate the effective permeability, which can provide valuable information about the mean pressure field in the medium.

From Eq. (5.48) we can obtain

$$\langle P(\mathbf{r}) \rangle = \frac{\mathbf{v}}{\langle k \rangle} \cdot \int |\mathbf{r} - \mathbf{r}'|^{2-d} d\mathbf{S}', \quad (5.54)$$

where $\langle k \rangle$ is the average permeability and $|\mathbf{r} - \mathbf{r}'|^{2-d}$ is the Green function for this problem in d dimensions. We should keep in mind, however, that $G(\mathbf{r}, \mathbf{r}') = \ln |\mathbf{r} - \mathbf{r}'|$ in two dimensions.

King (1987a) showed that this field-theoretic method can reproduce several known exact results. For example, it is known (Matheron, 1967) that, if the permeability distribution is log-normal, then the exact effective permeability in two dimensions is the geometric mean of the distribution, which the field-theoretic model also reproduces. Several other results obtained by variants of perturbation expansions (Bakr *et al.*, 1978; Dagan, 1981, 1982a, 1982b; Gutjahr and Gelhar, 1981; Mizell *et al.*, 1982) can also be reproduced by this formulation.

The main condition for the validity of this method is that the Green function $G(\mathbf{r}, \mathbf{r}')$ be analytic around $G_0(\mathbf{r}, \mathbf{r}')$, i.e., $G(\mathbf{r}, \mathbf{r}')$ must have a Taylor-series expansion. This condition is satisfied if the perturbed system is qualitatively similar to the unperturbed one. The condition for this is that the porous medium not be close to its p_c , where the unperturbed system is not similar to the true, perturbed medium. For single-phase flow through a porous medium, percolation does not play any role (unless the heterogeneities are broadly distributed), and thus this approach retains its validity.

5. Percolation methods

Most of the methods that have been reviewed so far are not exact and provide only approximate estimates of k and σ . The exact results discussed above are mostly applicable to spatially periodic media, which are not very realistic models of disordered porous media. The only exception to this is the exact solution of electrical conduction on a Bethe lattice (Stinchcombe, 1974; Straley, 1977b). For this solution, it is shown that near p_c , $\sigma \sim (p - p_c)^3$, i.e., $\mu = 3$. Thus this conductivity of the Bethe networks would provide a poor estimate of σ for three-dimensional networks (for which $\mu \approx 2$). However, there is a happy coincidence here! The microscopic conductivity σ_m (not the macroscopic conductivity σ) of a Bethe lattice obeys the following scaling law near p_c :

$$\sigma_m \sim (p - p_c)^2. \quad (5.55)$$

Since the critical exponent μ for the macroscopic conductivity of three-dimensional systems is also about 2 (see Table III), and in fact it has been conjectured to be exactly 2 (Gingold and Lobb, 1990), Eq. (5.55) indicates that the exact solution of Stinchcombe (1974) for σ_m on a Bethe lattice may be used for estimating the macroscopic conductivity of three-dimensional networks. For example, for a cubic network, $p_{cb} \approx 0.249$ (Table II), and if we use a Bethe lattice of coordination number 5, then $p_{cb} = 1/(5-1) = 0.25$, which is less than 0.1% larger than

that of the cubic network. Thus a Bethe lattice of coordination number 5 can be used for estimating the conductivity of a cubic network. Figure 30 compares the macroscopic conductivity σ of a cubic network obtained by Monte Carlo calculations and the microscopic conductivity σ_m of a Bethe lattice of coordination number 5. It is evident that the difference between the two, if any, cannot be detected. This idea was first used by Heiba *et al.* (1982).

Another percolation method of estimating the transport properties of disordered media was developed by Ambegaokar, Halperin, and Langer (AHL) in 1971. These authors argued that transport in a disordered medium with a broad distribution of conductances is dominated by those conductances whose magnitudes are larger than some characteristic value g_c , which is the smallest conductance such that the set of conductances $\{g_p | g_p > g_c\}$ forms a conducting sample-spanning cluster. Therefore transport in a disordered medium with a broad conductance distribution reduces to a percolation problem with threshold value g_c . Shante (1977) and Kirkpatrick (1979) extended these ideas by assigning all local conductances with values $g_p \geq g_c$ the value g_c , and setting all conductances with values $g_p < g_c$ to be zero (since the contribution of such bonds is very small). They then arrived at a trial solution for the sample conductance of the form

$$g_e = ag_c [p(g_c) - p_c]^\mu, \quad (5.56)$$

which is just what we described in Sec. II. Here $p(g_c)$ denotes the probability that a given conductance is greater than or equal to g_c , and a is a constant. Equation (5.56) is now maximized with respect to g_c to obtain an estimate of g_c and thus g_e . Computer simulations of Berman *et al.* (1986) for two-dimensional networks with various conductance distributions (Gaussian, log-normal,

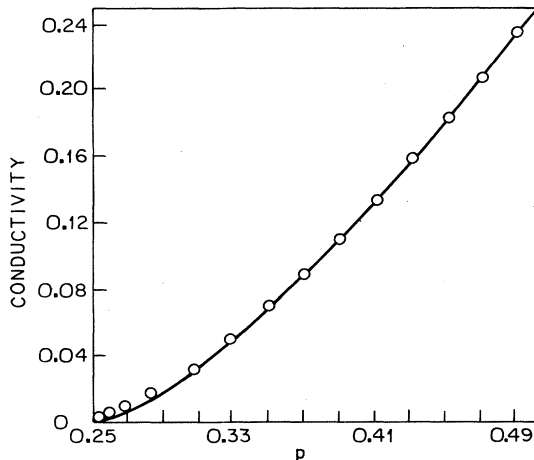


FIG. 30. Comparison of *macroscopic* conductivity of a cubic network, obtained by a Monte Carlo method, and *microscopic* conductivity of a Bethe lattice with $Z=5$.

flat, and cubic) confirmed the quantities accuracy of the AHL scheme even for relatively narrow distributions. Therefore calculating the effective transport properties of disordered media in which percolation does not seem to play any role can be reduced to determining the same properties for a percolating system. This indicates the broad applicability of percolation theory.

Katz and Thompson (1986, 1987) extended the ideas of Ambegaokar, Halperin, and Langer to estimate the permeability and electrical conductivity of porous media. In a porous medium the local hydraulic conductance is a function of the length l . Therefore the critical conductance g_c defines a characteristic length l_c . Since both flow and electrical conduction problems belong to the class of scalar percolation problems, the length that signals the percolation threshold in the flow problem also defines the threshold in the electrical conductivity problem. Thus we rewrite Eq. (5.56) as

$$g_e = \phi g_c(l)[p(l) - p_c]^\mu, \quad (5.57)$$

where the porosity ϕ ensures a proper normalization of the fluid or the electric-charge density. The function $g_c(l)$ is equal to $c_f l^3$ for the flow problem and $c_e l$ for the conduction problem. For appropriate choices of the function $p(l)$, the conductance $g_e(l)$ achieves a maximum for some $l_{\max} \leq l_c$. In general l_{\max}^f for the flow problem is different from l_{\max}^c for the conduction problem, because the transport paths have different weights for the two problems.

If $p(l)$ allows for a maximum in the conductance which occurs for $l_{\max} \leq l_c$, then we can write

$$l_{\max}^f = l_c - \Delta l_f = l_c \{1 - \mu/[1 + \mu + l_c \mu p''(l_c)/p'(l_c)]\}, \quad (5.58)$$

$$l_{\max}^c = l_c - \Delta l_c = l_c \{1 - \mu/[3 + \mu + l_c \mu p''(l_c)/p'(l_c)]\}. \quad (5.59)$$

If the pore-size distribution of the medium is very broad, then $l_c \mu p''(l_c)/p'(l_c) \ll 1$, and Eqs. (5.58) and (5.59) reduce to

$$l_{\max}^f = l_c [1 - \mu/(1 + \mu)] \approx \frac{1}{3} l_c, \quad (5.60)$$

$$l_{\max}^c = l_c [1 - \mu/(3 + \mu)] \approx \frac{3}{5} l_c. \quad (5.61)$$

Using these, we can establish a relation between σ and k . Writing

$$\sigma = a_1 \phi [\phi(l_{\max}^c) - p_c]^\mu \quad (5.62)$$

and

$$k = a_2 \phi (l_{\max}^f)^2 [p(l_{\max}^f) - p_c]^\mu, \quad (5.63)$$

we obtain to first order in Δl_c or in Δl_f

$$p(l_{\max}^c) - p_c = -\Delta l_f c p'(l_c). \quad (5.64)$$

To obtain the constants a_1 and a_2 , Katz and Thompson (1986) assumed that at a local level the rock conductivity

is σ_f , the conductivity of the fluid (usually brine) that saturates the pore space, and that the local pore geometry is cylindrical. These imply that $a_1 = \sigma_f$ and $a_2 = 1/32$. Therefore one obtains

$$k = a_3 l_c^2 \sigma / \sigma_f , \quad (5.65)$$

where $a_3 = 1/226$. A similar argument leads to (Katz and Thompson, 1987)

$$\frac{\sigma}{\sigma_f} = \frac{l_c^c}{l_c} \phi S(l_c^c) , \quad (5.66)$$

where $S(l_c^c)$ is the volume fraction (saturation) of connected pore space involving pore widths of size l_c^c and larger.

Equations (5.65) and (5.66) involve no adjustable parameters. Every parameter is fixed and precisely defined. To obtain the characteristic length l_c , Katz and Thompson (1986, 1987) proposed to use mercury porosimetry, discussed in Sec. III.C.1. As we discussed there, mercury porosimetry is a percolation process. Consider a typical mercury porosimetry curve in which the pore volume in the injected mercury is obtained as a function of the pressure; see Fig. 31. As can be seen, in the initial portion of the curve the curvature is positive. This portion is obtained before a sample-spanning cluster of pores, filled with mercury, has been formed. There is also an inflection point beyond which the pore volume increases rapidly with the pressure. This inflection point signals the formation of the sample-spanning cluster. Therefore from the Washburn equation [Eq. (3.4)] we must have $l \geq -4\sigma_{mv} \cos\theta / P_i$, where P_i is the pressure at the inflection point. Then $l_c = -4\sigma_{mv} \cos\theta / P_i$ defines the characteristic length l_c .

Figure 32 compares the logarithm of the permeability for a set of sandstones, calculated using Eq. (5.65), with the measured values. The dashed lines mark a factor of 2. No adjustable parameter has been used, and the agreement between predictions and theory appears to be very good. Note that, once l_c is determined from a mercury

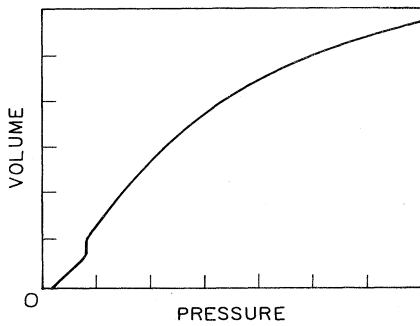


FIG. 31. Volume-pressure curve during a typical mercury porosimetry experiment. The pressure at the jump defines l_c (see the text) (from Katz and Thompson, 1986).

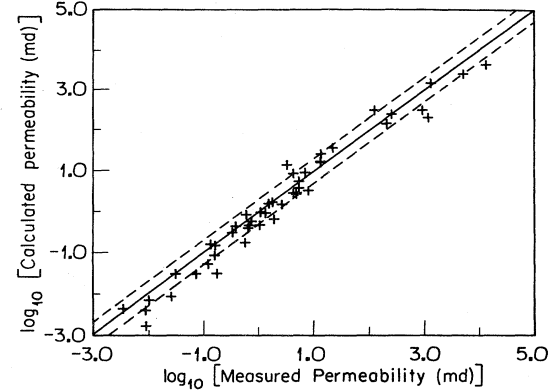


FIG. 32. Comparison of predicted (solid line) and measured (\times) permeabilities. Dashed lines mark a factor of two deviations from the predicted values (from Katz and Thompson, 1986).

injection curve, the saturation $S(l_c^c)$ can also be determined immediately. Figure 33 compares the calculated and measured σ/σ_f . As in the case of permeability, no adjustable parameter has been used for calculating σ/σ_f . Katz and Thompson (1986, 1987) contend that l_c can be estimated from mercury injection curves with an error of at most 15%. However, the error in the constant 1/226 in Eq. (5.65) can be as large as a factor of 2. We emphasize that Eqs. (5.65) and (5.66) are *not* in general exact, but appear to provide very accurate estimates of k and σ . Note that the exponent μ can take on its value for continuum percolation, discussed in Sec. II. Of course, this depends on the structure of the pore space.

Some related work should be mentioned here. Swanson (1981) had already recognized that during mercury injection (or flow of any nonwetting fluid in a porous medium) large pores dominate the flow paths, and that the inflection point in the pore volume-pressure curve signals the formation of a sample-spanning cluster. Thus he postulated a relation between the permeability and the capillary pressure curve. He maximized the product of

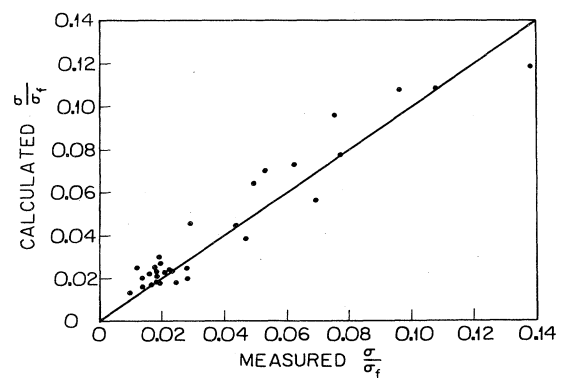


FIG. 33. Comparison of predicted (line) and measured electrical conductivity of porous media (from Katz and Thompson, 1987).

length and saturation, both of which can be estimated from the mercury injection curve, and obtained

$$l \sim (S^2 l^2)_{\max}, \quad (5.67)$$

where l_{\max} is a length scale very similar, both qualitatively and numerically, to the length scale l_c introduced by Katz and Thompson (1986, 1987). The agreement between this correlation and the experimental data is very good, which is not entirely surprising given the similarity between Swanson's l_{\max} (not to be confused with Katz and Thompson's l_{\max}) and l_c . However, it should be noted that the transport paths considered by Swanson were appropriate for electrical conduction, not the fluid flow problem. Banavar and Johnson (1987) and Le Doussal (1989) calculated the coefficient a_3 in Eq. (5.65) slightly differently from Katz and Thompson (1986, 1987). For example, Banavar and Johnson (1987) gave $a_3 \approx 7.68 \times 10^{-3}$, which should be compared with Katz and Thompson's value, $a_3 = 1/226 \approx 4.42 \times 10^{-3}$. However, Banavar and Johnson's predictions are still within the error bars of Fig. 32. Nyame and Ilbston (1980) used an empirical parameter similar to l_c to describe permeability in cement paste. Hagiwara (1984) used Archie's law to replace S^2 in Eq. (5.67) with σ to obtain $k \sim \sigma l^2$, which appears again to agree with the data.

Finally, the ideas of Ambegaokar, Halperin, and Langer and of Katz and Thompson can also be extended for calculating the permeability of fractured rocks. Indeed, Charlaix, Guyon, and Roux (1987) used arguments very similar to those of Katz and Thompson to calculate the permeability of fracture networks with a broad distribution of fracture apertures. They can also be used for obtaining an estimate of the permeability of a porous medium saturated by a *non-Newtonian* fluid (Sahimi, 1993a).

6. Random-walk methods and network simulations

The methods discussed so far are analytical techniques by which exact or approximate expressions for k and σ of a porous medium are derived. We now discuss two *numerical* methods which are in some sense exact because the quantities of interest can, in principle, be obtained to any desired or affordable accuracy.

The first method is based on random walks. As discussed in Sec. II, D_e (and σ) can be calculated from the relation between the mean-square displacement of a random walker and its effective diffusivity, $\langle r^2(t) \rangle = 2dD_e t$. The first application of this idea for determining transport properties of composite or disordered systems appeared in a paper of Haji-Sheikh and Sparrow (1966), who studied heat conduction in a composite solid. Since this paper, many authors have used random-walk methods to study transport in disordered media. In the context of percolation problem, Brandt (1975) appears to have been the first to use this method to study the diffusion of noble gases in glasses. But the method was popularized by de Gennes (1976), who made an analogy

between the motion of a random walker in a disordered medium and that of an ant in a labyrinth. Mitescu and Roussenq (1976) followed de Gennes' idea and performed extensive simulations on percolation clusters. Havlin and Ben-Avraham (1987), Haus and Kehr (1987), and Hughes (1993) provide extensive reviews of this subject. Bunde *et al.* (1985) considered a general two-component mixture, in which both phases allow transport, and formulated a random-walk model for calculating the conductivity of such a mixture. Using vectorization on a supercomputer and multispin coding, one can make the computer algorithm for simulating random walks in a disordered medium highly efficient; see Sahimi and Stauffer (1991) for details.

One can facilitate the random-walk simulations by using *first-passage-time* equations. The idea is that, if a random walker moves in a homogeneous region of the system, there is no need to spend unnecessary time to simulate detailed motion of the walker. The walker can take large steps to pass quickly through a homogeneous region and arrive at the interface between the two phases. The necessary time for taking large steps can be calculated *analytically*. Thus unlike conventional simulations in random networks, in which the length of each step of the walk is only one lattice bond and each time a step is taken the time is increased by one unit, in first-passage-time simulations the walker takes long steps (providing its step does not take it outside of a phase), and the time is increased by an amount appropriate to that step. This basic idea was first used by Sahimi, Heiba, *et al.* (1982) for simulating hydrodynamic dispersion in a porous medium by a random-walk method; their work will be discussed in Sec. VI. In the context of calculating the effective conductivity, diffusivity, and reaction rate of a disordered medium, Zheng and Chiew (1989) and Kim and Torquato (1990, 1991) appear to be the first to have used this method. Let us now discuss briefly the first-passage-time simulation for conductivity and diffusivity.

Consider a multiphase system that consists of n phases with conductivities $\sigma_1, \dots, \sigma_n$ and volume fractions ϕ_1, \dots, ϕ_n . In a first-passage-time simulation one constructs the largest (imaginary) concentric sphere of radius R around a randomly chosen point in phase i , which just touches the multiphase interface; suppose that the random walker is initially at the center of the imaginary sphere. The mean time τ_m for the particle to reach a randomly selected point on the surface of the sphere is $\tau_m(R) = R^2 / (2d\sigma_i)$, where d is the dimensionality of the system. This time is recorded, and the process of construction of the sphere and the time a point on its surface is reached is repeated, until the random walker comes within a very small distance of the multiphase interface. One then computes the mean time necessary for crossing the boundary τ_b and the probability of crossing the boundary, which is dependent upon the ratio of the conductivities of the two phases. If the random walker crosses the interface and enters a new phase, it finds itself in a new homogeneous phase, and therefore the process

of sphere construction is repeated. If the reference phase is taken to be phase 1, then the *overall* effective conductivity of the system is given by (Kim and Torquato, 1990)

$$\frac{\sigma}{\sigma_1} = \frac{\left\langle \sum_i \tau_{1m}(R_1) + \sum_j \tau_{1m}(R_j) \right\rangle}{\left\langle \sum_i \tau_m(R_i) + \sum_j \tau_b(R_j) \right\rangle}, \quad (5.68)$$

where $\tau_{1m}(R)$ is the mean first-passage (hitting) time for a walker in a homogeneous sphere of radius R , i denotes the number of phases j for paths crossing the interface, and $\langle \rangle$ denotes an average over all realizations. Equation (5.68) is valid in the limit of long times.

The first-passage-time simulation is particularly effective for simulating transport in continuum models of porous media. The efficiency of the method decreases, however, as the porosity of the pore space decreases, since the search for the construction of the imaginary sphere becomes time consuming. Near p_c the method is not efficient at all, and the vectorized version of the conventional random-walk simulation (Sahimi and Stauffer, 1991) should be used.

Random-walk methods are particularly useful for estimating the electrical conductivity of porous media made of an insulating granular matrix saturated with a conducting pore fluid such as brine. A traditional method such as the finite-element technique is notoriously time consuming for such porous media, since even if we use only 20^3 grains (a modest number), a very fine finite-element mesh with roughly 10^9 nodes would be required to solve the Laplace equation accurately, a prospect that is totally impractical. For this reason alone, random-walk methods are the preferred technique for estimating diffusivity and conductivity in porous media. Evans *et al.* (1980), Abbasi *et al.* (1983), Nakamo and Evans (1983), and Akanni *et al.* (1987) used random-walk methods to study both ordinary and Knudsen diffusion in a variety of porous media made of random dispersions of penetrating or nonpenetrating spheres (or disks in two dimensions). Likewise, Smith and Huijzen (1984) used the method to investigate Knudsen diffusion in a random assemblage of spheres. More recently, Schwartz and Banavar (1989) used random-walk simulations to calculate the electrical conductivity of the grain-consolidation model of Roberts and Schwartz (1985), discussed in Sec. III.B, with multisize particles. The results, shown in Fig. 34 in terms of the formation factor $F = \sigma_f / \sigma$, are in excellent agreement with the experimental data of Guyon *et al.* (1987) for sintered binary composites and with other experimental data for similar systems (Oger *et al.*, 1986). In practice, the grain particles are not usually spherical, but in a random-walk simulation the particles can have any shape. Schwartz, Banavar, and Halperin (1989) also calculated the electrical conductivities of a system that was originally a packing of spherical rubber grains but was exposed to a uniaxial pressure applied to deform the particles. To model the system they constructed an unconsolidated sphere

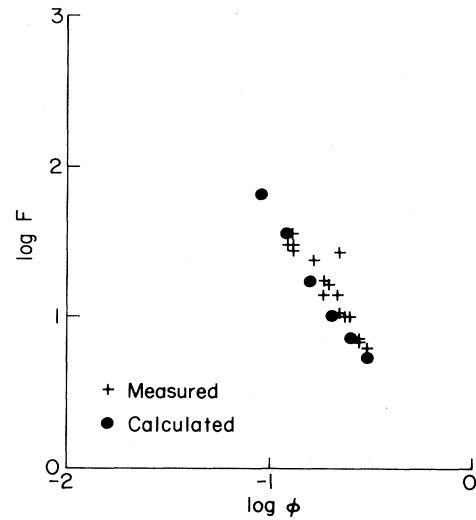


FIG. 34. Comparison of experimental data for formation factor F of sintered binary composites with random-walk simulation results. ϕ is the porosity of the system (from Schwartz and Banavar, 1989).

pack with a given particle distribution and then compressed the system in one direction by a given α_c . This resulted in a system of spheroidal grains, which were then allowed to grow along the three axes. Thus a sphere of radius R at (x_0, y_0, z_0) was replaced by the spheroid

$$\alpha_c^{2/3}(x - x_0)^2 + \alpha_c^{2/3}(y - y_0)^2 + \alpha_c^{-4/3}(z - z_0)^2 = R^2.$$

Note that the resulting system is no longer isotropic, and one has to calculate a conductivity tensor. The results of Schwartz, Banavar, and Halperin (1989) for this system were in good agreement with the measurements of McLachlan *et al.* (1987). In order to speed up random-walk simulations in porous media that have *macroscopic* inhomogeneities such as layering, Schwartz, Banavar, and Halperin (1989) introduced a *weak* bias in their simulations. This caused the random walker to sample the pore space more efficiently, because in the direction of the bias the travelled distance was proportional to N_s rather than $N_s^{1/2}$, where N_s is the number of steps. Although the ideas of biased diffusion for estimating the conductivity of inhomogeneous systems is rather old (Miller and Abrahams, 1960), Schwartz, Banavar, and Halperin (1989) appear to have been the first to apply it to inhomogeneous porous media.

In contrast with diffusivity and conductivity, there is *no* random-walk method for estimating the permeability of a porous medium, because there is no general relation between k , σ , and D_e . This is not totally surprising, as σ and D_e are calculated from the solution to the Laplace equation, which is a scalar equation, whereas k is calculated from the solution to the Stokes equation, a vector equation. Thus one cannot expect to have a general relation between these quantities. This lack of a general rela-

tion between a scalar and a vector system is well known in statistical physics. Effective properties of scalar percolation (for example, D_e or σ) are not, in general, related to those of vector percolation (for example, the elastic moduli). Properties of the Heisenberg and Ising models do not seem to be related at all.

In the absence of a random-walk algorithm, the main numerical means of estimating the permeability of a disordered pore space has been computer simulation using a network model. Of course the same networks can also be used for estimating the diffusivity and conductivity of the pore space. A pore-throat (bond) shape (for example, cylindrical, channel-like, etc.) and a flow regime (for example, laminar) are assumed. The flow problem is then solved analytically for a single pore, from which an expression is obtained for the flow rate q_i in pore i in terms of the pressure drop along the pore and the length and effective radius of the pore. In most cases the pressure drop across a pore body, where pore throats meet, is ignored. One then writes down a mass balance for each node, or each pore body, which simply means that the net flow rate reaching it is zero. Writing down such a mass balance for every interior node of the network results in a set of simultaneous equations for nodal pressures, from the solution of which the pressure field in the network, and thus the permeability, can be calculated. The boundary conditions are usually an imposed flow rate or pressure gradient in one direction and periodic boundary conditions in the other directions. One usually distributes the effective sizes of the pore throats according to a probability density function which represents the pore-size distribution.

Various versions of this network simulation have been used in the last four decades. As already mentioned, Owen (1952) appears to have been the first to do relatively extensive computations with a three-dimensional network of large pore bodies and very narrow pore throats, and estimated the formation factor. Fatt (1956) used a two-dimensional network of pore throats with distributed effective sizes and calculated permeability and relative permeabilities for two immiscible fluids. In the 1960s there were several works in which network models were used for calculating permeability, conductivity, and formation factors and for investigating the relationship between them (Fatt, 1960; Nicholson, 1968; Rink and Schopper, 1968; Greenberg and Brace, 1969; Weinbrandt and Fatt, 1969). This type of simulation was continued in the 1970s (Nicholson and Petropoulos, 1971, 1975, 1977; Shankland and Waff, 1974; Dullien, 1975), in the 1980s (Koplik, 1982; Koplik *et al.*, 1984; Seeburger and Nur, 1984; Doyen, 1988; Constantinides and Payatakes, 1989), and in the 1990s (David *et al.*, 1990). These works vary in the amount of detail included in the network model, the sizes of the networks used, and so on, but the essential idea behind all of them is the same as that discussed above. On the other hand, Bryant *et al.* (1991) developed a network model based on Finney's random close packing of equal spheres (Finney, 1968), without invoking any major assumption regarding the microstruc-

ture of the network, and calculated the permeability of the network. Chu and Ng (1989) used a somewhat similar method. Bryant *et al.* (1991) showed that the calculated permeability agrees well with the data, thus confirming the general validity of network models for calculating the permeability of a pore space. Finally, Adler (1985a, 1985b, 1985c, 1985d) studied flow and transport in a variety of deterministic fractal networks.

7. Relation between permeability and electrical conductivity

As discussed above, a general relation between the permeability and electrical conductivity of porous media probably does not exist. Although many empirical and semiempirical relations between k and σ have been proposed in the past, almost all of them "work" only for certain classes of porous media and not for other porous media. For example, although Wong *et al.* (1984) found that $\sigma \sim \phi^m$ and $k \sim \phi^{2m}$, this relation is restricted to their model and is not expected to hold for a general porous medium. Johnson *et al.* (1986), however, introduced a well-defined parameter Λ , defined by

$$\Lambda = 2 \frac{\int |E(\mathbf{r})|^2 dV_p}{\int |E(\mathbf{r})|^2 dS_p} \equiv \frac{V_p}{S_p}, \quad (5.69)$$

where $E(\mathbf{r})$ is the potential in the electrical conduction problem, and V_p and S_p are, respectively, the pore volume and the pore surface area. Note that V_p/S_p is a geometrical parameter that can be measured and is *independent* of any transport process. On the other hand, Λ is a dynamical property, defined for a specific problem, and cannot be measured by geometrical analysis alone. Since $E(\mathbf{r})$ can vanish in certain regions of the pore space (for example, an isolated region), Λ is roughly a measure of *dynamically connected* pores of the medium. Johnson *et al.* (1986) proposed that for three-dimensional porous media

$$k \simeq a_4 \frac{\Lambda^2}{8F} = a_4 \frac{\Lambda^2}{8} \frac{\sigma}{\sigma_f}, \quad (5.70)$$

where $a_4 = O(1)$. It should be said at the outset that, for the reasons discussed above, this relation [and Eqs. (5.65) and (5.66)] cannot *in general* be exact, although, because of the meaning of Λ , it is certainly appealing. If we compare Eq. (5.70) with Katz and Thompson's (1986) relation, Eq. (5.65), we obtain

$$a_3 l_c^2 = a_4 \frac{\Lambda^2}{8}. \quad (5.71)$$

This is immediately indicative of the possibility that Λ can be measured, since l_c is obtained from a mercury injection curve. Various authors have tested the validity of Eq. (5.70) (Banavar and Johnson, 1987; Straley *et al.*, 1987; Banavar *et al.*, 1988; Schwartz and Banavar, 1989; Saeger *et al.*, 1991; Kostek *et al.*, 1992), using a variety of numerical and analytical methods as well as experimental data for well-defined systems. Avellaneda and

Torquato (1991) investigated the relation between k and σ and derived the conditions under which an approximate relation between k and σ may be expected. It now appears that (Kostek *et al.*, 1992), unless the system contains two widely different relevant length scales, Eq. (5.70) would be very accurate.

8. Relation between permeability and nuclear magnetic resonance

Many years ago, Timur (1969) suggested that NMR may be used as a way of measuring k . This may seem to be impractical, since most of the fluid in a porous medium is stored in the pore bodies, whereas k and other transport properties are controlled by the pore throats. Various authors (for example, de Gennes, 1982; Banavar *et al.*, 1985) have investigated this issue. In particular, Kenyon *et al.* (1988) studied the relation between NMR and the permeability of 56 water-saturated sandstones. They found that the decay of proton magnetization $M_z(t)$ is described by a stretched exponential,

$$M_z(t) = m_0 \exp[-(t/T_1)^{\delta_1}], \quad (5.72)$$

and that $\log k$ shows a very strong correlation with $\log(\phi^4 T_1^2)$, where ϕ is the porosity of the system. Figure 35 presents the data plotted in this fashion. From this figure we obtain

$$k \sim (\phi^4 T_1^2)^{\delta_2}, \quad (5.73)$$

where $\delta_2 \approx 0.7$. Billardo *et al.* (1991) carried out NMR experiments on, and measured the permeabilities of, 44 different sandstones and found that Eq. (5.73) fits their data very well. Banavar and Schwartz (1987) investigat-

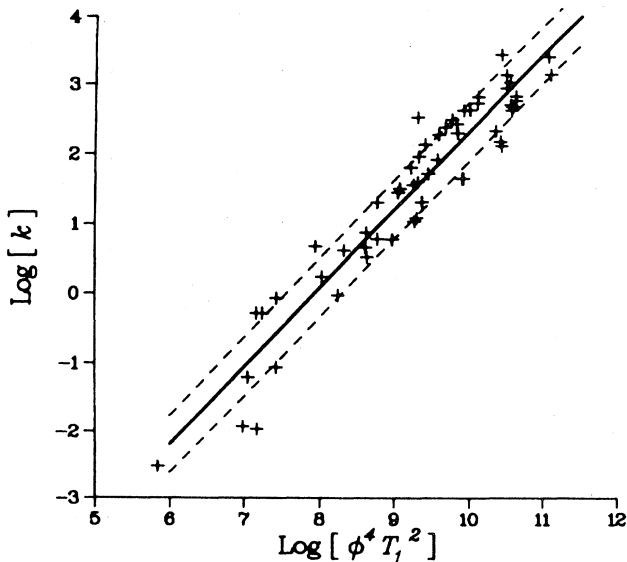


FIG. 35. Correlation of permeability k of sandstones with porosity ϕ and NMR relaxation time T_1 (from Kenyon *et al.*, 1988).

ed the same problem in the grain-consolidation model of Roberts and Schwartz (1985) and the shrinking-tube model of Wong *et al.* (1984) and reached the same conclusion. These results may seem surprising until we ask ourselves: What is the meaning of the relaxation time T_1 ? The protons in the hydrogen of water molecules carry nuclear magnetic moment, which enables them to align themselves with an externally applied field. But because water molecules at room temperature are thermally agitated, only a few of the protons actually align themselves with the external field; these are, however, detectable. If the external field is removed, the system will go back to its equilibrium configuration. The time that the system needs to do this is also the same as the time that it needs to build up its external magnetization after the external field has been applied. This time is usually denoted by T_1 , and is called spin-lattice relaxation time for protons. Why should T_1 be related to k ? Experiments show that, if one measures T_1 for water saturating a porous medium, one finds T_1 to be much smaller than it is for the same water in the bulk. This is because T_1 for water is affected strongly by surface relaxation mechanisms, and thus it is expected to be sensitive to the microstructure of the porous medium and provide insight into the structure of the pore space. Thus it appears likely that NMR can serve as a means of measuring k .

Thompson *et al.* (1989) used deuterium NMR to study sandstones, carbonate rocks, and synthetic porous samples. The reason for using deuterium instead of protons is that (Williams and Fung, 1982) it has a much smaller magnetic moment than protons. Thompson *et al.* measured T_{1p} , the longitudinal relaxation time in the rotating frame, found that the magnetization $M_z(t)$ obeys a stretched exponential similar to Eq. (5.70), with T_1 replaced by τ_{SE} , the corresponding stretched-exponential relaxation time. They argued that the parameter l_c [see Eqs. (5.58) and (5.71)] is proportional to a time scale τ_{NMR} , the NMR relaxation time. Their experimental data appear to be in complete agreement with this argument. Moreover, they showed that their data are fully consistent with

$$k \sim (T_{1p} \phi)^2 \sim (\tau_{NMR} \phi)^2, \quad (5.74)$$

which, in some sense, is consistent with Eq. (5.73), except that the exponents of T_{1p} (or τ_{NMR}) and T_1 in these equations are not the same. Thompson *et al.* (1989) mentioned that their data could be fitted with an equation similar to (5.73), but the quality of the resulting fit would be slightly worse than that provided by (5.74). They also showed that T_{1p} is proportional to the width of the pore-size distribution and also the water saturation in a partially saturated porous medium. Since NMR measurements can be made at depth in the earth with well-logging tools, they provide one of the few means of estimating *in situ* permeabilities and saturations.

9. Dynamic permeability

So far, we have discussed the static permeability of a porous medium. But what can we say about its dynamic permeability? If we measure dynamic permeability, can it provide extra information about the structure of the porous medium? Dynamic permeability $\tilde{k}(\omega)$ is defined by a generalized Darcy's law

$$\langle \mathbf{v}(\omega) \rangle = -\frac{\tilde{k}(\omega)}{\eta} \nabla P(\omega), \quad (5.75)$$

where ω is the frequency and $\nabla P(\omega) = \nabla P^{-i\omega t}$. This problem has been investigated by several groups. Au-riault *et al.* (1985) made measurements of $\tilde{k}(\omega)$ to test the validity of Eq. (5.75). Charlaix *et al.* (1988) also measured $\tilde{k}(\omega)$ for a variety of fused-glass beads and crushed glass in a frequency range of 0.1 Hz to 1 kHz. Johnson *et al.* (1987), Sheng and Zhou (1988), Zhou and Sheng (1989), Chapman and Higdon (1992), and Knackstedt *et al.* (1993) studied the problem theoretically and numerically. [Some errors in the studies of Sheng and Zhou were corrected by Chapman and Higdon (1992).] Let us summarize some of the more important results, most of which were derived by Johnson *et al.* (1987).

We obviously have to use Eq. (5.75) together with

$$T(\omega)\rho_f \frac{\partial \langle \mathbf{v} \rangle}{\partial t} = -\nabla P \quad (5.76)$$

as the starting point, where $T(\omega)$ is the frequency-dependent tortuosity (a dimensionless quantity) and ρ_f the density of the fluid. $T(\omega)$ and $\tilde{k}(\omega)$ are related to each other:

$$\tilde{k}(\omega) = \frac{i\eta\phi}{T(\omega)\omega\rho_f}, \quad (5.77)$$

where $i = (-1)^{1/2}$. As $\omega \rightarrow 0$, we have $\tilde{k}(\omega) \rightarrow k$, and

$$\lim_{\omega \rightarrow 0} T(\omega) = \frac{i\eta\phi}{k\omega\rho_f}. \quad (5.78)$$

Johnson *et al.* (1987) showed that in the high-frequency limit

$$\lim_{\omega \rightarrow \infty} T(\omega) = T_\infty + C_\infty (-i\omega)^{-1/2}, \quad (5.79)$$

where $C_\infty = kK_f/(\eta\phi)$, K_f being the bulk modulus of the fluid. Moreover, one has

$$T_\infty = \phi F, \quad (5.80)$$

for any porous medium, a result that is generally attributed to Lord Rayleigh. Johnson *et al.* (1987) also showed that in the high-frequency limit one has

$$\lim_{\omega \rightarrow \infty} T(\omega) = T_\infty \left[1 + \left(\frac{i\eta}{\omega\rho_f} \right)^{1/2} \frac{2}{\Lambda} \right], \quad (5.81)$$

$$\lim_{\omega \rightarrow \infty} \tilde{k}(\omega) = \frac{i\eta\phi}{T_\infty \omega\rho_f} \left[1 - \left(\frac{i\eta}{\omega\rho_f} \right)^{1/2} \frac{2}{\Lambda} \right] \quad (5.82)$$

[compare Eqs. (5.81) and (5.79)], so that the *high-*

frequency limit provides information on Λ and thus on k through Eq. (5.70). Moreover, Johnson *et al.* (1987) proposed that

$$T(\omega) = T_\infty + \frac{i\eta\phi}{\omega k \rho_f} \left[1 - \frac{4iT_\infty^2 k^2 \omega \rho_f}{\eta \Lambda^2 \phi^2} \right]^{1/2}, \quad (5.83)$$

$$\tilde{k}(\omega) = k \left[\left[1 - \frac{4iT_\infty^2 k^2 \omega \rho_f}{\eta \Lambda^2 \phi^2} \right]^{1/2} - \frac{iT_\infty k \omega \rho_f}{\eta \phi} \right]^{-1}. \quad (5.84)$$

These results, together with those of Sheng and Zhou and the experimental data of Charlaix *et al.* (1988), also indicate that, in general, $\tilde{k}(\omega)$ obeys the following scaling equation:

$$\frac{\tilde{k}(\omega)}{k} = f(\omega/\omega_c), \quad (5.85)$$

where $\omega_c = \eta\phi/(T_\infty k \rho_f)$ is a characteristic frequency at which a crossover in $\tilde{k}(\omega)$ from a viscous flow regime to an inertial one takes place. The function $f(\omega/\omega_c)$ is found to be universal, independent of the microstructure of the porous medium. Johnson (1989) showed that Eq. (5.84) works extremely well when compared with numerical simulations, and is also obeys Eq. (5.85). Therefore, although Eq. (5.85) tells us that we cannot gain much microstructural information about the porous medium by just measuring $\tilde{k}(\omega)$ [since $f(\omega/\omega_c)$ is universal], Eq. (5.82) can be used to obtain k , the static permeability of the porous medium (via Λ). The experimental data of Charlaix *et al.* (1988), as well as the analytical and numerical calculations of Sheng and Zhou (1990), Chapman and Higdon (1992), and Knackstedt *et al.* (1993), seem to support the validity of Eq. (5.85).

VI. HYDRODYNAMIC DISPERSION

So far we have largely discussed flow and transport processes that involve only one fluid and one fluid phase. This section may be considered as the beginning of Part II of this paper, which discusses phenomena at the next level of complexity, namely, those that involve at least two fluids and one or two fluid phases. The most important of such phenomena is hydrodynamic dispersion, which is discussed in this section. Miscible displacement processes, which are generalizations of dispersion phenomena in which the viscosities of the two fluids are *not* the same, will be discussed in Sec. VII. Two-phase flows will be discussed in Sec. VIII.

A. The phenomenon of dispersion

When two miscible fluids are brought into contact, with an initially sharp front separating them, a transition zone develops across the initial front, the two fluids slowly diffuse into one another, and after some time they develop a diffused mixed. If one assumes that the volumes of the two fluids do not change upon this mixing, then

the net transport of one of the fluids across any arbitrary plane can be represented by Fick's second law of diffusion,

$$\frac{\partial C}{\partial t} = D_m \nabla^2 C . \quad (6.1)$$

Here C is the concentration, t the time, and D_m the molecular diffusivity. This mixing process is independent of whether or not there is a convective current through the medium. However, if the fluids are also flowing, then there will be some additional mixing of a different sort: convective mixing. This mixing, called *hydrodynamic dispersion*, is caused by a nonuniform velocity field, which in turn may be caused by the morphology of the medium, the fluid flow condition, and chemical or physical interactions with the solid surface of the medium. Dispersion is important to a wide variety of processes such as miscible displacements in enhanced oil recovery, salt water intrusion in coastal aquifers, where fresh and salt waters mix by a dispersion process, *in situ* study of the characteristics of an aquifer, where a classical method of determining such characteristics is to inject fluid tracers in it and measure their travel times, and the pollution of surface waters because of industrial and nuclear wastes. Dispersion phenomena also occur in flow and reaction in packed-bed chemical reactors; these have been studied extensively by chemical engineers for a long time (see, for example, Bernard and Wilhelm, 1950).

B. Mechanisms of dispersion processes

In steady flow through a disordered porous medium, the *transit time*, or *first-passage time*, of a fluid particle between entrance and exit planes depends on the path, or streamline, that it follows through the pore space. A population of particles passing the entrance plane at the same instant will arrive at the exit plane by a set of streamlines with a *distribution* of transit times. Thus a solute concentration front will spread in the mean flow direction as it passes through the medium. The resulting first-passage-time distribution (FPTD) is a measure of *longitudinal dispersion* in a porous medium.

Likewise, a population of particles passing simultaneously through a restricted area of the entrance plane will not follow entirely the mean flow to the exit plane, but will be dispersed in the transverse directions as well, that is, the population and the set of streamlines traveled with have a wider distribution of exit locations than of entrance locations. Thus a concentration front will also spread laterally on the way to the exit plane. The distribution of the first-passage times for crossing the system at a given transverse plane is a measure of *transverse dispersion* in a porous medium.

Two basic mechanisms drive dispersion in macroscopically homogeneous, microscopically disordered porous media; these arise in the pore-level velocity field forced on the flowing fluid by the irregularity of the pore space. The first mechanism is *kinematic*: streamtubes divide

and rejoin repeatedly at the junctions of flow passages in the highly interconnected pore space. The consequent tangling and divergence of streamlines is accentuated by the widely varying orientations of flow passages and coordination numbers of the pore space. The result is a wide variation in the lengths of the streamlines and their downstream transverse separations. The second mechanism is *dynamic*: the speed with which a given flow passage is traversed depends on the flow resistance or hydraulic conductance of the passage, its orientation, and the local pressure field. The two mechanisms conspire to produce a broad first-passage-time distribution between entrance and exit plane. These two mechanisms suggest two possible geometrical aspects of dispersion processes, defined with respect to the mean velocity direction, i.e., a longitudinal effect due to the differences between the velocity components in the direction of mean flow and a transverse effect due to the differences between local velocity components orthogonal to the direction of the mean flow.

These mechanisms of dispersion do *not* depend on molecular diffusion. Diffusion modifies the effects of the two basic mechanisms by moving material from one streamline to another and also by the usually weaker streamwise diffusion of material relative to the average velocity. The solid matrix of a porous medium of course acts locally as a separator of streamlines and thus as a barrier to diffusion, and therefore the modification of dispersion by diffusion depends on pore-space morphology and how it in turn affects local flow and concentration fields. The effect of molecular diffusion is usually important only in microscopically disordered porous media, where it acts to transfer the tracer particles out of slow or stagnant regions of the pore space.

C. The convective-diffusion equation

Dispersion processes in microscopically disordered and macroscopically isotropic and homogeneous porous media are usually modeled based on the convective-diffusion equation (CDE),

$$\frac{\partial C}{\partial t} + \langle v \rangle \cdot \nabla C = D_L \frac{\partial^2 C}{\partial x^2} + D_T \nabla_T^2 C , \quad (6.2)$$

where $\langle v \rangle$ is the macroscopic mean velocity, C the macroscopic mean concentration, and ∇_T^2 the Laplacian in transverse directions. For the sake of simplicity we delete $\langle \rangle$ and denote the magnitude of the average velocity vector by v . Thus the basic idea is to model dispersion processes as anisotropic diffusional spreading of concentration, the diffusivities being the longitudinal dispersion coefficient D_L and the transverse dispersion coefficient D_T . One important goal of any study of dispersion is to investigate the conditions under which dispersion processes in a give environment *cannot* be represented by the convective-diffusion equation.

Dispersion is said to be *macroscopically diffusive* or Gaussian if it obeys the CDE. If a particle population is

injected into the medium at $\mathbf{r}_0=(x_0, y_0, z_0)$ at $t=0$, for macroscopically diffusive dispersion, the probability density $P(\mathbf{r}, t)$ obeys the Gaussian distribution

$$P(\mathbf{r}, t) = (8\pi^3 D_L D_T^2 t)^{-3/2} \exp \left[-\frac{(x - x_0 - vt)^2}{4D_L t} - \frac{(y - y_0)^2}{4D_T t} - \frac{(z - z_0)^2}{4D_T t} \right], \quad (6.3)$$

where $P(\mathbf{r}, t)d\mathbf{r}$ is the probability that a particle is in a plane between \mathbf{r} and $\mathbf{r}+d\mathbf{r}$ at time t , and $\mathbf{r}=(x, y, z)$. $P(\mathbf{r}, t)$ is proportional to C/C_0 , where C_0 is the concentration at $t=0$, and therefore Eq. (6.3) represents a solution of Eq. (6.2). If one defines $Q(\xi - \xi_0, t)dt$ as the probability that a particle, beginning in the plane at ξ_0 , will cross, *for the first time*, a plane at ξ between t and $t+dt$, then from Eq. (6.3) one can easily obtain the first-passage-time distribution

$$Q(\xi - \xi_0, t) = |\xi - \xi_0| (4\pi D_\xi t^3)^{-1/2} \times \exp[-(\xi - \xi_0 - v_\xi t)^2 / 4D_\xi t], \quad (6.4)$$

where D_ξ and v_ξ are the dispersion coefficient and the mean flow velocity in the ξ direction, respectively. Various moments of Q yield information about the flow field and the dispersion processes. For example, for the longitudinal direction we have

$$\langle t \rangle = \frac{L}{v}, \quad (6.5)$$

and

$$\langle t^2 \rangle = \langle t \rangle^2 \left[1 + \frac{2D_L}{Lv} \right], \quad (6.6)$$

where $L = \xi - \xi_0$. In general, one can easily show that for large L and to the leading order one has $\langle t^n \rangle \sim \langle t \rangle^n$, where $n > 1$ is any integer number. Of course, this is true if the convective-diffusion equation is applicable, and therefore one way of showing that the CDE cannot describe a dispersion process in a certain medium is to show that $\langle t^n \rangle / \langle t \rangle^n$ ($n > 1$) is *not* a constant and one needs more information to describe various moments of the first-passage-time distribution. This will be discussed later in this section.

D. Dispersion in a tube

Historically, Griffiths (1911) was the first to report some experimental results that demonstrated the essence of the dispersion process in a tube with diffusional effects present, but without mathematical treatment. He observed that a tracer fluid injected into a system of water spreads out symmetrically about a plane in the cross section which moves with the speed of the flow. He commented that: "It is obvious that the movement of the center of the column of the tracers must measure the mean

speed of flow." It turned out that this was not as obvious as Griffiths had thought! Forty two years later, Taylor (1953) pointed out that this is a rather startling result for two reasons. First, because the water at the center of the tube moves with twice the mean speed of the flow (the Hagen-Poiseuille flow), the water at (or near) the center must approach the column of tracer, absorb the tracer as it passes through the column, and then reject the tracer as it leaves on the other side of the column. Secondly, although the velocity is asymmetrical about the plane moving at the mean speed, the column of tracer spreads out symmetrically.

Taylor (1953) and Aris (1956) studied dispersion in a cylindrical capillary tube of radius R . Starting from the convective-diffusion equation for a tube,

$$\frac{\partial C}{\partial t} + 2v_m \left[1 - \left(\frac{r}{R} \right)^2 \right] \frac{\partial C}{\partial x} = D_m \left[\frac{\partial^2 C}{\partial r^2} + \frac{1}{r} \frac{\partial C}{\partial r} + \frac{\partial^2 C}{\partial x^2} \right], \quad (6.7)$$

where v_m is the mean flow velocity in the tube, and defining a *mean* concentration C_m by

$$C_m = \frac{\int_0^{2\pi} \int_0^R C(r, x) r dr d\theta}{\int_0^{2\pi} \int_0^R r dr d\theta} = \frac{2}{R^2} \int_0^R Cr dr, \quad (6.8)$$

they showed that in the limit of long times

$$\frac{\partial C_m}{\partial t} = D_L \frac{\partial^2 C_m}{\partial x_1^2}, \quad (6.9)$$

where $x_1 = x - v_m t$ (the moving coordinate with respect to the mean flow velocity), and

$$D_L = D_x + \frac{R^2 v_m^2}{48D_r}, \quad (6.10)$$

where the subscripts x and r signify the fact that D_x and D_r are the contributions of axial and radial molecular diffusion, respectively. That is, if in Eq. (6.7) we delete $\partial^2 C / \partial x^2$ (i.e., neglect axial diffusion), D_x will also be deleted from Eq. (6.10); of course, $D_x = D_r = D_m$. Note that in Taylor-Aris dispersion D_L depends *quadratically* on v_m . We define a Péclet number Pe by $Pe = Rv_m/D_m = \tau_D/\tau_C$, where $\tau_D = R^2/D_m$ is the diffusion time and $\tau_C = R/v_m$ is the convection time. Thus Pe is simply a measure of the competition between diffusion and convection. Then Eq. (6.10) is rewritten as

$$\frac{D_L}{D_m} = 1 + \frac{1}{48} Pe^2. \quad (6.11)$$

Aris (1956) also showed that for a cylindrical tube with a cross section of *any* shape, one has

$$D_L = D_m + \delta_s \frac{l_s^2 v_m^2}{D_m}, \quad (6.12)$$

where l_s is a length scale of the tube and δ_s a shape factor

that depends on the shape of the cross section. For example, for an elliptical cross section where the major and minor semiaxes are a and b , respectively, one has $L_s = a$ and

$$\delta_s = \frac{1}{48} \frac{24 - 24e^2 + 5e^4}{24 - 12e^2}, \quad (6.13)$$

where $e = [1 - (b^2/a^2)]^{1/2}$. For a circular cross section, $b = a$, $e = 0$, and $\delta_s = 1/48$, as expected. For dispersion in a duct of parallel plates with fully developed laminar flow, $l_s = h$ and $\delta_s = 2/105$, where h is the half-width of the channel. Thus the quadratic dependence of D_L on v_m is independent of the shape of the cross section: it is the result of the competition between the equally strong molecular diffusion and convection.

Aris (1956) conjectured that *any* initial distribution of concentration will ultimately approach a Gaussian distribution. Chatwin, in a series of papers (see, Chatwin, 1977, for earlier references to his work), proved this. Further important work on dispersion in tubes was done by Horn (1971) and Brenner (1980). In particular, Brenner (1980) generalized Taylor-Aris dispersion significantly and employed local and global spaces (for example, in the tube problem r is the local space and x is the global one). One can also exploit the equivalence between Langevin and Fokker-Planck equations and derive the Taylor-Aris results (Van den Broeck, 1982).

E. Dispersion in spatially periodic media

At the next level of complexity are spatially periodic porous media. We have already discussed diffusion, electrical conduction, and flow in such models of porous media. Brenner (1980), Brenner and Adler (1982), Eidsath *et al.* (1983), and Koch *et al.* (1989) examined theoretically dispersion in spatially periodic porous media, and Gunn and Pryce (1969) measured the longitudinal dispersion coefficient in flow parallel to one of the axes of a simple cubic lattice of spherical particles. In particular, Koch *et al.* (1989) showed that, for a square array of cylinders or a cubic array of spheres, and in the limit $Pe \rightarrow \infty$, D_L depends quadratically on Pe and D_T approaches a constant value. These findings are in total contradiction with dispersion in *disordered* porous media, for which both D_L and D_T have a weaker dependence on Pe and, in particular, D_T does not reach a constant value (see below).

F. Models of dispersion in macroscopically homogeneous porous media

Many researchers have carried out experimental studies of dispersion, almost exclusively, in beadpacks, unconsolidated sandpacks, and sandstones. Some of the results, mainly for unconsolidated sands, were compiled by Fried and Combarous (1971). Work on sandstones, compiled by Perkins and Johnston (1963) and Legaski

and Katz (1967) shows, however, that dispersion in consolidated porous media is similar to that in unconsolidated media. Figure 36 collects experimental data for D_L/D_m for sandpacks, showing that there are five different regimes of dispersion. A similar plot can be made for D_T/D_m . For porous media the Péclet number is defined as $Pe = d_g v / D_m$, where d_g is frequently taken to be the average diameter of a grain or bead. The five dispersion regimes, shown in Fig. 36, are as follows.

(i) $Pe < 0.3$. This is the regime in which convection is so slow that diffusion controls dispersions almost completely. In this regime, we have *isotropic* dispersion such that (Brigham *et al.*, 1961; Koplik, Redner, and Wilkinson, 1988)

$$\frac{D_L}{D_m} = \frac{D_T}{D_m} = \frac{1}{F\phi}, \quad (6.14)$$

where, as usual, F is the formation factor and ϕ is the porosity of the medium. The quantity $1/(F\phi)$ varies commonly between 0.15 and 0.7, depending on the porous medium. Because of this isotropy, a concentrated sphere of solute will remain a sphere [rather than developing into an ellipsoid as indicated by Eq. (6.3)], but will increase in size as dispersion progresses.

(ii) $0.3 < Pe < 5$. This is the transition regime in which convection contributes to dispersion, but the effect of diffusion is still quite strong. D_L/D_m appears to increase with Pe , although it is difficult to say how!

(iii) $5 < Pe < 300$. This is the power-law regime. Convection dominates dispersion, but the effect of diffusion cannot be neglected, and one can write

$$\frac{D_L}{D_m} \sim Pe^{\beta_L}, \quad (6.15)$$

$$\frac{D_T}{D_m} \sim Pe^{\beta_T}. \quad (6.16)$$

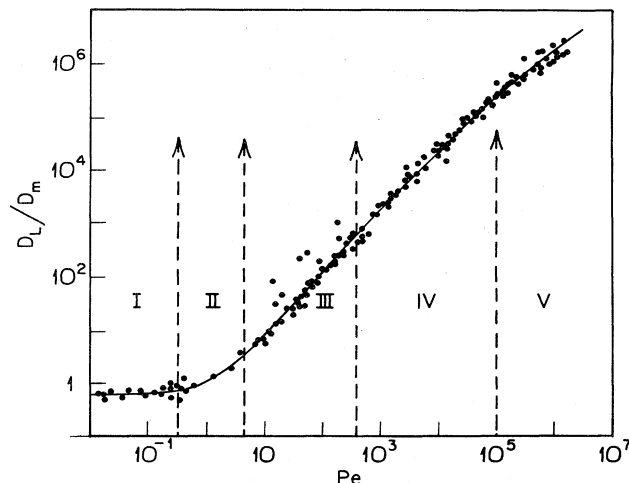


FIG. 36. Experimental data for longitudinal dispersion coefficient D_L vs Péclet number Pe in the five different regimes. D_m is the molecular diffusivity, and the curve is a guide to the eye (from Fried and Combarous, 1971).

The average values of β_L and β_T from all the available experimental data are $\beta_L \approx 1.2$ and $\beta_L \approx 0.9$. We call this regime the *boundary-layer* dispersion after Koch and Brady (1985), since, as we shall show below, this regime is consistent with the diffusive boundary layers near the solid surface, first found by Saffman (1959), where diffusion transfers materials from the very slow regions near the solid walls to faster streamlines.

(iv) $300 < Pe < 10^5$. This is the regime of pure convection. Simple dimensional analysis indicates that

$$\frac{D_L}{D_m} \sim Pe, \quad (6.17)$$

$$\frac{D_T}{D_m} \sim Pe. \quad (6.18)$$

This is usually called *mechanical dispersion*. In this case dispersion is simply the result of a stochastic velocity field induced by the randomly distributed pore boundaries.

(v) $Pe > 10^5$. This is the turbulent dispersion regime. The Péclet number is no longer the only correlating parameter, and the Reynolds number should also be used.

There is a sixth dispersion regime that is not evident in Fig. 36. This is the so-called *holdup dispersion* (Koch and Brady, 1985), first studied by Carberry and Bretton (1958), Turner (1959), and Aris (1959). In this case, the solute is trapped in a dead-end region or inside the solid grains, from which it can escape only by molecular diffusion. One has

$$\frac{D_L}{D_m} \sim Pe^2, \quad (6.19)$$

$$\frac{D_T}{D_m} \sim Pe^2, \quad (6.20)$$

indicating a strong dependence of D_L and D_T on Pe . In a porous medium near its percolation threshold p_c , there are many dead-end pores, and therefore this regime is relevant to such a porous medium.

Bacri *et al.* (1987) used an acoustic technique (Bacri *et al.*, 1984) to measure D_L for three different porous media. They showed that pore-level disorder strongly affects D_L and its dependence on Pe , and were able to observe power laws (6.15)–(6.20), depending on the breadth of the pore-size distribution and connectivity of the pore space.

Having gained a qualitative understanding of dispersion in porous media and what we may expect, let us now review and discuss various models of dispersion in macroscopically homogeneous porous media.

1. Statistical-kinetic models

These models are mathematical formulations either of the motion of a solute molecule (Beran, 1968; Todorovic, 1970) or of an abstract entity, e.g., a “point.” Various versions of this model were developed by Scheidegger

(1965), Todorovic (1971, 1975, 1982), and Chaudhari and Scheidegger (1965). The Chaudhari-Scheidegger approach assumes that the solute concentration in a “cell” of a porous medium is a Markovian variable, and in this sense their approach is somewhat different from the rest.

Beran (1968) treated a one-dimensional system; he assumed that the velocity field is an asymptotically stationary stochastic process and that two velocities separated by a large but finite time are uncorrelated. He invoked a formal analogy between a simple random walk and the position of the solute molecules and then invoked a central-limit theorem to assert that the probability $P(x, t)$ [the one-dimensional analog of Eq. (6.3)] is Gaussian. By invoking an ergodic theorem, Beran asserted that $P(x, t)$ is proportional to $C(x, t)$, the solute concentration, but did not calculate the probability density for the velocities v_1, v_2, \dots, v_n of the solute particle after 1, 2, ..., n steps. The construction of this probability density is perhaps the most fundamental problem in the development of a model of dispersion. Todorovic (1970) also developed a theory of longitudinal dispersion and extended his treatment to transverse dispersion (Todorovic, 1971) and to the situation wherein a time-dependent injection of solute particles at a boundary is specified (Todorovic, 1975). Using a Markov process, he argued that the displacement $x(t)$ of the solute particle at time t is a Brownian process, and therefore its probability density is Gaussian. Bear (1972) and Chaudhari and Scheidegger (1965) also suggested that the theory of Markov processes can be used for modeling dispersion processes. The problem with these approaches is that (i) a Gaussian distribution for the concentration profile is guaranteed, and (ii) they do not provide a method of actually calculating the dispersion coefficients; therefore they are purely phenomenological and formal and have no practical use.

2. Fluid-mechanical models

These models are based on three basic components: (i) a *Lagrangian* description of the motion of solute-containing fluid through a single pore; (ii) specific assumptions about the medium, e.g., homogeneity and isotropy; and (iii) calculation of quantities of interest as statistical averages. In a Lagrangian approach the motion of a tracer particle is followed, and the tracer's average velocity and the dispersion coefficients are defined as the time-rate of change of the mean and mean-square positions, respectively. The works of Scheidegger (1954), Day (1956), de Josselin de Jong (1959), Saffman (1959, 1960), Haring and Greenkorn (1970), and Bear (1972) belong to this group of models. Saffman's work is the most general of these and hence is discussed briefly. His model consisted a network of randomly oriented and distributed straight capillaries, in each one of which the flow was uniform. The path of fluid particles was regarded as a random walk in which the length, direction, and duration of each step are random variables.

Saffman was careful to introduce a dynamical basis for

his model, founded explicitly on fluid-mechanical ideas. He assumed that all the pores had an equal circular cross section of radius R , and that flow was laminar in all tubes. Saffman distinguished five cases in his first paper:

(i) $t_c \ll t_r$, where t_c is the convective time spent by a fluid particle in the pore and t_r the time required for appreciable radial diffusion of this particle, $t_r = R^2/(8D_m)$ (the fluid particle jumps a distance $R/2$ from one streamline to another). Thus radial diffusion is negligible and the duration of a step is $t = t_c = l/v_m$.

(ii) The fluid particle is on a streamline close to the pore wall, i.e., its speed is small and molecular diffusion occurs. The duration of a step is then $t = t_r + l/v_m$, i.e., the particle makes *one jump* from the streamline close to the pore wall to another whose speed is v_m , and then is convected out of the pore.

(iii) $t_r < t \ll t_a$, where t_a is the time for appreciable axial diffusion; $t_a = l^2/(2D_m)$. The effect of axial diffusion is negligible and $t = t_r + l/v_m$.

(iv) $t_r < t \leq t_a$, which means that the pore is very narrow and $t = l/v_m$.

(v) $t_a \ll t$. Thus the duration of a step is $t = t_a$.

Saffman found that in all cases D_T is given by

$$D_T = \frac{3}{16} lv . \quad (6.21)$$

However, D_L was found to depend on the regime considered. If

$$D_L = \frac{1}{2} v l S^2 , \quad (6.22)$$

then

$$S^2 = \frac{1}{3} \ln \frac{3vt_a}{l} + \frac{1}{12} \left[\ln \frac{6vt_r}{l} \right]^2 - \frac{1}{4} \ln \frac{6vt_r}{l} + \frac{19}{24} , \quad (6.23)$$

if

$$\frac{vt_a/l}{n_s^{1/2} (\ln 3vt_a/l)^{1/2}} \ll 1 ; \quad (6.24)$$

$$S^2 = \frac{1}{6} \ln \frac{27vT_m}{2l} + \frac{1}{12} \left[\ln \frac{6vt_r}{l} \right]^2 - \frac{1}{4} \ln \frac{6vt_r}{l} + \frac{19}{24} , \quad (6.25)$$

if $\ln n_s \gg 2$, and

$$\begin{aligned} \frac{3vt_r/l}{n_s^{1/2} (\ln n_s^{1/2})} &\ll 1, & \frac{3vt_a/l}{n_s^{1/2} (\ln n_s^{1/2})} &\gg 1 ; \\ S^2 &= \frac{1}{48} \left[\ln \frac{54vT_m}{l} \right]^2 , \end{aligned} \quad (6.26)$$

if $\ln n_s \gg 2$, and

$$\frac{4vt_r/l}{n_s^{1/2} \ln n_s^{1/2}} \gg 1, \quad \frac{4vt_a/l}{n_s^{1/2} \ln n_s^{1/2}} \gg 1 ,$$

where n_s is the mean number of steps taken by the fluid

particles after a large time T_m , at which D_L and D_T are measured, and is equal to $3\langle x \rangle/(2l)$, with $\langle x \rangle$ being the mean longitudinal position at time T_m . If we neglect the constant $19/24$ in Eqs. (6.23) and (6.25), which is usually much smaller than the other terms in these equations, Saffman's results can be summarized as

$$\frac{D_L}{D_m} \sim Pe(\ln Pe)^\alpha . \quad (6.27)$$

where $\alpha = 1$ or 2 . Equation (6.27) can now be compared with Eq. (6.15). If we take $\alpha = 1$ and fit the experimental data to this equation, the resulting fit would be as accurate as that provided by Eq. (6.15) if $\beta_L \approx 1.25$. On the other hand, if we take $\alpha = 2$, the resulting fit would be compatible with Eq. (6.15) if $\beta_L \approx 1.15$. This explains two interesting features of all experimental data: (i) The data indicate that β_L is either about 1.13–1.16 [obtained by Legaski and Katz (1967) for Bandera sandstone, by Salter and Mohanty (1982) for Berea sandstone, and by Blackwell *et al.* (1959) for packed unconsolidated sands], or about 1.24–1.30 [reported by Brigham *et al.* (1961) and Pakula and Greenkorn (1971) for glass beads, and by Legaski and Katz (1967) for Boise and Nordosaria sandstones and for dolomites], with an overall average of about 1.2, as mentioned above. (ii) β_L is probably not universal; it depends on the strength of competition between molecular diffusion and convection, which in turn depends on the pore shapes. On the other hand, Eq. (6.21) is *not* completely compatible with Eq. (6.16), since most data [see, for example, Blackwell (1962)] indicate that $\beta_T \approx 0.9$, as mentioned above. It is probable that β_T , like β_L , is *not* universal.

Saffman also found that dispersion *cannot* be described by a convective-diffusion equation, unless T_m is sufficiently large. Saffman's analysis clearly indicates the significance of molecular diffusion for dispersion in microscopically disordered porous media, no matter how small it may be, as long as it is not exactly zero. In the absence of molecular diffusion, a fluid particle, which is travelling along a streamline very close to a pore wall, will need huge amounts of time to escape from this region, and $D_L = 0$. However, diffusion intervenes and transfers the fluid particle to a much faster streamline. The logarithmic terms in Eqs. (6.23)–(6.26) are exactly due to such singularities in the dispersion process.

Saffman's results are presumably valid if Pe is large but finite. In his second paper (Saffman, 1960), he considered the case in which Pe is "less than some large value" and found that both D_L and D_T depend quadratically on Pe . The agreement between Saffman's results and various experimental data ranges from reasonable to good. In this author's opinion, Saffman's work is the most detailed and careful analysis of dispersion in microscopically disordered porous media and has not been fully appreciated. However, his work also has its shortcomings. Saffman did not allow for the possibility of a pore-size distribution (all pores were assumed to have the same radius). Haring and Greenkorn (1970) rederived some of Saffman's results

assuming a pore-size distribution. Moreover, in Saffman's work the flow field is represented by a sort of mean-field approximation, and there are no correlations between successive steps of the walk. This restriction can also be removed by Monte Carlo calculations in network models of pore space, as was first done by Sahimi *et al.* (1982); these calculations will be discussed below. Finally, it is worth mentioning that the logarithmic singularities found by Saffman were rediscovered by Aronovitz and Nelson (1984) in what they called "diffusion in steady flow" through a porous medium, which is nothing but the hydrodynamic dispersion discussed here!

3. Continuum models: Volume-averaging methods

We have already discussed this method in Sec. V, where we reviewed single-phase flow problems. The works of Whitaker (1967), Bachmat (1969, 1972), Gray (1975), Carbonell and Whitaker (1983), Eidsath *et al.* (1983), Koch and Brady (1985), and Plumb and Whitaker (1988a) fall into this class of methods. For example, Plumb and Whitaker (1988a) start from the convective-diffusion equation for the liquid or pore (β) phase

$$\frac{\partial C}{\partial t} + \nabla \cdot (C \mathbf{v}_\beta) = \nabla \cdot (D_m \nabla C), \quad (6.28)$$

with the boundary conditions

$$-\mathbf{n}_{\beta\sigma} \cdot D_m \nabla C = 0 \text{ at } S_{\beta\sigma}, \quad (6.29)$$

$$C = \mathcal{J}(\mathbf{r}, t) \text{ at } S_{\beta\sigma}, \quad (6.30)$$

and the initial condition $C = C_0(\mathbf{r})$, using the same technique discussed in Sec. V, and derived the following equation for the average concentration:

$$\epsilon_\beta \frac{\partial \langle C \rangle^\beta}{\partial t} + \nabla \cdot (\epsilon_\beta \langle \mathbf{v}_\beta \rangle^\beta \langle C \rangle^\beta) = \nabla \cdot (\epsilon_\beta \mathbf{D}^* \cdot \nabla \langle C \rangle^\beta), \quad (6.31)$$

where \mathbf{D}^* is the dispersion tensor given by

$$\mathbf{D}^* = D_m \left[\mathbf{I} + \frac{1}{V_\beta} \int_{A_{\beta\sigma}} \mathbf{n}_{\beta\sigma} \cdot \mathbf{f} dA \right] - \langle \mathbf{v}_\beta \mathbf{f} \rangle^\beta. \quad (6.32)$$

This analysis shows that on a large enough length scale, such that the porous medium is homogeneous, a convective-diffusion equation for the average concentration, Eq. (6.31), holds. Note that \mathbf{D}^* contains two terms. One is the contribution of molecular diffusion, while the other is due to hydrodynamic transport. As before, there is an unknown function \mathbf{f} which has to be determined. In practice, \mathbf{f} can be determined if a model of pore space is specified. However, if the pore space is disordered, then the numerical calculation of \mathbf{f} is no easier than any other numerical method that may be used to solve Eq. (6.31) directly.

A more sophisticated version of this method was developed by Koch and Brady (1985). These authors first formally related the average concentration field to the

probability distribution of solid material and then derived the effective dispersion coefficients in the *high-porosity limit*, including the relevant proportionality constants. A particular advantage of their method is that the fluid-mechanical aspects of the problem are treated *without* any approximations. It can also be extended to the case in which dispersion is not Gaussian and does not obey a convective-diffusion equation (see below). A major disadvantage of the method is that the assumption of high porosity has to be made in order to make the method numerically predictive. Koch and Brady (1985) also used their method to derive expressions for the dispersion coefficients in the various regimes discussed above.

4. Network models

These models belong to the class of fluid-mechanical models already discussed, except that the mean-field nature of a model like that of Saffman (1959, 1960) and the absence of disorder and heterogeneity are explicitly lifted. As already mentioned, Torelli and Scheidegger (1972) appear to have been the first to propose a random network model for studying dispersion processes in porous media, although they did not report any result. Torelli (1972) did simulate dispersion processes in flow through a random network, but his results pertain to a dispersion not related to what we are interested in here.

Sahimi *et al.* (1982) were the first who used random network models of porous media to simulate dispersion. In their method, one first determines the flow field in the network by the method discussed in Sec. V.B, where we reviewed network models for calculating the permeability of a porous medium. Then tracer particles are injected into the network at random at the upstream plane $x=0$. Each particle selects a streamline at random. The travel time for a given pore is given by $t = l/v_p$, where l is the length of the pore and v_p is the pore flow velocity. Complete mixing at the nodes is assumed, and therefore the probability that a pore is selected, once a particle has arrived at a node, is proportional to the flow rate in that pore. The first-passage-time distributions for the particles are computed by fixing the longitudinal or lateral positions and measuring the time at which the particles arrive at these positions for the first time. It is easy to see that D_ζ , the dispersion coefficient in the ζ direction, is given by

$$D_\zeta = \int_0^\infty Q(\zeta - \zeta_0, t) (S_\zeta^2 / 2t) dt, \quad (6.33)$$

where $\zeta_0(x_0)$ is the starting position of the particles, $S_x^2 = (x - x_0 - vt)^2$, and $S_\zeta^2 = (\zeta - \zeta_0)^2$ for $\zeta = y$ or z .

However, this random-walk method is appropriate for mechanical dispersion, since pore-level molecular diffusion has been ignored. To include the effect of molecular diffusion and simulate the boundary-layer dispersion, the following method was adopted (Sahimi and Imdakm, 1988). The convective time t_c for travelling

along a streamline in a pore is first calculated. If $t_c \gg t_r$, where t_r is the radial diffusion time scale discussed above, then one sets $t = t_c + t_r$, since the tracer has enough time to diffuse to a faster streamline. To simulate holdup dispersion, the tracer particles are allowed to diffuse into the dead-end pores of the network. Transport in such pores is only by molecular diffusion. In a series of papers, Sahimi *et al.* (Sahimi, Heiba, *et al.*, 1982; Sahimi, Davis, and Scriven, 1983; Sahimi, Heiba, *et al.*, 1986; Sahimi, Hughes, *et al.*, 1986) and Sahimi and Imdakm (1988) showed that these network models can reproduce and simulate all of the regimes of dispersion discussed above. In particular, Eqs. (6.14)–(6.20) can all be reproduced by these models.

de Arcangelis, Koplik, *et al.* (1986) proposed another method, which they called the “probability propagation algorithm.” In this method a one-dimensional convective-diffusion equation is assumed to hold for each pore of the network,

$$\frac{\partial C}{\partial t} + v_m \frac{\partial C}{\partial x} = D_m \frac{\partial^2 C}{\partial x^2}. \quad (6.34)$$

Consider a network of tubes $\{ij\}$. The concentration C_{ij} in each tube obeys Eq. (6.34), with the initial condition $C_{ij}(x_{ij}, 0) = 0$ and three boundary conditions: (i) a unit pulse of input flux at node i at $t=0$,

$$\sum_{\{j\}} S_{ij} \left[v_{mij} C_{ij} - D_m \frac{\partial C_{ij}}{\partial x_{ij}} \right]_{x_{ij}=0} = \delta(t), \quad (6.35)$$

where S_{ij} is the cross-section area of tube ij and v_{mij} is the mean flow velocity in that tube; (ii) a common concentration $C_i(t)$ at the starting junction, $C_{ij}(0, t) = C_i(t)$ for all j ; and (iii) a sink at each tube end, $C_{ij}(l, t) = 0$, for all j , corresponding to the fact that a tracer reaching the end acts as a source for the junction problem at the new node. The first-passage-time probability is given by $q_{ij}(t) = -S_{ij} D_m \partial C_{ij}(l, t) / \partial x_{ij}$. Equation (6.34) is easily solved in the Laplace transform space. The solution is given by

$$\hat{C}_{ij}(x, \lambda) = A_{ij} \exp(\alpha_{ij} x) + B_{ij} \exp(\beta_{ij} x), \quad (6.36)$$

$$\alpha_{ij}, \beta_{ij} = [v_{ij} \pm (v_{ij}^2 + 4D_m \lambda)^{1/2}] / (2D_m), \quad (6.37)$$

where A_{ij} and B_{ij} are determined from the above boundary conditions and λ is the Laplace transform variable conjugate to t . Then it is easy to see that

$$\hat{q}_{ij}(\lambda) = \hat{C}_{ij}(\lambda) S_{ij} \frac{\alpha_{ij} - \beta_{ij}}{\exp(-\beta_{ij} l) - \exp(-\alpha_{ij} l)}. \quad (6.38)$$

Having determined $\hat{q}_{ij}(\lambda)$, we obtain the first-passage-time distribution $\hat{Q}(L, \lambda)$ for the *entire* network,

$$\hat{Q}(L, \lambda) = \sum_{\Gamma} \prod_{i,j \in \Gamma} \hat{q}_{ij}(\lambda), \quad (6.39)$$

where the sum is over *all* paths Γ from the inlet to the outlet of the network.

To compute this sum efficiently, de Arcangelis, Koplik,

et al. (1986) ordered the nodes of the network in decreasing pressure order, starting with the inlet and finishing with the outlet. At each node i , a quantity $\hat{Q}_i(\lambda)$ is introduced that is a partial sum of Eq. (6.39), over paths running from the inlet to site i . For a delta-function input of tracer, one initially has $Q_I = 1$ at the inlet I and $Q_i = 0$ elsewhere. One then proceeds recursively through the pressure-ordered node list, propagating the quantity Q from each node i to its network neighbors j according to the rule $\hat{Q}_j(\lambda) \rightarrow \hat{Q}_j(\lambda) + \hat{Q}_i(\lambda) \hat{q}_{ij}(\lambda)$, $\hat{Q}_i(\lambda) \rightarrow 0$. After all the internal nodes have been propagated once in this way, the quantity $\hat{Q}_0(\lambda)$ at the outlet contains all terms of Eq. (6.39) corresponding to purely downstream paths. However, because molecular diffusion is present, the tracer motion includes upstream paths as well. Hence, after one sweep through the network, one has $\hat{Q}_n \neq 0$ for internal nodes n . By repeated sweeps through the network, the contributions of paths with progressively more upstream steps are included. Once $\hat{Q}(L, \lambda)$ is determined, it is inverted to the time domain and D_L is calculated using Eq. (6.33). Note that this method, in the mechanical dispersion regime (i.e., with no diffusion), is equivalent to the random-walk method of Sahimi and co-workers. de Arcangelis, Koplik, *et al.* (1986) showed that this method can reproduce the results for both mechanical and boundary-layer dispersion. The method is very efficient as long as the network is well connected. For percolation networks near p_c the method is very inefficient because calculating the sum in Eq. (6.39) becomes very time-consuming.

In a later paper, Koplik, Redner, and Wilkinson (1988) used another method for studying dispersion in random networks. In this method, one first calculates the flow field throughout the network by the method already discussed. Assuming that dispersion in each pore obeys a convective-diffusion equation, Eq. (6.35) with its right-hand side being zero (which is simply a statement of the continuity of mass at each node) is written for all interior nodes of the network. The resulting set of linear equations for nodal concentrations is solved (in the Laplace transform space), from which D_L is calculated. Roux *et al.* (1986) used the same method, except that they used a transfer matrix (Derrida and Vannimenus, 1982), originally invented for calculating the effective conductivity of percolation networks. Sahimi and Jue (1989) used a somewhat similar method to study dispersion of *large* molecules in porous media, i.e., molecules whose hydrodynamic radius is comparable to the pore sizes.

G. Long-time tails: Dead-end pores versus disorder

As already discussed, molecular diffusion transfers fluid particles into and out of stagnant, dead-end, or low-velocity regions of the pore space. Many experimental measurements of the concentration distribution during dispersion indicate the presence of a long-time tail in the concentration profiles. Diffusion into and out of the stagnant regions is often used to explain such long-time

tails. Such a phenomenon has, in fact, been of great interest for a long time. Carberry and Bretton (1958), Aris (1959), and Turner (1959) were probably the first who studied dispersion in systems with stagnant regions. In particular, Aris (1959) showed that $D_L/D_m \sim Pe^2$, a result that was rediscovered by Koch and Brady (1985). In the early 1960s there were several studies of the relation between the observed long-time tails and the effect of dead-end pores. Deans (1963) and Coats and Smith (1964) attributed the long-time tails to the presence of dead-end pores, which can cause long delays in travel times and hence long tails in the concentration profiles. They developed a semiempirical model to account for this, which will be discussed below. Brigham (1974) and Baker (1977) found that trapping in the dead-end pores is needed to describe dispersion in carbonate rocks but not in sandstones. They proposed that the origin of stagnant regions in carbonate rocks is either regular or bimodal porosity. This was recently disputed by Gist *et al.* (1990), who measured dispersion coefficients in a variety of sandstones and carbonate rocks. Their mercury capillary-pressure data for Austin chalk and Indiana limestone indicated the presence of bimodal porosity, yet no long-time tails were observed in the measured concentration profiles.

Deans (1963), Coats and Smith (1964), Passioura (1971), Baker (1977), Rao *et al.* (1980), and Salter and Mohanty (1982) have all investigated the effects of long-time tails and dead-end pores. In Baker's model, which is the most sophisticated, it is assumed that a fraction ϕ_f of the pore volume is available for flow, while $1 - \phi_f$ is the stagnant or dead-end fraction. A one-dimensional convective-diffusion equation is assumed (thus ignoring transverse dispersion), modified to account for the effect of the stagnant regions:

$$\phi_f \frac{\partial C_f}{\partial t} + (1 - \phi_f) \frac{\partial C_s}{\partial t} + v \frac{\partial C_f}{\partial x} = D_L \frac{\partial^2 C_f}{\partial x^2}, \quad (6.40)$$

where C_f and C_s are the concentrations of the flowing and stagnant regions, respectively. This equation is augmented by a mass balance between the stagnant and flowing fluids

$$(1 - \phi_f) \frac{\partial C_s}{\partial t} = k_c (C_f - C_s), \quad (6.41)$$

where k_c is the mass transfer coefficient. k_c^{-1} can be interpreted as the time that the fluid particles spend in the stagnant regions. Equations (6.40) and (6.41), with the appropriate initial and boundary conditions, are then solved. Normally, ϕ_f and k_c are not known *a priori* and are treated as adjustable parameters.

Bacri, Rakotomalala, and Salin (1990), who used an acoustic technique to measure the concentration and velocity profiles in dispersion in unsaturated porous media (i.e., dispersion in one fluid phase while another immiscible fluid is also present), Charlaix, Hulin, and Plona (1987), who measured dispersion coefficients and concentration profiles in sintered-glass bead packs, and Gist

et al. (1990), who did the same in a variety of sandstones and carbonate rocks, all used the Coats-Smith-Baker model to fit their data and found very good fits. However, while Bacri *et al.* (1990a) attributed the long-time tails in their data to the fact that the length of their medium was too short to allow for the development of Gaussian dispersion (see Fig. 37), Charlaix, Hulin, and Plona (1987) and Gist *et al.* (1990) attributed this to the heterogeneous nature of their porous medium. Thus it is important to understand why the Coats-Smith-Baker model is able to provide such good fits to the data (see below).

From their studies of dispersion in consolidated porous media, Gist *et al.* (1990) identified two cases in which long-time tails can occur. The first case is that of a heterogeneous porous medium, when the permeability contrast between various regions is strong enough. This gives rise to a long-time tail in the concentration profile. The second case is that of a narrow pore-size distribution, in which the permeability heterogeneities are due to defects in the packing density. If the long-time tails are in

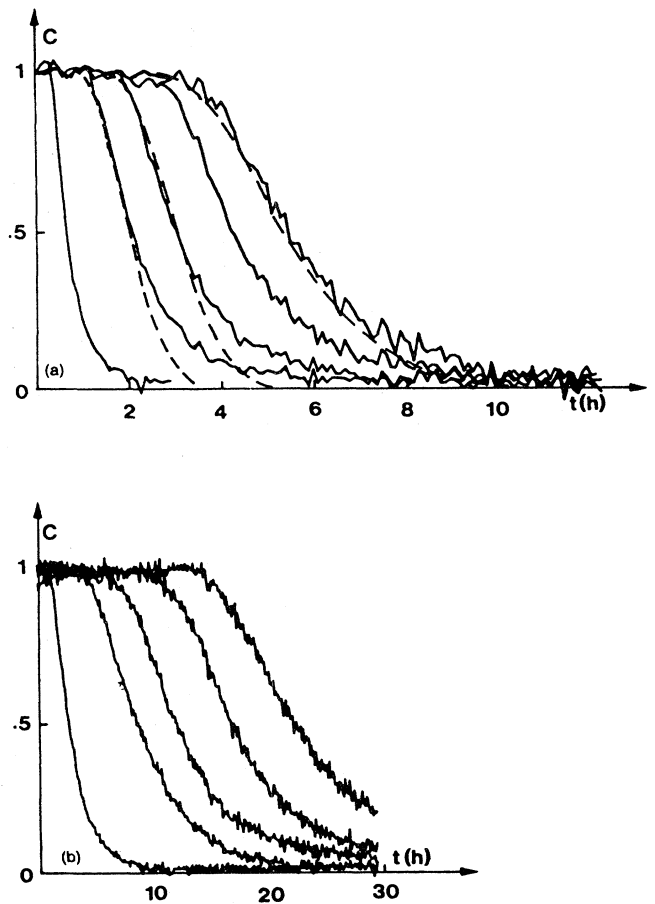


FIG. 37. Unsaturated concentration profiles at different cross sections of the porous medium: (a) Mean flow velocity, $v = 3.6$ cm/hr; (b) $v = 0.9$ cm/hr. The dashed lines correspond to a Gaussian profile. Observe the long time tails of the profiles for short distances x (from Bacri, Rakotomalala, and Salin, 1990).

fact due to permeability heterogeneities, the implications for the scale up of laboratory results to field conditions can be important. For example, the Coats-Smith-Baker model predicts that the long-time tails will disappear if k_c^{-1} is much smaller than the total travel time of the fluid particles [this is easily seen by inspecting Eqs. (6.40) and (6.41)], whereas long-time tails will persist if there are strong permeability heterogeneities at any length scale. This is also consistent with studies and measurements of tracer dispersion in groundwater flow in heterogeneous aquifers (Pickens and Grisak, 1981). Before we go on and explain this complex phenomenon, let us first study dispersion in short porous media, a closely related subject.

H. Dispersion in short porous media

As mentioned above, Bacri, Rakotamalala, and Salin (1990) attributed the long-time tails of their concentration profiles to the small size of their sample. Thus dispersion in short porous media is of significance, because then the mixing zone will be large compared with the medium's length. Brenner (1962) was probably the first to investigate this issue, but Brigham (1974) made a comprehensive and definitive analysis of the problem.

Let us first give the solution of a one-dimensional convective-diffusion equation for a porous medium of length L and various boundary and initial conditions. We define the dimensionless quantities

$$\alpha_{\pm} = \frac{L \pm vt}{(4D_L t)^{1/2}}$$

$$\beta_{\pm} = [L \pm v(t - V_{\text{inj}}/q_f)]/[4D_L(t - V_{\text{inj}}/q_f)]^{1/2}$$

where q_f is the volumetric flow rate and V_{inj} is the total volume of injected tracer solution. For a step change in inlet concentration at time $t=0$, the convective-diffusion equation provides an outlet solution given by Brigham (1974),

$$C = \frac{1}{2} \operatorname{erfc}(\alpha_-) + \frac{1}{2} \exp(Lv/D_L) \operatorname{erfc}(\alpha_+), \quad (6.42)$$

where $\operatorname{erfc}(z)$ is the complementary error function. The solution for a pulse input of total volume V_{inj} is found by superimposing two step-change solutions. The outlet concentration in this case was found by B. S. Carey [as quoted by Gist *et al.* (1990)],

$$C = \frac{1}{2} \operatorname{erfc}(\alpha_-) + \frac{1}{2} \exp(Lv/D_L) \operatorname{erfc}(\alpha_+) - \frac{1}{2} \operatorname{erfc}(\beta_-) - \frac{1}{2} \exp(Lv/D_L) \operatorname{erfc}(\beta_+). \quad (6.43)$$

If one is interested only in observation times $t \gg V_{\text{inj}}/q_f$, then the above solution can be simplified to

$$C = \left[\frac{L}{2\pi} \right] \{ [D_L(t - V_{\text{inj}}/q_f)]^{-1/2} - (D_L t)^{-1/2} \} \times [\exp(-\beta_-^2) + \exp(-\alpha_-^2)] \quad (6.44)$$

Gist *et al.* (1990) used Eq. (6.44) to fit their concentra-

tion profiles and found that the resulting fits are as accurate as those provided by the Coats-Smith-Baker model.

Brigham (1974) showed that if the Coats-Smith-Baker model is adjusted at the effluent boundary to account for the difference between *in situ* and flowing concentrations, then the above solutions for the convective-diffusion equation in a finite-size sample and for that of the Coats-Smith-Baker model will be essentially identical. This explains why Bacri, Rakotamalala, and Salin (1990) could fit their data for a short porous medium with the Coats-Smith-Baker model.

Koch and Brady (1987) also considered dispersion in porous media of short-to-moderate lengths. They derived an expression for the Fourier transform of the concentration and the effective dispersion coefficients. They showed that the characteristic time τ_{KB} for reaching a diffusive transport described by the convective-diffusion equation is related to a Péclet number Pe_1 by

$$\tau_{\text{KB}} \sim \text{Pe}_1^{-2/3}, \quad (6.45)$$

where $\text{Pe}_1 = dv/D_m$ and d is the typical grain size *before* the grains are fused to produce a consolidated porous medium. They found qualitative agreement between Eq. (6.45) and the data of Charlaix, Hulin, and Plona (1987). Bacri, Rakotamalala, and Salin (1990) also used the Koch-Brady expression for the concentration profile, but found only qualitative agreement between the predictions and their data, whereas the Coats-Smith-Baker model provided an accurate fit to the data. Perhaps the reason for this discrepancy is that the Koch-Brady results are valid in the limit of high porosities, whereas the data of Bacri *et al.* (1990) and Charlaix, Hulin, and Plona (1987) are both for lower porosities. Koch and Brady (1987) also proposed that τ_{KB} could be taken to be the same as k_c^{-1} in the Coats-Smith-Baker model. Finally, Han *et al.* (1985) measured both D_L and D_T in three different unconsolidated porous media made of packed particles, and varied the Péclet number from 10^2 to 10^4 . They used three types of packings, namely, uniform-size particles and a narrow and a broad size distribution. In all cases, they found that if the length of their packed column was shorter than some critical length, the convective-diffusion equation would not be able to predict their data, and that this critical length depended on Pe such that the larger the Pe, the larger the critical length for achieving a diffusive dispersion regime. This is in qualitative agreement with the prediction of Koch and Brady (1987), Eq. (6.45). However, Han *et al.* (1985) observed no time dependence for D_T in their short porous media, whereas D_L was found to be time dependent before the critical length was reached.

I. Dispersion in fractal porous media and percolation networks

In this section we discuss dispersion in percolation networks, which is relevant to dispersion in macroscopically heterogeneous porous media. Moreover, as Katz and

Thompson (1986, 1987) showed, flow in a porous medium with a broad pore-size distribution may be mapped onto an equivalent percolation problem. The same must be true about dispersion, since a broad pore-size distribution gives rise to a broad distribution of pore flow velocities, which in turn affects dispersion strongly. There are two features of percolation networks that can influence dispersion. One is the fact that there are a large number of dead-end pores near p_c , and thus holdup dispersion can be important. The second is the fact that for length scales shorter than the percolation correlation length ξ_p , the sample-spanning cluster and its backbone are fractal objects, and thus dispersion is not expected to be described by a convective-diffusion equation. We call this regime fractal dispersion. Two important characteristic quantities are the dispersivities $\alpha_L = D_L/v$ and $\alpha_T = D_T/v$ (which are proportional to each other, but α_L is usually larger than α_T). Physically, the dispersivities represent the macroscopic length scale over which a convective-diffusion equation can describe dispersion, and thus in some sense, they are similar to ξ_p .

In their simulations of dispersion in percolation networks, Sahimi *et al.* (Sahimi, Heiba, *et al.*, 1982, 1986; Sahimi, Davis, and Scriven, 1983; Sahimi, Hughes, *et al.*, 1983b) found that, as p_c is approached, the dispersivities also increase dramatically. This can be attributed to the fact that near p_c the transport paths are very tortuous, resulting in a broad first-passage-time distribution and thus large dispersivities. Figure 38 shows the results for dispersion in a percolating square network. The increase in dispersivities and thus the dispersion coefficients near p_c were confirmed by Charlaix, Hulin, and Plona (1987, 1988) and Hulin, Charlaix, *et al.* (1988), who studied tracer dispersion in model porous media and measured the D_L . Charlaix *et al.* (1988) constructed two-dimensional hexagonal networks of pores whose effective

diameters were of the order of millimeters. They found that as the fraction of open pores decreased, D_L increased sharply and Eq. (6.15) was satisfied. But even when dispersion coefficients were measured quite close to p_c , the quadratic dependence of D_L/D_m on Pe [Eq. (6.19)] was *not* observed (although the fraction of dead-end pores is large near p_c), presumably because the exchange time between the flowing fluids and the dead-end regions was so long that it could not be detected during their experiment. Hulin, Charlaix, *et al.* (1988) measured D_L in bidispersed sintered glass materials prepared from mixtures of two sizes of beads. They observed that when the porosity was decreased from 30% to 12%, D_L increased by a factor of 30. The results of these studies also indicated that dispersion is more sensitive to *large-scale* inhomogeneities of a porous medium than to its detailed local structure. Somewhat similar results were obtained by Charlaix, Hulin, and Plona (1987).

We should mention here a paper of de Gennes (1983a) in which he studied dispersion near p_c . De Gennes (1983a) presented a very long discussion and derivation to show that, in calculating D_L , the average flow velocity that one must use has to be based on the *total* travel time of the tracer particles in the sample-spanning cluster, rather than the travel time along the backbone alone. Intuitively, this is clear, and even in experimental measurements of the concentration profiles and D_L there is no way to measure the travel time along the backbone alone; what is routinely measured is the total travel or transit time.

What are the scaling laws for D_L and D_T near p_c ? From our discussions so far, it must be clear that D_L and D_T are sensitive to the structure of the porous medium. Similar to fractal diffusion discussed in Sec. II, we may define a crossover time τ_{co} such that for $t \gg \tau_{co}$ dispersion is Gaussian or diffusive and follows a convective-diffusion equation, whereas for $t \ll \tau_{co}$ dispersion is nondiffusive, with the crossover taking place at about $t \approx \tau_{co}$. For dispersion near p_c , this time scale can be estimated from

$$\tau_{co} \sim \frac{\xi_p^2}{D_L}. \quad (6.46)$$

To derive the scaling laws for D_L and D_T , we must consider separately the various dispersion regimes discussed above. Let us first introduce two random-walk fractal dimensionalities by

$$\langle \Delta x^2 \rangle \sim t^{2/d_w^l}, \quad (6.47)$$

$$\langle y^2 \rangle \sim \langle z^2 \rangle \sim t^{2/d_w^t}, \quad (6.48)$$

where $\langle \Delta x^2 \rangle = \langle (x - \langle x \rangle)^2 \rangle = \langle x^2 \rangle - \langle x \rangle^2$. These two equations are defined for length scales $L \ll \xi_p$. Two average flow velocities can also be defined. If an average velocity v_c is defined in terms of the travel time in the

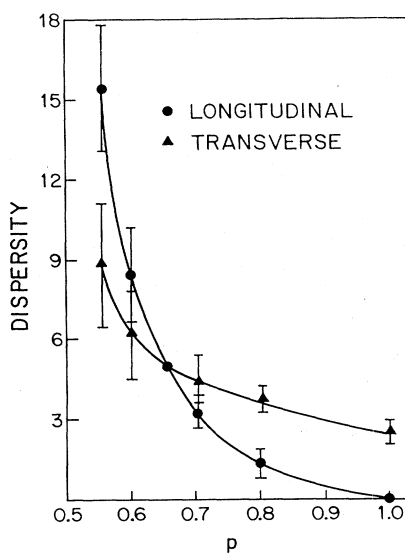


FIG. 38. Dispersivities in a percolation network (from Sahimi, Hughes *et al.*, 1986).

sample-spanning cluster, then near p_c , $v_c \sim k/X^A$, or

$$v_c \sim (p - p_c)^{\mu - \beta_p} \sim \xi_p^{-\theta}, \quad (6.49)$$

where, $\theta = (\mu - \beta_p)/\nu$, the critical exponents μ and β_p were already defined in Sec. II, and we assumed that the critical exponents of k and σ (or g_e) are equal. On the other hand, if an average particle velocity v_B is defined in terms of the travel times along the backbone, then $v_B \sim k/X^B$, or

$$v_B \sim (p - p_c)^{\mu - \beta_B} \sim \xi_p^{-\theta_B}, \quad (6.50)$$

where, $\theta_B = (\mu - \beta_B)/\nu$. For length scales $L \ll \xi_p$, we should replace ξ_p in Eqs. (6.49) and (6.50) by L , and therefore $v_c \sim L^{-\theta}$, and $v_B \sim L^{-\theta_B}$, respectively. We also define a *macroscopic* Péclet number

$$\text{Pe}_m = \frac{v \xi_p}{D_e}, \quad (6.51)$$

where v can be either v_c or v_B . For $L \ll \xi_p$, we replace ξ_p in Eq. (6.51) by L . Having defined these quantities, we can now investigate the scaling of the dispersion coefficients and τ_{co} near p_c .

(i) Let us first consider the small-Péclet-number regimes discussed above. In this case convection has no effect, and $D_L \sim D_T \sim D_e \sim (p - p_c)^{\mu - \beta_p}$, as before. For $L \ll \xi_p$, we have

$$d_w^l = d_w^t = 2 + \theta. \quad (6.52)$$

Moreover

$$\tau_{co} \sim (p - p_c)^{-\mu - 2\nu + \beta_p} \sim \xi_p^{2+\theta}, \quad (6.53)$$

so that $\tau_{co} \sim L^{2+\theta}$ for $L \ll \xi_p$. These equations are valid for the entire sample-spanning cluster in the limit $\text{Pe}_m \rightarrow 0$. For dispersion along the backbone θ is replaced everywhere with θ_B . Moreover, we have $\langle t^n \rangle \sim \langle t \rangle^n$, where $n > 1$ is an integer, and therefore for $L \ll \xi_p$ we have $\langle t^n \rangle \sim (L^2/D_e)^n$, so that

$$\langle t^n \rangle \sim L^{n(2+\theta)}. \quad (6.54)$$

(ii) Suppose now that dispersion takes place only in the backbone of the network and that Pe_m is relatively large. Although any porous medium has a large number of dead-end pores near its p_c , as the experiments of Charlaix *et al.* (1988) indicated, the medium has to be extremely close to p_c if the effect of the dead-end pores is to be seen, so that dispersion along the backbone has practical importance. For dispersion in the backbone, we have $D_L/D_e \sim \text{Pe}_m$ and $D_T/D_e \sim \text{Pe}_m$ (mechanical dispersion), and the logarithmic correlation indicated by Eq. (6.27) is neglected in scaling analyses, which means that $D_L \sim D_T \sim \xi_p v_B \sim \xi_p^{1-\theta_B} \sim (p - p_c)^{\mu - \beta_B - \nu}$. Using the numerical values of μ , β_B , and ν given in Table III, we obtain $D_L \sim D_T \sim (p - p_c)^{-0.56}$ in two dimensions, and $D_L \sim D_T \sim (p - p_c)^{0.04}$, so that D_L and D_T diverge in two dimensions but vanish very weakly in three dimensions.

This demonstrates the strong effect of the backbone structure on dispersion processes. The backbone can be approximated by nodes, links, and blobs. Links are the bonds or pores that connect the blobs and the remaining multiply-connected bonds aggregate together in the blobs. The blobs are very dense in two dimensions, providing a wide variety of paths for the fluid particles with a broad first-passage-time distribution. As a result, D_L and D_T diverge as p_c is approached. On the other hand, the blobs are not very dense in three dimensions, which means that the FPTD is not broad enough to give rise to divergent D_L and D_T . In a hypothetical porous medium modeled by a Bethe lattice, $D_L \sim D_T \sim (p - p_c)^{1/2}$, which indicates the strong effect of closed loops of a network (which are absent in Bethe lattices) on D_L and D_T . For $L \ll \xi_p$, we have $D_L \sim D_T \sim L^{1-\theta_B}$, which means that

$$d_w^l = d_w^t = 1 + \theta_B. \quad (6.55)$$

Equation (6.55) implies that in two dimensions $\langle \Delta x^2 \rangle \sim \langle y^2 \rangle \sim t^{1.26}$, and in three dimensions $\langle \Delta x^2 \rangle \sim \langle y^2 \rangle \sim \langle z^2 \rangle \sim t^{0.97}$. That is, one has *superdiffusion* in two dimensions, i.e., a diffusion process in which the mean square displacements grow with time faster than linearly. This should be contrasted with fractal diffusion which is always *subdiffusive* [i.e., the mean-square displacement grows sublinearly with time; see Eqs. (2.19) and (2.20)]. The time scale τ_{co} is given by

$$\tau_{co} \sim (p - p_c)^{-\mu + \beta_B - \nu} \sim \xi_p^{1+\theta_B}, \quad (6.56)$$

which should be compared with Eq. (6.53) (replacing θ by θ_B). For $L \ll \xi_p$, we have $\tau_{co} \sim L^{1+\theta_B}$. It is easy to show that $\langle t^n \rangle \sim (p - p_c)^{-\nu - n(\mu - \beta_B)} \sim \xi_p^{1+n\theta_B}$, and $\langle t \rangle \sim \xi_p^{1+\theta_B}$, so that $\langle t^n \rangle / \langle t \rangle^n \sim \xi_p^{1-n}$. That is, from the scaling of $\langle t \rangle$ one cannot obtain the scaling of $\langle t^n \rangle$ for $n > 1$. For $\xi_p \gg L$, we have

$$\langle t^n \rangle \sim L^{1+n\theta_B}, \quad (6.57)$$

which should be compared with Eq. (6.54) if we replace θ by θ_B .

(iii) Now consider holdup dispersion discussed above. We have, $D_L \sim (v_c \xi_p)^2 / D_e$, which is the same as Eq. (6.19) in which the length scale is ξ_p and the diffusivity D_m has been replaced by D_e , as suggested by de Gennes (1983). We can therefore write $D_L \sim \xi_p^{2-\theta} \sim (p - p_c)^{-2\nu + \mu - \beta_p}$, with a similar result for D_T , and thus $D_L \sim (p - p_c)^{-1.5}$, and $D_L \sim (p - p_c)^{-0.17}$ in two and three dimensions, respectively. That is, dispersion coefficients always diverge as p_c is approached. This divergence is undoubtedly because of the contribution of dead-end pores and the long times that the particles spend there. For $L \ll \xi_p$, we have $D_L \sim L^{2-\theta}$, which means that

$$d_w^l = d_w^t = \theta, \quad (6.58)$$

and therefore $\langle \Delta x^2 \rangle \sim t^{2.3}$ and $\langle \Delta x^2 \rangle \sim t^{1.1}$ in two and three dimensions, respectively, with similar results for

the transverse direction. That is, one *always* has superdiffusive transport when holdup dispersion is dominant. The time scale τ_{co} is given by

$$\tau_{co} \sim (p - p_c)^{-\mu + \beta_p} \sim \xi_p^\theta, \quad (6.59)$$

and $\tau_{co} \sim L^\theta$ for $L \ll \xi_p$. It is now straightforward to show that $\langle t^n \rangle \sim (p - p_c)^{-n\nu(\theta+2)+\nu} \sim \xi_p^{n(\theta+2)-1}$, so that $\langle t^n \rangle / \langle t \rangle^n \sim \xi_p^{-1}$, and therefore scaling of $\langle t \rangle$ is *not* enough for obtaining that of $\langle t^n \rangle$ for any $n > 1$. In the $L \ll \xi_p$ regime we have

$$\langle t^n \rangle \sim L^{n(\theta+2)-1}. \quad (6.60)$$

Aside from Eqs. (6.52) and (6.53), all of the above equations were derived by Sahimi (1987) and were confirmed by Monte Carlo simulations of Sahimi and Imdakm (1988) and Koplik, Redner, and Wilkinson (1988). The fact that $\langle t^n \rangle / \langle t \rangle^n$ depends on n means that *there is no unique time scale for characterizing dispersion in the fractal regime*. Koplik, Redner, and Wilkinson (1988) also proposed an elegant and general scaling form for the first-passage-time distribution given by

$$Q(t) = \frac{1}{\tau_D} F_s \left[\frac{t}{\tau_D}, \frac{\tau_c}{\tau_D} \right], \quad (6.61)$$

where τ_D and τ_c are the diffusion and convective time scales, respectively, and $\tau_D \sim \xi_p^{2+\theta}$ [see Eq. (6.53)], which is also the largest time that the fluid particles can spend in the dead-end pores, since the length of the longest dead-end branches is of the order ξ_p . The scaling function F_s has the following limiting behavior:

$$F_s(x, y) \rightarrow \begin{cases} F_1(x) & \text{as } y \rightarrow \infty, \\ y F_2(x) & \text{as } y \rightarrow 0. \end{cases} \quad (6.62)$$

The case of pure diffusion corresponds to $y = \tau_c / \tau_D \rightarrow \infty$, while the convective limit corresponds to $y \rightarrow 0$. Numerical simulations support this scaling representation of $Q(t)$.

Gist *et al.* (1990) used the percolation ideas of Katz and Thompson (1986, 1987) to study and quantify dispersion in porous media. Following Sahimi and co-workers (Sahimi *et al.*, 1982; Sahimi, Davis, and Scriven, 1983; Sahimi, Heiba, Davis, and Scriven, 1986; Sahimi, Hughes, Scriven, and Davis, 1986), they argued that the fundamental quantity to be considered is the ratio ξ_p / d_g , where d_g is the mean grain size. Since (see Sec. II) $\xi_p / d_g \sim (X^A)^{-\nu/\beta_p} \sim (X^A)^{-2}$, and because X^A is roughly proportional to the fluid saturation S , we can write

$$\frac{\xi_p}{d_g} \sim S^{-2}. \quad (6.63)$$

Gist *et al.* (1990) derived a relation between $\alpha_r = \alpha_L / d_g$ and ξ_p / d_g using the percolation model. Their final result is

$$\alpha_r \sim \left[\frac{\xi_p}{d_g} \right]^{2.2} \sim S^{-4.4}. \quad (6.64)$$

Their data for sandstones, epoxies and carbonates supported this relation. This confirms the relevance of percolation to dispersion in porous media and the scaling laws discussed above.

The last question to be addressed is: What is the equation for the probability density function $P(\mathbf{r}, t)$ in the fractal dispersion regime? For Gaussian dispersion $P(\mathbf{r}, t)$ is given by Eq. (6.3), and in Sec. II we discussed $P(\mathbf{r}, t)$ for fractal diffusion. For fractal dispersion, Sahimi (1987) proposed the following equation for $P(\mathbf{r}, t)$, in the limit of long times

$$P(\mathbf{r}, t) \sim t^{-d_s/2} \exp \left[-\alpha_1 \left(\frac{|x - \langle x \rangle|}{t^{1/d_w^l}} \right)^{\nu_p^l} \right. \\ \left. - \alpha_2 \left(\frac{|y|}{t^{1/d_w^t}} \right)^{\nu_p^t} - \alpha_3 \left(\frac{|z|}{t^{1/d_w^l}} \right)^{\nu_p^t} \right], \quad (6.65)$$

where α 's are constant and as we already showed, $d_w^l = d_w^t$ for most cases. Here d_s is the spectral dimension (Alexander and Orbach, 1982), $d_s = 2D_p / d_w$, and $\nu_p^l = d_w^l (d_w^l - 1)^{-1}$, and $\nu_p^t = d_w^t (d_w^t - 1)^{-1}$. This equation, which reduces to Eq. (6.3) when $D_p = d$ and $d_w^l = d_w^t = 2$, is an extension of Eq. (2.21). Monte Carlo simulations of Sahimi and Imdakm (1988) seem to support it, but no rigorous derivation of it is yet available, and the matter is still an open question (Sahimi and Hughes, 1993).

J. Dispersion in heterogeneous porous media

Dispersion in macroscopically heterogeneous media has attracted considerable attention by *both* hydrologists and *politicians* in the past two decades as a result of growing concerns about pollution and water quality. Because of intensifying exploitation of groundwater, and the increase in solute concentrations in aquifers due to saltwater intrusion, leaking repositories, and use of fertilizers, dispersion in heterogeneous porous media has been a main topic of research. Moreover, dispersion in miscible displacement processes is an important phenomenon during oil recovery processes, and depending on the magnitudes of D_L and D_T and other physical parameters of the process, dispersion can help or hurt a miscible displacement process and its efficiency. What follows is a brief review of the main methods for studying dispersion in macroscopically heterogeneous porous media.

1. Continuum models: Large-scale volume-averaging techniques

In studying transport in heterogeneous porous media, one should define clearly a heterogeneous medium. Halldorsen and Lake (1984) discussed *four* scales of averaging which were microscopic, macroscopic, megascopic, and gigascopic scales. They also devised statistical techniques for estimating the distribution of heterogeneities

in oil reservoirs. Bhattacharya and Gupta (1983) discussed a variety of length scales ranging from kinetic and Taylorian to the Darcy scales, while Dagan (1986) considered length scales ranging from pore to laboratory to formation to regional levels. Cushman (1984) provided a brief review of the general problem of the development of N -scale transport equations. A complete treatment of the problem at all these length scales is not currently available.

We remind the reader that dispersion in heterogeneous porous media is purely mechanical, arising as a result of large-scale spatial variations of the permeability of the medium and the resulting random velocity field. Thus Eqs. (6.17) and (6.18) are generally expected to hold in which the length scale used in Pe may be the permeability correlation length ξ_k . In this sense, dispersion in a heterogeneous system is somewhat *simpler* than that in microscopically disordered but macroscopically homogeneous media.

Plumb and Whitaker (1988a, 1988b) [see also Thompson and Gray (1986)] considered a *two-scale* problem and developed a large-scale averaging technique for determining the macroscopic transport equation. The starting point of their analysis was Eq. (6.31), which was then averaged over regions in which the permeability varied spatially. They derived a macroscopic equation for the average concentration which contained such terms as $\nabla\nabla\nabla\{\langle C \rangle^\beta\}$ and $\nabla\nabla\partial\{\langle C \rangle^\beta\}/\partial t$, indicating that dispersion in macroscopically heterogeneous porous media does not, in general, obey a convective-diffusion equation. If so, this can give rise to time- and scale-dependent dispersion coefficients which are in some sense similar to those for fractal dispersion near and at p_c discussed above. The work of Plumb and Whitaker is valuable in that it demonstrates clearly the deviations of dispersion in heterogeneous porous media from a conventional CDE description. The main problem with the approach of Plumb and Whitaker (1988a, 1988b) is that, except for very simplified models of pore space, the numerical solution of their equation is extremely difficult to obtain. The problem has to be solved first at the local level in order to use the solution as the starting point for determining the solution of the macroscopic equation. Moreover, as discussed above, the main contribution to dispersion in a heterogeneous medium comes from large scale variations of the permeability of the medium, and local or pore-level events such as diffusion do not play an important role, and it is not clear how such large scale permeability variations can be incorporated into the computations.

Koch and Brady (1988) also studied dispersion in heterogeneous porous media using averaging techniques. They were able to show that if the correlations length ξ_k for the permeability fluctuations is finite, dispersion is diffusive and obeys a CDE. However, if ξ_k is divergent, then fractal dispersion occurs in which the mean square displacements grow with time faster than linearly, completely similar to fractal dispersion near and at p_c for length scales $L \ll \xi_p$. The conclusion is that the length

scale ξ_k plays a role very similar to ξ_p . Moreover, Koch and Brady (1988) showed that in the fractal regime the space-time evolution of the concentration is *universal*, and is *uniquely* related to the covariance of the permeability field. This is again completely similar to fractal dispersion near p_c .

2. Continuum models: Stochastic-spectral methods

This method has been popular with geologists and hydrologists, and has been used extensively. The main motivation for using such methods is that the complex geohydrological structures of aquifers, the nonuniformity and unsteadiness of flow, and other influencing factors make dispersion a very complex phenomenon. Field measurements of dispersivities are often costly and time consuming. For example, one needs to drill many observation wells to monitor the spread of solute concentrations, and the spreading itself is often very time consuming and slow, and a few years may be needed for completing the investigations. The level of uncertainties in all of the operations and measurements is quite high, and therefore stochastic methods have been advocated so that the concepts of randomness, uncertainty, and errors can be introduced into the models and analyses.

In the early years of investigating this problem, the convective-diffusion equation served as the starting point for analyzing field data and the treatment of the problem was deterministic. However, a considerable amount of data has indicated unequivocally that D_L and D_T measured in a field are larger by several orders of magnitude than those measured in a laboratory, and a completely deterministic approach cannot explain such data. Moreover, the apparent dispersivities α_L and α_T seem to increase with the transit times of the tracer particles, similar to those near p_c in the regime $L \ll \xi_p$. Figure 39,

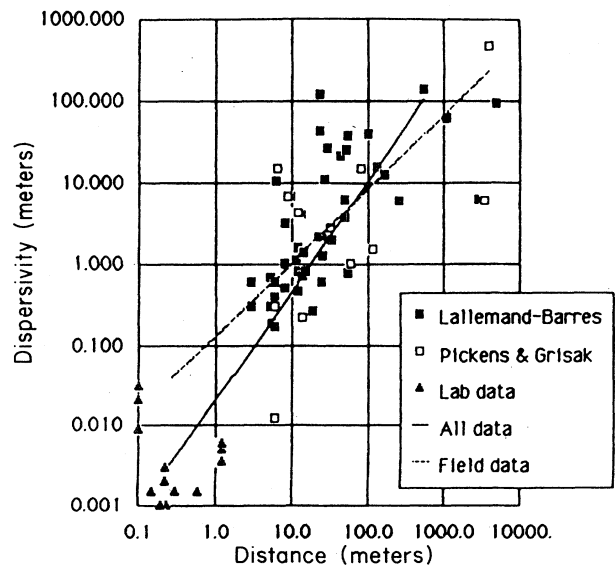


FIG. 39. Field-scale dispersivities vs distance from the tracers' injection point (from Arya *et al.*, 1985).

taken from Arya *et al.* (1988), demonstrates this phenomenon very clearly. As the distance from the source increases, so does the dispersivity, and no asymptotic limit in which it is constant is apparent. It is now well established that dispersion in heterogeneous porous media is dominated by large-scale permeability heterogeneities. Warren and Price (1961) seem to be the first to investigate dispersion in heterogeneous media, taking into account the effect of permeability heterogeneities. They used a Monte Carlo method which will be discussed in the next subsection. Early analytical studies of this problem, using stochastic concepts, were carried out by Mercado (1967) and Buyevich *et al.* (1969), but not all the ingredients were known at that time, and it has been only in the last decade or so that a more comprehensive analysis of this problem has become possible.

To give the reader some ideas about stochastic-spectral models of dispersion in heterogeneous media, let us discuss briefly the work of Gelhar *et al.* (1979), which is representative of this class of models. The starting point

is the CDE at the local level,

$$\frac{\partial C}{\partial t} + \frac{\partial}{\partial x}(vC) = \frac{\partial}{\partial x} \left[D_L \frac{\partial C}{\partial x} \right] + \frac{\partial}{\partial z} \left[D_T \frac{\partial C}{\partial z} \right], \quad (6.66)$$

where it is assumed that C , D_L , and D_T , which are *local* properties, are random processes with

$$C(x, z, t) = C_m(x, t) + c(x, z, t), \quad (6.67)$$

$$v = v_m + u, \quad (6.68)$$

$$D_L = D_{Lm} + d_L, \quad (6.69)$$

$$D_T = D_{Tm} + d_T \quad (6.70)$$

where subscript m denotes a mean value, e.g., $C_m(x, t) = \langle C(x, z, t) \rangle$, with the averaging being taken with respect to the vertical depth z . $c(x, z, t)$, d_L , and d_T are *fluctuations* such that their mean values are zero. If we substitute Eqs. (6.67)–(6.70) into Eq. (6.66) and take the average of both sides, we find that

$$\frac{\partial C_m}{\partial t} + \frac{\partial}{\partial x}(v_m C_m) + \frac{\partial}{\partial x} \langle uc \rangle = \frac{\partial}{\partial x} \left[D_{Lm} \frac{\partial C_m}{\partial x} \right] + \frac{\partial}{\partial x} \left\langle d_L \frac{\partial c}{\partial x} \right\rangle + \frac{\partial}{\partial x} \left\langle d_T \frac{\partial c}{\partial z} \right\rangle, \quad (6.71)$$

where we have now used the fact that the mean quantities are independent of z . We subtract Eq. (6.71) from Eq. (6.66) and use the coordinate $\xi = x - v_m t$ to obtain

$$\begin{aligned} \frac{\partial C}{\partial t} + u \frac{\partial C_m}{\partial \xi} + \frac{\partial}{\partial \xi} (uc - \langle uc \rangle) &= D_{Tm} \frac{\partial^2 c}{\partial z^2} + \frac{\partial}{\partial \xi} \left[d_L \frac{\partial C_m}{\partial \xi} \right] + D_{Lm} \frac{\partial^2 c}{\partial \xi^2} + \frac{\partial}{\partial z} \left[d_T \frac{\partial c}{\partial z} - \left\langle d_T \frac{\partial c}{\partial z} \right\rangle \right] \\ &\quad + \frac{\partial}{\partial \xi} \left[d_L \frac{\partial c}{\partial \xi} - \left\langle d_T \frac{\partial c}{\partial \xi} \right\rangle \right]. \end{aligned} \quad (6.72)$$

8

If the perturbation u is small, then the second-order terms (numbered 3, 7, and 8) can be neglected and one obtains an approximate equation of the form

$$\frac{\partial c}{\partial t} + u \frac{\partial C_m}{\partial \xi} = D_{Tm} \frac{\partial^2 c}{\partial z^2} + d_L \frac{\partial^2 c}{\partial \xi^2} + D_{Lm} \frac{\partial^2 c}{\partial \xi^2}, \quad (6.73)$$

so that, even at this level of approximation, one already has the additional term $d_L \partial^2 c / \partial \xi^2$. Equation (6.73) is solved by assuming that the permeability is a statistically-homogeneous random process. To solve this equation, one introduces the spectral representation of the random variables. If the field permeability k_f is written as, $k_f = k_m + k$, where $k_m = \langle k_f \rangle$, and $\langle k \rangle = 0$, then

$$k = \int_{-\infty}^{\infty} e^{i\omega z} dZ_k(\omega), \quad (6.74)$$

where ω is the wave number and $Z_k(\omega)$ is a complex process with orthogonal increments. The random processes u , c , d_L , and d_T also have similar spectral representations. Based on the experimental results of Harleman and Rumer (1963) that α_L seems to be proportional to

$k_f^{1/2}$, it is easy to show that $d_L / D_{Lm} = 3k / (2k_m)$. If we introduce a spectral representation for c

$$c = \int_{-\infty}^{\infty} e^{i\omega z} dZ_c(\omega), \quad (6.75)$$

then Eq. (6.73) becomes

$$\frac{\partial y}{\partial t} + a_T v_m \omega^2 y - D_{Lm} \frac{\partial^2 y}{\partial \xi^2} = V_s(\xi, t) \quad (6.76)$$

with

$$y = dZ_c,$$

$$V_s = v_m \frac{dZ_k}{k_m} G,$$

$$G = -\frac{\partial C_m}{\partial \xi} + \frac{3}{2} a_L \frac{\partial^2 C_m}{\partial \xi^2},$$

and $a_L = D_{Lm} / v_m$ and $a_T = D_{Tm} / v_m$. The cross spectrum of u and c , $S_{uc}(\omega)$, and the spectrum of k , $S_{kk}(\omega)$, can be

represented by [see, for example, Lumley and Panofsky (1974)]

$$S_{uc}(\omega) = E(dZ_u dZ_c^*) , \quad (6.77)$$

$$S_{uc}(\omega) = \frac{S_{kk}(\omega)^2}{k_m^2} \left\{ v_m G \frac{1-e^{-\beta t}}{a_T \omega^2} - \left[\frac{\partial G}{\partial t} - D_{Lm} \frac{\partial^2 G}{\partial \xi^2} \right] \left[\frac{1-(1+\beta t)e^{-\beta t}}{a_T^2 \omega^4} \right] \right\} , \quad (6.79)$$

where $\beta = a_T v_m \omega^2$. Similarly, $\langle uc \rangle$ is given by

$$\langle uc \rangle = A v_m G - B \left[\frac{\partial G}{\partial t} - D_{Lm} \frac{\partial^2 G}{\partial \xi^2} \right] , \quad (6.80)$$

and

$$A = \int_{-\infty}^{\infty} \frac{S_{kk}(\omega)}{k_m^2} \frac{1-e^{-\beta t}}{a_T \omega^2} d\omega ,$$

$$B = \int_{-\infty}^{\infty} \frac{S_{kk}(\omega)}{k_m^2} \frac{1-e^{-\beta t}}{a_T^2 \omega^4} d\omega .$$

Using all of these results, Eq.(6.71) is rewritten as

$$\begin{aligned} \frac{\partial C_m}{\partial t} &= (A + a_L) v_m \frac{\partial^2 C_m}{\partial \xi^2} - B \frac{\partial^3 C_m}{\partial \xi^2 \partial t} - 3a_L A v_m \frac{\partial^3 C_m}{\partial \xi^3} \\ &\quad + 3a_L B \frac{\partial^4 C_m}{\partial \xi^3 \partial t} + \left[a_L B v_m + \frac{9}{4} a_L^2 A v_m \right] \frac{\partial^4 C_m}{\partial \xi^4} \\ &\quad + \dots . \end{aligned} \quad (6.81)$$

Equation (6.81) shows that average concentration C_m does not obey a convective-diffusion equation, a result similar to what was obtained by Plumb and Whitaker (1988b). The rest of the analysis is clear: a spectrum $S_{kk}(\omega)$ is assumed and the quantities A and B are calculated. Having determined A and B , one can proceed to analyze Eq. (6.81). Gelhar and Axness (1983) extended this analysis to three-dimensional heterogeneous media and found that the dispersion coefficients depend linearly on the average velocity, which is not surprising [see Eqs. (6.17) and (6.18)].

The above method assumes that all of the randomness is due to the permeability field k_f . An alternative approach relies on a stochastic representation of the velocity (Tang *et al.*, 1982), and develops an ensemble average equation containing coupling between the velocity and concentration fluctuations [which is similar to that found by Gelhar *et al.* (1979)], that leads to a coefficient in the stochastic transport equation which is similar to D_L in a conventional CDE. This term, the *ensemble dispersion coefficient*, depends upon the variance-covariance structure of the velocity field. If neighboring velocities are uncorrelated, the ensemble dispersion coefficients increase as a function of travel distance from the source. If the covariance of the velocity field is an exponentially-decaying function, then ensemble dispersion coefficients reach a constant value. This analysis shows clearly the

$$S_{kk}(\omega) = E(dZ_k dZ_k^*) , \quad (6.78)$$

where E denotes the expected value, and $*$ denotes the complex conjugate. Since $dZ_u/v_m = dZ_k/k$, we obtain

effect of correlations in the stochastic treatment of dispersion. Stochastic models of the type that we discussed here can be useful if an adequate representation of the velocity or permeability fields is available, in which case the problem is in some sense *simpler* than dispersion in microscopically disordered and macroscopically homogeneous porous media, because one does not have to be concerned about boundary-layer and holdup dispersion mechanisms, which are generally very difficult to treat accurately. The interested reader should consult Dagan (1986, 1987) and Haldorsen and Damsleth (1990) for more details and references on stochastic modeling of transport in heterogeneous porous media.

3. Monte Carlo methods

We have already discussed in Sec. IV the model of heterogeneous porous media that was developed by Warren and Price (1961), Warren and Skiba (1964), and Heller (1972), and its improvement by Smith and Freeze (1979) and Smith and Schwartz (1980, 1981a, 1981b) who incorporated short-range correlations between the neighboring blocks. In addition, Smith and Schwartz used an algorithm for the motion of particles that included both deterministic and random displacements. In their simulations, a tracer particle is released in the flow field. For each time step a velocity is calculated by linearly interpolating the value from four surrounding values (in a two-dimensional system). The particle is then moved a distance that is fixed by the magnitude of the time step and the velocity. This is the deterministic portion of the displacement. Relocation from the deterministic position is accomplished first by moving the particle a distance d_x in a direction that coincides with the flow vector, and second a distance d_y in a direction normal to it. The random displacements d_x and d_y are calculated from

$$d_x = (24D_{Ll}\Delta t)^{1/2}(0.5 - [R]) , \quad (6.82)$$

$$d_y = (24D_{Tl}\Delta t)^{1/2}(0.5 - [R]) , \quad (6.83)$$

where Δt is the time step, $[R]$ a random number uniformly distributed in $(0,1)$, and D_{Ll} and D_{Tl} are *local* dispersion coefficients. Using this model, Smith and Schwartz investigated many aspects of dispersion in heterogeneous media and showed that strong permeability heterogeneities give rise to non-Gaussian dispersion. They also showed that when the permeability correlation

length ξ_k is of the order of the system length, a unique dispersion coefficient may not be possible to define.

4. Fractal models

In the discussion of models of heterogeneous media we mentioned Hewett's (1986) work on modeling of transport in heterogeneous porous media. Hewett analyzed vertical porosity logs and found that their distributions often obey fractal statistics. More precisely, they obey a fGn with $H > 0.5$. Analysis of fGn data is best done by using the rescaled range $R(l)/S(l)$, where $R(l)$ is the range of the accumulated departure from the mean of the variable (whose sample is the fGn), and $S(l)$ is the standard deviation. [We note that this notation is standard; see, for example, Feder (1988).] This method was first proposed by Hurst *et al.* (1965), and is ideally suited in uncovering the long-range correlations. In mathematical terms, if the variable takes the value $e(l)$ at position l , $R(l)$ is given by

$$R(l) = X_{\max}(l, L) - X_{\min}(l, L), \quad 1 \leq l \leq L, \quad (6.84)$$

where

$$\langle e \rangle_L = \frac{1}{L} \sum_{l=1}^L e(l), \quad (6.85)$$

$$X(l, L) = \sum_{u=1}^l [e(u) - \langle e \rangle_L], \quad (6.86)$$

and $S(l)$ is given by

$$S = \left\{ \frac{1}{L} \sum_{l=1}^L [e(l) - \langle e \rangle_L]^2 \right\}^{1/2}. \quad (6.87)$$

It can be shown that for fGn one has

$$R/S = \left(\frac{L}{2} \right)^H. \quad (6.88)$$

Vertical porosity logs analyzed by Hewett (1986) produced values $H \approx 0.7$ to -0.8 , indicating long-range positive correlations. Typical data are shown in Fig. 40. The exponent H , so obtained, was subsequently used for generating fractal distributions of the permeability of the reservoir with long-range correlations. In his work, the dispersivity α_L is predicted to vary with time as

$$\alpha_L \sim t^{2H-1}, \quad (6.89)$$

so that with $H \approx 0.75$ one obtains $\alpha_L \sim t^{0.5}$. A similar result was obtained by Philip (1986), Ababou and Gelhar (1990), and Neuman (1990), and is also implicitly assumed by Arya *et al.* (1988). Philip's work also predicted that at short times, $\alpha_L \sim t$, and the constraint $0.5 < H < 1$ was also proposed, consistent with Hewett's analysis of porosity logs.

These results demonstrate most definitively the relevance of fractal statistics to modeling heterogeneous media and transport processes in such media. Using these results, transport processes were simulated in a series of papers by the Chevron group (Hewett and Behrens, 1988; Mathews *et al.*, 1989; Emanuel *et al.*, 1989). The processes that were simulated were a miscible displacement and a waterflood (a process in which water is injected into the medium to displace the oil; see Sec. VIII), which is an immiscible displacement process. These simulations showed that fractal statistics lead to substantial improvements in the prediction of process performance.

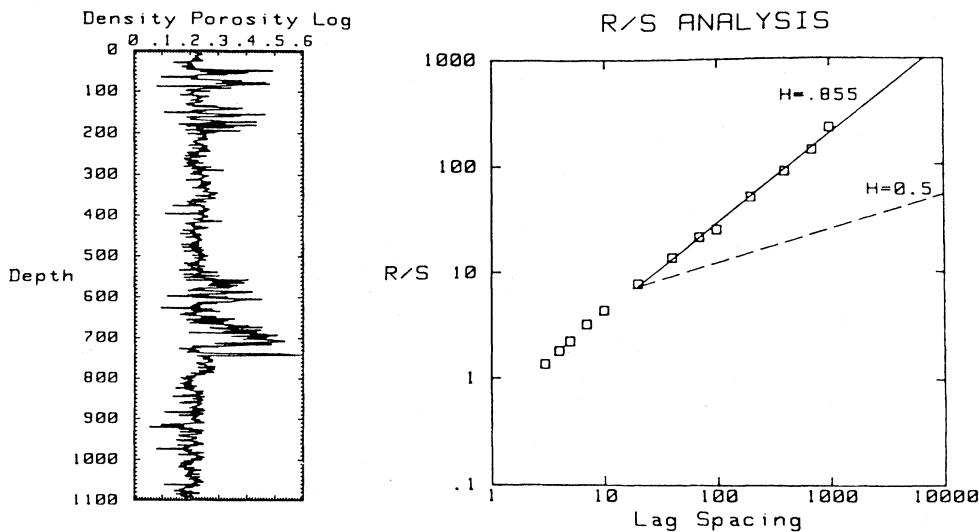


FIG. 40. Typical porosity logs of heterogeneous media and their R/S analysis, as explained in the text (from Hewett, 1986).

A different approach to the application of fractal geometry to transport in heterogeneous media was proposed by Wheatcraft and Tyler (1988). These authors were motivated by the experimental observations of Sudicky and Cherry (1979), Pickens and Grisak (1981), Sudicky and Frind (1982), Sudicky *et al.* (1985), and Molz *et al.* (1983), numerical simulations of Hewett (1986) and Arya *et al.* (1988), and Monte Carlo simulations of Smith and Schwartz (1980, 1981a, 1981b) who had found that dispersion coefficients and dispersivities are often scale dependent. They generated fractal and self-similar heterogeneities and, using a Lagrangian random-walk model of dispersion, showed that dispersion coefficients and dispersivities grow with the distance travelled. Although their model does seem to provide an explanation for the observed dependence of the dispersivities on time and length scales in terms of fractal concepts, their random-walk algorithm is not adequate enough to provide quantitative information, because their random walk is "unbiased," whereas if the motion of the tracer particles is to be modelled by a random walk, it has to be a biased walk, the bias being generated dynamically by the flow field.

K. Dispersion in fractured rocks

Dispersion in fractured rocks is important to both oil recovery processes and groundwater flow, and has received attention from researchers in both fields. However, unlike the simpler problem of flow in fractured rocks, dispersion in such media has not received the true attention that it deserves, primarily because of two reasons. One is that, as already discussed, appropriate models of fractured rocks are still being developed, and studies of dispersion in fractured rocks have mostly been delayed until such models are developed. The second reason is the level of complexity involved in such studies.

Previous studies of dispersion in fractured rocks can be divided into two groups. In the first group are studies that investigated transport in a single fracture. This group includes the works of Grisak and Pickens (1980), Neretnick (1980), D. H. Tang *et al.* (1981), Noorishad and Mehran (1982), and Lowell (1989). These studies were concerned with the effect of the matrix on transport through a single fracture. Some of these works were analytical, while others required numerical simulations. They are useful for modeling of transport in a network of fractures, since a fracture network simulation requires the solution of the problem at the level of a single fracture. The second group includes the works of Schwartz *et al.* (1983) and Smith and Schwartz (1984), who studied dispersion in a discrete network of interconnected fractures, and are perhaps the most advanced studies of transport in fractured rocks. But before we describe these, let us discuss first the continuum models that have been used to study transport and dispersion in fractured rocks, namely, the double-porosity and related models

which are widely used in the petroleum industry for reservoir simulation.

1. The double-porosity and related models

The petroleum industry has relied heavily on the double-porosity model discussed above for simulating transport and dispersion in fractured rocks. Typical of such attempts are those of Kazemi (1969), Closmann (1976), Kazemi *et al.* (1976), Gilman and Kazemi (1983), Thomas *et al.* (1983), and Dean and Lo (1988). The main problem with these works is that while the models are mathematically elegant and contain enough adjustable parameters to match the limited available data, they often lack predictive ability, in the sense that if new data become available, all parameters have to be fitted to the new data. This is perhaps because such parameters do not have any clear physical meaning; their sole purpose is to reproduce a certain set of data and, as such, they cannot be expected to be constant for a variety of different data. More recent continuum works include those of Firoozabadi and Hauge (1990) and Firoozabadi *et al.* (1991), where references to earlier works can also be found. These authors used simple structural models (for example, fracture blocks in series) to investigate transport processes. They found analytical solutions for certain problems, but the model of the rock that they used was too simple for this solution to be applicable to more general cases. The petroleum engineering literature contains many of such models, and a review of such works is beyond the scope of this paper. The reader should consult Chen (1989) for a complete review of this class of models.

Recently, Hughes and Sahimi (1993) developed a general formulation for simulating transport in double-porosity media. Their model takes into account the effect of the distribution of hydraulic conductivities and the interconnectivity of the pores and fractures. As such, the model is much more realistic than the previous models and can be used for simulation of transport processes in fractured rocks.

2. Fracture network models

In the works of Schwartz *et al.* (1983) and Smith and Schwartz (1984), the rock is represented by a two-dimensional network of interconnected discrete fractures. Such models were already discussed in the Secs. IV and V. The fractures are oriented at various angles with respect to the direction of the macroscopic mean flow. After calculating the flow field throughout the network, tracer particles are released into the network and their motion, which is governed by a random walk biased by the macroscopic mean flow, is monitored. Thus their model is completely similar to that of Sahimi *et al.* (1982) for dispersion in pore networks. It is found that the most important controlling factor is the orientation

of the fracture sets with respect to the macroscopic mean flow, and that in most cases dispersion is *not* Gaussian or diffusive.

As already mentioned, several careful experimental studies have indicated that fracture networks may be fractal objects. If so, dispersion in such networks should also be fractal, with dispersivities and dispersion coefficients that vary with time and length scales. Even though the fracture networks used by Schwartz *et al.* (1983) and Smith and Schwartz (1984) were not fractal, their study did indicate the possibility of fractal dispersion. On the other hand, assuming that a fracture network is a fractal object, Ross (1986) provided some arguments about the variations of the dispersivities with the scale of observations and the distance traveled.

L. Dispersion in stratified porous media

The last topic to be discussed in this section is dispersion in stratified porous media. Natural rocks are often stratified, made of various layers in which the structural and transport properties may vary greatly from stratum to stratum. For this reason, dispersion and transport in stratified porous media have always been of interest. The earliest studies on transport in stratified porous media appear to be those of Konce and Blackwell (1965) and Goddin *et al.* (1966), who studied the displacement of oil by water or a solvent in a stratified porous medium. However, these works do not belong to this section and will be discussed briefly in Sec. VIII.

Marle *et al.* (1967) and Güven *et al.* (1984, 1985) applied Taylor-Aris dispersion theory discussed above to a system of N strata that communicate with one another. Marle *et al.* (1967) obtained a complex integral expression for the longitudinal dispersion coefficient involving porosity, velocity, and *local* transverse dispersion coefficient which were all functions of the distance perpendicular to the strata. Lake and Hirasaki (1981) and Van den Broeck and Mazo (1983, 1984) also considered Taylor-Aris dispersion in a stratified medium. In particular, Van de Broeck and Mazo (1983, 1984) derived several interesting results, including the first-passage-time distribution and the longitudinal dispersion coefficient. Gelhar *et al.*'s work discussed above can be thought of as a method of studying dispersion in two-dimensional stratified porous media, since their equations were averaged over the vertical distance z and the permeability field was assumed to depend on the distance perpendicular to the strata. Plumb and Whitaker (1988a, 1988b) used their large-scale volume-averaging method discussed above to study dispersion in stratified porous media.

In a seminal paper, Matheron and de Marsily (1980) studied dispersion analytically in a two-dimensional stratified porous medium, using analytical methods and asymptotic expansions. The direction of the flow velocity was assumed to be parallel to the bedding and constant for a given stratum. It was further assumed that the

component of the velocity along the direction of macroscopic flow field is a weakly stationary stochastic process. The permeability was assumed to be an isotropic stochastic process and the medium was assumed to be of infinite extent in *both* directions. Matheron and de Marsily (1980) showed that under such conditions dispersion is *never* diffusive. The reason is that since the system is infinitely large and heterogeneous, a travelling tracer particle always samples new regions and strata with new heterogeneities. As a result, a diffusive regime can never be reached. Matheron and de Marsily also showed that if dispersion is to be Gaussian, then the integral of the covariance of the velocity (or permeability) must be zero, as its Laplace transform must depend linearly on the Laplace transform variable λ near $\lambda=0$. However, for most realistic situations, this will not be the case. On the other hand, if the macroscopic flow is *not* strictly parallel to the stratification (i.e., a small but finite perpendicular flow component is added), then dispersion will asymptotically be Gaussian if this integral is finite.

Bouchaud *et al.* (1990) extended Matheron and de Marsily's work by looking at a random walk in a two-dimensional stratified medium containing random velocity fields. If the velocities in the x (macroscopic flow) direction are a function of the vertical distance, then Bouchaud *et al.* showed that

$$\langle \Delta x^2 \rangle \sim t^{3/2}, \quad (6.90)$$

i.e., one has superdiffusion, and that there are large sample-to-sample fluctuations. The probability density $P(x, t)$, when averaged over various environments (realizations of the medium), was found to be non-Gaussian and approximately given by

$$\langle P(x, t) \rangle \sim t^{-3/4} f(x/t^{3/4}), \quad (6.91)$$

where $f(u)$ is a scaling function with the properties that $f(u) \sim \exp(-u^\delta)$ for $u \gg 1$, with $\delta = 4/3$. These results show clearly the non-Gaussian nature of dispersion in strongly heterogeneous media, and the inadequacy of a convective-diffusion equation for describing it.

From our discussion of dispersion processes in rocks, it is clear that these phenomena are very sensitive to the spatial heterogeneities of rocks. For this reason, dispersion has been advocated as a sensitive probe of the structure of heterogeneous rocks. Moreover, it is clear that superdiffusion is a generic property of dispersion in heterogeneous media with long-range correlations and, as such, it is very different from pure diffusion in such media, which is usually subdiffusive and very slow.

VII. MISCELLY DISPLACEMENT PROCESSES

In the last section we discussed dispersion processes which involve two fluids and one fluid phase. The viscosities and densities of the two fluids were assumed to be equal. In this section we discuss the displacement of one fluid by another miscible fluid having a different viscosity and density. If we inject a fluid into a system

saturated with another fluid, and if the two fluids mix in all proportions and their mixture remain a single phase, the two fluids are said to be *first-contact miscible*. Intermediate-molecular weight hydrocarbons such as propane and butane have this property. In other situations, the injected and in-place fluids may form two different phases, i.e., they are not first-contact miscible. However, mass transfer between the two phases and repeated contact between them can achieve miscibility; this is usually called *multiple contact* or *dynamic miscibility*. In the petroleum industry, the miscible injection fluids that achieve either first-contact or dynamic miscibility are usually called miscible solvents. In this review we restrict ourselves to first-contact miscible problems, since modeling multiple contact miscibility involves thermodynamic phase equilibria calculations that are beyond the scope of this paper.

Miscible displacement processes have received considerable attention since early 1950s. In the 1950s and early 1960s over 100 projects were undertaken to study the feasibility and economics of miscible displacement processes as effective tools of increasing oil production. In most of these projects hydrocarbon miscible flooding was used. However, most of the hydrocarbons used are normally less viscous than the oil and this viscosity contrast, together with the so-called gravity segregation, make a miscible displacement much less efficient than desired. For this reason, miscible displacement processes have not been used as widely as immiscible displacement processes, such as water flooding, in oil recovery processes. In most miscible displacement processes the injected fluid is either a hydrocarbon or, less frequently, flue gas, nitrogen, or CO_2 . The temperature and pressure that one needs for miscibility of the oil and these agents are often so high that they limit the number of prospective reservoirs. For example, CO_2 and medium-to-heavy hydrocarbons become miscible only at high temperatures and pressures (Sahimi *et al.*, 1985; Sahimi and Taylor, 1991). Another negative factor is the cost of a miscible displacement process. It may happen that a miscible displacement is more efficient in terms of the amount of the recovered oil than an immiscible process, but the total cost of the miscible displacement (including the cost of transporting the fluid agent to the oil field from other locations) is so high that makes it unattractive from an economical point of view. Flue gas and nitrogen have only limited application as agents of a miscible displacement process in deep and high pressure reservoirs. In the United States, CO_2 has the greatest potential for miscible displacement and oil recovery, but its availability is questionable.

In this section, we review and discuss important aspects of miscible displacement processes. Since the publication of a paper of Paterson (1984) in which a connection between miscible displacement processes and diffusion-limited aggregates was suggested, there has been a great deal of interest in such phenomena, especially in the physics community. We review in this section a

few important continuum models of miscible displacements and contrast them with the statistical and DLA-like models. We also discuss the stability of miscible displacement processes. This section is by no means exhaustive. The interested reader can consult, for example, the monograph by Stalkup (1984) which provides a detailed discussion of these processes, the classical methods of studying them, and the experimental data.

A. Factors affecting miscible displacement processes

As discussed by Stalkup (1984), many factors contribute to the efficiency of a miscible displacement. Among the most important of these are the following.

(i) *Mobility ratio*: The mobility λ_i of a fluid i is defined as the ratio of the effective permeability of the rock and the fluid's viscosity: $\lambda_i = k_i / \eta_i$. When one fluid displaces another, the mobility ratio M is defined as the ratio of the mobilities of the displaced and displacing fluids, and is one of the most important influencing factors in any displacement process. Normally, M is not constant because mixing changes the effective viscosities of the two fluids. If, in addition to the solvent, another fluid such as water is also injected into the medium, as is often done in order to reduce the mobility of the solvent, then it is not completely clear how to define an effective value of M . In many miscible displacement processes, one has to deal with more than one displacing front. For example, in tertiary oil recovery processes (which are undertaken when a process such as water flooding is no longer effective) there is usually more than one displacing front. The problem of defining an effective M is even more complex in such a situation, and no completely satisfactory method has been developed yet.

(ii) *Dispersion*: Dispersive mixing can decrease the viscosity and density contrasts between the displacing and displaced fluids, and in many cases this can be very useful. As discussed in Sec. VI, three major contributing factors to dispersion are microscopic and macroscopic variations of fluid velocities (or the permeabilities), and molecular diffusion, all of which help mixing of the two miscible fluids. Since longitudinal dispersion coefficient is usually much larger than the transverse dispersion coefficient, more mixing takes place in the direction of macroscopic flow. Even at the level of a single pore, it is difficult to study rigorously dispersive mixing of two fluids of unequal viscosities. In essence, we have to rework the Taylor-Aris dispersion theory, except that the viscosity of the mixing zone depends on the concentrations of the two fluids. To the best of this author's knowledge, and also to his surprise, no serious attempt has ever been made to tackle this problem. Since, as discussed in Sec. VI, pore space heterogeneities strongly affect D_L and D_T , this implies that such heterogeneities also affect miscible displacements.

Mobility ratio and gravity also affect dispersion. If $M > 1$, viscous instability develops (see below) in which

case the displacement is no longer a simple process. However, if $M < 1$, the usual dispersion mechanisms discussed in Sec. VI will be operative. Moreover, since no instability develops, the effect of pore space heterogeneities is also suppressed. On the other hand, if in a miscible displacement a less dense fluid displaces a denser fluid, then gravity suppresses the effect of dispersive mixing.

In some situations, longitudinal dispersion affects a miscible displacement more strongly than transverse dispersion, and vice versa. For example, when large fingers of the displacing fluids develop, which is often the case when $M > 1$, then there would be a large surface area on the sides of the fingers which allows for significant transverse dispersion to occur. This can help join the fingers, stabilize the displacement, and increase its efficiency. By contrast, longitudinal dispersion can only take place at the tip of the fingers, and therefore its effect is much weaker than that of transverse dispersion. For this reason, models that ignore transverse dispersion are usually not adequate for describing a miscible displacement.

(iii) *Reservoir stratification:* We have already discussed the effect of stratification on dispersion. Obviously, if dispersion is affected by stratification, so also are mixing and miscible displacement. It is clear that the displacing fluid preferentially chooses the strata with higher permeabilities. As a result, large amounts of the displaced fluids can be left behind in the strata with low permeabilities. If we try to displace this fluid by injecting more displacing agent into the low permeability strata, some of the agent will inevitably enter the high permeability strata and do "nothing," since such strata have already been swept by the displacing fluid, and this is not very efficient. The effect of stratification is even stronger when $M > 1$. Another phenomenon that affects miscible displacements in stratified media is the crossflow of displacing and displaced fluids between the strata. Depending on the direction of the displacement process, crossflows can help or hurt the efficiency of the process. Another factor that influences miscible displacements is dead-end pores. We already discussed the effect of dead-end pores on dispersion which, in turn, affects mixing and displacement.

B. Viscous fingering

If the displacing and displaced fluids are first-contact miscible, and if $M < 1$, then the displacement process is very simple and efficient. The displaced fluid moves ahead of the displacing fluid, the displacement front is stable, and there is a mixed zone between the pure displacing and displaced fluids regions. However, as in any other aspect of life, a real miscible displacement process is not as simple as this. If $M > 1$, the front is unstable, and many fingers of the displacing fluid develop that penetrate the displaced fluid leaving behind large amounts of the displaced fluid. These fingers have very

irregular shapes, and their formation reduces strongly the efficiency of the displacement process. Figure 41, taken from Habermann (1960), shows the effect of M on the formation and shape of the fingers. The experiments were carried out in a quarter of the so-called five-spot geometry, made of consolidated sand. The porous medium was essentially two dimensional. It is clear that as M increases the amount of swept oil decreases, and thin and

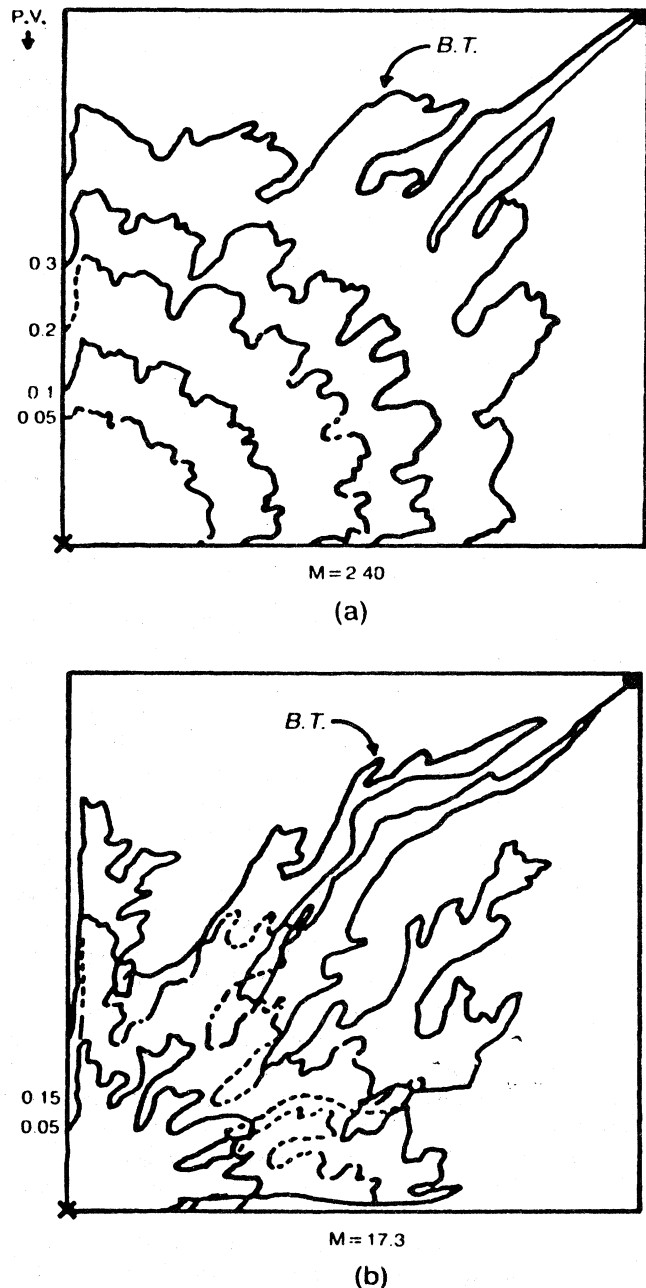


FIG. 41. Patterns of viscous fingering in a five-spot geometry as a function of the mobility ratio M . B.T. denotes the breakthrough, the point at which the displacing fluid first reaches the producing well, while P.V. denotes the pore volume of the injected fluid (from Habermann, 1960).

long fingers of the displacing fluid are formed.

Why do these fingers form? Collins (1961) gives a simple but very clear illustration to explain this phenomenon. Suppose that a porous medium is saturated with oil, and a displacing fluid is injected into the medium to displace it. Assume that dispersion is negligible. The displacing fluid displaces the oil linearly, i.e., if the porous medium is homogeneous, the front will remain a flat plane throughout the process. Suppose now that the displacing fluid encounters a small region of higher permeability. Then the front will travel faster in that region and produce a bump that is a distance ϵ ahead of the rest of the front. If k , ϕ , and ΔP are, respectively, the permeability, porosity, and pressure difference along the medium, then using Darcy's law we can write

$$\frac{dx_f}{dt} = \frac{k \Delta P}{\eta_f \phi [ML + (1-M)x_f]} , \quad (7.1)$$

when x_f is the position of the front, L the medium's length, and $M = \eta_0/\eta_f$. Similarly, we can write

$$\frac{d(x_f + \epsilon)}{dt} = \frac{k \Delta P}{\eta_f \phi [ML + (1-M)(x_f + \epsilon)]} , \quad (7.2)$$

and therefore

$$\frac{d\epsilon}{dt} = \frac{-k \Delta P (1-M)}{\eta_f \phi [ML + (1-M)x_f]^2} \epsilon = c \epsilon , \quad (7.3)$$

if $\epsilon \ll x_f$, and hence $\epsilon = \epsilon^{ct}$. However, $c > 0$ if $M > 1$, which means that ϵ grows exponentially with t , and a long thin finger is formed, but it dies out if $M < 1$. Although this example is too simple, it does illustrate the effect of M in the formation of viscous fingers. We should remark that finger formation is not restricted to miscible displacements, and can also occur in immiscible displacements, which will be discussed in Sec. VIII. Because of its significance, viscous fingering has been studied for a long time, and several review papers have discussed the subject. Among these are those of Wooding and Morel-Seytoux (1976), who reviewed viscous fingering in a porous medium, Bensimon *et al.* (1986) and Saffman (1986) who discussed immiscible viscous fingering only in a Hele-Shaw cell (see below), and Homsy (1987) who considered the problems in both Hele-Shaw cells and porous media. Viscous fingering also belongs to the general class of pattern-selection problems, and Kessler *et al.* (1988) have provided a comprehensive review of the subject. Therefore it is clear that the subject is both important and well-reviewed, and hence we restrict ourselves to a review of the most interesting and important results.

There have also been many experimental studies of viscous fingering, both in miscible and immiscible displacements. Some of these include those of Blackwell *et al.* (1959), Benhan and Olson (1963), Slobod and Thomas (1963), Greenkorn *et al.* (1965), Kyle and Perrine (1965), Perkins *et al.* (1965), Mahaffey *et al.* (1966), Perkins and Johnston (1969), and more recently, those of Pa-

terson (1981, 1983, 1985), Paterson *et al.* (1982), Park *et al.* (1984), Chen and Wilkinson (1985), Måløy *et al.* (1985, 1987), Nittman *et al.* (1985), Ben-Jacob *et al.* (1986), Daccord *et al.* (1986), Lenormand *et al.* (1988), Tabeling and Libchaber (1986), and Bacri *et al.* (1991). Most of these experiments were carried out in either a Hele-Shaw cell, or a porous medium with microscopic disorder. Flow in the Hele-Shaw cells was either rectilinear or radial. The fluids were mostly oil and water, in the case of immiscible displacements, or oil and a miscible fluid. Most of the experimental works were also accompanied by a linear stability analysis (see below), and most authors were interested in the qualitative aspects of the displacement process, e.g., the shape of the fingers and the effect of M on them. Some of these experiments will be compared with the theoretical predictions. In addition, viscous fingering and pattern formation in viscoelastic media (Van Dame *et al.*, 1987a, 1987b), and with smectic and nematic liquid crystals (Buka *et al.*, 1986; Horváth *et al.*, 1987a) have also been studied. Finally, Horváth *et al.* (1987b) studied viscous fingering in a Hele-Shaw cell with a set of parallel grooves on one of the plates to investigate the effect of an uniaxial anisotropy on the morphological phase diagram of the system.

Before we go on with the review of the subject, we would like to remind the reader that our policy throughout this review has always been to mention, and give credit to, the first important work on any subject we discuss. Hence, we should mention that Hill (1952) appears to be the first who published experimental and simple analytical results on viscous fingering. Later, Saffman and Taylor (1958) and Chouke *et al.* (1959) did the first rigorous analysis of the problem. Homsy (1987) suggested that one must call this phenomenon the "Hill instability" problem, instead of the now-popular "Saffman-Taylor instability." We take a middle-of-the-road approach and refer to this as the "Hill-Saffman-Taylor instability."

C. Miscible displacements in Hele-Shaw cells

The simplest system to study flow problems in a Hele-Shaw cell (Hele-Shaw 1898), which is an essentially two-dimensional system confined between two parallel plates of length L , separated by a small distance b . For single-phase flow, in the absence of dispersion, and in the limits of small Reynolds number and small b/L , the governing equations are the continuity equation, $\nabla \cdot \mathbf{v} = 0$, and Darcy's law, Eq. (5.1). The equivalent permeability k of the cell is $k = b^2/12$. These equations are the same as those of two-dimensional incompressible fluids in a porous medium. As long as dispersive mixing is absent, the same analogy is also valid between viscous fingers in Hele-Shaw cells and a two-dimensional porous medium. If dispersion is present, the analogy breaks down because, as we discussed in Sec. VI, transverse dispersion is always present in a porous medium, whereas a Hele-Shaw cell with its thin gap cannot support significant transverse

dispersion in the third direction. With dispersion present, we have to add a convective-diffusion equation to the set of governing equations, and keep in mind that the fluid viscosity η is now dependent upon the concentration C . The solution to this set of equations depends on the value of the Péclet number, which was already discussed in Sec. VI, and on two other dimensionless groups, which are [see Homsy (1987)]

$$A = \frac{\eta_1 - \eta_2}{\eta_1 + \eta_2} = \frac{M - 1}{M + 1}, \quad (7.4)$$

$$G = \frac{gk(\rho_1 - \rho_2)}{v(\eta_1 + \eta_2)}. \quad (7.5)$$

Let us first outline the general approach to stability analysis of miscible displacements, as we refer to it frequently in the subsequent subsections. In Sec. VII D we shall present a more quantitative description of the approach, but for now we restrict ourselves to a qualitative description.

The standard method of stability analysis of miscible (or immiscible) displacements can be summarized as follows. In the first step the governing equations are introduced which represent the unperturbed quantities. Next, one introduces perturbations into the dependent variables of the model. This results in a set of equations which, when subtracted from the unperturbed model, yields the governing equations for the perturbations. In the next step, the governing equations for the perturbations are solved either analytically or numerically, from the solution of which stability criteria are obtained. Clearly, if the perturbations grow with time, then the displacement is unstable. At first, this may seem to be a straightforward exercise which can be carried out with essentially no difficulty. However, the governing equations for the perturbations are often nonlinear and difficult to solve, even numerically. In that case, the equations are linearized in order to make the computations more tractable. This results in a *linear stability criterion* which is useful for the onset of stability, but cannot be used for predicting the long time behavior of the displacement process. One common feature of linear stability theory is that one can decompose the initial perturbations into separate Fourier components, so that the stability of each component can be investigated separately. This often simplifies the problem considerably. This also suggests that Fourier analysis (also known as spectral analysis) is a very convenient way to solve the perturbation equations. It also introduces the terminology of wave theory, and thus the stability criterion may be expressed in terms of perturbations that have wavelengths greater or less than a critical value. Of course, if the critical wavelengths can be measured, then the stability criterion can be much more quantitative.

Dispersion limits the wavelengths or frequencies of the Fourier components that can be unstable, which is why it usually has a positive effect on a miscible displacement. In the presence of dispersion the problem is always time

dependent, transport coefficients such as the viscosity and dispersion coefficients are concentration (and hence time) dependent, and one cannot find a physical steady-state solution. Chouke was the first who analyzed the effect of dispersion, but his results appeared almost 30 years after their derivation in an Appendix to the paper of Gardner and Ypma (1982). For now we assume that the disturbances are of the form of normal modes proportional to $\exp(i\omega t + i\alpha y)$. Chouke considered the case of a jump in viscosity, i.e., a base-case solution in which longitudinal dispersion is absent, but allowed both longitudinal and transverse dispersion to act on the disturbances. His result for ω is then given by

$$\omega = \frac{1}{2} [A\alpha - \alpha^3 Pe^{-2} - \alpha(\alpha^2 Pe^{-2} + 2A\alpha Pe^{-1})^{1/2}], \quad (7.6)$$

where the cutoff wave number is given by

$$\alpha_c = A Pe/4, \quad (7.7)$$

and ω is maximum when

$$\alpha_m = (2\sqrt{5} - 4) A Pe/4. \quad (7.8)$$

Thus the Péclet $Pe = LV/D_m$ provides a physical mechanism for the introduction of a cutoff length scale. Equation (7.6) should be compared with the result in the absence of dispersion, i.e., when $Pe \rightarrow \infty$, $\omega = (A + G)\alpha$, which is unphysical because it implies that smaller wavelengths are even more unstable than the larger ones. In this subsection, we present a mostly qualitative discussion of the available results. In the next subsection, where we discuss the results for porous media, we give a more quantitative discussion, most of which is also applicable to Hele-Shaw cells. Homsy (1987) provides an excellent and comprehensive review of the subject, and what follows in this subsection is essentially a summary of his discussion, plus our own remarks and comments and the review of the works since the publication of his review.

In the early 1960s several attempts were made to investigate the stability of miscible displacements in both the Hele-Shaw cells and porous media. The approach of introducing small perturbations that we discussed above was taken by Perrine (1961) and Wooding (1962). In particular, Wooding (1962) treated the stability of a time-dependent base solution, and considered buoyancy-driven fingering. By expressing the disturbance quantities as a Hermite expansion and truncating the expansion beyond the first term, he obtained a dispersion relation which was qualitatively similar to Eq. (7.6). He also argued that all disturbances will die out if dispersion is given enough time to act. Another approach was based on a macrostatistical method, first used by Scheidegger and Johnson (1961), in which the fingers are treated statistically. Thus only the average cross-sectional areas occupied by the fingers are taken into account, and the shape and size of the individual fingers are neglected. Dougherty (1963), Koval (1963), and Perrine (1963) used this approach and

took into account the effect of dispersion. In all cases, one ends up with nonlinear equations which have to be solved numerically in order to study instability.

Schowalter (1965) studied fingering in which both density and viscosity variations are present. Although, as discussed above, the governing equations do not allow a steady base solution, he assumed one anyway and obtained a dispersion relation and a cutoff wave number. Heller (1966) considered horizontal miscible displacement in a rectangular system, and studied the early growth or decay of perturbations using a Fourier analysis. He also included the effect of dispersion and approximated the profiles by straight-line segments (or "ramp-shaped" profiles as he called them), and obtained the dependence of the growth exponent on the wave number. However, the assumption of straight-line segments for the profiles makes his results of limited applicability.

Peters *et al.* (1984) considered a miscible displacement process, took into account the effect of dispersion, and performed a Fourier analysis to derive a linear stability criterion. Tan and Homsy (1986) considered this problem for the case of no density difference, and a situation in which the concentration dependence of the viscosity is given by $\eta(C) = \exp(-C \ln M)$. The flow was rectilinear and the domain was unbounded. Both isotropic and anisotropic media were considered, and a quasi-steady-state assumption was made. They showed that, for the isotropic case, Chouke's result is essentially correct in the sense of predicting correctly the magnitude of the growth rates and the preferred wave numbers. However, they also found that at longer times dispersion causes a shift to larger wave lengths, and stabilizes the flow to some extent. Tan and Homsy (1986) also showed that transverse dispersion causes a shift to smaller length scales, as expected. Hickernell and Yortsos (1986) considered the case in which the solvent is injected into the system whose amount varies with time. This results in a spatially varying mobility profile. They ignored the effect of dispersion and showed that a finite thickness of the zone of viscosity variations provides a cutoff scale. Chang and Slattery (1986) showed that, when there is a steep change in concentration and $M > 1$, the displacement can be unstable at the injection boundary. But, if the concentration is changed sufficiently slowly with time at the entrance to the system, the displacement will be stable to small perturbations, *regardless of the value of M*.

In some situations, dispersion can play a role similar to that of surface tension in immiscible displacements. As we shall discuss in Sec. VIII, surface tension is responsible for *tip splitting* in the fingers, which is the main mechanism of pattern formation, and dispersion can cause a similar phenomenon in miscible displacements. The experiments of Wooding (1969) in a Hele-Shaw cell, in the presence of buoyancy forces, are indicative of this phenomenon. In Wooding's experiments, transverse dispersion causes lateral *spreading* of the fingers, as expected. However, because of this spreading, the tips of the fingers can become unstable since their typical

breadth exceeds the cutoff length scale, which is also set by transverse dispersion. Because of this instability, tip splitting can occur if Pe exceeds a critical value which, according to Tan and Homsy (1987), depends on both A and M . For example, at $M = e^3$, $250 < (\text{Pe}/A_r)_{\text{critical}} < 300$, if dispersion is isotropic (i.e., $D_L = D_T$), where A_r is the aspect ratio of the cell. Note that if transverse dispersion is weak, then tip splitting may not happen at all, because before it can start one must have spreading of the fingers, which can happen only if transverse dispersion is strong enough.

Numerical simulations of miscible displacements in rectilinear flows (such as those in Hele-Shaw cells) with weak dispersion (high values of Pe) are particularly difficult. The first attempt in this direction was made by Peaceman and Rachford (1962), using finite-difference methods, which was not successful because of large numerical errors that dominated the solution. Since their pioneering attempt, a lot of effort has been dedicated to this problem. The main reason for this difficulty was that for large values of Pe, viscous fingering can occur on many scales, and there is no unique power of Pe with which one can rescale all lengths. Zimmerman and Homsy (1991) proposed a method which appears to tackle this problem to a large extent. They used Fourier transforms to recast the system of partial differential equations, governing flow and dispersion into an ordinary differential equation for the Fourier coefficients. Then they used a two-dimensional Hartley transform, which for an arbitrary function $g(x, y)$ is given by

$$G(\alpha_x, \alpha_y) = \frac{1}{(N_x N_y)^{1/2}} \sum_x \sum_y \text{cas} \left[\frac{2\pi x \alpha_x}{N_x} + \frac{2\pi y \alpha_y}{N_y} \right] g(x, y), \quad (7.9)$$

where N_x and N_y are the number of collocation points, α_x and α_y are the wave numbers in the longitudinal and transverse directions, respectively, and $\text{cas}(x)$ is the so-called "cosine and sine" function, formed by summing the cosine and sine of its argument. The advantage of using the Hartley transform is that it can be easily inverted, because it is its own inverse. An efficient method for computing a two-dimensional discrete transform via $N_x + N_y$ discrete fast Hartley transforms has been devised by Bracewell *et al.* (1986). Zimmerman and Homsy (1991) used the Taylor-Aris result, Eq. (6.12), to relate D_L to Pe, in which they used $\delta_s = 2/105$, the appropriate value for flow between two parallel plates (Hele-Shaw cell), and assumed that $D_T = D_m$ (i.e., a constant, velocity-independent D_T). As such, the results are valid only for Hele-Shaw-like geometries, although the authors claimed that the results are also valid for porous media. Over a wide range of value of Pe, they observed a variety of phenomena, including spreading, tip splitting, shielding, and pairing. In a shielding process, one finger gets

ahead of its neighbors and grows explosively. Eventually, the tip of the finger spreads out and *shields* the neighboring fingers. Pairing is a phenomenon by which pairs of fingers join and form a larger finger. This phenomenon has been observed both with isotropic dispersion ($D_L = D_T$) and anisotropic dispersion. It can also be found in immiscible fingering as was shown by Tryggvason and Aref (1985) and Kessler and Levine (1986). According to Tan and Homsy (1987), pairing occurs because of unequal cross-flow about neighboring fingers. This allows a finger to spread, which shields the growth of the neighboring finger and results in its eventual collapse. If tip splitting is absent, then pairing eventually results in the reduction of the number of fingers to one or two.

The results of Zimmerman and Homsy (1991) also indicated great sensitivity in the complex two-dimensional fingering patterns that evolve on the size of the initial noise. However, when an averaging was performed over the cross-section area, it was found that the one-dimensional average concentration profiles were similar with large Pe and small D_m/D_L . This means that it may be possible to describe nonlinear viscous fingers by a one-dimensional model, which is invariant with respect to Pe and D_m/D_L , for large Pe and small D_m/D_L . In a sense, this is the same as the idea of Scheidegger and Johnson (1961) already mentioned above. It is also similar to the work of Fayers (1988), who constructed an approximate one-dimensional model with adjustable parameters that had clear physical meaning. Koval (1963) and Todd and Longstaff (1972) also constructed empirical one-dimensional models which could predict the evolution of the average concentration profile well. But because of their empirical nature, they could not provide much insight into the mechanisms of viscous fingering. Finally, Christie and Bond (1987) developed a numerical method for the evolution of both linear and nonlinear fingers. They used a finite-difference method for the longitudinal direction and Fourier decomposition in the transverse direction.

The effect of the cell geometry is significant. Wilson (1975) and Paterson (1985) studied miscible viscous fingering in a radial Hele-Shaw cell both theoretically and experimentally. Paterson (1985) ignored dispersion and obtained the following relation for ω

$$\omega = Am - 1, \quad (7.10)$$

where m is a discrete azimuthal wave number. This equation indicates that there is no cutoff azimuthal wave number, which is not surprising. Thus Paterson (1985) suggested that in a radial Hele-Shaw cell, and in the absence of dispersion, fingers can form on *all* length scales, down to the size of the gap between the plates. Based on a heuristic argument using the concept of energy dissipation in the gap, Paterson (1985) estimated that the cutoff wavelength is approximately $4b$. Figure 42, taken from his work, shows the pattern of miscible viscous fingers in a radial Hele-Shaw cell. While his experimental results

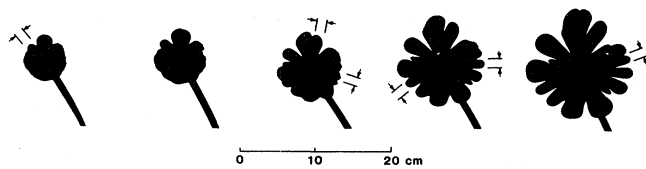


FIG. 42. Viscous fingers in a radial Hele-Shaw cell. The gap between the plates is $b=0.3$ cm, and the exposures are, from left to right, at $t=12, 17, 21, 26$, and 31 sec, respectively. The indicated distance is $4b$ (from Paterson, 1985).

appear to agree with his rough estimate of the cutoff wavelength, Paterson's argument in the general case in which dispersion is present is not expected to hold, because, as discussed above, transverse dispersion (however small in a Hele-Shaw cell) helps the fingers to spread, which leads to tip splitting. Thus fingers cannot form down to the scale b . This has been discussed in details by Homsy (1987). Finally, mention should be made of the experiments of Nittman *et al.* (1985) and Daccord *et al.* (1986). These authors used a viscoelastic fluid to study fingering in both radial and rectilinear Hele-Shaw cells. Their viscous fingers show very localized tip splitting and shieldings which are also much stronger than those obtained with a Newtonian fluid. The viscous fingers also have a fractal structure with a fractal dimension close to that of diffusion-limited aggregates, which will be discussed below. These results contradict those obtained with Newtonian fluids discussed above, and remain unexplained.

D. Miscible displacements in porous media

Since the 1950s there have been many experimental studies of miscible displacements in porous media, most of which were made of sand or other unconsolidated materials. In particular, Slobod and Thomas (1963) and Perkins *et al.* (1985) used x-ray techniques to make visualization studies of viscous fingers. Normally, one can observe viscous fingers over length scales that are several times larger than the typical pore size. Since in these experiments the transverse Pe (i.e., the Péclet number based on D_T instead of D_m) is relatively low, finger growth is probably due to the spreading phenomenon discussed above. A careful examination of the pictures taken during the experiments of Slobod and Thomas (1963) and Perkins *et al.* (1965) shows no tip splitting. However, Habermann's (1960) and Mahaffey *et al.*'s (1965) experiments do show tip splitting due to shielding, similar to those in a Hele-Shaw cell already discussed. The dominant length scale in all of these experiments is much larger than a typical pore size. However, if one carries out experiments in a porous medium in which Pe increases with decreasing length scales, one can no longer claim that the dominant length scale is much larger than the typical pore size. An example is the work of Paterson *et al.* (1982) who studied miscible viscous fingers in packed beds. The viscous finger patterns that they ob-

tained are similar to diffusion-limited aggregates. This indicates that, for a given pore space there is a crossover between the continuum and discrete description. An important and interesting question is the shape of viscous fingers for the case in which there is no mechanism for the creation of a cutoff scale, e.g., in the absence of dispersion. These will be discussed below where we present discrete models of viscous fingering.

How can we describe miscible displacements and viscous fingers in a porous medium? One method is based on averaged continuum equations, most of which were discussed above and the rest are reviewed below. This can then describe any instability that is smooth on the length scale of the continuum equations. Thus all of the above discussions regarding miscible displacements in Hele-Shaw cells and similar geometries are equally applicable to porous media, provided that dispersion phenomena discussed in Sec. VI are properly taken into account. For example, the approach of Zimmerman and Homsy (1991) can be used for miscible displacement in porous media if, instead of what they used, we use the appropriate equations for the velocity (or Pe) dependence of D_L and D_T , discussed in Sec. VI. In the strict absence of dispersion (i.e., the limit $\text{Pe} \rightarrow \infty$, where Pe is based on D_L or D_T and not D_m), viscous fingers will occur on all scales, with growth rates that increase with decreasing scale. This means that a scale will be reached for which a continuum description is no longer appropriate, and one has to develop a pore-level model. Such models are discussed below. The initial-value problem in this case is ill posed, but one can seek solutions that contain discontinuities. Since dispersion is absent in this case, there will be a step jump in the viscosity profiles (from the displacing to the displaced fluids). As a result, the pressure obeys the Laplace equation, and the pressure and fluid fluxes are continuous across the front separating the displaced and displacing fluids. One may have all sorts of singularities in the solution, and different nonuniformities can appear in different boundary value problems. For example, Shraiman and Bension (1984) and Howison (1986) investigated cusp formation in viscous fingering.

Even since Paterson (1984) pointed out an analogy between DLA processes and viscous fingering in the limit $A=1$ ($M=\infty$) and in the absence of dispersion, there has been considerable interest in this subject. But, before we review and discuss this body of work, we first discuss briefly continuum approaches to miscible displacements and their stability in porous media. As we already pointed out, most of the methods that we discussed for miscible displacements in Hele-Shaw cells are also applicable to porous media, provided that the effect of dispersion is properly taken into account.

1. Continuum approaches to miscible displacements in porous media

In the petroleum industry, a standard approach to miscible displacements in porous media is based on solving

the governing equations with finite-difference techniques. The earliest of such methods was that of Peaceman and Rachford (1962) mentioned above, while the works of Giordano and Salter (1984), Giordano *et al.* (1985), and Christie and Bond (1987) represent the latest of such attempts. There are two major problems with such methods. The first is that the resolution of the results is often poor, making it very difficult to investigate viscous fingers. The second problem is that the initiation of instabilities in this method requires permeability variations. However, the results are often very sensitive to the initial permeability variations that are used in the simulations. Although supercomputer technology has made it possible to use very fine finite-difference grids, the results do not yet agree quantitatively with the experimental data, unless a very large and detailed mesh is used.

An alternative approach is based on the method of weighted residuals, proposed by Tan and Homsy (1987) and Hatzivramidis (1988). Fourier expansions (or a spectral method) and Chebyshev polynomials are used in this method, which are accurate and relatively efficient. To obtain numerical solutions of the resulting equations, collocation methods are used which means that these equations are solved exactly at the collocation points. One can also use a fast fourier transform (FFT) to refine the grids. Even the system with the refined grid can be solved more efficiently than those with the standard finite-difference method. However, the method can become complex if simulations for long times are needed. Moreover, FFTs can be used if the number of grid points is an integral power of two, which means that most of the advantage gained from the use of FFTs can be lost. Finally, one usually has to use periodic boundary conditions in order to avoid the so-called Gibbs phenomenon, which is characterized by wiggly outlet concentration curves. Hatzivramidis (1988) compared the results of his spectral method with simulation results and found good agreement between the two. Other continuum methods were discussed when we reviewed miscible displacements in Hele-Shaw cells.

2. Linear stability analysis of miscible displacements in porous media

We have already given a qualitative discussion of how a stability analysis of miscible displacements is performed. In this subsection we provide a more quantitative discussion of this. The main goals of this subsection are to illustrate, (i) how a linear stability analysis is actually carried out, and (ii) how far an analysis can take one. We emphasize again that most of this discussion is also applicable to Hele-Shaw cells. A detailed discussion of such stability analyses is given by Yortsos (1990). What follows is a summary of his discussion.

As already discussed in Sec. VI, dispersion coefficients depend on the mean flow velocities, and the precise form of the dependence depends on the value of the Pe. How-

ever, for simplicity, we assume that D_L and D_T are related to the flow velocities v_x and v_y through the relations (Bear 1972)

$$D_L = D_m + \alpha_L |v| + (\alpha_L - \alpha_T) v_x^2 / |v| , \quad (7.11)$$

$$D_T = D_m + \alpha_T |v| + (\alpha_L - \alpha_T) v_y^2 / |v| , \quad (7.12)$$

which describe longitudinal and transverse dispersion coefficients in terms of the corresponding dispersivities α_L and α_T , and the molecular diffusion coefficient D_m . For convenience, we shall follow the notation in Yortsos and Zeybek (1988) and Yortsos (1990) to obtain the system

$$\phi \frac{\partial C}{\partial t} + v_x \frac{\partial C}{\partial x} + v_y \frac{\partial C}{\partial y} = \frac{\partial}{\partial x} \left[D_L \frac{\partial C}{\partial x} \right] + \frac{\partial}{\partial y} \left[D_T \frac{\partial C}{\partial y} \right] , \quad (7.13)$$

$$\frac{\partial v_x}{\partial x} + \frac{\partial v_y}{\partial y} = 0 , \quad (7.14)$$

$$v_x = -\frac{k}{\eta} \frac{\partial P}{\partial x} , \quad (7.15)$$

$$v_y = -\frac{k}{\eta} \frac{\partial P}{\partial y} . \quad (7.16)$$

Implicit in the above continuum description is the assumption that the local Péclet number $Pe_l = vl/D_m$, is small.

The base state corresponding to constant injection at concentration C_i , and rate v in a rectilinear flow geometry is given by the well-known diffusive profile (Tan and Homsy, 1986)

$$\bar{C} = \frac{1}{2} \operatorname{erfc}(\xi/2t^{1/2}) , \quad (7.17)$$

$$\frac{\partial \bar{P}}{\partial \xi} = -\frac{1}{\lambda(\bar{C})} , \quad (7.18)$$

where $\xi = (x - vt)/L$ is a moving coordinate, λ denotes a normalized mobility (inverse of viscosity), and lengths are scaled with D_{L0}/v , where D_{L0} is the base-state dispersion coefficient. Using normal modes for concentration and flow rate, respectively,

$$\{C', v'_x\} = \{\Sigma, \Phi\} \exp(i\omega t + i\alpha y) , \quad (7.19)$$

the following eigenvalue problem is obtained:

$$\Sigma_{\xi\xi} - (\epsilon\alpha^2 + \omega)\Sigma = \Phi C_\xi - L_c(\Phi C_\xi)\xi , \quad (7.20)$$

$$\lambda(\lambda^{-1}\Phi_{xi})_\xi - \alpha^2\Phi = -\alpha^2 R \Sigma , \quad (7.21)$$

where the mobility dependence is taken to be (Tan and Homsy, 1986)

$$\lambda(C) = \exp(RC) , \quad (7.22)$$

and $R = \ln M$. The subscripts denote derivatives with respect to the variables. Two important terms, ϵ and L_c ,

$$\epsilon = \frac{D_m + \alpha_T v}{D_m + \alpha_L v} , \quad (7.23)$$

$$L_c = \frac{\alpha_L v}{D_m + \alpha_L v} , \quad (7.24)$$

appear in Eq. (7.20). ϵ is a measure of flow-induced anisotropic dispersion, which is characteristic of porous media, while L_c is a measure of the contribution of mechanical dispersion to total dispersion. It must be stressed that in the works of Chouke (1959) and of Tan and Homsy (1986) the term containing L_c in (7.20) is absent, thereby restricting their conclusions to essentially constant (although still anisotropic) dispersion. Zimmerman and Homsy (1991) used velocity-dependent dispersion coefficients, although their functional forms were different from (7.11) and (7.12).

Based on our discussion in the previous subsections, one expects that the onset of instability and related features would be dictated by the sharpest mobility contrast, namely, that associated with a step concentration profile, which also allows for an analytical solution given by (Yortsos and Zeybek, 1988)

$$\alpha R [1 + L_c \gamma_0 \tanh(R/2)] = 2\gamma_0(a + \gamma_0) , \quad (7.25)$$

where

$$\gamma_0 = (\epsilon\alpha^2 + \omega)^{1/2} > 0 . \quad (7.26)$$

In general, the solution of (7.25) leads to parabolic like profiles, examples of which are shown in Fig. 43. The case $L_c = 0$ corresponds to the result of Tan and Homsy (1986): for unfavorable mobility ratio ($R > 0$) large wavelengths are unstable, while a strong stabilization due to transverse dispersion is exerted at smaller wavelengths. A cutoff wave number can be identified

$$\alpha_c = \frac{R}{2(\epsilon + \epsilon^{1/2})} . \quad (7.27)$$

As expected, α_c increases with increasing unfavorable mobility, and with an increase in the ratio of longitudinal to transverse dispersion ($1/\epsilon$). However, the limits of the continuum description should be kept in mind. The size

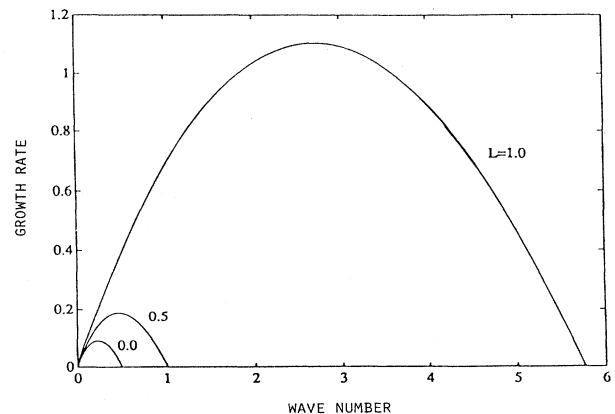


FIG. 43. Step-profile results for the growth rate vs the wave number for various values of the parameter L (from Yortsos and Zeybek, 1988).

of the most unstable disturbance scales with the characteristic length, which for large enough flow rates becomes equal to the dispersivity α_L , which is normally a multiple of the typical pore size (or the length scale of the heterogeneity). It is apparent that a possible conflict may develop between the above result and the continuum description, precluding meaningful predictions over scales of the order of the microscale.

While the case $L_c = 0$ leads to expected results, a distinct sensitivity develops as L_c takes nonzero values (see Fig. 43). This effect is present only because of the velocity dependence of the dispersion coefficients, and it can be best quantified in terms of the combination

$$B = (RL_c/2)\tanh(R/2) - 1 - \epsilon^{1/2}. \quad (7.28)$$

The following may then be shown (Yortsos and Zeybek, 1988):

(i) When $B < 0$ (which is *always* the case if $L_c = 0$), at small enough viscosity ratio and for $L_c \neq 0$, the cutoff wave number is finite

$$\alpha_c = \frac{1}{2}R\epsilon^{-1/2}(-B), \quad (7.29)$$

although it increases as L_c or B does.

(ii) On the other hand, when $B > 0$, a finite cutoff does not exist, with the rate of growth increasing indefinitely at large α as

$$\omega \sim B(B + 2\epsilon^{1/2})\alpha^2 > 0. \quad (7.30)$$

Clearly, such is the case for a sufficiently high (but finite) mobility contrast, as long as $L_c \neq 0$, as shown in Fig. 43. This unexpected and rather remarkable result was obtained on the basis of a step base state, which is subject to a singular behavior in the large (as well as in the small) α region. To better understand the proper dependence, Yortsos and Zeybek (1988) attempted a more rigorous asymptotic analysis valid for base states near a step profile, namely, for

$$\bar{C} = \frac{1}{2}\operatorname{erfc}(b\zeta), \quad (7.31)$$

where $b \gg 1$. Their results showed that the step profile prediction, inequality (7.30), is invalid at large α , when $B > 0$, and in fact a cutoff wave number does exist. However, the latter was found to increase monotonically and without bound as b increases, namely, as the profile becomes steplike, provided that $B > 0$. Thus the essential predictions, that qualitatively different instability behavior is obtained by changing the sign of B , remain intact. Most of the above results were confirmed by the recent experimental study of Bacri *et al.* (1991).

The implications of the above are straightforward. Due to the dependence of the dispersion coefficients on the flow velocity, an essential feature of hydrodynamic dispersion in porous media, and for mobility ratios that exceed a critical value dictated by the given process conditions, a miscible replacement is predicted to be unstable *at all wavelengths*. Under such conditions, there is no

finite preferred mode, and in fact the above continuum description is ill-posed and breaks down.

This remarkable result raises serious doubts about our ability to describe the conditions for the onset of instability in miscible displacements. Recall that the result is an outcome of several hypotheses, including the validity of a continuum description, with dispersion represented in terms of a passive solute and formulated in terms of a conventional convective-diffusion equation. If the present predictions are to be taken seriously, the breakdown of the continuum hypothesis beyond a finite M calls for an alternative description to the present CDE-based description. One concludes that at least for large enough mobility ratios, our present description of miscible displacements is inadequate, particularly at the early, and the most important, stage of the process. Thus although Zimmerman and Homsy (1991) used a CDE, it is not clear that the formulation is actually applicable to the early stages of the growth of the fingers. Clearly, additional fundamental work is needed. The above analysis demonstrates clearly the significance of anisotropic dispersion (i.e., the inequality of D_L and D_T). Of course, all of the above results are limited to linear fingers, and nonlinear fingers require full numerical simulations of the above equations, provided that the proper forms of the velocity-dependence of the dispersion coefficients are used.

One problem with all of the above approaches, including those of Tan and Homsy (1986, 1987), Zimmerman and Homsy (1991), and Yortsos and Zeybek (1988) is that it is difficult to incorporate the effect of rock heterogeneity into such models, especially if it is strongly disordered with correlations over many length scales, in which case not only the above approaches cannot account for such effects, a continuum description may not even be valid to begin with. This is certainly the case if the pore space is fractal. For this reason, discrete models, which are flexible enough for including the effect of pore space disorder, offer an alternative to the continuum formulations. Such an alternative is very useful for obtaining insight into the effect of disorder on viscous fingering. We now review and discuss the discrete models.

E. Discrete models of miscible displacements

In this section we discuss discrete models of miscible displacements, and compare their performance with the experimental data and the predictions of continuum models.

1. Diffusion-limited aggregation

In the DLA model one starts with an occupied site (the “seed”) of a lattice, located either at the center of the lattice or on its edges. Random walkers are released, one at a time, far from the seed particle and are allowed to move randomly on the lattice. If they visit an empty site

adjacent to an occupied one, the aggregate of the occupied sites advances by one site and occupies the last site visited by the walker. The walker is removed, another one is released and so on. Now, imagine that the aggregate represents a displacing fluid, and the empty sites represent the displaced or the defending fluid. Thus the original seed particle represents the point at which the displacing fluid is injected into the system. Since the particles perform their random walks on the empty sites, the probability $P(\mathbf{r})$ of finding the particle at a position \mathbf{r} in this region obeys the Laplace's equation, $\nabla^2 P = 0$. Because the walkers never move into the aggregate, the probability of finding them there is zero. If the walkers are reflected at the "walls" of the system, one has $(\nabla P)_n = 0$, where n denotes normal to the wall. Finally, the mean speed at which the front between the displacing and displaced fluids advances is proportional to the probability on the side of the displaced fluid next to the front, i.e., $\mathbf{v} = (\nabla P)_n$. But these are essentially the same equations for the displacement of a viscous fluid by a miscible inviscid one, *in the absence of dispersion*. In other words, a miscible displacement in the limits $M = \infty$ and no dispersion can be simulated by this algorithm. The DLA model was originally invented by Witten and Sander (1981, 1983) to simulate aggregation of small particles, and Meakin and many others have studied it extensively [see Meakin (1988) for a review of the subject]. Paterson (1984) was the first to note the above analogy between the DLA model and miscible displacements.

There are, however, several problems with this analogy. Recall that a miscible displacement can be unstable if $M > 1$. The DLA algorithm produces an aggregate that, (i) has a fractal structure with a fractal dimension of about $D_{\text{DLA}} \approx 1.7$ and 2.45, in two and three dimensions, respectively; and (ii) it contains a large number of very tiny fingers in which tip splitting occurs at all times. Chen and Wilkinson (1985) displaced glycerine by oil in an etched-glass network and showed that, if the system is perfectly ordered (all pores have the same size), then the fingers form ordered (dendrites) patterns (see Fig. 44), in which growth occurs mostly along the coordinates of the system, whereas the DLA algorithm would generate a random fractal for exactly the same situation. The reason is that the surface of a DLA structure is dominated by noise: random walkers taking *random trajectories* arrive there one at a time, which makes the surface very rough. Thus one has to somehow reduce the noise. Two algorithms were introduced to accomplish this. In the first, one introduces a "sticking probability," the probability p_s that the front will advance by one unit once a random walker is in an empty site next to the aggregate. The DLA case corresponds to $p_s = 1$. However, if we let p_s to be very small, then the surface of the aggregate becomes very smooth, because a random walker will encounter the front many times (roughly $1/p_s$ times on average) before the front actually advances. This was discussed by Meakin (1986).

The second method is due to Tang (1985) and Sz  p

et al. (1985). In this method, each time an empty site next to the front is visited by a random walker, a counter registers the event. The front does not advance to an empty site in its neighborhood unless the empty site has been visited at least n_v times, so that $n_v = 1$ corresponds to the DLA case, and $n_v = \infty$ represents the mean-field (noiseless) limit of the DLA model. Kert  sz and Vicsek (1986) showed that this modification of the DLA algo-

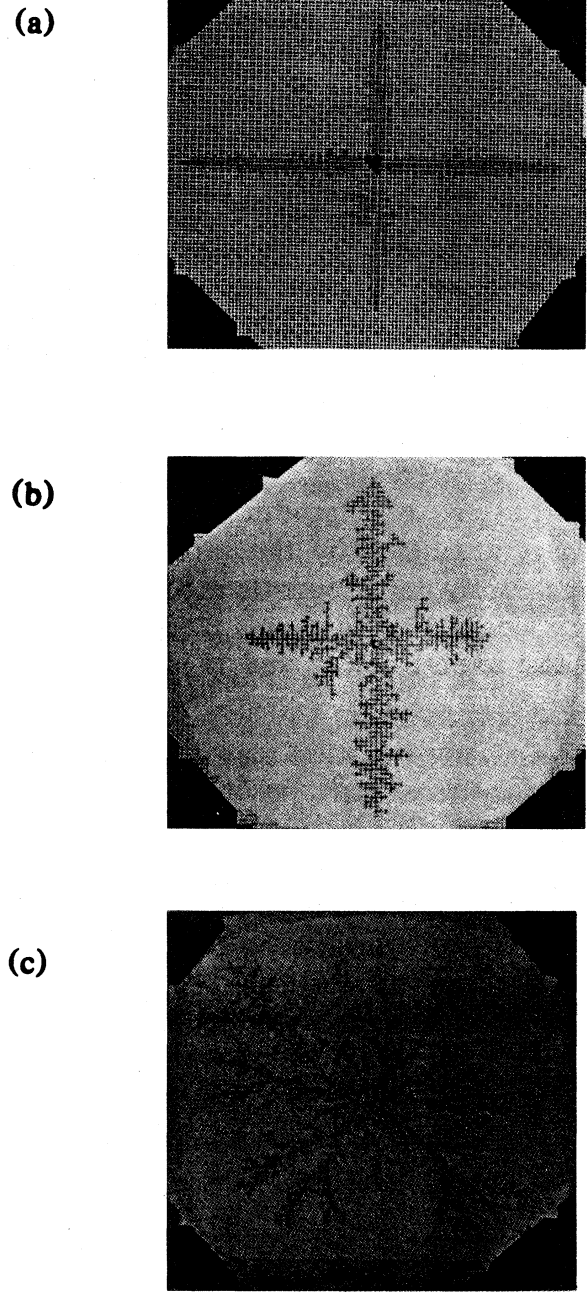


FIG. 44. Patterns of viscous fingers in an etched-glass network. In (a) all pores have the same radius, while in (c) the network is completely disordered (from Chen and Wilkinson, 1985).

rithm can reproduce the patterns obtained by Chen and Wilkinson [see also Siddiqui and Sahimi (1990a)].

If, in an unstable miscible displacement, we reverse the direction of the pressure gradient and allow the more viscous fluid to displace the less viscous (or inviscid) one, the displacement will be stable. This can be simulated by allowing the displaced fluid to advance each time the n_v visits occur. This was suggested by Paterson (1984) and Tang (1985), and may be called anti-DLA (since it essentially represents the reverse of the DLA process). Paterson (1984) compared the results of such simulations with the experimental data of Habermann (1960) and found reasonable agreement. C. Tang (1985) compared his results with the exact steady-state solution of Saffman and Taylor (1958), and the exact unsteady-state solution of Shraiman and Bensimon (1984), and found excellent agreement. Therefore this aspect of DLA-based simulation of miscible displacements is clarified.

There are several other aspects of DLA-based simulations of miscible displacements that deserve careful consideration. The first one is whether this type of simulation can be generalized to the case of finite values of M . The next question is whether this type of simulation can be a *quantitative* tool for simulating miscible displacements in a *disordered* porous medium, at least in the limit $M = \infty$. The third aspect is the fact that this type of simulation shows a sensitive dependence on the lattice size, and therefore it is highly important to establish links between the parameters of the simulations and the physical parameters that can be measured. Next is how to generalize the DLA algorithm for a porous medium with a pore size or a permeability distribution (as in a heterogeneous medium). The next issue is whether it is possible to generalize such techniques to include the effect of dispersion since, as we discussed above, dispersion plays a fundamental role in miscible displacements, whereas in most of published papers using this kind of simulations, this effect has completely been ignored. We shall investigate these issues, but we first review briefly a few models related closely to the DLA algorithm.

Before closing this subsection, we would like to mention that the DLA algorithm has been generalized to include the effect of surface tension, as in an immiscible displacement in a Hele-Shaw cell, which is the classical Hill-Saffman-Taylor problem. This method was suggested by Sz  p *et al.* (1985) and Kadanoff (1985). The problem is to force the probability $P(\mathbf{r})$ at the interface between the two fluids to have a value of the form

$$P(\mathbf{r}) = a_1 \kappa + a_2 , \quad (7.32)$$

2. The dielectric breakdown model

This model was proposed by Niemeyer *et al.* (1984) to study dielectric breakdown. A discrete version of the Laplace's equation is solved in which, as the boundary condition, the unknown function is specified at the boundary. In the context of a miscible displacement, the unknown function is the pressure, so the simulation is appropriate only for the case of a viscous fluid and an inviscid fluid. At each step of the simulation, one site on the boundary is selected for growth, the probability of selection being proportional to a power of the gradient of the unknown function. This algorithm is usually called the dielectric breakdown model (DBM). The same acronym is used by Ben-Jacob *et al.* (1985) to denote dense branching morphology. The DBM can also be simulated by a random walk technique. The method would be similar to that of DLA, except that in the DBM the front advances to a nearest-neighbor empty site if this site is visited by a random walker *which also crosses the front* (whereas in the DLA model the front advances as soon as the empty site is visited by the walker). Thus the boundary conditions at the front are *not* the same for the DBM and the DLA.

3. Gradient-governed growth model

DeGregoria (1985) and Sherwood and Nittman (1986) introduced an algorithm for simulating miscible displacements at finite values of M , and in the absence of dispersion. The model is usually called the gradient-governed growth model (GGGM). This is essentially an extension of the DBM to the case in which both fluids have a finite viscosity. A discrete version of the Laplace equation is solved in the region occupied by each fluid to yield the pressure field. One point on the front is advanced at each time step, with the selection probabilities proportional to the local pressure gradients. The model is *wrong* in a microscopic sense, because the velocity field is determined

assuming the entire front is moving instantaneously, yet only one bond at the front is moved at a time. DeGregoria (1985) and Sherwood and Nittmann (1986) used this model to simulate miscible displacement at finite values of M , in the absence of dispersion. Using a 100×100 square network, DeGregoria (1985) obtained reasonable agreement with Habermann's (1960) data. Sherwood (1986) used the same model for investigating the size distribution of the islands of the displaced fluid that are formed when the displacing fluid completely surrounds a portion of the displaced fluid.

4. The two-walker model

This method was proposed by Siddiqui and Sahimi (1990a) for simulating miscible displacements at finite values of M , in the absence of dispersion, *using only random walkers*. Since the pressure in each fluid region obeys the Laplace equation, one random walker for each fluid region (displacing and displaced) is used. Because in the absence of dispersion and surface tension the front always advances forward, both random walkers advance the front, upon contacting it, with a probability proportional to $p_1 = (M+1)^{-1}$, for the particle in the displacing fluid region, and $p_2 = M/(M+1)$, for the particle in the displaced fluid region. As such, this model can be thought of as the random walk version of the GGGM. Because of different mobilities of the two fluids, the lengths of each step of the random walkers are *different* in each fluid region. The results of this model are in complete agreement with those obtained with DBM and GGGM. Siddiqui and Sahimi (1990a) also generalized the model to the case in which there is a pore size or pore permeability distribution. In this case, the random walkers take each step with a probability proportional to the pore permeabilities (see also Meakin, 1987; Blumberg Selninger *et al.*, 1989). A somewhat similar model was proposed by Leclerc and Neale (1988), although the precise relation between these two models is not clear to us.

5. Probabilistic models that include the effect of dispersion

The discrete models discussed so far do not explicitly take into account the effect of dispersion. We now discuss three models that can accomplish this, two of which use probabilistic arguments and are discussed in this subsection, while the third one is completely deterministic and will be discussed in the next section.

The first of the two probabilistic models is due to King and Scher (1987, 1990), whose details are as follows. Consider first the case of miscible displacement *without* dispersion. For point injection of fluids the governing equations are

$$\frac{\partial C}{\partial t} + \mathbf{u} \cdot \nabla C = \delta^2(\mathbf{x}), \quad (7.33)$$

$$\mathbf{u} = \mathbf{v}/q_r = \nabla \times (\psi \hat{\mathbf{z}}), \quad (7.34)$$

where q_r is the injection rate (volume per unit thickness per unit time), ψ is the stream function, and $\delta^2(\mathbf{x})$ is the two-dimensional Dirac delta function. The injected volume of fluid provides a natural time variable

$$\tau = \int_0^t q_r(t') dt' / \psi. \quad (7.35)$$

Note that the viscosity function is a bulk fluid property. Mixture viscosities η_m are well represented by the following formula due to Koval (1963)

$$\frac{\eta_m(C)}{\eta_1} = (1 - C + CM^{1/4})^{-4}. \quad (7.36)$$

If there is no dispersion, then the solution is simple: A concentration bank $C=1$ displacing $C=0$, which are also what the diffusion-limited aggregation model predicts. However, in general, the concentrations need not form a bank. To develop a probabilistic model, King and Scher (1987, 1990) interpreted $(\partial C / \partial \tau) d^2x$ as a *two-dimensional* probability density function for concentration evolution. Equations (7.33) and (7.34) tell us that we can write

$$\frac{\partial C}{\partial \tau} d^2x = - \frac{\partial C}{\partial \xi_1} \frac{\partial \psi}{\partial \xi_1} d\xi_1 d\xi_2 = -dC d\psi, \quad (7.37)$$

where ξ_1 and ξ_2 are local tangential and normal coordinates on the front. Equation (7.37) can now be given a probabilistic interpretation. The probability of concentration evolution at \mathbf{x} [i.e., $(\partial C / \partial \tau) d^2x$] is the product of the probability $d\psi$ of fluid flow through \mathbf{x} and the probability dC of a concentration gradient moving through \mathbf{x} . For a given *realization*, one samples the cumulants C and ψ , i.e., determines the flux contour $C=r_1$, and the streamline $\psi=r_2$, and calculates their intersection in the plane, which is also the point at which concentration is modified. Here r_1 and r_2 are two random numbers uniformly distributed in $(0,1)$.

In a simulation, one has to employ a probabilistic interpretation of the finite-difference version of Eq. (7.33). We integrate this equation over a rectangular spatial region A_{ij} and time interval $\Delta\tau$ to obtain δC_{ij} , the change in the average concentration C_{ij} . This is given by

$$\delta C_{ij} = - \frac{\Delta\tau}{\Delta x \Delta y} \oint_{\partial A_{ij}} \bar{C} d\psi. \quad (7.38)$$

Obviously, if $\delta C_{ij} / \Delta C$ is properly normalized, then it can be interpreted as the growth probability at site ij . One now has to fix ΔC . If we choose $\Delta C=1$, we have a situation similar to the diffusion-limited aggregation model (i.e., a cluster of $C=1$ surrounded by a cluster of $C=0$). According to Eq. (7.38), the growth probability is nonzero only when the boundary integral overlaps the cluster edge. This method has the advantage that finite values of M can be used in the simulations. But it also implies that very large clusters *cannot* be generated with this method.

We can now add the effect of dispersion. Consider first the static case $\mathbf{v}=0$. The evolution equation is simply

the diffusion equation, $\partial C / \partial T - D_L \nabla^2 C = 0$, where $T = D_L t$ (King and Scher assumed the equality of D_L and D_T , which is not justified). In discrete form

$$\delta C_{ij} = \frac{\Delta T}{\Delta x \Delta y} \oint_{\partial A_{ij}} \hat{n} \cdot \nabla \bar{C} dl , \quad (7.39)$$

which should be compared with Eq. (7.38). If the time step ΔT satisfies $\Delta T / (\Delta x \Delta y) \leq \Delta C$, then

$$\frac{\delta C_{ij}}{\Delta C} = - \sum_{\text{faces}} \oint_{\partial A_{ij}} \left[\frac{\Delta T}{\Delta x \Delta y \Delta C} \right] (-\hat{n} \cdot \nabla \bar{C}) dl . \quad (7.40)$$

For the full problem (convection and diffusion) we can split the time evolution as

$$\phi \frac{\partial C}{\partial t} = q_r \frac{\partial C}{\partial \tau} + \phi D_L \frac{\partial C}{\partial T} . \quad (7.41)$$

In this equation $\partial / \partial t$ represent separate convection and dispersion processes. Convective evolution is described by Eq. (7.39), while dispersion evolution is represented by Eq. (7.41). Thus we have a sequential finger evolution in which convection initiates the growth, which is then modified or moderated by dispersion. If we fix the time interval δt , then $\delta \tau = (q_r / \psi) \delta t$, and $\delta T = D_L \delta t$, which then define the Péclet number $Pe = \delta \tau / \delta T$. In practice, $\delta \tau$ is set by $\delta \tau = \Delta \tau = \Delta x \Delta y \Delta C$, implying that $\Delta T = \Delta \tau / Pe$. In most of practical cases, $Pe > 1$, and Eq. (7.41) is properly normalized. However, if $Pe < 1$, δT is subdivided into n_D intervals to obtain $\Delta T = (\delta \tau / Pe) n_D$, where $n_D > Pe^{-1}$.

King and Scher (1990) simulated miscible displacements with dispersion for various values of M and obtained reasonable agreement with the data of Habermann (1960). It is interesting to note that, although in the GGGM and the two-walker model dispersion is not present *explicitly*, the numerical algorithms seem to contain implicitly the effect of dispersion.

The second probabilistic method is due to Araktingi and Orr (1988). In this model the porous medium is represented by a three- or two-dimensional system of cubic (square) grid blocks. At the beginning of each time step the pressure field is calculated, given the distribution of permeability and the current distribution of fluid viscosities. Tracer particles that carry a finite concentration of displacing fluid are injected into the system and are moved with velocities based on the pressure field. The velocities are calculated at the midpoint between pressure nodes. Velocities for particles that are not on such nodes are obtained by linear interpolation. After moving the particles by convection to their current position, the effect of dispersion is simulated by random perturbations of particle positions in the longitudinal and transverse directions. As discussed in Sec. VI, for diffusive dispersion the standard deviations of the motion of the particles are given by, $\sigma_x = (2D_L t)^{1/2}$, and $\sigma_y = (2D_T t)^{1/2}$. Thus the distribution of the particles about a mean position can be simulated by multiplying these standard deviations by a number between -6 and $+6$. This number is obtained by adding a sequence of 12

random numbers, distributed normally with a zero mean and unit standard deviation, to -6 . The values $+6$ and -6 were selected because, on a practical basis, the probability of a particle moving beyond 6 standard deviations on either side of the mean is less than 1%. After the particles arrive at their new position, the current time step is determined. To avoid having particles travel a distance greater than a grid block, the time step is chosen to allow measurement equal to half of a grid block length (or width), travelled at the highest existing velocity. The new pressure field is calculated, and a new position for each particle is determined. This procedure is repeated many times. It should be noted that both this method and that of King and Scher require *a priori* estimates of D_L and D_T .

Araktingi and Orr (1988) compared their results with the experimental data of Blackwell *et al.* (1959), using $D_L = 1.6 \times 10^{-3} \text{ cm}^2/\text{sec}$, and $D_T = 6.5 \times 10^{-5} \text{ cm}^2/\text{sec}$. Figure 45 compares their results with the data and the agreement is very good. Although this method suffers from fluctuations due to the limited number of particles used in the simulation, the ensemble-average properties over several realizations compare well with the data of Blackwell *et al.* (1959). Note that the probabilistic method suggested by Araktingi and Orr (1988) is very similar to Monte Carlo method of Smith and Schwartz (1980, 1981a, 1988b) for studying dispersion. The only difference is that Araktingi and Orr (1988) treated the case in which the viscosities of the two fluids were *not* the same. The main disadvantage of these models is their long simulation times. This is especially true when the effects of gravity and transverse dispersion are to be included in the simulations.

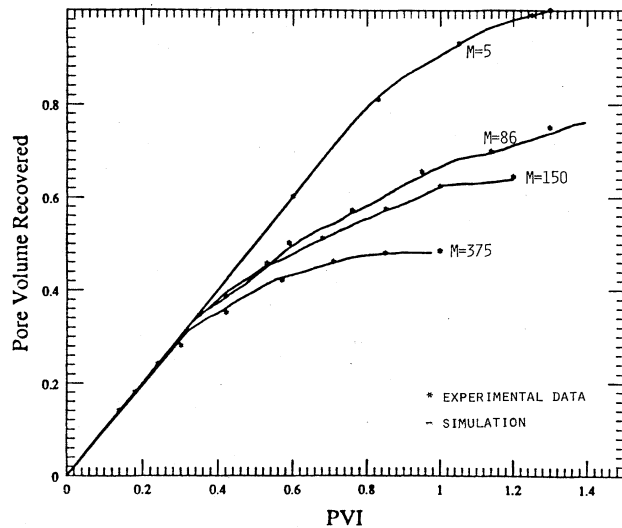


FIG. 45. Comparison of the predicted recovery vs pore volume injected (PVI) with the experimental data of Blackwell *et al.* (1959), for various values of mobility ratio M and grid sizes (from Araktingi and Orr, 1988).

6. Deterministic models that include the effect of dispersion

These models were invented for investigating viscous fingers in pore networks. Nobles and Janzen (1958) had already used analog resistor networks to study the effect of M on miscible displacements. Random networks and deterministic flow models were originally proposed by Simon and Kelsey (1971, 1972), but their model was too simple and the networks used were too small. There are two such models, one of which is applicable to miscible displacements in the absence of dispersion, while the other can also take into account the effect of dispersion.

Let us first discuss the case in which dispersion is neglected. The porous medium is represented by a network of interconnected pores, usually assumed to be cylindrical tubes with distributed radii. Consider a tube of length l_{ij} and radius R_{ij} which connects nodes i and j , of which a portion x_{ij} is occupied by the displacing fluid and the rest by the displaced fluid. The pressure difference $P_i - P_j$ along the tube is given by

$$P_i - P_j = 8\eta_2(x_{ij}/M + l_{ij} - x_{ij})q_{ij}/(\pi R_{ij}^4) = \frac{q_{ij}}{g_{ij}}, \quad (7.42)$$

where η_2 is the viscosity of the displaced fluid, q_{ij} the flow rate in the tube between i and j , and g_{ij} is the hydraulic conductance of the tube. At each node i of the network we have conservation of fluid fluxes, $\sum_j q_{ij} = 0$, which, when written for the interior nodes of the network, yields a set of linear equations for the nodal pressures. The boundary conditions are such that at the injection point $P=1$, while at the production point $P=0$. After determining the nodal pressures, we move the front a distance

$$\Delta x_{ij} = \frac{q_{ij}}{\pi R_{ij}^2} \Delta t, \quad (7.43)$$

into one of the pores adjacent to the interface. We choose the time step Δt to be the time necessary to exactly move the front to reach a node through the fastest tube. We then update all other fronts (i.e., we move them into the slower pores adjacent to the front and *partially* fill such pores) and, for the new configurations of the regions of displacing and displaced fluids, calculate the pressure field and repeat the entire process. This method was used by Chen and Wilkinson (1985), King (1987b), Siddiqui and Sahimi (1990a), and Ferer *et al.* (1992) to investigate miscible displacements without dispersion. The main advantage of this method is that it allows one to investigate the effect of pore-level or large-scale heterogeneities on the displacement process. It is also free of the type of noise that is generated by the DLA-type models.

The second method is capable of taking into account the effect of dispersion. As in the first model, we first calculate the pressure field throughout the network. There is, however, one difference between this case and the first case: the portion x_{ij} is occupied by a *mixture* of displac-

ing and displaced fluid with an effective viscosity η_m given by, e.g., Eq. (7.36). Thus M should be calculated and used in Eq. (7.42) based on the effective viscosity η_m and the viscosity η_2 of the displaced fluid, i.e., $M = \eta_2/\eta_m$. We then assume that within each pore a one-dimensional convective-diffusion equation governs the concentration distribution, whose solution is given by Eqs. (6.36) and (6.37). Using the fact that C is a conserved quantity, and employing the distribution of pore velocities, we can determine the concentration distribution in the entire network, since for every node i , we can write $\sum_j S_{ij}J_{ij} = 0$, where $J_{ij} = v_{ij}C_i - D_m \partial C_i / \partial x$ is the total flux (convective plus diffusive) in the pore that connects sites i and j , and S_{ij} is the cross section area of pore ij . This equation, when written for every node of the network, yields a set of linear equations for the C_i 's, the concentration at site i , which is solved numerically. Once the concentration distribution is determined, we proceed as in the first case except that the distance Δx_{ij} that the front moves in a pore is given by $\Delta x_{ij} = J_{ij}/(\pi R_{ij}^2 \Delta t)$. The advantage of this method is that one does not need to provide D_L and D_T as phenomenological inputs to the model, as is done in the models of King and Scher (1987, 1990) and Araktingi and Orr (1988). It also allows one to investigate the effect of rock heterogeneities on miscible displacements in the presence of dispersion.

F. Relation between miscible displacements and diffusion-limited aggregation

In the previous subsections we described the DLA and other discrete models. Among these the DLA model and its two-walker generalization are the only ones that use *only* random walkers, and thus, from a computational point of view, they can be very efficient. Therefore, the relevant question is whether such random walk methods can predict *quantitatively* miscible displacements without dispersion. At first the answer may seem affirmative, since the governing equations for both phenomena and processes are identical. However, this only guarantees that the universal properties of the two processes to be the same, but not the equality of nonuniversal quantities of interest. For example, as far as a petroleum or chemical engineer is concerned, the most important quantity to calculate is the volume fraction S_b of the displaced fluid at the breakthrough point, i.e., at the point at which a sample-spanning cluster of the displacing fluid is formed, since this is a quantitative measure of the efficiency of the displacement process. Murat and Aharony (1986) and Meakin *et al.* (1989) used the DLA model and the DBM to simulate viscous fingers in the absence of dispersion. They found that the two models are not always the same, but their results were not conclusive.

Chan *et al.* (1986, 1988), Sahimi and Siddiqui (1987), and Siddiqui and Sahimi (1990a) made a more definitive study of this problem. As explained by Sahimi and Siddiqui, the proper comparison is between the DLA model and the deterministic model in the absence of dispersion,

because in an actual experiment the front does not advance one pore at a time, as in the DBM and GGGM, but advances in several pores simultaneously, which is the basis of the deterministic model. Thus they computed S_b using both models and found them to be generally different. Moreover, they found that although the fractal dimensions of the two models are identical if the pore system is well connected, the two models are characterized by different fractal dimensions if the pore system is poorly connected, e.g., if the pore space is a percolation cluster near the percolation threshold. Chan *et al.* (1986, 1988) argued essentially along the same lines as those of Sahimi and Siddiqui, except that their model of pore space was different from that of Sahimi and Siddiqui. In the model of Chan *et al.*, the porous medium is represented by a network of interconnected *tubes and chambers*. The tubes have small diameter, and thus contribute most of the resistance to fluid flow. These tubes connect the grid points of the network a distance l apart at which the chambers are located. The chambers have volumes much greater than those of the tubes, thus making a negligible contribution to the hydrodynamic resistance. The fluid capacity of each chamber, i.e., its volume per specified volume l^3 , is a randomly distributed quantity. Chan *et al.* showed that, unless the distribution of the fluid capacity of the chambers is exponential, the predicted values of S_b by their model and the DLA model will be different. The conclusion is that although the DLA model often provides a good description of the universal properties of miscible displacements without dispersion, the mapping between the two problems is not exact but approximate, although a very good one in many situations.

G. Crossover from fractal to compact displacement at finite mobility ratios

Since the universal properties of viscous fingering, in the limit $M \rightarrow \infty$ and without dispersion, and those of diffusion-limited aggregates are the same, one may conclude that viscous fingers are fractal objects in the limit $M = \infty$. But what about the case of viscous fingers at finite values of M ? We already know that viscous fingers may be unstable if $M > 1$, which might mean that they are fractal objects for *any* $M > 1$, with the instability manifesting itself with the fractal structure. However, this implies that the density of the displacing fluid would vanish as the displacement proceeds, since this is a general property of any fractal object. This means that very thin sections of fluids would have to support a vast and tenuous network of the fingers at the tip. In fact, if the displaced fluid has a finite mobility, one would expect the fingers to become *thicker*, as opposed to thinner fingers with the fractal behavior. However, for $M > 1$ the displacement can be unstable, if dispersion effects are absent, and we cannot expect it to be smooth. The cluster of the displacing fluid is also not compact, since there is no intermediate length scale between the size of the sys-

tem and that of a pore. Thus, as argued by King (1987b), only the *surface* of the viscous fingers (i.e., the front between the two fluids) can have a fractal-like character, and this can be interpreted as the manifestation of the instability of the process. This argument is supported by the simulations of King (1987b), Blunt and King (1988), Siddiqui and Sahimi (1990a), and Ferer *et al.* (1992) who used the deterministic model, and by those of Siddiqui and Sahimi (1990b) who used the two-walker method. Even the surface roughness and its fractal character should gradually disappear as the size of the system increases. This is supported by the work of King and Scher (1990) who argued that if the linear size of the system exceeds a crossover size N_{co} , then there would be a crossover from a fractal-like behavior to a compact displacement, where N_{co} is given by

$$N_{co} \sim \left(\frac{M-1}{2} \right)^{1/D_{DLA}}. \quad (7.44)$$

King and Scher (1990) called this *viscous relaxation*. Earlier Monte Carlo simulations of DeGregoria (1986), who used the gradient-governed growth model, also supported this. DeGregoria observed that, for finite values of M , the volume fraction of displaced fluid increases as the size of the system increases, which implies increased stability. Note that Eq. (7.44) implies that no such crossover can occur if $M \rightarrow \infty$. Using renormalization-group methods, Lee *et al.* (1990) also reached the same conclusion. They showed that there exist *two* fixed points on a renormalization flow diagram: The Eden point, corresponding to a compact, nonfractal structure such as what one obtains with $M=1$, which is stable, and the diffusion-limited aggregation point, corresponding to a fractal structure, which is what one obtains in the $M = \infty$ limit, which they showed it to be a saddle point. This implies that for *any* finite M viscous fingers "eventually" approach a Euclidean limit, in the sense of taking up a compact shape, perhaps with a fractal or rough surface, where "eventually" means either long times, or very large length scales, or a fine enough grid. Furthermore, Lee *et al.* (1990) proposed the crossover scaling law

$$m_c(R) \sim R^d F\left(\frac{R^\delta}{M}\right), \quad (7.45)$$

where m_c is the "mass" of the cluster of displacing fluid, R the radius of gyration of the cluster, d the dimensionality of the system, and δ a crossover exponent. $F(x)$ is a scaling function with the properties that $F(x) \sim 1$ for $x \ll 1$, and $F(x) \sim x^\alpha$ for $x \gg 1$, with $d + \alpha\delta = 2$.

These results have two practical implications. The first is that the scale up of numerical or laboratory experiments of unstable displacements ought to be done with caution since, as suggested by Eq. (7.45), there will always be a crossover to a stable displacement if one waits long enough, or if the scale up is done for a large enough scale. The other implication is that heterogeneities of a scale of the order of the crossover length N_{co} or larger dominate viscous fingering (see also below).

H. Miscible displacements in heterogeneous porous media

Miscible displacements in macroscopically heterogeneous porous media have also been studied by various methods, although these studies are not as extensive as those for macroscopically homogeneous porous media. For example, Tan and Homsy (1992) used their continuum model to study miscible displacements in heterogeneous porous media, in which the heterogeneities were modeled as stationary random functions of space. The permeability correlation length ξ_k was finite. They found that the fingers grow linearly in time in a manner similar to that of homogeneous media. This result is not surprising since ξ_k was assumed to be finite. As an example of discrete simulations, we mention Araktingi and Orr's (1988) simulations in which they assumed that the mean of the permeability distribution is independent of the location, and that the spatial correlation between any two regions depends only on the distance between them. A heterogeneity index HI was used to characterize a permeability field, which was defined by

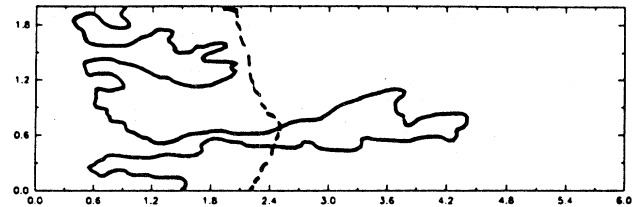
$$HI = \sigma_{\ln k}^2 \hat{\xi}_k , \quad (7.46)$$

where $\sigma_{\ln k}$ is the standard deviation of log permeability and $\hat{\xi}_k$ is the dimensionless correlation length of permeability $\hat{\xi}_k = \xi_k / L$, L being the system length. HI combines the variability (as measured by $\sigma_{\ln k}$) and the spatial correlations of the permeability field. Figure 46 compares their simulation results for two values of M and three values of HI. It is clear that for low values of HI, i.e., a more homogeneous porous medium, the effect of M is strong, which is expected. However, as HI increases the effect of M diminishes, and the shape of the fingers is dominated by the permeability heterogeneities. For example, for $HI=0.77$, the shapes of the fingers are almost identical for $M=1$ and 20. If this is the case, then a simple generalization of a DLA-based model (or any other random-walk method) should suffice for simulating miscible displacements in heterogeneous reservoirs, since as discussed in Sec. VI, pore-level dispersion is not important in heterogeneous porous media, and the velocity field fluctuations, induced by the permeability field, is the only important factor, and this effect is easily captured by a DLA-like model.

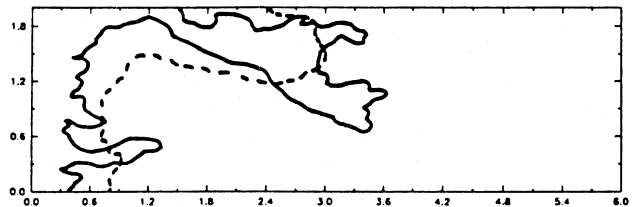
One of the factors that distinguishes a heterogeneous porous medium from a homogeneous one is the extent of the spatial correlations in the permeability distribution. If there are no spatial correlations, or they are of finite extent and very short, we do not expect a miscible displacement in the heterogeneous medium to be very different from that in a homogeneous one. One way of incorporating the effect of long-range permeability correlations is of course through the use of fractal statistics that we already discussed in Sec. VI. Emanuel *et al.* (1989) and Mathews *et al.* (1989) used such statistics in their simulations of displacement processes. They showed that using such statistics leads to significant im-

provement in the predictive ability of their models. These authors used finite-difference techniques for solving their equations, which may limit the size of the system and the extent of correlations that they can simulate (since one usually needs a very fine grid structure with finite-difference techniques in order to achieve reliable accuracy). On the other hand, Sahimi and Knackstedt (1993) used a random-walk model to study miscible displacements in heterogeneous porous media, in which the permeabilities obeyed a fBm discussed earlier. They showed that M does not play any important role, and the permeability heterogeneities control the performance of the displacements.

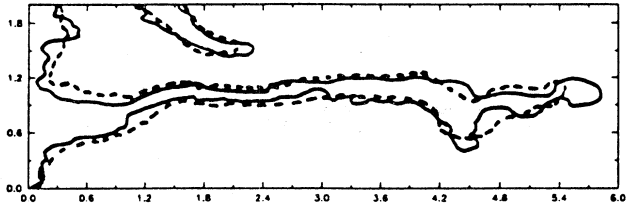
At the end of this section we should again emphasize the role of dispersion (both microscopic and macroscopic) and permeability heterogeneities in any miscible displacement process. In the past few years, the physics literature has witnessed an explosion of papers on misci-



a. Displacement in Permeability Field with $HI=0.25$



b. Displacement in Permeability Field with $HI=0.29$



c. Displacement in Permeability Field with $HI=0.77$

FIG. 46. Comparison of viscous finger patterns for various values of heterogeneity index (HI). Dashed curves are for $M=1$, while solid curves are for $M=20$ (from Araktingi and Orr, 1988).

ble displacements and their relation with growth phenomena. While these studies have added to our understanding of miscible displacements, most of them would be of limited use in practical (field) applications, unless they adequately take into account the effect of dispersion and permeability heterogeneities. Unfortunately, most of the papers in the physics literature lack this fundamental requirement.

VIII. TWO-PHASE FLOW AND IMMISCIBLE DISPLACEMENT PROCESSES

We now turn our attention to two-phase flows in rocks. A large number of factors can affect this class of phenomena, among which are capillary, viscous, and gravity forces, the viscosities of the two fluids and the interfacial tension separating them, chemical and physical properties of the surface of the pores, i.e., whether or not there are surface active agents, or whether the surface is fractal, the morphology of the pore space, and the wettability of the fluids. Obviously, two-phase flows and the displacement of one fluid by another in porous media involve a set of complex phenomena, and to date no model has been developed that can take into account the effect of all of these factors.

A. Wettability and its measurement

Generally speaking, the rock-fluid interactions are what we call wettability. It has a strong effect on the flow of two immiscible fluids in a porous medium, conventional and enhanced oil recovery processes, and many other phenomena (for example, coating operations), and has been studied for a long time by petroleum engineers (Bartell and Miller, 1928; Owens and Archer, 1971; Salathiel, 1973; McCaffery and Benion, 1974; Batycky *et al.*, 1981), and others. It is also known that oil recovery process itself can alter reservoir wettability (Wagner and Leach, 1959; Reed and Healy, 1977).

Consider, as an example, a situation in which a drop of water is placed on a surface immersed in oil. Then a contact angle is formed that can vary anywhere from 0° to

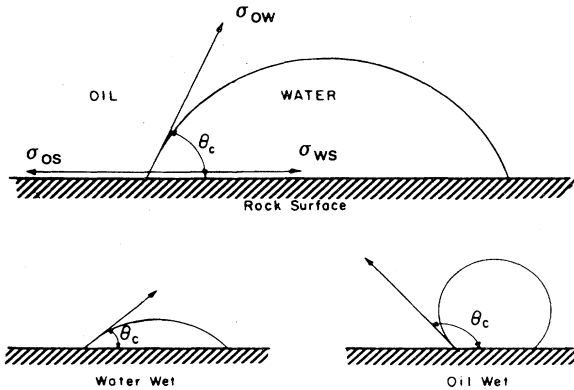


FIG. 47. Formation of contact angle between a liquid and a solid surface (from Anderson, 1986).

180° . A typical situation is shown in Fig. 47. The three different surface tensions are related by the Young-Dupré equation

$$\sigma_{ow} \cos \theta = \sigma_{os} - \sigma_{ws}, \quad (8.1)$$

where σ_{ow} is the interfacial tension between oil and water, and σ_{os} and σ_{ws} are the surface tensions between oil and the solid surface, and water and the solid surface, respectively. Normally, the contact angle θ is measured through the water phase. Strictly speaking, if $\theta < 90^\circ$, the surface is preferentially water-wet. However, in practice, $\theta < 65^\circ$ for water-wet systems, while $105^\circ < \theta < 180^\circ$ for oil-wet systems. If $65^\circ < \theta < 105^\circ$, the system is said to be *intermediately-wet*, and has no strong preference for any of the two fluids. Another important case is *mixed wettability*, in which the wettability of the surface changes from pore to pore or from one portion of the surface to another. This is caused by *chemical heterogeneity* of the surface, and is actually the situation one has to deal with in most oil reservoirs.

The study of moving contact lines and contact angles goes back to Washburn (1921) who proposed Eq. (3.4). This equation is invalid if the length of the tube (for which the equation was intended) is much longer than its diameter, and if the diameter is small enough that gravity cannot have a significant effect on the shape of the moving contact line or meniscus. Fisher and Lark (1979) accumulated experimental evidence in support of this equation. However, Eq. (3.4) neglects the details of the surface and its effect on the moving contact line: it provides only an overall picture of what happens. For example, in almost all cases of practical interest, one has to deal with the no-slip boundary condition. Huh and Scriven (1971) were the first to analyze moving contact angles and lines and claimed that, with no-slip boundary condition, the stresses at the contact line become *divergent* (or the total dissipation diverges). They attributed this to the existence of, among other things, discontinuous processes around the contact line. As pointed out by Dussan and Davis (1974), this anomaly is due to the fact that Huh and Scriven (1971) had worked with a *planar* interface, and that their equations failed to satisfy the normal stress boundary condition at the interface between the two fluids. It is now well known that there are two ways of removing the singularity. If the advancing fluid wets the solid surface perfectly, then a thin precursor film forms ahead of the contact line and the dissipation divergence (which is logarithmic) is cutoff at the film thickness. On the other hand, if the advancing fluid does not wet the surface completely, slip can occur within a length l_θ from the contact line. This length can act as a cutoff and prevent the divergence of the total dissipation. These matters has been reviewed by Dussan (1979).

On a moving contact line the interface exerts a force $\sigma_{fs} \cos \theta_D$, where θ_D is the apparent *dynamic* contact angle (as opposed to a static contact angle θ_S which is well defined on a homogeneous surface), and σ_{fs} is the surface tension between the fluid and the solid. There is also an

additional viscous force F_v on the contact line. If the capillary number Ca [Eq. (3.8)] is small, F_v would also be small compared with the capillary forces, except within a distance l_θ from the contact line. This gives us a method of measuring F_v from θ_D , measured far from the contact line since, $F_v = \sigma_{fs}(\cos\theta_D - \cos\theta_S)$. Roughness, chemical heterogeneity and other factors can make this picture more complex, which will be discussed below. The dynamic contact angle θ_D can be measured by optical methods (see, for example, Hoffman, 1975).

Many methods have been devised for measuring the wettability of a system, and Anderson (1986) has given a thorough discussion of them. Here, we restrict ourselves to three quantitative methods. More details are given by Anderson (1986).

1. Contact-angle measurements

There are several methods for measuring the contact angles. These include the tilting plate method, capillary rise method, tensiometric methods, vertical rod method, cylinder method, and sessile drops or bubbles method, and Adamson (1990) discusses most of them. However, the petroleum industry does not use most of these methods, because they work best when one deals with pure fluids, and clean, artificial cores which are rarely encountered in practice. The most popular method in the petroleum industry is the sessile drop method (see, for example, McCaffery, 1972), and its modification by Treiber *et al.* (1972). In the latter method the mineral to be tested is put in a test cell which is made of inert material. This prevents the contamination of the surface which can alter the true contact angle. Two flat and polished mineral crystals are mounted parallel to one another, that are usually either quartz or calcite crystals (sedimentary rocks are composed of such crystals). The apparatus has to be completely clean so that the true contact angle can be measured. The cell containing the mineral crystals is then filled with de-oxygenated synthetic formation brine. It usually takes a few days for the oil-crystal interface to be clearly established (this is called *aging*). Then the two crystals are displaced parallel to each other to shift the oil drop. Thus the brine can move over a portion of the surface that was covered with oil. In this way an *advancing* contact angle θ_A is measured. Usually, it takes a day or two before θ_A reaches its equilibrium value. The surface is aged again, the water is advanced again, and so on. The sessile drop method is similar to this procedure, except that only one flat crystal is used. A drop of oil is formed at the end of a fine capillary tube and brought into contact with the flat surface (see Fig. 47).

If the oil contains surface-active agents, θ_A increases with aging until an adsorption equilibrium is reached. This may take a long time. Usually, the measured contact angles show hysteresis, that is, the contact angle θ_A of an interface that was recently advanced differs from the apparent contact angle θ_R that recently receded.

This hysteresis is presumably due to the existence of many metastable positions of the contact line. The difference $\theta_A - \theta_R$ can be as large as 60° . According to Adamson (1990) there are at least three reasons for this hysteresis which are, (1) surface roughness, (2) surface heterogeneity, and (3) surface immobility on a macromolecular scale. As pointed out by Morrow (1970, 1976), surface roughness and pore geometry can affect the contact line between the two fluids and the surface, and thus change the apparent contact angle. If the surface is smooth, then θ is fixed. However, in an actual reservoir there are sharp edges which give rise to a wide range of contact angles. Figure 48, taken from Morrow's work, demonstrates this clearly. The contact angles θ_A and θ_R were measured on a roughened teflon surface, while the intrinsic angle θ_E was measured on a smooth teflon surface; we shall return to this later. Moreover, compositional heterogeneity of a surface gives rise to θ_A and θ_R that can change from pore to pore, and one problem with contact angle measurements is that they cannot take such effects into account. In addition, no information can be gained about the absence or presence of various coatings on the pore surface of a reservoir rock.

2. Amott method

In this method (Amott, 1959) a core is prepared by centrifuging under brine until the residual oil saturation

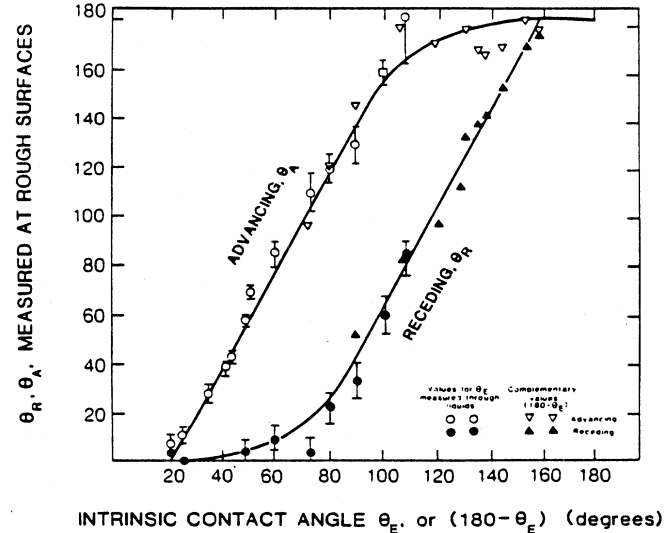
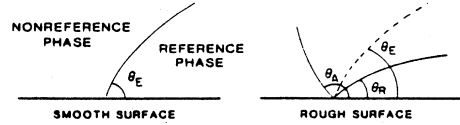


FIG. 48. Recently advanced and recently receded contact angles θ_A and θ_R , measured on roughened Teflon vs intrinsic contact angle θ_E measured on smooth Teflon. The contact angles were changed by changing the salinity (from Morrow, 1976).

(ROS) is reached. This is the volume fraction of oil in the pore space, residing in isolated finite clusters of pores, that can no longer be displaced by the brine in the centrifuge. Then four steps are taken for measuring the wettability of the core. (i) The core is immersed in oil, and the volume of water displaced by free or spontaneous imbibition of oil into the core is measured, in a period of time that may be as long as one or two weeks. (ii) The core in oil is centrifuged until the irreducible water saturation (IWS), i.e., the water saturation that can no longer be reduced by centrifuging, is reached and the total amount of displaced water is measured. (iii) The core is immersed in brine, and the volume of oil displaced by water is measured. (iv) Finally, the core is centrifuged in brine until residual oil saturation is reached, and the total amount of displaced oil is measured. To decide whether the core is water or oil wet, two quantities are calculated. One is $R_o = V_{wi}/V_{wt}$, where V_{wi} is the water volume displaced by free imbibition of oil, and V_{wt} is the total volume of water displaced by free and forced (centrifugal) displacements. The second quantity is $R_w = V_{oi}/V_{ot}$, where the notations have similar meanings. Now, if the reservoir is water wet, then $R_w > 0$ and $R_o = 0$, because in a water-wet reservoir there can be no free imbibition of oil (it has to be forced into the medium), and vice versa. In a sense, the method measures the average wettability of the system. Sometimes, an index $I_w = R_w - R_o$ is measured which can vary anywhere from +1 (completely water-wet reservoirs) to -1 (completely oil-wet reservoirs). According to Cuiec (1984), for $0.3 \leq I \leq 1$ the reservoir must be considered as water-wet, for $-0.3 \leq I \leq 0.3$ it is intermediately-wet, and for $-1 \leq I \leq -0.3$ it is oil-wet. The main problem is that if the reservoir is close to being intermediately-wet, then the method is not very sensitive or accurate, simply because free imbibition of either fluid cannot take place in significant amounts.

3. U.S. Bureau of Mines method

This method was developed by Donaldson *et al.* (1969) and, like the Amott method, also measures the average wettability of the system. It compares the work necessary for one fluid to displace the other. The wetting fluid requires less work to displace the non-wetting fluid from the core than the opposite. It can be shown (see, for example, Morrow, 1970) that the required work is proportional to the area under the capillary pressure curve (in a capillary pressure-water saturation plot; see Sec. III). If the reservoir is strongly water-wet, most of the water will imbibe freely into the core, and the area under the curve for water will be very small. Thus the capillary pressure curves for the two displacements are measured, and a wettability index $I_w = \log(A_o/A_w)$ is calculated, where A_o and A_w are the areas under the oil- and water-drive curves, respectively. Obviously, if $I_w > 0$, then the reservoir is water-wet, and if $I_w < 0$, it is oil-wet. If, $I_w \approx 0$, then the reservoir is close to being intermediately-wet.

B. Dependence of dynamic contact angle and capillary pressure on capillary number

Stokes *et al.* (1990) studied the velocity dependence of $\cos\theta_D - \cos\theta_S$ by a method which, in a sense, belongs to the class of contact angle measurement methods, except that its details are very different from those of the methods discussed above, and it also appears to be more sensitive. They measured the capillary pressure P_c across the interface as a function of the contact-line velocity v . P_c can be measured very accurately by superimposing a small-amplitude oscillatory flow on a larger steady-state flow and measuring the response. Stokes *et al.* (1990) generated the oscillatory flow by a plunger that was coupled to the fluid through latex membrane, and was driven at frequency ω by an audio speaker. The steady-state flow was varied by raising a reservoir of the advancing fluid. Between the reservoir and the sample a narrow-bore and long tube was inserted to guarantee that the flow rate was constant. The interface between a mineral oil and a glycerol-methanol mixture was measured in a 1-mm diameter 30-cm long Pyrex tube. Two Omega pressure transducers were used to measure both the pressure and velocity. The AC outputs of the transducers were amplified, and the harmonic content measured with several amplifiers. When the glycerol mixture was advanced, $\theta_A = 65^\circ$, and $\theta_R = 45^\circ$ were measured, which indicated that the surface of the tube was somehow disordered.

These experiments indicated that for a tube of radius R

$$\cos\theta_D - \cos\theta_A = \frac{R}{2\sigma_{fs}}(P_c - P_t) = a \text{ Ca}^x, \quad (8.2)$$

where P_t is the total pressure, $a \approx 3.1 \pm 1$, and $x \approx 0.4 \pm 0.05$. This implies that $P_c \sim v^x$. For homogeneous surfaces the velocity dependence of θ_D has been studied by several authors. For example, Cox (1985) found that for θ_D measured a distance r from the contact line one has

$$g(\theta_D, M) = g(\theta_0, M) + [\ln(r/l_\theta) + B_1] \text{Ca}, \quad (8.3)$$

where g is a simple analytic function, M the viscosity ratio of the two fluids, θ_0 the actual contact angle at lengths smaller than l_θ , and B_1 a constant that depends on the model. Molecular dynamics simulations of Koplik *et al.* (1988a) confirmed this equation if one takes $\theta_0 = \theta_S$. This equation implies $x = 1$ for an intermediately-wet fluid on a homogeneous surface, which is different from Eq. (8.2). This can be attributed to the roughness or heterogeneity of the surface, an effect which is apparently strong enough to change the exponent from unity to about 0.4. This indicates the significance of surface roughness and its effect on contact angle (see below). On the other hand, Rillaerts and Joos (1980) correlated data from several different systems by plotting $\cos\theta_D - \cos\theta_S$ versus $\text{Ca}^{1/2}$, which is close to Eq. (8.2), and Hoffman (1975) proposed somewhat more complex correlations which can describe many different sets

of data for all $0 \leq \theta_D \leq 180^\circ$. For example, at low values of Ca he obtained, $\theta_D \sim \text{Ca}^{1/3}$ (which is known as Tanner's law). Weitz *et al.* (1987) also measured the velocity dependence of the capillary pressure (and hence θ_D) between two fluids in a *porous medium*, and proposed the correlation

$$P_c \simeq \frac{\sigma_{fs}}{r_t} (-1 + B_2 \text{Ca}^x), \quad (8.4)$$

where r_t is a typical radius of pore throats. Their measurements indicated that, $x \simeq 0.5 \pm 0.1$, and $B_2 \simeq 300$, which are compatible with the results of Stokes *et al.* (1990). de Gennes (1988) used scaling arguments and proposed that

$$P_c \simeq \frac{\sigma_{fs}}{r_t} \text{Ca}^{2/3} T_p^{5/3}, \quad (8.5)$$

where T_p is a tortuosity factor. Although this result is almost consistent with Eq. (8.4), it does not seem to agree with the result of Stokes *et al.* There is, however, one major difference between the experiments of Stokes *et al.* (1990) and Weitz *et al.* (1987): the former experiments were done in a *tube*, whereas the latter ones were performed in a *porous medium*. Whether this can explain the discrepancies between these experiments and de Gennes' prediction is not yet clear.

C. The effect of surface roughness on contact angles

We have already mentioned the experimental work of Morrow (1970, 1976), who investigated the effect of surface roughness on contact angles. There have also been a few recent theoretical studies of the effect of a heterogeneous surface on moving contact angles and contact lines (Joanny and de Gennes, 1984; Pomeau and Vannimenus, 1985; Robbins and Joanny, 1987; Joanny and Robbins, 1990). For example, Joanny and Robbins (1990) studied the motion of a contact line on a surface with periodic heterogeneities. Although such heterogeneities do not usually occur on natural surfaces, their study can provide clues as to how such problems may be studied on a real heterogeneous surface. They considered the case in which the contact line is advanced at a constant force F or a constant velocity v . In the first case, motion starts if $F > F_{C1}$, where F_{C1} is some threshold force which is related to the static θ_A or θ_R defined above. For smooth heterogeneity, they found that, $F - F_{C1} \sim v^2$. If the contact line is moved at a constant velocity, the results are somewhat different: one has two regimes, namely, the weak and strong pinning regimes. In the strong pinning regime, which is more interesting and relevant, there is another threshold F_{C2} which approaches F_{C1} as the surface becomes more heterogeneous. For smooth heterogeneities, they obtained $F - F_{C2} \sim v^{2/3}$. Similar results were obtained by Raphael and de Gennes (1989).

D. Fluid distribution on fractal surfaces: Hypodiffusion versus hyperdiffusion

In Sec. III we discussed fractal properties of pore surfaces. Fractality of pore surfaces can have interesting implications for fluid distributions at low wetting-phase saturations. This was discussed by de Gennes (1985), Melrose (1988), Davis (1989), Davis *et al.* (1990) and Toledo *et al.* (1990). In this section, we briefly discuss their results and their implications.

We assume that one of the fluids strongly wets the system, so that even at very low saturations the wetting phase remains hydraulically connected through thin films. The capillary pressure is given by the Young-Laplace equation

$$P_c = 2H\sigma_{ff}, \quad (8.6)$$

where H is the mean curvature of the interface between the two phases, and σ_{ff} the interfacial tension between the two fluids. This equation is valid when both phases are present in large amounts. However, if the wetting phase is present only in the form of thin films, then one has to use the augmented Young-Laplace equation

$$P_c = 2H\sigma_{ff} + \Pi(h), \quad (8.7)$$

where h is the thickness of the film, and $\Pi(h)$ is the disjoining pressure. At saturations below the percolation threshold, the wetting phase exists as thin films or *pendular structures* at intergranular contacts, or in nooks and crannies provided by the pore surface features or overhangs. Thus at a given capillary pressure, the liquid volume is proportional to r^{3-D} , and since $r \sim 1/P_c$, we must have

$$S_w \sim P_c^{-(3-D)}. \quad (8.8)$$

Using Eq. (8.8) Davis (1989) analyzed Melrose's (1988) data, and found that they are well-described by it with $D \simeq 2.55$. This is in the range of fractal dimensions reported by Katz, Thompson, Krohn and others discussed in Sec. III. If the capillary contribution, $2H\sigma_{ff}$, is small compared to the disjoining pressure, then $P_c \simeq \Pi(h) \sim h^{-m_{di}}$, and therefore

$$S_w \sim P_c^{-1/m_{di}}. \quad (8.9)$$

Similar relations can be developed for the hydraulic conductivity k_w of the wetting phase. Thus, if only thin films are present, then since $k_w \sim h^3$, we find

$$k_w \sim P_c^{-3/m_{di}} \sim S_w^3, \quad (8.10)$$

and if only the pendular structures are present, distributed fractally, then

$$k_w \sim S_w^{3/m_{di}(3-D)} \quad (8.11)$$

If our porous medium, and its low wetting-phase saturation, is now immersed in a reservoir of a wetting phase, it will spontaneously imbibe the wetting phase. The satura-

tion of the wetting phase will obey a convective-diffusion equation in which the dispersion coefficient D_{Lc} is given by

$$D_{Lc} = -\frac{k_w}{\eta_w} \frac{dP_c}{dS_w}. \quad (8.12)$$

D_{Lc} is usually called the capillary dispersion coefficient. Depending on the wetting-phase saturation, one can have three distinct regimes. If $D_{Lc} \rightarrow 0$ as $S_w \rightarrow 0$, the invading front of the wetting phase will disperse less than that in a diffusive front. This is called *hypodiffusion*. If D_{Lc} approaches a constant as $S_w \rightarrow 0$, then we have a diffusive dispersal of the front. Finally, if $D_{Lc} \rightarrow \infty$ as $S_w \rightarrow 0$, then the front will disperse faster than that in a diffusive front, and is called *hyperdiffusion*. From Eqs. (8.9)–(8.12) we obtain

$$D_{Lc} \sim S_w^\alpha, \quad (8.13)$$

$$\alpha = [3 - m_{di}(4 - D)]/[m_{di}(3 - D)]. \quad (8.14)$$

Therefore if $m_{di} < 3/(4 - D)$, we will have capillary hypodiffusion, if $m_{di} > 3/(4 - D)$, we will be in the regime of capillary hyperdiffusion, while $m_{di} = 3/(4 - D)$ will give rise to a capillary diffusive front.

Bacri *et al.* (1985) carried out experiments in which water imbibed in a pre-wet sandstone (i.e., a porous medium with irreducible water saturation) and observed hyperdiffusion. Bacri, Rosen, and Salin (1990) studied the same problem in a porous medium with glass beads that were totally wetted by water, and with polymethylmethacrylate (PMMA) beads that were partially wetted by oil and water. In the porous medium with glass beads, they observed hyperdiffusion again, whereas PMMA beads did not allow this to happen. They also studied the same phenomenon in a porous medium with a mixture of glass and PMMA beads, and observed hyperdiffusion even when the fraction of glass beads was small (but not smaller than the critical volume fraction for percolation). Toledo *et al.* (1990) analyzed the data of Nimmo and Akstin (1988) using the above scaling laws. Nimmo and Akstin (1988) reported measurements of P_c and k_w at low saturations in the presence of air in several compacted samples of Oakley sands, which is a clayey soil. On the other hand, Viani *et al.* (1983) provided data on disjoining pressure of clayey solids, which indicate that they are well-described by $\Pi(h) \sim h^{-1/2}$, i.e., $m_{di} = 1/2$. Using this value of m_{di} , Toledo *et al.* (1990) showed that the above scaling laws hold for 9 different samples with a fractal dimension between 2.35 and 2.67, with an average of about 2.5. Davis *et al.* (1990) also analyzed Ward and Morrow's (1987) data on capillary pressure-saturation curves in the presence of air in several low permeability sandstones. Two distinct regimes were found. One was in the lowest saturation region where $D \approx 2$. The other was in a higher saturation region for which $2.6 \leq D \leq 2.9$, which is consistent with the range of fractal dimensions discussed in Sec. III. Finally, Novy *et al.* (1989) developed a network model of two-phase flow in porous

media to test the above scaling laws, and found qualitative agreement between their simulations and the scaling laws.

The wettability of a medium affects strongly its transport as well as thermodynamic properties such as the capillary pressure curves. There is a strong correlation between the shape of the capillary pressure curves of a medium and its transport properties. Thus we first discuss the effect of wettability on capillary pressure curves.

E. Effect of wettability on capillary pressure

We have already discussed in Sec. IV capillary pressure curves and how they can be used for extracting information about the pore size distribution of the porous medium. In this section, we discuss the effect of wettability on capillary pressure curves. Let us first introduce the terminology that is frequently used in the oil industry. In *drainage* a nonwetting phase displaces a wetting phase from a porous medium, while during *imbibition* a wetting phase displaces a nonwetting phase.

With sintered porous teflon and clean fluid pairs, Morrow (1970, 1976), McCaffery and Benion (1974), and Morrow and McCaffery (1978) studied two-phase relative permeabilities (discussed below) and capillary pressure curves in porous media that are uniformly wettable. They took, as an independent measure of wettability, the intrinsic contact angle θ_E made by the fluid pairs on smooth teflon surfaces, and studied two processes. The first is *primary displacement*, i.e., the reduction of the saturation of a reference phase from 100% to the residual saturation (RS) by injection of a nonreference phase. The second is *secondary displacement* that follows primary displacement, i.e., reduction of the nonreference phase saturation to the RS by injection of the reference phase. On the basis of the capillary pressure (and relative permeability) behavior in the sequence of primary and secondary displacements, they identified three regimes of wettability: (i) *wetted*, in which primary displacement is drainage and secondary displacement is imbibition; (ii) *intermediately-wetted*, in which primary and secondary displacements are both drainage, and (iii) *nonwetted*, in which primary displacement is imbibition and secondary displacement is drainage. The second case is very interesting: because primary displacement is drainage, one intuitively expects secondary displacement to be imbibition. However, in the intermediate wettability regime the operative contact angle appears to give the more strongly wetting characteristics to the phase being displaced, whether it be the reference phase or the nonreference phase.

Figure 49(b), taken from Killins *et al.* (1953), shows the capillary pressure curves for a typical wetted regime. The measurements were done on a water-wet Berea sandstone. The primary process, denoted by 1 on the curve, was a drainage process in which oil displaced water and was terminated at A, where irreducible water saturation was reached. This is followed by process 2, a spontane-

ous imbibition of water into the core, up to point B at which $P_c = 0$. Beyond B, the water had to be forced into the medium (curve 3), characterized by a negative P_c , until point C and the residual oil saturation were reached. Note the two typical knees, one at the beginning of drainage, and the other at B. This figure should be compared with Fig. 49(a) which is typical of capillary pressure curves in nonwetted porous media. The curves were measured in an oil-wet Berea sandstone treated with Drifilm (to render it strongly oil-wet). Note that in both processes 1 (spontaneous imbibition of oil) and 2 (drainage of oil by water) the capillary pressure curve takes on negative values. Moreover, the imbibition curve rises steeply, and the drainage curve proceeds slowly, except near the original starting point A. Finally, Fig. 49(c), measured by Morrow and McCaffery (1978), shows capillary pressure curves for typical intermediately-wet systems.

In order to compare capillary pressure curves measured on different cores from the same reservoir, and to take into account the effect of permeability and porosity of each core, the curves are usually replotted in terms of the Leverett J function, Eq. (3.5). As long as the wettability of all cores is the same, the $\cos\theta$ term of Eq. (3.5) is a simple numerical factor, but if different fluids are used with cores of the same reservoir, then this term becomes important. Figure 50 shows the effect of contact angle on capillary pressure, as measured by Morrow (1970). As the contact angle increases, the return curve of the capillary pressure (to the left of the dashed curve) becomes steeper, which is in agreement with Fig. 49(c), since increasing θ implies the tendency of the system towards intermediate wettability. In fact, in the last curve on the left (shown by ■) the advancing contact angle θ_A is about 77° which, as discussed above, is well within the range of intermediate wettability.

There is yet another wettability regime that is of great practical importance. This is the so-called *mixed wettability* regime (Owens and Archer, 1971; Treiber *et al.*, 1972; Salathiel, 1973; Craig, 1977), in which some pores are wetted by one fluid, while others are wetted by the other fluid. There is evidence that over the course of geological times oil displaces brine from a portion of the pore space. Depending on the nature and composition of the oil, those portions of the pore wall that are separated from the crude oil by only a thin film or a tiny pendular

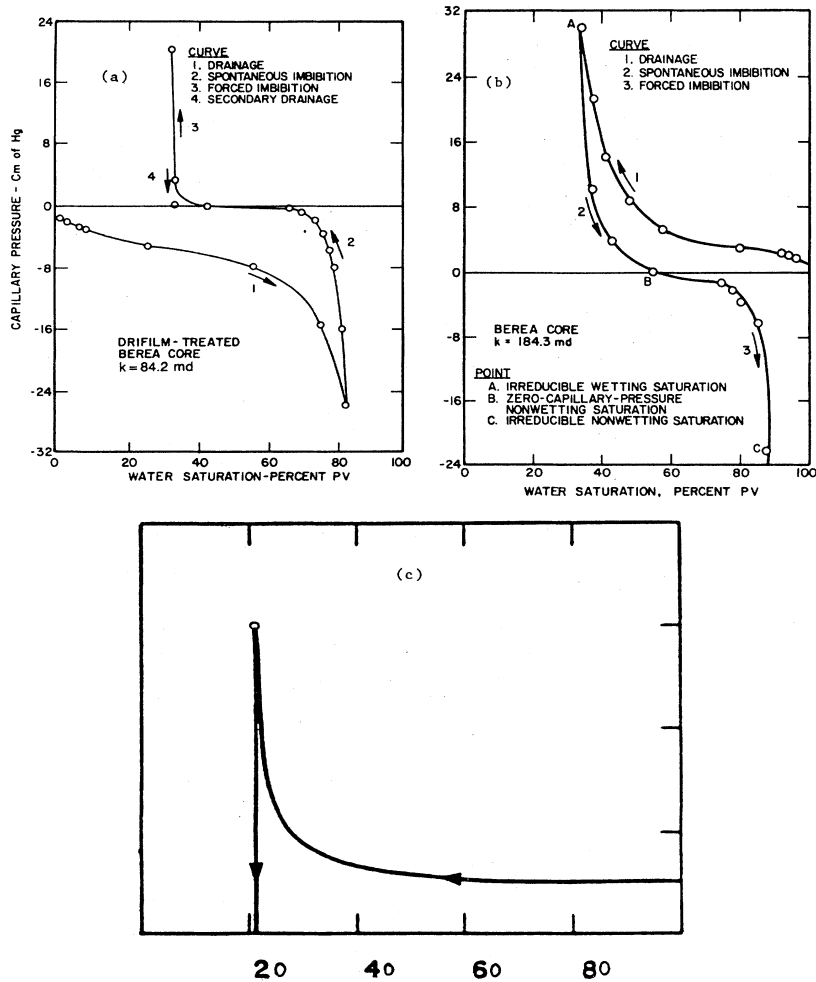


FIG. 49. (a) Typical capillary pressure curves for the wetted regime, (b) for a nonwetted porous medium [from Killins *et al.* (1953)], and (c) for an intermediately-wet system (from Morrow and McCaffery, 1978, reproduced from Anderson, 1987a).

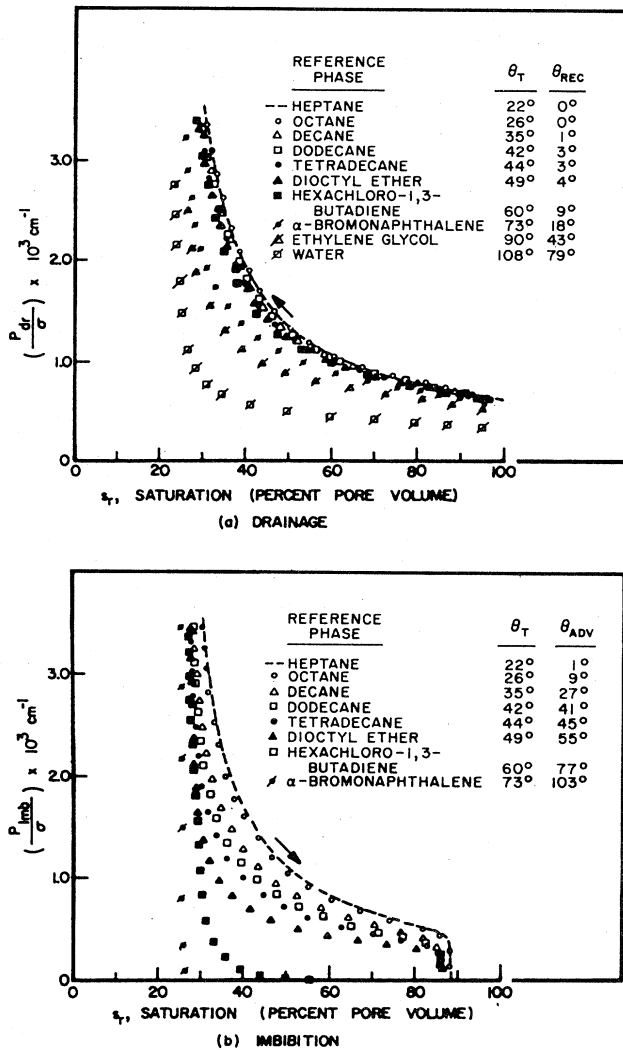


FIG. 50. Effect of contact angle on capillary pressure curves (from Morrow, 1970, reproduced from Anderson, 1987a).

structure of brine may become oil-wet owing to diffusion and adsorption or stronger chemical interactions with constituents of the oil phase. One widely cited interaction is the deposition by the crude of polar organic surfactants upon the surface of the rock (Brenner *et al.*, 1943; Salthiel, 1973; Melrose, 1982). In any event, it appears that migration, accumulation and deposition processes can generate a distribution of surface wetting preferences, the small pores that have not been invaded

by oil remaining water-wet, while the larger pores that have been occupied by oil becoming more or less oil-wet. Figure 51 shows capillary pressure curves for a system in which a fraction Y of the pores was invaded by oil and became oil-wet. $Y=0$ corresponds to a totally water-wet system, while $Y=1$ is representative of a totally oil-wet porous medium. These various wettability regimes also affect transport properties of porous media, which will be discussed below. More complete discussions of the effect of wettability on capillary pressure curves are given by Melrose (1965, 1968), Heiba (1985), and Anderson (1987a).

F. Immiscible displacement processes

We now discuss displacement of one fluid by another immiscible fluid. This process is controlled and affected by a variety of factors that were mentioned at the beginning of this section. We already discussed the effect of wettability and contact angles on capillary pressure, and shall discuss their effect on transport properties of the porous medium in two-phase flow later. Among the remaining factors, the capillary number Ca and the mobility ratio M have the greatest importance. Depending on how the displacement process proceeds, many different regimes may arise. A very careful discussion and classification of imbibition processes and how to distinguish between them was given by Payatakes and Dias (1984). We give here a summary of their classification and discussion and expand on them if appropriate.

(i) *Spontaneous imbibition*, which we already mentioned in the context of capillary pressure curves.

(ii) *Constant influx, constant Ca imbibition*, which occurs if a pressure drop ΔP is applied to the medium, and if it is adjusted as the invading fluid expels more fluids from the medium. If $M \leq 1$, then we must maintain $\Delta P \geq 0$, and vice versa. If for $M \leq 1$ the applied pressure dominates capillary forces, we shall no longer be dealing with an imbibition process.

(iii) *Quasistatic imbibition*, which happens when the flow rate of the displacing fluid is vanishingly small. In this case, the interface between the displacing and displaced fluid advances in only one pore at a time.

(iv) *Dynamic invasion with constant flow rate of the displacing fluid*. This can be done either at favorable mobility ratio ($M \leq 1$) or at an unfavorable one ($M > 1$). To achieve this, a large pressure drop ΔP is applied to the porous medium, which can be so large that it would dom-

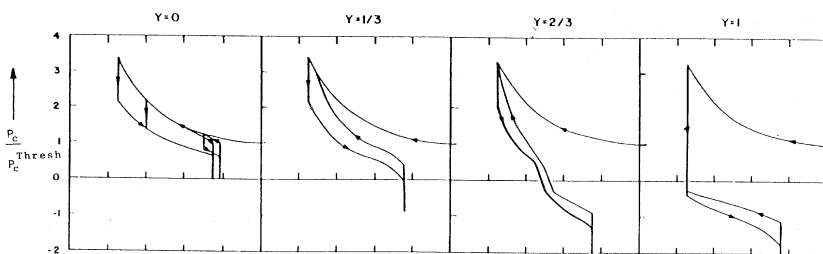


FIG. 51. Capillary pressure curves for porous media with mixed wettability. Y is the fraction of oil-wet pores (from Heiba, 1985).

inate capillary forces. The interface advances in *many* pores at any given time. For $M > 1$ viscous fingers can develop.

Note that the reverse of at least some of these imbibition processes can be considered as drainage processes. At the end of these processes, the displaced fluid exists only in the form of isolated blobs or clusters of finite sizes that cannot be displaced by any of the above processes. In order to mobilize and displace such blobs, the capillary number has to be significantly increased, which then gives rise to three other displacement processes which are (Payatakes and Dias, 1984) quasistatic and dynamic displacements of blobs, both of which are time-dependent phenomena, and steady-state dynamic displacement. The last process is achieved if the displacing and displaced fluids are simultaneously injected into the porous medium. After some time, a dynamic equilibrium is reached and the macroscopic flow rate becomes constant. This problem was recently investigated by Siddiqui and Sahimi (1993) using computer simulations, and has been discussed, from an experimental point of view, by Craig (1971). Payatakes (1982) has given an excellent discussion of blob mobilization and displacement in porous media. Therefore we shall not discuss the last three processes in great detail.

Before describing various theoretical and experimental studies on immiscible displacement in porous media, let us remind the reader that, unlike miscible displacement processes, immiscible displacements in Hele-Shaw cells have no direct relevance to those in a porous medium. This can be seen easily by realizing that the interface in a Hele-Shaw cell is sharp, whereas it is diffused in a porous medium due to the disordered structure of the medium. The interested reader can consult Bensimon *et al.* (1986), Saffman (1986), and Homsy (1987) regarding two-phase flows in a Hele-Shaw cell.

1. Spontaneous imbibition

The driving force for spontaneous imbibition is capillary suction, and because of this the smallest pore bodies which are next to the interface are always invaded. At any given time step, many pore-level interfaces advance in the porous medium. Usually, the displacement takes place at small but finite capillary numbers. Moreover, the value of C_a , which depends on the extent of the process, does not remain a constant, but varies over a range of values. This was demonstrated nicely in the experiments of Legait and Jacquin (1982) who studied spontaneous imbibition of water in sandstones containing oil at $M=225$. They reported that the rate of oil displacement increased strongly with time. When the same experiment was carried out at $M=1$, the same phenomenon was observed, albeit in a much weaker manner.

When relatively large values of C_a are created, a transition zone develops in which there is a high saturation gradient. As the interface advances in the medium, two separate regions develop. One is in front of the transition

zone in which the saturation of the displaced fluid is high. The other moves behind the transition zone in which the saturation of the displacing fluid is high. This region expands as the interface advances. The transition zone remains essentially the same throughout the displacement, except when the interface nears the end of the porous medium. For this reason, this region is called *stabilized zone*. Although Bail (1956) argued that under conditions used in regular imbibition in oil reservoirs, the length of this zone is not very large, its dynamics are interesting because it affects the efficiency of the displacement, and it is also in this region where oil blobs are formed by the disconnection of the displaced fluid by the displacing fluid.

2. Quasistatic imbibition

One main difference between this process and spontaneous imbibition is that in this process at any given step only one pore is invaded by the displacing fluid. This can be done by adjusting the backpressure so that the *narrowest* pore throat is invaded, while the interface at other larger throats remains essentially motionless. Since even the largest pore throats are smaller than the pore body to which they are connected, once a pore body is invaded, all of the throats that are also connected to it are also invaded. As soon as the interface enters such throats, the smallest pore body that is connected to them is invaded and so on. Thus at any given step of the displacement the smallest pore body that is accessible from the surface through a continuous path of the displacing fluid is invaded.

When the displacing fluid forms a sample-spanning cluster of invaded pore bodies (and the associated pore throats), a *breakthrough* is achieved. Just before the breakthrough the displaced fluid is mostly connected. However, as the displacement proceeds small blobs of the displaced fluid are formed which get trapped. At the end of this process, one may end up with a large number of isolated blobs whose volume fraction is significant. The value of this volume fraction depends on the morphology of the pore space. In unconsolidated media it varies between 0.14 and 0.2 (Chatzis *et al.*, 1983), whereas in consolidated rocks it is anywhere between 0.4 and 0.8 (Wardlaw and Cassan, 1978).

Experimental data of Raimondi and Torcaso (1964), Egbogah and Dawe (1980), and Chatzis *et al.* (1983) indicate that the size distribution of the blobs, when expressed in terms of the number of pore bodies they occupy, follows the power law

$$n_{sb} \sim s^{-\tau_b}, \quad (8.15)$$

where n_{sb} is the number of blobs of size s . Egbogah and Dawe (1980) found that the size of the blobs varied between 1 and 10 grain volumes, but most of them were around $s=1$. Although the data of Chatzis *et al.* (1983) show an apparent disagreement with Eq. (8.15), if one plots them as a function of the number of pore bodies

they occupy, they become consistent with Eq. (8.15). This equation reminds us immediately of Eq. (2.9), the scaling law for the number of finite percolation clusters of s sites. Indeed, as we shall discuss below, an appropriate percolation model can be devised to model such a quasistatic displacement.

3. Imbibition at constant flow rates

This is very similar to spontaneous imbibition except that in this case we need to adjust a backpressure in order to keep the flow rate constant. There has been some controversy regarding the role of M in the displacement process. There are some older papers (for example, Geffen *et al.*, 1951; Donaldson *et al.*, 1966) in which it was claimed that for fluids with identical wettability characteristics M does not have any significant effect. More recent works do not agree with this. Le Febvre du Prey (1973) investigated systematically the effect of M on relative permeabilities (i.e., the permeability to a fluid phase divided by the permeability of the medium) to two-phase flows, by studying displacements in sintered porous media in which Ca varied between 10^{-7} and 5×10^{-3} . He found that the higher the viscosity of one of the fluids, the lower the relative permeability of the other fluid, and this effect was found to be even more important than the wettability effect. This effect is presumably due to the fact that the high viscosity of the fluid gives rise to a film of the fluid residing on the pore walls, which denies pore volume to the other fluid and decreases its relative permeability.

Abrams (1975) found that the residual oil saturation in short porous media correlates well with the group $M^{-0.4}\text{Ca}$, where $10^{-7} \leq \text{Ca} \leq 10^{-2}$. Egbogah and Dawe (1980) found that for $M \leq 1$ the blob size distribution became much broader, took on bimodal and even trimodal shapes, and the average blob size increased dramatically.

4. Dynamic invasion at constant flow rates

The driving force for this process is an applied pressure drop, since the role of capillary forces is of secondary importance. If $M > 1$, we shall have an unstable displacement, which will be discussed later. Therefore, for now, we consider only the $M < 1$ case. There is a small transition zone in this process in which the saturations of both phases change with time. If the capillary pressure is negligible compared to the applied pressure, we shall have several advancing interfaces in as many pores at any given stage of the displacement. Because the driving force is the applied pressure, the microscopic interfaces choose the *largest* accessible pore throats (to minimize the resistance). Thus the structure of the sample-spanning cluster of the displacing fluid resembles that in a drainage process. However, this does not necessarily mean that smaller throats will not be selected: local pressures are also important and can cause the invasion of smaller throats by the advancing fluid. Since in the tran-

sition zone the saturation of the phase changes with time, the value of Ca cannot remain constant, even though the flow rate can be kept constant.

As in the previous cases, the advancing fluid creates isolated blobs of the displaced fluid. Whether these blobs become stranded or not depends on many factors. Ng and Payatakes (1980) and Payatakes *et al.* (1980) argued that the stranding of the blobs depends on Ca , the length of the blob in the direction of the macroscopic flow, and the sizes of the pore bodies and pore throats in which the blobs reside. If a very large blob is created, initially it is mobile, but later on it breaks into several smaller blobs, and the breaking process continues until they are small enough to be stranded.

5. Displacement of blobs: Choke-off versus pinch-off

If the displaced fluid is incompressible, then at the end of both imbibition and dynamic invasion one obtains many isolated blobs or clusters of the displaced fluid, whose displacement is the main goal of oil recovery processes. Usually, the mobilization and displacement of oil blobs require relatively high capillary numbers, say $\text{Ca} > 10^{-4}$. However, the value of Ca depends on several factors, including the shape and size of the blobs, the morphology of the porous medium, especially around the regions where the blobs reside, and the contact angle. For $\text{Ca} > \text{Ca}_c$, where Ca_c is a critical value of Ca , the blobs start to move. If $\text{Ca} - \text{Ca}_c$ is small, then we obtain what is called quasistatic displacement of the blobs. During this process one blob moves downstream, while one or two may move upstream. A blob may get reentrapped if it arrives at a pore body where all throats that are connected to it are too small for the blob's movement, in which case one needs an even higher Ca to move such blobs.

A moving blob is almost certain to break into smaller blobs by one of the following mechanisms. In *pinch-off* the velocity of the moving blob becomes small for a long enough time that the blob collapses into several smaller blobs. In *dynamic breakup* (Payatakes, 1982) a blob advances in two or more pore throats simultaneously, which can easily happen if the coordination number of the pore space is large enough. For this to happen, the value of Ca has to be large enough that even if two pore throats connected to the same pore body have different effective sizes, there can still be enough force to move the blob into both pores. If the blob completely evacuates the pore body, it breaks into two or more smaller blobs, depending on how many pore throats it enters.

There is yet another mechanism for blob breakup which is usually called *choke-off* or *snap-off*, and was first discussed by Pickell *et al.* (1966). Roof (1970), Mohanty *et al.* (1980, 1987), and Arriola *et al.* (1983) have discussed this phenomenon in detail. Chokeoff signals the breakup of a small drop from the leading tip of a nonwetting thread that tries to pass through a narrow constric-

tion. Roof (1970) conducted several experiments and demonstrated this phenomenon nicely. He considered choke-off in a toroidal pore throat, assumed that there is a thin lubrication film on the surface, and showed that choke-off occurs if the curvature of the interface at the throat is larger than the curvature of the tip of the thread. If the throat is nonaxisymmetric, then Roof showed that the same phenomenon happens except that it takes place faster than the toroidal case, because the film has easier access to the point of rupture as a result of the fact that some parts of the cross section are not filled by the nonwetting film. He also showed that before choke-off occurs, the tip of the nonwetting fluid thread has to travel a distance of several pore-throat diameters beyond the original throat. Therefore choke-off is important if the ratio of the pore body and pore throat diameters is large, and this was demonstrated by Wardlaw (1982) and Li and Wardlaw (1986a, 1986b). Hammond (1983) made a careful study of this phenomenon by solving the problem of slow adjustment of lubricated threads and drops in axisymmetric, straight capillaries, and constricted tubes. He used a lubrication theory and showed that it is not sufficient for the lubrication film to be unstable for choke-off to happen. One must also have a sufficient amount of wetting liquid in the film near the incipient neck to form a bridge across the tube because, while the neck is being formed, the thread on either side bulges and isolates the local wetting fluid from the rest. He estimated that for rupture to occur, the thickness l_f of the wetting fluid, normalized by the tube radius, must be larger than $\pi/6$. He also estimated that the time scale for the growth of a perturbation large enough to cause the rupture of a thread in a constriction is at least of the order $l_f^{-2}D\eta_1/\sigma_{fs}$, where D is the diameter of the tube.

Finally, just as blobs breakup into several smaller blobs, they can also coalesce. This happens when two interfaces that belong to two different blobs pass through the same throat and are pressed against each other for a long enough time. Constantinides and Payatakes (1991) used a network model to investigate the likelihood of collision and coalescence of blobs in a porous medium. Their results indicated that the wetting characteristics are more important than Ca , M , or θ , and that the probability of coalescence, given a collision, decreases as θ increases. They found this probability to vary between 0.03 to 0.15. Thus the breakup and coalescence phenomena give rise to a series of complex dynamical processes, in which the displaced fluid can break, but form a larger cluster again at a later time. Lenormand and Zarcone (1985b) presented nice experimental realizations of these phenomena in a micromodel. These are fascinating phenomena, for a review of which the reader can consult Payatakes (1982).

G. Models of two-phase flow and displacement

Similar to all the phenomena discussed so far, there are two classes of models of two-phase flow and displacement

in porous media. One of them relies on continuum equations, averaged over a suitably defined representative volume. This is the classical engineering approach whose major elements and achievements were already discussed in the previous sections. The literature on this class of model is enormous, and there is no possibility of reviewing it in this paper. We refer the reader to Collins (1961), Bear (1972), Scheidegger (1974), and Marle (1981) for complete discussions of this class models. The models in the second class are discrete or statistical. In this section we review them for two-phase flow problems. The literature on this class of models has also grown dramatically in the last few years, and it would be difficult to review everything that has been done.

1. Continuum equations and relative permeabilities

Whitaker (1986b) studied flow of two immiscible fluids in porous media. Starting with the continuity and Stokes' equations for each phase, and using the appropriate boundary and initial conditions, he derived the following equations for the average flow velocity and volume fraction of the phases β and γ

$$\mathbf{v}_\beta = - \frac{\mathbf{K}_\beta}{\eta_\beta} \cdot (\nabla \langle P_\beta \rangle^\beta - \rho_\beta \mathbf{g}) + \mathbf{K}_{\beta\gamma} \cdot \mathbf{v}_\gamma , \quad (8.16)$$

$$\frac{\partial S_\beta}{\partial t} + \nabla \cdot \mathbf{v}_\beta = 0 , \quad (8.17)$$

$$\mathbf{v}_\gamma = - \frac{\mathbf{K}_\gamma}{\eta_\gamma} \cdot (\nabla \langle P_\gamma \rangle^\gamma - \rho_\gamma \mathbf{g}) + \mathbf{K}_{\gamma\beta} \cdot \mathbf{v}_\beta , \quad (8.18)$$

$$\frac{\partial S_\gamma}{\partial t} + \nabla \cdot \mathbf{v}_\gamma = 0 , \quad (8.19)$$

where all notations are as before. Note that Eqs. (8.16) and (8.18) contain two terms, the first of which is the usual Darcy's law, written for each phase, while the second one is a cross term that couples the two phases. These equations are valid if $Ca \ll 1$ and if moving contact lines discussed above do not have a significant effect. Equations (8.16) and (8.18) were first proposed by Raats and Klute (1968) and de Gennes (1983b) based on physical arguments, although somewhat similar equations had been conjectured by Rose (1972). Whitaker (1986b) was the first to derive Eqs. (8.16)–(8.19). In analogy with the thermodynamics of irreversible processes, one may assume that $\mathbf{K}_{\beta\gamma} = \mathbf{K}_{\gamma\beta}$. Generally speaking, the coupling terms in Eqs. (8.16) and (8.18) are not significant unless $\eta_\beta \approx \eta_\gamma$ (in which case a thin film of one phase covers the walls of a pore whose bulk volume is filled with the other phase). However, Kalaydjian and Legait (1987) and Goode and Ramakrishnan (1993) showed that such coupling terms might be important in certain cases even if η_β and η_γ are not close to each other. Some of the most convincing evidence for insignificance of the cross terms of Eqs. (8.16) and (8.18) was provided by Yadav *et al.* (1987). They experimented with a wetting and a nonwet-

ting fluid and showed that the permeability of both phases in drainage, measured when the opposite phase was solidified *in situ*, was the same as that typically measured for Berea sandstones. The phase permeabilities K_β and K_γ are supposed to be known, but in practice one calculates them by the use of the relations

$$K_\beta = K k_{r\beta}, \quad (8.20)$$

with a similar equation for the γ phase, where $k_{r\beta}$ is the relative permeability (RP) to the β phase, a concept that has been used for many decades in the petroleum industry. A major problem in two-phase flow in porous media is the prediction of the RPs. Unlike the absolute permeability, $k_{r\beta}$ has been found to depend on many parameters, including saturation and saturation histories of the fluids (Johnson *et al.*, 1959; Naar *et al.*, 1962), pore space morphology (Morgan and Gordon, 1970), the wetting characteristics of the fluids (Owens and Archer, 1971; McCaffery and Benion, 1974), sometimes on the viscosity ratio (Odeh, 1959; Le Febre du Prey, 1973), and Ca (Leverett, 1939; Taber, 1969). Moreover, forty years ago it was recognized (Richardson *et al.*, 1952) that the relative permeability to a phase typically becomes small or altogether negligible when its saturation is less than a critical value which is distinctly above zero. This is of course the signature of a percolation problem which will be discussed below. The reason $k_{r\beta}$ apparently depends on the saturation history of a phase, i.e., the way that saturation has been reached, is that there are presumably multiple shapes that satisfy the Stokes equation, which is made nonlinear by the free interfaces. This dependence naturally gives rise to *hysteresis* in RPs, which is discussed shortly.

2. Measurement of relative permeability

There are many methods of measuring RPs (see Anderson, 1987b). One method that is routinely used is as follows. The porous medium is initially filled with the wetting phase, and both wetting and nonwetting fluids are injected into the medium at a constant flow rate. When the steady state has been reached, the pressure drop across the medium is recorded. From the knowledge of the flow rate and pressure drop the phase permeabilities k_β and k_γ are calculated, using Eqs. (8.16) and (8.18). The phase saturations can also be determined by several methods, the simplest of which is by weighing the sample before and after the injection. Since the absolute permeability of the medium is already known (see Sec. V), the relative permeability to the wetting phase at this particular value of saturation is calculated. In the next stage, the injected amount of non-wetting fluid is increased, and the procedure is repeated. In this way, the RP to the wetting phase is obtained. By reversing the procedure one can obtain the RP to the nonwetting phase, and so on. The reader should consult Anderson (1987b) and Heaviside (1991) for more details on measurement of RPs.

3. The effect of wettability on relative permeability

We have already discussed the effect of wettability on capillary pressure. It is clear that wettability and contact angles should also affect the RPs, and this is indeed the case. Figure 52(a) shows typical oil-water RP curves for a strongly water-wet system, while Fig. 52(b) shows the same for a strongly oil-wet porous medium. While the difference between the two RP curves for the oil phase is not very large, there is a dramatic difference between the RPs to the water phase. Note also the existence of a finite saturation (i.e., a percolation threshold) at which the RP vanishes. Normally, if a system is strongly water-wet, there is little or no hysteresis in the RPs to the water phase. This can be seen clearly in the experimental data of Morrow and McCaffery (1978). They measured RPs in a teflon core with nitrogen as the nonwetting fluid and heptane ($\theta=20^\circ$) and dodecane ($\theta=42^\circ$) as the wetting phase. They found that there is no hysteresis in the wetting-phase RP. Figure 53 shows the data of McCaffery and Benion (1974) and Morrow and McCaffery (1978) for the three different wettability re-

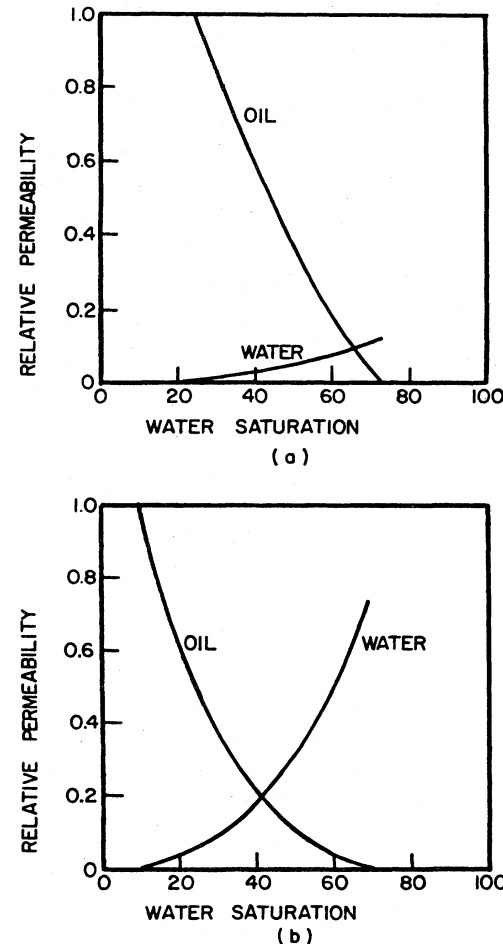


FIG. 52. Typical relative permeability curves: (a) for a water-wet system; (b) for an oil-wet porous medium (from Craig, 1971, reproduced from Anderson, 1987b).

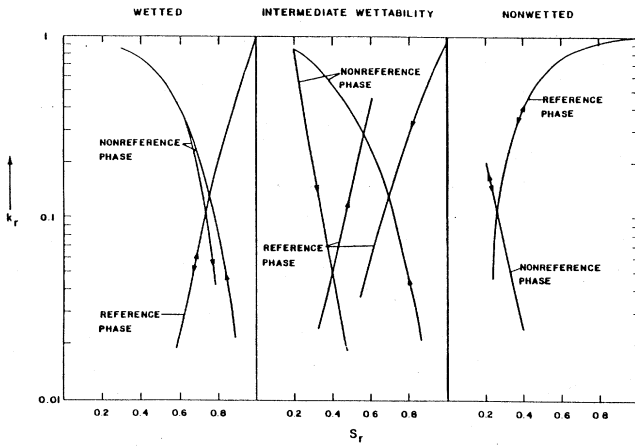


FIG. 53. Relative permeability k_r vs the reference phase saturation S_r for various regimes of wettability. The contact angles for the wetted and nonwetted cases were 49° and 130°, respectively (from McCaffery and Benion, 1974, and Morrow and McCaffery, 1978).

gimes discussed above, namely, wetted, intermediately-wetted, and nonwetted cases. In this figure the reference phase refers to the displaced phase, while the nonreference phase refers to the displacing phase, and S_r is the saturation of the reference phase. The differences between the three cases are rather large. For example, in the nonwetting case, the contact angle for the nonreference phase was more than 130°, whereas in the wetted case it was at most 49°. Figure 54 is an even clearer demonstration of the effect of contact angle and wettability on RP's, in which Y is the fraction of oil-contacted pores rendered oil-wet in the primary drainage (such pores were initially water-wet). These curves exhibit four processes, which are primary drainage (the core is saturated 100% with water), followed by a primary imbibition (started at the end of primary drainage), and then followed by secondary drainage and secondary imbibition. It is obvious that wettability strongly affects the trends in RP's, and one major theoretical challenge is to predict such trends. This is the subject of the next two subsections.

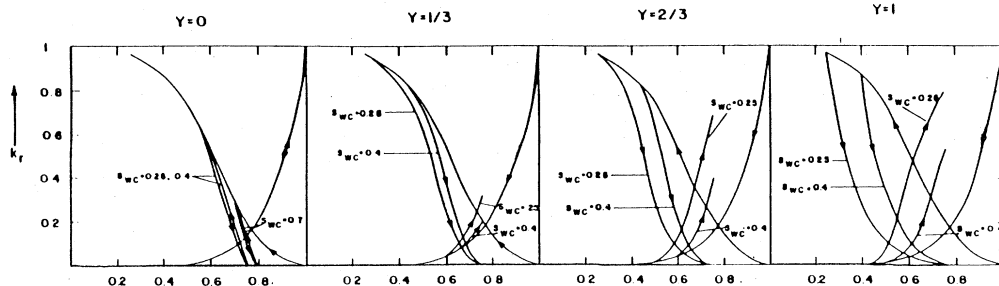


FIG. 54. Relative permeability curves for varying fractions Y of oil-contacted pores rendered oil-wet after an oilflood (from Heiba, 1985).

H. Percolation models of capillary-controlled two-phase flow and displacement

In this section we discuss statistical and network methods of two-phase flow and displacement in porous media. Some of these are based on percolation concepts and their variants and, strictly speaking, are applicable only when Ca is very small. There are other models that are presumably valid even when Ca is finite (in which case both capillary and viscous forces are relevant). The limit $Ca \rightarrow \infty$ is of course the case of miscible displacements already discussed in Sec. VII.

1. Random-percolation models

At the outset we should point out that the fundamental assumption in all percolation models of two-phase flow is that the occupation probability p is proportional to the capillary pressure. Without such an assumption, it would be difficult to make a one-to-one correspondence between a percolation model and the two-phase flow problem. Although in some percolation models such as invasion percolation (see below) the occupation probability is not defined, an analogue of it can be calculated easily.

The first random-percolation model of two-phase flows in porous media was suggested by Larson (1977), with the details given in Larson *et al.* (1977, 1981a, 1981b). In Larson *et al.* (1981a) the authors proposed a model for drainage. The porous medium was represented as a cubic network of bonds and sites with distributed sizes. It was assumed that a bond next to the interface is penetrated by the displacing fluid if the capillary pressure at that point exceeds a critical value, which implies that the radius of the bond has to exceed a critical radius r_{min} . This is the same radius that is defined by Eq. (3.9), which implies that during drainage the largest pore throats are invaded by the nonwetting fluid (which is similar to dynamic invasion). All bonds that are connected to the (nonwetting) displacing fluid by a path of pores or bonds, whose effective radii are larger than r_{min} , are considered accessible, the accessibility being defined in the sense of percolation discussion in Sec. II. It was also assumed that all accessible bonds, whose radii are at least as large

as r_{\min} , are filled with the nonwetting fluid. This is of course not true, since an interface which starts at one external face of a porous medium has to travel along a certain path before it reaches an accessible and potentially eligible bond. Larson *et al.* (1981a) also assumed that the displaced fluid is compressible, so that even if a blob of it is surrounded by the displacing fluid, it can still be invaded. This does not, however, result in a serious error, as we discuss below.

In their next paper, Larson *et al.* (1981b) proposed a percolation model of imbibition in order to calculate the residual nonwetting phase saturation S_{rw} and its dependence on Ca . To do this, they modeled the creation of isolated blobs of the nonwetting phase by a random site percolation (see Sec. II). At the site percolation threshold of the network, they calculated the fraction $\hat{g}(s)$ of the active sites that are in clusters of length s in the direction of flow and argued that this represents the desired blob size distribution. To calculate S_{rw} , they assumed that once a blob is mobilized, it is permanently displaced which, as discussed above, is not always the case, because a blob can get trapped again, can join another blob and create a larger one, and so on.

The fundamental assumption behind the work of Larson *et al.* work is that pore-level events are controlled by capillary forces. It is possible to use simple scaling arguments to estimate the values of Ca for which this assumption is valid. The capillary pressure across the interface is proportional to

$$P_c \sim \frac{\sigma_{ow} \cos \theta}{l}, \quad (8.21)$$

where l is a typical grain size. On the other hand, the viscous pressure drop is proportional to

$$P_{vis} \sim \frac{\eta_w v l}{k}, \quad (8.22)$$

where η_w is the viscosity of the wetting phase. Therefore

$$\frac{P_{vis}}{P_c} \sim \frac{Ca}{k_d} \quad (8.23)$$

where $k_d = k/l^2$ is a dimensionless permeability which is small (of order 10^{-3} or smaller), because k is controlled by the narrowest throats in the medium. It follows that for capillary-controlled displacements, one must have $Ca \ll 1$, and in practice one has $Ca \sim 10^{-5} - 10^{-6}$. Experimental data (Le Fabvre du Prey, 1973; Amaefule and Handy, 1982; Chatzis and Morrow, 1984) seem to support this, since they indicate that S_{rw} is constant for $Ca < Ca_c$, where Ca_c is the critical value of Ca for capillary-controlled displacement, and S_{rw} decreases only when $Ca > Ca_c$. Larson *et al.* (1981b) compiled a wide variety of experimental data and compared them with their predictions.

Heiba *et al.* (1982, 1983, 1984, 1992) further developed these ideas and used them for calculating relative permeabilities for all regimes of wettability discussed above. Heiba *et al.* (1982) distinguished between bonds (pore

throats) that are *allowed* to a phase, and those that are actually occupied by the phase. Then, given a pore size distribution of the pore space, they calculated the pore size distribution of the allowed pores and the occupied pores. Consider, for example, a displacement process in which one fluid is strongly wetting, while the other one is completely nonwetting. Then, according to percolation model of Heiba *et al.* (1982, 1992), during primary drainage the pore size distribution of the pores occupied by the displacing (nonwetting) phase is given by Eq. (3.10), since the *largest* throats are occupied by the nonwetting fluid, and during imbibition the pore size distribution of the pores occupied by the displacing (wetting) phase is given by Eq. (3.12), because the *smallest* pores are occupied by the wetting phase. One can, in a similar fashion, derive expressions for the pore size distribution of the pores occupied by the displacing and displaced fluids during secondary imbibition and drainage. Once such pore size distributions are determined, calculating the permeability of each fluid phase (and therefore the RP) reduces to a problem of percolation conductivity, because when we calculate the permeability of a given phase, the conductance (or effective radii) of the bonds occupied by the other phase can be set to zero, since the two phases are immiscible. Therefore any of the methods discussed in Sec. V can be used for calculating the RPs to the phases. These ideas were first developed by Heiba *et al.* (1982) and were implemented by them and by Sahimi *et al.* (1986a) on a variety of networks. Figure 55, taken from Sahimi *et al.* (1986a), shows the results obtained with a cubic network. A comparison between this figure and Figs. 53 and 54 shows that all qualitative, and many quantitative, aspects of the experimental data are reproduced by the model. Note that, as discussed in Sec. III, drainage is better described by a bond percola-

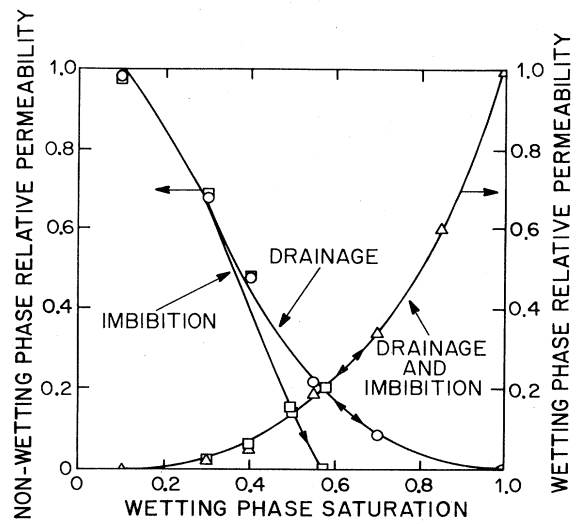


FIG. 55. Relative permeability curves for a strongly wetting and a completely nonwetting porous medium, as predicted by the random-percolation model. Data are shown with \circ and \square (from Sahimi, Heiba *et al.*, 1986).

tion process, whereas imbibition is more complex (see below).

In two subsequent papers, Heiba *et al.* extended their model to the case in which the porous medium is intermediately-wet, or has mixed wettability characteristics (Heiba *et al.*, 1983), and to the case where there are *three immiscible phases* in the medium (for example, oil, water, and gas). Consider the case of an intermediately-wetted medium. As discussed above, in such a case both primary and secondary displacement processes are drainage. Therefore the formulas developed by Heiba *et al.* (1982, 1992) for drainage can be easily extended and modified for this case. Heiba *et al.* (1983) showed that their model can predict all relevant features of RPs and capillary pressure for intermediately-wetted a porous media (see Fig. 53). Ramakrishnan and Wasan (1984) used similar ideas and developed expressions for RPs and also considered the effect of Ca on them. Just as the residual saturations S_r depend on Ca (in fact $S_r \rightarrow 0$ as $\text{Ca} \rightarrow \infty$, which is the limit of miscible displacements), the RPs also depend on Ca. Normally, If Ca is small RPs do not show a great sensitivity to Ca. Evidence for this is provided by the experimental data of Amaefule and Handy (1982). However, as Ca increases the RP curves lose their curvature, and in the limit $\text{Ca} \rightarrow \infty$ they become straight lines. Ramakrishnan and Wasan (1984) developed formulae that can take this effect into account. Levine and Cuthiell (1986) used an effective-medium approximation and a percolation model similar to that of Heiba *et al.* to calculate the RPs to two-phase flow systems.

2. Random site-correlated bond percolation models

Chatzis and Dullien (1982) used a network model in which the sites represented the pore bodies to which random radii were assigned, and the bonds represented the pore throats whose effective radii were correlated with those of the sites. Using this model, Chatzis and Dullien (1982, 1985), Diaz *et al.* (1987), and Kantzas and Chatzis (1988) simulated RP and capillary pressure curves for sandstones. On the other hand, Wardlaw *et al.* (1987) determined experimentally the correlations between the pore bodies and pore throats sizes, and found that there are little, if any, such correlations in Berea sandstones but larger correlations for the Indiana limestone. Li *et al.* (1986), Constantinides and Payatakes (1989), and Maier and Laidlaw (1990, 1991b) also proposed network models in which the sizes of the pore bodies and pore throats were correlated. In spite of the fact that the correlated model is much more detailed than a simple random bond model, and despite extravagant claims made by Chatzis and co-workers about the superiority of the model, the RP predictions of their model are not different in any significant way from those of the random percolation model.

3. Invasion percolation

This model was first proposed by Lenormand and Bories (1980), Chandler *et al.* (1982), and Wilkinson and Willemsen (1983). In this model the network is initially filled with a fluid called the *defender*. To each site of the network is assigned a random number uniformly distributed in $[0,1]$. Then the displacing fluid (the *invader*) is injected into the medium which displaces the defender at each time step by choosing the site next to the interface that has the smallest random number. If we interpret the random numbers as the resistance that the sites offer to the invading fluid, then choosing the site with the smallest random number is equivalent to selecting a pore with the largest size, and hence this model simulates a drainage process. A slightly more tedious procedure can be used for working with bonds instead of sites. Two versions of the model have been developed. In one model the defender is incompressible, and therefore if its blobs are surrounded by the invader, they become trapped. This was studied by Chandler *et al.* (1982) and Wilkinson and Willemsen (1983). In the second model, trapping is ignored (i.e., one tries to displace an infinitely compressible defender). This was studied by Wilkinson and Barsony (1984). Note that invasion percolation represents a dynamical growth process, as opposed to random percolation which is static.

There is a close connection between invasion percolation without trapping and random percolation. This connection was first found by Wilkinson and Barsony (1984) by Monte Carlo simulations. Some theoretical arguments were also given by Chayes *et al.* (1986). Wilkinson and Barsony (1984) hypothesized that the exponent $\Delta = vD_p$ of invasion percolation without trapping is the same as that of random percolation, and this was supported by their Monte Carlo simulations. An exact solution of the problem on the Bethe lattice (Nickel and Wilkinson, 1983) also confirmed this. Therefore invasion percolation without trapping seems to be in the universality class of random percolation.

For invasion percolation with trapping, Monte Carlo simulations of Wilkinson and Willemsen (1983) and those of others indicated that, $D_p(d=2) \approx 1.82$, somewhat smaller than $D_p(d=2) = 91/48 \approx 1.896$ for random percolation, whereas for $d=3$ no significant difference between invasion and random percolation models was observed. Therefore the effect of trapping seems to be negligible in three dimensions. However, it is not yet established rigorously that invasion percolation with trapping does not belong to the universality class of random percolation.

From a conceptual point of view, invasion percolation is definitely a more appropriate model of immiscible displacements than the random percolation models discussed above. The most obvious reason for this is the fact that there is a well-defined interface that starts from one side of the system and displaces the defender in a sys-

tematic and realistic way. Thus, the concepts of history, and the sequence of invading pores according to a physical rule are naturally built into the model.

Let us summarize the *experimental* evidence in support of invasion percolation model of two-phase flows. Lenormand and Zarcone (1985a) displaced oil (the wetting fluid) by air (the nonwetting fluid) in a large and transparent two-dimensional etched network and obtained $D_p \approx 1.82$, consistent with two-dimensional computer simulations of invasion percolation with trapping. Jacquin (1985) and Shaw (1987) also performed experiments that gave strong support to the validity of invasion percolation. For example, Shaw (1987) showed that if a porous medium, filled with water, is dried by hot air, the dried pores (i.e., those filled with air) form an invasion percolation cluster with the fractal dimension that is found in computer simulations. Stokes *et al.* (1986) used a cell packed with unconsolidated glass beads, an essentially three-dimensional pore system. The wetting fluid was water or a water-glycerol mixture, while the nonwetting fluid was oil. When oil displaced water (drainage), the resulting patterns were consistent with invasion percolation description of the process. Chen and Wada (1986) used a technique in which one uses index matching of the fluids to the porous matrix to "look" inside the porous medium. Their observations were consistent with invasion percolation model. Chen and Koplik (1985) used small two-dimensional etched networks, with oil and air as the wetting and nonwetting fluids, respectively, and found that their drainage patterns were consistent with the assumptions and results of invasion percolation. Finally, Lenormand and Zarcone (1985b) used two-dimensional etched networks and a variety of wetting and nonwetting fluids (oil, different water-sucrose solutions, air), and showed that their drainage experiments are all completely consistent with an invasion percolation description of this phenomenon. Therefore although all these porous media were man-made, and we still do not have any experimental evidence from two-phase flow in a natural porous medium, there is little doubt that invasion percolation is an appropriate description of capillary-controlled two-phase flow in porous media, especially in the case of drainage.

A large number of authors have used an invasion percolation algorithm or its variants to simulate two-phase flow in porous media. Some of them (Lin and Slattery, 1982; Mohanty and Salter, 1982; Katz *et al.*, 1988; Roux and Wilkinson, 1988; Blunt and King, 1990, 1991; Jerauld and Salter, 1990) were concerned mainly with calculating the RPs and conductivities of invasion percolation clusters. Some of these authors did not mention invasion percolation, although their model was similar to invasion percolation. Others concerned themselves with fundamental properties of invasion percolation clusters. For example, Wilkinson (1986) and Sahimi and Imdakm (1988) derived the scaling laws that the capillary pressures, RPs, and dispersion coefficients obey near the residual saturations (see below). Furuberg *et al.* (1988) studied the probability $Q(r, t)$ (where $r = |\mathbf{r}|$) that a site,

a distance r from the injection point, is invaded at time t . They found that a dynamic scaling governs $Q(r, t)$

$$Q(r, t) \sim r^{-1} f(r^{D_p}/t), \quad (8.24)$$

where $f(u)$ is a scaling function with the *unusual* property that $f(u) \sim u^{a_1}$ ($u \ll 1$), and $f(u) \sim u^{-a_2}$ ($u \gg 1$), i.e., $f(u)$ vanishes at both ends. This dynamic scaling implies that the most probable point at which the growth of the interface takes place is at $r \sim t^{1/D_p}$. The reason for this unusual limiting behavior of $f(u)$ is that at time t , most of the region within the distance r has already been invaded, and new sites close to the interface that can be invaded are rare. Roux and Guyon (1989) argued that the exponents a_1 and a_2 are given by, $a_1 = 1$, and $a_2 = \tau_p + \sigma_p - D_h/D_p - 1$, where τ_p , σ_p , and D_p are the usual percolation exponents and fractal dimension (Sec. II), and D_h is the fractal dimension of the *hull* (or external surface) of percolation clusters, where $D_h(d=2) = 1 + 1/\nu = 7/4$, and $D_h(d=3) \approx D_p$.

Laidlaw *et al.* (1988) considered two different algorithms for invasion percolation. One of them was the usual one defined above, while in the other one the displacing fluid invaded *all* accessible sites less than a given size. They found that while the fractions of invading fluid in the two cases are different (which is expected), their scaling properties are the same. Meakin (1991) studied invasion percolation on substrates with multifractal distribution of bond threshold probabilities. He found that the spatial correlation does not change the fractal properties of invasion clusters. However, certain differences may appear in the scaling of the hulls of the clusters. Maier and Laidlaw (1991a) investigated the existence of dimensional invariants (such as B_c defined for random percolation in Sec. II) in invasion percolation. Finally, Bakurov *et al.* (1990) proposed a dynamical percolation model of oil displacement, and developed a quasi-quantum-mechanical formulation for it. Their model is closely related to invasion percolation.

4. Random percolation with trapping

Random percolation with trapping was developed by Sahimi (1985) and Sahimi and Tsotsis (1985) to model catalytic pore plugging of porous media. In this problem the pores of a porous medium plug as the result of a chemical reaction and deposition of the solid products on the surface of the pores. Large (macro-) pores take a long time to be plugged, and if they are surrounded by small (micro-) pores that quickly plug, they are trapped and cannot be reached by the reactants. Accurate computer simulations of Dias and Wilkinson (1986), who proposed the same model for two-phase flow problems, indicated that most properties of random percolation with trapping in both two and three dimensions are the same as those of random percolation discussed in Sec. II. However, this may not be the case if, as in the problem considered by Sahimi and Tsotsis, the pore sizes are

broadly distributed.

More rigorously, a trapping transition for random percolation can be defined as follows (Pokorný *et al.*, 1990). One starts with a random percolation model and at any fraction p of open bonds removes from the network all the bonds which are part of the infinite cluster. A trap is then defined as the connected component of what remains of the network. For $p \approx 1$, all traps are of finite size. As p approaches p_c , a trapping transition occurs at p_t below which there is an infinite trap. Aizeman and Grimmett [quoted by Pokorný *et al.* (1990)] proved that $p_t > 1 - p_c$. Pokorný *et al.* (1990) showed that $p_t \approx 0.52$ for the square network, and that trapping transition is described by the critical exponents of random percolation.

5. Crossover from fractal to compact displacement

Although we discussed relative-permeability RP curves for *both* imbibition and drainage in terms of a percolation model, there are certain qualitative differences between the two that need to be discussed. A clue to these differences is already evident in the RP curves. The RP to the nonwetting phase during primary imbibition by a strongly wetting fluid vanishes only at $S_{rw} = 0$, i.e., the nonwetting phase is completely expelled from the medium and the wetting phase fills the system; see Fig. 55. This indicates that imbibition is an essentially compact displacement. However, during drainage by a completely nonwetting fluid, the RP to the wetting phase vanishes at a finite value of S_{rw} , i.e., the nonwetting phase does not fill the porous medium, and a fractal percolation cluster is formed. This was already predicted by the percolation model of Heiba *et al.* (1982, 1992), and was also nicely demonstrated by Lenormand and Zarcone (1984) who used a two-dimensional etched network, injected mercury into the system (drainage), and then withdrew it (imbibition). The cluster formed during imbibition was totally compact and filled the etched network.

A definitive study of this problem was made by Cieplak and Robbins (1988, 1990). In this study the porous medium was represented by a two-dimensional array of disks with random radii, where the underlying lattice was either a triangular or a square network. The limit of low Ca was considered, and the displacement dynamics were modeled as a stepwise process where each unstable section of the interface moved to the next stable or nearly stable configuration. Their simulations showed that there are three basic types of instability and the corresponding growth mechanisms. (i) *Burst* happens when, at a given capillary pressure P_c , no stable arc connects two disks, and therefore the interface simply jumps forward to connect to the nearest disk. (ii) *Touch* happens when an arc that connects two disks, intersects another disk at a wrong contact angle θ . In this case, the interface connects to this third disk. (iii) *Overlap* happens when two nearby arcs overlap. There is no need for the disk to

which both arcs are connected, and it can be removed from the interface. Figure 56 illustrates these three growth mechanisms.

To simulate the growth of the interface P_c is fixed and the stable arcs are found. If instabilities are found, local changes are made to remove them. Then, P_c is increased by a small amount (to simulate a capillary-controlled invasion), the interface is advanced, possible instabilities are removed again, and so on. As in invasion percolation with trapping, if the invading fluid surrounds a blob of the displaced fluid, the blob is kept intact for the rest of the simulation. If all disks have the same radius, the resulting patterns are very regular and faceted which also preserve the symmetry of the lattice. This is in agreement with the experiments of Ben-Jacob *et al.* (1985). However, when the radii of the disks are randomly distributed, then the behavior of the system depends on the contact angle θ . To quantify the effect of θ , we define an interface width w . When θ is near 180° , i.e., one has a drainage process, then the phenomenon is an invasion percolation and w is of the order of pore size. However, Cieplak and Robbins (1988, 1990) showed that as θ decreases the cluster of invading fluid becomes more compact and w increases; see Fig. 57. Finally, at a critical contact angle θ_c , w diverges according to a power law

$$w \sim (\theta - \theta_c)^{-\nu_\theta}, \quad (8.25)$$

where $\nu_\theta \approx 2.3$ in their two-dimensional simulations. The critical angle θ_c was found to depend on the porosity ϕ of the system, for example, $\theta_c \approx 29^\circ$ for $\phi = 0.322$, and $\theta_c \approx 69^\circ$ for $\phi = 0.73$. The exponent ν_θ was found to be universal. The compactness of the cluster for $\theta < \theta_c$ is consistent with the imbibition picture discussed above.

The divergence of w at θ_c is clearly due to the transition from fractal to compact growth. For large θ , growth occurs mainly by burst, similar to invasion percolations, and the growth pattern is independent of θ . However, as $\theta \rightarrow \theta_c$, the overlap and touch phenomena become more important, and the interface is unstable for almost any configuration of the local geometry. Thus the growth pattern changes, and hence w diverges.

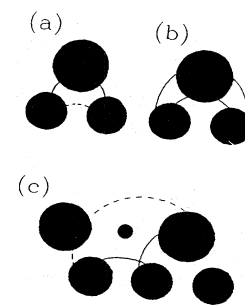


FIG. 56. Three types of instability and growth that occur during an immiscible displacement: (a) burst, (b) touch, and (c) overlap of arcs (from Cieplak and Robbins, 1990).

6. Roughening and pinning of fluid interfaces: Dynamic scaling of rough surfaces

Although the available experimental data, the percolation model of Heiba *et al.* (1982, 1992) for RP's, two-dimensional experiments of Lenormand and Zarcone (1984), and simulation of Cieplak and Robbins (1988, 1990) all indicated a major difference between drainage and imbibition, we still have not discussed the nature of the interface during imbibition. The cluster of the invading fluid during imbibition is compact, but capillary forces lead to random local pinning of the interface which results in its roughening. This rough interface has

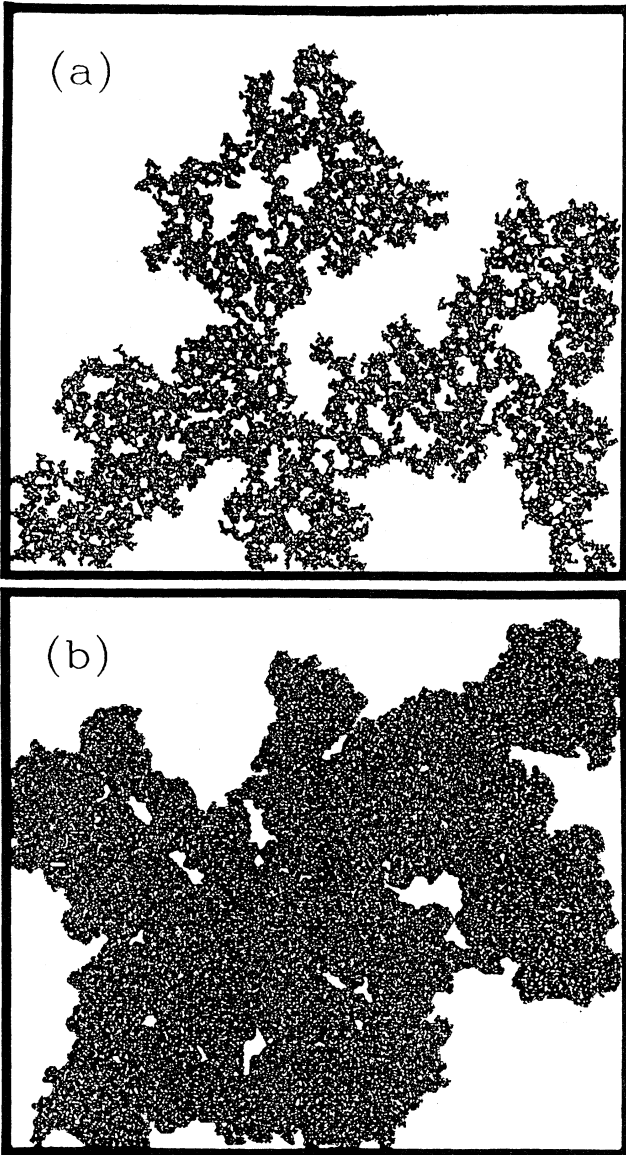


FIG. 57. The effect of contact angle on the shape of the invading cluster: (a) $\theta=179^\circ$; (b) $\theta=58^\circ$. The cluster in (a) represents a drainage process, while the one in (b) represents imbibition (from Cieplak and Robbins, 1990).

a self-affine (anisotropic) fractal structure, which was demonstrated by the experiments of Rubio *et al.* (1989) and Horváth *et al.* (1991a). The self-affinity of such rough interfaces was first suggested by Cieplak and Robbins (1988), but it was not quantified.

Rubio *et al.* (1989) performed their experiments in a thin (essentially two-dimensional) porous medium made of tightly packed clean glass beads of various diameters. Water was injected into the porous medium to displace the air in the system. The motion of the interface was recorded and digitized with high resolution. The experiments of Horváth *et al.* (1991a) were very similar (see below). Before embarking on an analysis of the results of Rubio *et al.* (1989) and Horváth *et al.* (1991a), let us review briefly the dynamics of rough surfaces and interfaces.

The roughness of the interface is characterized by the width $w(L)$ defined as, $w(L)=\langle [h(x)-\langle h \rangle_L]^2 \rangle^{1/2}$, where h is the height of the interface at position x , and $\langle h \rangle_L$ is its average over a horizontal segment of length L . According to the scaling theory of Family and Vicsek (1985) for growing rough surfaces, one has the scaling form at time t

$$h(x)-\langle h \rangle_L \sim t^{\beta} f(x/t^{\beta/\alpha}), \quad (8.26)$$

where α and β are two critical exponents that satisfy the scaling relation

$$\alpha + \frac{\alpha}{\beta} = 2, \quad (8.27)$$

and the scaling function $f(u)$ has the properties that, $|f(u)| < c$ for $u \gg 1$, and $f(u) \sim L^\alpha f(Lu)$ for $u \ll 1$, where c is a constant. It is then easy to see that

$$w(L,t) \sim t^{\beta} g(t/L^{\alpha/\beta}), \quad (8.28)$$

where $g(u)$ is another scaling function, and therefore

$$w(L,\infty) \sim L^\alpha. \quad (8.29)$$

Note that $w(L,t)$ is a measure of the correlation length along the direction of growth. A variety of surface growth models and the resulting dynamical scaling can be described by the stochastic differential equation proposed by Kardar, Parisi, and Zhang (1986) (KPZ)

$$\frac{\partial h}{\partial t} = \sigma \nabla_T^2 h + \frac{v_g}{2} |\nabla h|^2 + \mathcal{N}(\mathbf{r},t), \quad (8.30)$$

where σ is the surface tension, v_g is the growth velocity perpendicular to the interface, and \mathcal{N} is a noise term. Kardar *et al.* (1986) considered the case in which the noise was assumed to be Gaussian with the correlation

$$\langle \mathcal{N}(\mathbf{r},t) \mathcal{N}(\mathbf{r}',t') \rangle = 2A \delta(\mathbf{r}-\mathbf{r}',t-t'), \quad (8.31)$$

where A is the strength of the noise. For this model it has been proposed that (Kim and Kosterlitz, 1989; Hentschel and Family, 1991)

$$\alpha = \frac{2}{d+2}, \quad (8.32)$$

$$\beta = \frac{1}{d+1}, \quad (8.33)$$

for a d -dimensional system.

Another stochastic equation was proposed by Koplik and Levine (1985)

$$\frac{\partial h}{\partial t} = \sigma \nabla_T^2 h + v_g + A \mathcal{N}(r, h), \quad (8.34)$$

a linear equation whose noise term is more complex than that of the KPZ equation. A similar equation was used by Bruinsma and Aeppli (1984) to describe the motion of the interface between the spins-up and the spins-down domains of an Ising model. For this model, the numerical work of Kessler *et al.* (1991) indicated that $\alpha(d=2) \approx 0.75$. It is now easy to see why a pinning transition occurs by considering Eq. (8.34) in zero transverse dimension

$$\frac{\partial h}{\partial t} = v_g + A \mathcal{N}(h). \quad (8.35)$$

If $v_g > A \mathcal{N}_{\max}$, where \mathcal{N}_{\max} is the maximum value of \mathcal{N} , then $\partial h / \partial t > 0$, and the interface always moves with a velocity fluctuating around v_g . If, however, $v_g < A \mathcal{N}_{\max}$, the interface will eventually arrive at a point where $v_g + A \mathcal{N} = 0$, and get pinned down. Therefore for a fixed v_g there has to be a pinning transition at some finite value of A . Indeed, Stokes *et al.* (1988) performed fluid displacement experiments in random packs of monodisperse glass beads in pyrex tubes and measured the capillary pressures at which such a pinning transition takes place. The reader is referred to Family and Vicsek (1991) for a variety of models and experiments in random media and the accompanying surface growth phenomena.

Now that we have equipped ourselves with this description of rough interfaces, let us now go back to the experiments of Rubio *et al.* (1989) and Horváth *et al.* (1991a). Rubio *et al.* (1989) found that $\alpha \approx 0.73$, significantly different from $\alpha = 1/2$, predicted by Eq. (8.32), but consistent with the result of Kessler *et al.* (1991). Horváth *et al.* (1990) reanalyzed the data at Rubio *et al.* and obtained, $\alpha \approx 0.91$, larger than all other values. Horváth *et al.* (1991a) conducted their own experiments in a Hele-Shaw-like cell, packed randomly and homogeneously with glass beads, and displaced the air in the system with glycerol-water mixture, and obtained, $\alpha \approx 0.81$, and $\beta \approx 0.65$. Although this value of α is close to that of Rubio *et al.*, as analyzed by Horváth *et al.* (1990), and although these α and β satisfy the scaling relation (8.27), they are significantly different from the predictions of Eqs. (8.32), but their α is consistent with the result of Kessler *et al.* Martys *et al.* (1991) employed the model of Cieplak and Robbins (1988) discussed above and showed that below θ_c one has, $\alpha \approx 0.81$, in perfect agreement with the result of Horváth *et al.* (1991a).

How can we explain these beautiful results? As of the time of writing this review, this question has not found a definitive answer. Several models and explanations have been introduced. For example, Zhang (1990a) proposed a

modification of the KPZ model in which the distribution of the noise amplitude is of power-law form

$$P(A) \sim A^{-(\mu_n + 1)}, \quad (8.36)$$

which is interesting, since such a distribution implies long-range correlations in the noise (similar to fBm discussed in Sec. IV). Horváth *et al.* (1991b) showed that the above experimental data can be fitted to this model if $\mu_n \approx 2.7$. Havlin *et al.* (1991) used an analogy between surface growth models and Lévy flights [i.e., random walks in which the walker takes steps whose length is distributed according to a distribution similar to (8.36)] to show that

$$\alpha = \frac{3}{\mu_n + 1}, \quad (8.37)$$

$$\beta = \frac{3}{2\mu_n - 1}, \quad (8.38)$$

so that with $\mu_n \approx 2.7$ we obtain $\alpha \approx 0.81$, in perfect agreement with the data. Equations (8.37) and (8.38) had been proposed by Zhang (1990b) and Krug (1991) as *lower bounds* to the true values of α and β . Of course, we still do not know why the noise amplitude should have a power-law distribution, or if it does, why this particular value of μ_n should fit the data. It may have to do with the geometry and the pore size distribution of the porous media used in these studies.

Another model was proposed by Tang and Leschhorn (1992) and Buldyrev *et al.* (1992). The latter authors also carried out an interesting experiment in which a paper was clipped to a ring, and was dipped into a basin filled with suspensions of ink or coffee. The fluid invaded the paper and formed a rough interface between the wet and dry regions. The roughness exponent was found to be $\alpha \approx 0.63$, completely different from the above data. Tang and Leschhorn (1992) and Buldyrev *et al.* (1992) argued that this phenomenon is related to *directed percolation*. In this process [for a review see Kinzel (1983)], the bonds of the network in a given direction are directed and diode-like, in the sense that they allow transport in only one direction; if the direction of the macroscopic potential is reversed, no global transport would take place. This induces a global anisotropy such that one needs *two* correlation lengths for characterizing the network. One is ξ_L , the longitudinal correlation length in the direction of macroscopic potential, while the other is ξ_T , in the transverse direction. The percolation thresholds p_{cd} of directed networks are much larger than those of random percolation. Near p_{cd}

$$\xi_L \sim (p - p_{cd})^{-\nu_L}, \quad (8.39)$$

$$\xi_T \sim (p - p_{cd})^{-\nu_T}. \quad (8.40)$$

One has, $\nu_L \approx 1.734$ and 1.27, and $\nu_T \approx 1.1$ and 0.735, for two and three dimensions, respectively.

Tang and Leschhorn (1992) and Buldyrev *et al.* (1992)

argued that $w(L) \sim \xi_T$ and $L \sim \xi_L$, and therefore

$$w(L) \sim L^{\nu_T/\nu_L}, \quad (8.41)$$

i.e., $\alpha = \nu_T/\nu_L \approx 0.63$ for $d=2$, which agrees with the experiments of Buldyrev *et al.* (1992), and the simulations of Tang and Leschhorn (1992). Barabási *et al.* (1992) extended these experiments to three dimensions, and obtained $\alpha \approx 0.5$. However, we should point out that the roughness of the interface in a natural porous medium such as sandstone is far more complex than whatever that has been considered in all of these experiments, and despite their elegance it remains to be seen whether these models and experiments are directly relevant to imbibition in natural porous media.

7. Finite-size effects on capillary pressure and relative permeability: Devil's staircase

Most of our theoretical discussion so far has been limited to systems that are essentially of infinite extent. If the system is of finite size, the dependence of macroscopic properties on the size L of the system can be investigated using finite-size scaling. But we have not investigated the effect of the size of a porous medium on its capillary pressure and relative permeability curves. Thompson *et al.* (1987b) measured the electrical resistance of a porous medium during mercury injection (drainage), and showed that the resistance decreases (the permeability increases) during the injection process in steps on devil's staircase (Mandelbrot, 1983), this is shown in Fig. 8. The steps were irreversible in that small hysteresis loops did not retrace the steps, and they were not reproduced on successive injections. When the number $N_{\Delta R}$ of resistance steps larger than ΔR was plotted versus ΔR , a power-law relation was found:

$$N_{\Delta R} \sim (\Delta R)^{\lambda_R}. \quad (8.42)$$

λ_R was found to vary between 0.57 and 0.81. It presumably depends on the strength of the competition between capillary and gravitational forces: $\lambda_R \approx 0.57$ signifies the limit of no gravitational forces, while $\lambda_R \approx 0.81$ presumably represents the limit in which gravitational forces are prominent. Based on the stepwise decrease of the resistance and the apparent first-order phase transition (see Fig. 8), Thompson, Katz, and Rashke (1987) concluded that mercury injection is not second order and should not be modeled by percolation, which usually represents a second-order phase transition. This was already mentioned in Sec. III.

However, simulation of this process by Katz *et al.* (1988), Roux and Wilkinson (1988), and Sahimi and Im-dakm (1988), and a related simulation of Batrouni *et al.* (1988) showed that such a stepwise decrease in the resistance can be predicted by a (random or invasion) percolation process. The reason for this stepwise decrease in the sample resistance is that, in a *finite sample*, penetration of any pore by mercury causes a *finite* change in the resis-

tance (or, in order to cause a finite change in the resistance, the capillary pressure should also change by a finite amount), but as the sample size increases, the size of the step changes decreases such that for a very large sample the steps would vanish and the resistance curves become continuous and smooth. Siddiqui and Sahimi (1993) simulated this process using invasion and random percolation models which showed clearly the effect of sample size on the resistance curve. Using a percolation model, Roux and Wilkinson (1988) showed that, for a three-dimensional porous medium of size L ,

$$N_{\Delta R} \sim L^{3(\mu-\nu)/(\mu+3\nu)} (\Delta R)^{-3\nu/(\mu+3\nu)}, \quad (8.43)$$

so that $\lambda_R = 3\nu/(\mu+3\nu) \approx 0.57$, which agrees well with the experimental result in the absence of gravity. Thus, while sample size effects are important, the stepwise decrease in the resistance of the sample during mercury injection is still consistent with a percolation description of this process discussed in Sec. III, and with that of two-phase flow discussed in this section.

8. Immiscible displacements under the influence of gravity: Gradient percolation

So far, we have neglected the effect of gravity on an immiscible displacement. However, this effect cannot be neglected for three-dimensional porous media. The hydrostatic component of pressure adds to the applied pressure, and this creates a vertical gradient in the effective injection pressure. Because of this gradient, the fraction of accessible pores decreases with the height of the system. This effect was not taken into account in the percolation models described above. However, a modification of the invasion percolation by Wilkinson (1984), and by Sapoval *et al.* (1985) and Gouyet *et al.* (1988) succeeded in taking into account such effects. But before discussing these models, let us briefly describe a few experimental studies regarding the effect of gravity.

Clément *et al.* (1987) and Hulin *et al.* (1988) used the following procedure to study gravitational effects. They injected Wood's metal, which is a low-melting point liquid alloy, into the bottom of a vertical and evacuated crushed-glass column. The experiments were carried out at low values of C_a by controlling the flow velocity v . After the front reached a given height, they stopped the injection and let the liquid solidify. The horizontal sections of the front corresponding to various heights were then analyzed, and the correlation function $C(r)$ [see Eq. (3.55)] of the metal distribution in the horizontal planes was determined to see whether a fractal structure was formed.

Another series of experiments were carried out by Birovlev *et al.* (1991) in a *two-dimensional* porous medium. They used transparent two-dimensional models consisting of a monolayer of 1-mm glass beads placed at random and sandwiched between two plates. The system was filled with a glycerol-water mixture, which was displaced by air invading the system at one end.

The competition between gravity and capillary forces is usually expressed through the Bond number Bo which is defined as

$$Bo = \frac{\Delta\rho g R^2}{\sigma_{ow}}, \quad (8.44)$$

where $\Delta\rho$ is the density difference between the two fluids, g the gravity, and R the typical size of the grain. Wilkinson (1984) showed that in an immiscible displacement under gravity, the correlation length ξ_p does not diverge (unlike random and invasion percolation which have a diverging correlation length ξ_p), but it can reach a maximum value which is given by

$$\xi_g \sim Bo^{-\nu/(1+\nu)}, \quad (8.45)$$

so that $\xi_g \sim Bo^{-0.47}$ and $\xi_g \sim Bo^{-4/7}$ in three and two dimensions, respectively. In three dimensions, there is a transition region where both phases can percolate, and the width w of this region is given by

$$w \sim Bo^{-1}. \quad (8.46)$$

Similar results were obtained by Sapoval *et al.* (1985) and Gouyet *et al.* (1988) in the context of *gradient percolation*, which is a model in which a gradient G for the occupation probability p is imposed on one direction of the network [such a model had in fact been considered earlier by Trugman (1983), who called this a *graded percolation*]. They used arguments similar to Wilkinson's to show that

$$\xi_g \sim G^{-\nu/(1+\nu)}, \quad (8.47)$$

which is completely similar to Eq. (8.45), in which Bo has been replaced with G . The three-dimensional experiments of Hulin *et al.* (1988), and the two-dimensional experiments of Birovliev *et al.* (1991) were completely consistent with these results. For example, Birovliev *et al.* (1991) obtained $\xi_g \sim Bo^{-0.57}$, where the exponent 0.57 agrees completely with the theoretical prediction, $\nu/(1+\nu)=4/7 \approx 0.57$.

Wilkinson (1984) also derived an important result regarding the effect of gravity on the residual oil saturation. He showed by a scaling argument that the difference $S_{ro} - S_{ro}^0$, where S_{ro} is the ROS for $Bo \neq 0$ and S_{ro}^0 the corresponding value when $Bo=0$, is given by

$$S_{ro} - S_{ro}^0 \sim Bo^{\lambda_B}, \quad (8.48)$$

where $\lambda_B = (1+\beta_p)/(1+\nu)$, ν and β_p being the usual percolation exponents, so that $S_{ro} - S_{ro}^0 \sim Bo^{0.74}$, for a three-dimensional porous medium. Wilkinson (1984) also proposed a simple model for simulating invasion percolation under the influence of gravity, in which a bias, linearly proportional to the height of the interface, is added to the random numbers that are assigned to the sites in the usual invasion percolation. The simulation proceeds as in the usual invasion percolation by invading those sites in the vicinity of the interface that have the smallest numbers.

9. A phase diagram for displacement processes

Lenormand (1989) studied the crossovers between three regimes of displacements, namely, capillary-controlled displacements (represented by percolation models), unstable viscous displacements (represented by DLAs and their generalizations), and stable viscous displacements (represented by anti-DLAs). If L is the linear size of a porous medium, then, the boundaries of a percolation-type displacement scales as

$$Ca \sim L^{-(\mu+\nu+1)/\nu} \quad (8.49)$$

towards the stable viscous displacements, and as

$$Ca \sim L^{-(\nu+1)/\nu} \quad (8.50)$$

towards the unstable regime. Unstable viscous displacements can occur for

$$Ca \sim L^{-1}, \quad (8.51)$$

which extends towards percolation-type displacements as L increases. Stable displacements do not depend on the size of the system. These considerations lead to the phase diagram shown in Fig. 58. Fernández *et al.* (1991) also studied the crossover from invasion percolation to a DLA-type displacement. They found that on length scales much smaller (larger) than a crossover length scale L_{co} , invasion percolation (DLA) patterns are obtained. Moreover, they argued that

$$L_{co} \sim (\delta P_c)^{2/(2+D_i)}, \quad (8.52)$$

where δP_c is a measure of the spatial variations of P_c and D_i is the interface fractal dimension on small length scales, which they found to be $D_i \approx 1.3$ in two dimensions.

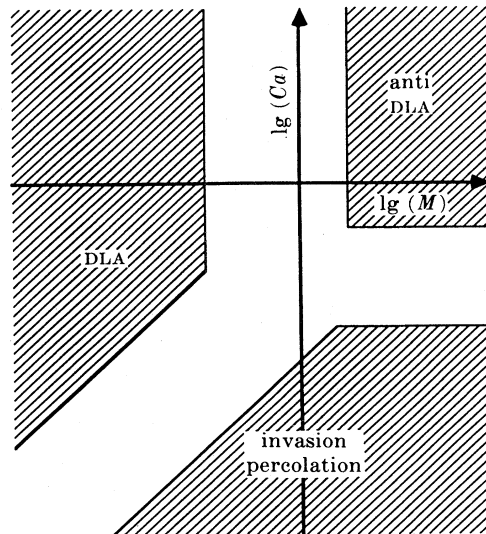


FIG. 58. Phase diagram for three types of displacement (from Lenormand, 1989).

10. Scaling laws for relative permeability and dispersion coefficients

One can derive scaling laws for capillary pressures, relative permeabilities, and dispersion coefficients near the residual saturations, to see whether the experimental data agree with such scaling laws. Wilkinson (1986) derived such scaling laws for capillary pressure and RPs, while Sahimi and Imdakm (1988) did the same for the dispersion coefficients. The main problem in deriving such scaling laws is relating the saturations S_w and S_{nw} of the wetting and nonwetting phases (and their residual values S_{rw} and S_{rnw}) to the occupation probability p and the percolation threshold of the system.

During drainage we are concerned with the point where the displacing nonwetting fluid first percolates. Since the trapping of the wetting phase is not important, S_{nw} is proportional to L^{D_p}/L^3 , if $L \ll \xi_p$. For $L \gg \xi_p$, we replace L with ξ_p , so that, $S_{nw} \sim \xi_p^{-\beta_p/\nu}$, and therefore

$$S_{nw} \sim (p - p_c)^{\beta_p}. \quad (8.53)$$

On the other hand, during imbibition we have

$$S_{nw} - S_{rnw} \sim \int_{p_c}^p X^4 dp \sim (p - p_c)^{1+\beta_p}. \quad (8.54)$$

Given these two equations, it is not difficult to derive the scaling laws for RPs and dispersion coefficients. Thus the relative permeability k_{rnw} to the nonwetting phase during drainage obeys $k_{rnw} \sim (p - p_c)^\mu$, or in view of (8.52)

$$k_{rnw} \sim (S_{nw})^{\mu/\beta_p}, \quad (8.55)$$

and during imbibition it obeys

$$k_{rnw} \sim (S_{nw} - S_{rnw})^{\mu/(1+\beta_p)}. \quad (8.56)$$

Similar results can be derived for the dispersion coefficients. Thus if near the residual saturations holdup dispersion is the dominant mechanism (see Sec. VI), then $D_L \sim (p - p_c)^{-2\nu + \mu - \beta_p}$. Therefore in drainage

$$D_L \sim (S_{nw})^{(\mu - \beta_p - 2\nu)/\beta_p}, \quad (8.57)$$

and in imbibition

$$D_L \sim (S_{nw} - S_{rnw})^{(\mu - \beta_p - 2\nu)/(1+\beta_p)}. \quad (8.58)$$

These results appear to agree with both simulations and experimental data. For example, Eqs. (8.56) and (8.57) imply that $D_L \sim S_{nw}^{-0.41}$, and $D_L \sim (S_{nw} - S_{rnw})^{-0.12}$, for drainage and imbibition, respectively. These are in agreement with experimental data of Delshad *et al.* (1985), which indicate very weak divergence of D_L near the residual saturations.

11. Comparison of invasion and random-percolation models

As we already saw, invasion percolation is a realistic model of capillary-controlled two-phase flow in porous

media. However, permeability and relative permeabilities are controlled by narrow pore throats and, moreover, the trapping of one phase by another seems to be insignificant in three dimensions. On the other hand, the random-percolation model of Heiba *et al.* (1982, 1992) provides analytical expressions for the pore-size distributions of the pores occupied by each phase during imbibition and drainage. These expressions greatly facilitate calculation of RPs, since many methods of calculating the permeability of a porous medium, discussed in Sec. V, can be used with such expressions for estimating RPs. Moreover, simulation of invasion percolation in a large three-dimensional network is costly and time consuming. Therefore, a practical question is: How do the predictions of invasion and random percolation models for RPs compare with the experimental data? Siddiqui and Sahimi (1993) compared the predictions of the two models, obtained with a simple cubic network, with the experimental data of Talash (1976) for Berea sandstones; see Fig. 59. It is clear that the predictions of the random-percolation model are at least as accurate as those of invasion percolation. We emphasize that this comparison is only for predicting the RPs, an important problem for simulation of two-phase flows. However, for other quantities of interest invasion percolation is a more realistic model than the random-percolation model.

I. Network models of immiscible displacements at finite capillary numbers

So far we have discussed capillary-controlled displacements, and in such processes viscous forces do not play any role. However, in practice, especially in oil recovery processes, it is often true that for a given displacement such as waterflooding of an oil reservoir, the capillary number Ca is relatively large so that viscous forces become important. In this section, we review and discuss network models of such processes.

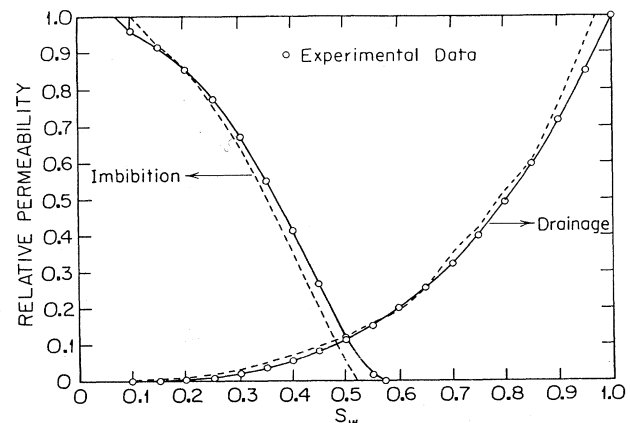


FIG. 59. Relative permeabilities as predicted by the random-percolation (solid curves) and invasion percolation (dashed curve) models. Circles represent experimental data (from Siddiqui and Sahimi, 1993).

The first of such models was apparently developed by Singhal and Somerton (1977), followed by the works of Mohanty *et al.* (1980) and Payatakes *et al.* (1980). In particular, Mohanty *et al.* (1980) used a square network of pore bodies and pore throats with distributed sizes, modelled the displacement of a nonwetting fluid by a wetting one, investigated the effect of pore body and pore throat size distributions, and simulated both low and relatively high Ca regimes.

Detailed, and to some extent quantitative, models of these phenomena were developed by Koplik and Lasseter (1984, 1985), Dias and Payatakes (1986a, 1986b), Leclerc and Neal (1988), and Lenormand *et al.* (1988). In Koplik and Lasseter's work, the pore space is modeled by a two-dimensional, but nonplanar, network of cylindrical pore throats and spherical pore bodies with distributed effective sizes. The local coordination number of the network was random. In general, the equations that have to be solved are those for the pressure field throughout the network, and those for saturations of the two phases. In a pore throat, the pressure drop ΔP is given by

$$\Delta P = -\frac{1}{g_{p1}} q_f + P_c - \frac{1}{g_{p2}} q_f , \quad (8.59)$$

where q_f is the flow rate, and g_{pi} is the single-phase flow conductance of fluid region i . The basic assumption behind equation (8.59) is that away from the interface the flow field in each fluid region is unaffected by the other fluid. Equation (8.59) gives rise to a nonlinear problem, if it is assumed that the radius of the meniscus between the two fluids, and thus the capillary pressure P_c change in some way as the meniscus passes from a pore body or pore throat into the contiguous pore throat or pore body. The nonlinear problem can be converted into a constrained linear one if one assumes that the meniscus stops at the interface during this passing period. The flow in the pore throat is, therefore, zero until the constraints are violated and the meniscus either moves forward into the pore body or back into the pore throat. If only one fluid is present in a pore body or pore throat, then P_c is of course dropped from Eq. (8.59). Using Eq. (8.59) and the fact that for each pore body one has the mass conservation law, $\sum_i q_{fi} = 0$, one obtains a set of equations for the pressure at the center of each pore body which can be solved by a number of methods. Then in a time step Δt , a meniscus m with velocity v_m moves a distance $v_m \Delta t$. This gives a new fluid distribution, and the process is repeated. Koplik and Lasseter assumed that the two fluids have the same viscosity ($M=1$), and did detailed computations to determine the rate of change of saturations from the fluid fluxes and to find out which fluids are crossing the pore-throat boundaries. As already discussed above, at relatively high Ca the viscosity ratio M is expected to have a significant effect, which Koplik and Lasseter's model did not capture. Their simulations were restricted to very small networks (10×10).

The model of Dias and Payatakes (1986a, 1986b) is, in some sense, more sophisticated than that of Koplik and

Lasseter, and at the same time it is simple enough to allow computations with larger networks. They used a square network of pores having converging-diverging segments with a sinusoidal profile. This model was first used by Payatakes *et al.* (1980) for simulating blob mobilization and dynamics, as discussed above. For single-phase flow through a pore the solution due to Tilton and Payatakes (1984) was used according to which

$$q_f = \frac{\pi c_0 d_p^3}{4\eta(-\Delta P_1)} \Delta P_{cd} , \quad (8.60)$$

where c_0 is a constant, d_p the smallest diameter of the pore (at the minimum of the sinusoidal profile), ΔP_1 a dimensionless pressure drop along the pore (which is a function of d_p) when the flow is creeping and the Reynolds number is unity, and ΔP_{cd} the pressure drop along the converging-diverging pore. For two-phase flow in the pore a lubrication approximation was used and the solution of the flow problem due to Sheffield and Metzner (1976) was used. For the capillary pressure across the interface the Washburn approximation, Eq. (3.4), was used. Various mechanisms of imbibition, similar to those discussed above, were then simulated. In their second paper, Dias and Payatakes (1986b) simulated mobilization of oil blobs using physical mechanisms that were discussed above. The calculated quantities included residual oil saturation and the distribution of the blobs. They found that ROS decreases with decreasing M , even for very small values of Ca. Moreover, for $M < 1$ ROS decreases as Ca does (if $Ca > 10^{-7}$), while for $M > 1$ ROS increases slightly with Ca in the range $10^{-7} \leq Ca \leq 5 \times 10^{-5}$, but for still higher values of Ca the ROS decreases rapidly as Ca increases. Finally, they found that a waterflood at finite values of Ca gives rise to blob populations in which most blobs occupy only one pore body, whereas as $Ca \rightarrow \infty$ larger blobs are also formed. These findings are all in qualitative agreement with the experimental data which we already discussed above.

The final model is due to Lenormand *et al.* (1988) which is completely similar to that of Leclerc and Neal (1988), that was mentioned in our discussion of miscible displacements in Sec. VII. More details of the work of Leclerc and Neal (1988) can be found in Kiriakidis *et al.* (1991). Blunt and King (1990, 1991) also used a similar model. Whereas Koplik and Lasseter as well as Dias and Payatakes replaced the actual nonlinear problem by a sequence of linear problems, Lenormand *et al.* (1988) solved the actual nonlinear problem. In their model the porous medium is represented by a network of bonds with distributed effective radii. Consider a pore between nodes i and j with radius r_{ij} for which the flow rate is given by

$$q_{ij} = \frac{\pi r_{ij}^4}{8l\eta_{ij}} (P_i - P_j - P_{cij})^+ , \quad (8.61)$$

where l is the length of the pore, P_i and P_j the pressures at i and j , and P_{cij} the capillary pressure in the pore. The mixture viscosity η_{ij} was taken to be η_{ij}

$=0.5[\eta_2(\alpha_i + \alpha_j) + \eta_1(2 - \alpha_i - \alpha_j)]$, where α_i is the fraction of the pore occupied by the fluid i . In Eq. (8.61) $+$ means that $q_{ij} = 0$ as long as $P_i - P_j < P_{cij}$. Because of this constraint, Eq. (8.60) is actually a nonlinear relation between the flow rate, and the nodal and capillary pressures. Because the actual nonlinear equations are solved, one can use any value of the capillary number Ca and mobility ratio M . Figure 60 shows the displacement patterns obtained with various values of Ca and M (in the figure C denotes the capillary number). Only the displacement of the wetting phase by a nonwetting phase was considered. Thus very low values of Ca correspond to invasion percolation, while very large values of Ca represent miscible displacements. These results are also in excellent agreement with the experiments of Lenormand *et al.* (1983) in two-dimensional etched networks. Lenormand *et al.* (1988) were also able to use relatively large networks (100×100) which is a distinct advantage over the methods Koplik and Lasseter, and Dias and Payatakes.

J. Stability of immiscible displacements in porous media

We now discuss the stability of immiscible displacements. But we first provide a qualitative discussion of the subject, and then follow it up with a more quantitative analysis.

Many years ago, van Meurs (1957) used displacing and displaced fluids of the same refraction index and studied immiscible displacements in porous media. Chouke *et al.* (1959), Perkins and Johnston (1969), White *et al.*

(1976), Peters and Flock (1981), Paterson *et al.* (1982, 1984a, 1984b), Måløy *et al.* (1985, 1987), Stokes *et al.* (1986), and Frette *et al.* (1990) provided more experimental results and insight. From these observations it appears that immiscible fingering can take place over many length scales, up to a macroscopic one, and therefore one may even use a characteristic length scale for characterizing what is seen. The main implications of most of these experimental works were discussed extensively by Homsy (1987), and can be summarized as follows. (i) If the invading fluid wets the porous medium, fingering can be characterized by some macroscopic length scale, such as the width of the fingers, whereas if it does not, fingering is limited to pore scales, in which case shielding dominates spreading (see Sec. VII) (recall that a displacement with a wetting fluid is compact). The characteristic macroscopic length scale decreases as Ca increases. These were confirmed by the careful experiments of Stokes *et al.* (1986), who also showed that when macroscopic fingering takes place, the width of the finger w scales with the permeability and Ca as $w/k^{1/2} \sim Ca^{-1/2}$. (ii) If the invading fluid is nonwetting, then one obtains fingers that form a percolation cluster. This was already discussed above. (iii) Finally, there is a transition zone just behind the interface where both phases are flowing. We should mention that Måløy *et al.* (1985, 1987) and Oxaal (1991) claimed that their viscous fingering patterns obtained with immiscible fluids are similar to diffusion-limited aggregation clusters which, as discussed in Sec. VII, are strictly applicable to miscible fluids in the limit $M = \infty$. Therefore it is not clear at all why there should be any similarities between the two phenomena.

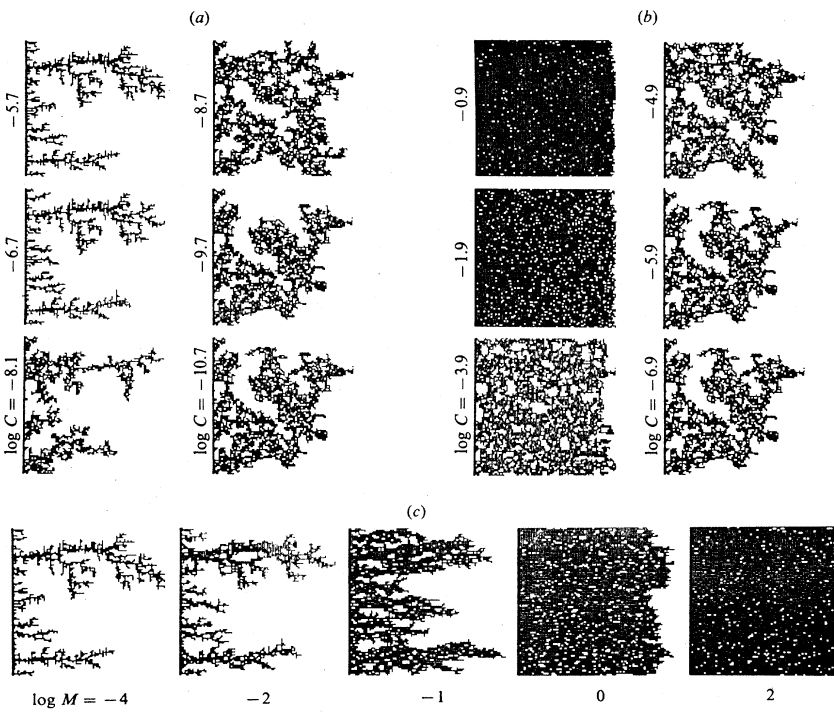


FIG. 60. Displacement patterns for different values of capillary number C and mobility ratio M (from Lenormand *et al.*, 1988).

Chouke *et al.* (1959) were the first to attempt a theoretical analysis of stability of two-phase flows in a porous medium. They ignored the transition zone and assumed that one fluid completely displaces another fluid. As the boundary condition at the interface they used Eq. (7.32), but replaced the microscopic surface tension by an *effective* surface tension for the *macroscopic* system. Although there is no theoretical justification for doing this, it does provide a reasonable description of some experimental works. Other authors (Outmans, 1962; Rachford, 1964; Hagoort, 1974; Peters and Flock, 1981; Huang *et al.*, 1984; Jerauld, Davis, and Scriven, 1984; Jerauld, Nitsche *et al.*, 1984; King *et al.*, 1984; Yortsos and Huang, 1986; Chikhliwala and Yortsos, 1988; Chikhliwala *et al.*, 1988; Yortsos and Hickernell, 1989) analyzed stability of immiscible displacements. Yortsos (1990) has given a detailed discussion of such analyses, a summary of which is as follows.

We consider the results that are obtained from displacements at a constant velocity v of a nonwetting fluid by the injection of a wetting fluid. The system is initially at a uniform saturation S_{iw} . Unidirectional flow is described by the equation

$$\phi \frac{\partial S_w}{\partial t} + v \frac{\partial f_w}{\partial S_w} \frac{\partial S_w}{\partial x} = - \frac{\partial}{\partial x} \left[f_w \frac{kk_{rw}}{\eta_w} \frac{dP_c}{dS_w} \frac{\partial S_w}{\partial x} \right], \quad (8.62)$$

with the initial and boundary conditions

$$S_w = S_{iw}, \quad t = 0, \quad (8.63)$$

$$S_w \rightarrow S_{iw}, \quad \text{as } x \rightarrow \infty, \quad (8.64)$$

$$f_w \left[1 + \frac{kk_{rw}}{v\eta_{rw}} \frac{dP_c}{dS_w} \frac{\partial S_w}{\partial x} \right] = f_0, \quad x = 0, \quad (8.65)$$

where f_w is the fractional flow of the wetting phase (i.e., the ratio of its flux and the total flux). If f_w has an upward convex segment, which is usually the case during imbibition, or during drainage of not strongly wetting phases, then the base state can be taken as the travelling steady-state solution of Eq. (8.62). Various upstream conditions, denoted by $-\infty$, are graphically shown in Fig. 61. We use dimensionless notations to simplify the discussion. A reduced saturation

$$S_{rd} = \frac{S_w - S_w^\infty}{S_w^{-\infty} - S_w^\infty} \quad (8.66)$$

and normalized mobilities (see Sec. VII),

$$\lambda_w(S_{rd}) = \frac{k_{rw}}{k_{rw}^{-\infty}}, \quad (8.67)$$

$$\lambda_{nw}(S_{rd}) = \frac{k_{rw}}{k_{rw}^{-\infty}}, \quad (8.68)$$

$$M = \frac{k_{rw}^{-\infty}}{k_{rw}} \frac{\eta_{nw}}{\eta_w}, \quad (8.69)$$

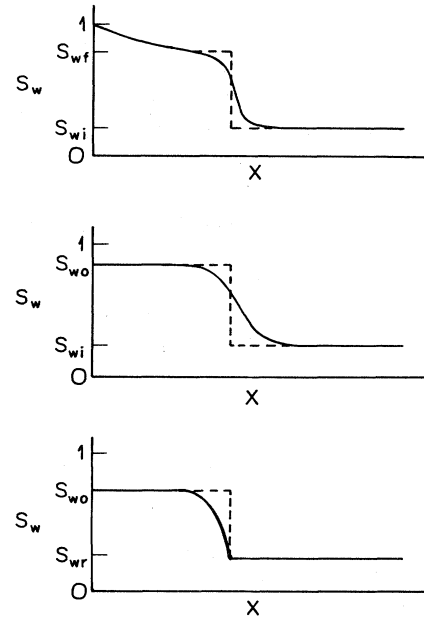


FIG. 61. Various upstream conditions for wetting-phase saturation S_w vs the axial distance X , used in the stability analysis of immiscible flows (from Yortsos, 1990).

$$\lambda_t = M\lambda_w + \lambda_{nw}, \quad (8.70)$$

$$\lambda_c = \left[\frac{k}{\phi} \right]^{1/2} \frac{1}{\sigma_{ow} \cos \theta} \frac{dP_c}{dS_w} < 0, \quad (8.71)$$

are used. Moreover, length scales will be measured by $L = (k/\phi)^{1/2}(S_w^{-\infty} - S_w^\infty)k_{rw}^{-\infty}/Ca$, which is the length over which the viscous and capillary forces are balanced. In this new notation we have

$$\lambda_{nw}\lambda_w\lambda_c \frac{dS_{rd}}{d\xi} = \lambda_t(fS_{rd} + f_w^\infty) - M\lambda_w, \quad (8.72)$$

$$\lambda_{nw} \frac{dP_c}{d\xi} = fS_{rd} + f_w^\infty - 1, \quad (8.73)$$

where $f = f_w^{-\infty} - f_w^\infty$, and $\xi = x/L$. We note that if $k_{rw}(S_w = S_{iw}) > 0$, i.e., if the saturation is mobile, then the downstream decay of the base state is exponential. In the opposite case we have

$$\frac{dS_{rd}}{d\xi} \sim -S_{rd}^{-m}, \quad (8.74)$$

where $0 < m < 1$ for secondary displacements, and $m > 1$ for primary displacements. Equation (8.74) is a manifestation of hypodiffusion discussed above.

To examine the stability of the system, the above equations are written in a moving coordinate and the stability of the resulting equations are studied using the general method discussed in Sec. VII. The following results are obtained.

(i) The rate of growth ω is bounded from above for all wave numbers α by the expression

$$\omega < -A_1\alpha^2 + A_2 A_3 \alpha, \quad (8.75)$$

where $A_1 = \min(-\lambda_{nw}\lambda_w\lambda_c/\lambda_t) > 0$, $A_2 = \max(df_w/dS_{rd}) > 0$, and $A_3 = \lambda_t(1)/\lambda_t(0) - 1 > 0$, where 1 and 0 correspond to upstream and downstream values of S_{rd} , respectively [see Eq. (8.66)]. Therefore, ω lies below the parabola on the right side of (8.75) and a cutoff wave number $\alpha_{co} \leq A_2 A_3 / A_1$, while the maximum growth rate ω_m does not exceed $(A_1 A_3)^2 / (4 A_1)$. These general results confirm what is expected, that long-wave instability is driven by mobility contrast (A_3), while short-wave stabilization is a result of capillarity (A_1).

(ii) One can develop large wavelength asymptotics, $\omega = \omega_1 \alpha + \omega_2 \alpha^2 + \dots$, where

$$\omega_1 = f \frac{\lambda_t(1) - \lambda_t(0)}{\lambda_t(1) + \lambda_t(0)}, \quad (8.76)$$

which is a generalization of the Saffman-Taylor condition, $\omega = \alpha(M-1)/(M+1)$, for Hele-Shaw cells. ω_2 is not zero but varies according to the upstream decay of the base state. For example, if the upstream decay is algebraic [see Fig. 61(a)], then one has $\omega = \omega_1 \alpha + \omega_2^* \alpha^2 \ln \alpha + \omega_3 \alpha^2 + \dots$, where

$$\omega_2^* = \frac{4\lambda_t(0)d\lambda_t/dS_{rd}|_{S_{rd}=1}}{k[\lambda_t(0) + \lambda_t(1)]}, \quad (8.77)$$

where k is a measure of the algebraic decay. Since $d\lambda_t/dS_{rd}|_{S_{rd}=1}$ is positive for unstable displacements, its existence indicates a stabilizing effect. Interestingly, this is due to mobility effects alone which adds to the process stability. Chikhliwala and Yortsos (1988) obtained the numerical solutions of the above equations to demonstrate the adequacy of the above expansions.

The geometries of the interface and the medium can have an important effect. For miscible displacements Tan and Homsy (1987) suggested an algebraic (rather than exponential) dependence for the time evolution of the disturbances. This suggestion was applied by Yortsos (1987b) to immiscible fluids in radial displacements. In this case, the base state profiles are sole functions of the similarity variable $\eta_s = r^2/t$. Perturbations are then sought in the following forms

$$S_{rd} = \bar{S}(\eta_s) + t^\delta s(\eta_s) e^{i\alpha\theta_a}, \quad (8.78)$$

$$P = \bar{P}(\eta_s) + t^\delta p(\eta_s) e^{i\alpha\theta_a}, \quad (8.79)$$

where \bar{P} and P are dimensionless capillary pressures, and θ_a is the azimuthal angle. If $\delta > 0$, then the interface is unstable. At low values of α one has the asymptotic expansion

$$\delta = -1 + \delta_1 \alpha + \delta_2 \alpha^2 + \dots \quad (8.80)$$

where δ_1 is equivalent to the Saffman-Taylor term, i.e., $\omega = \alpha(M-1)/(M+1)$, and δ_2 is inversely proportional to a capillary number Ca_m . Large Ca_m leads to instability, but if Ca_m is not too large, even $M > 1$ may not lead to instability. For $Ca_m < Ca_c$ the displacement is stable, where Ca_c is a critical value of Ca_m given by

$Ca_c = 2f/\omega_m$, and ω_m is a parameter independent of Ca . Finally, it should be pointed out that, as Yortsos (1987a) showed, immiscible displacements are equivalent to miscible displacements with equilibrium adsorption. This analogy relates (S, f_w) to the flowing and adsorbed concentrations (C_f, C_{ad}) .

K. Two-phase flow in heterogeneous and stratified rock; continuum models and large-scale averaging

So far, our discussion of two-phase flows has been restricted to macroscopically homogeneous porous media. Most reservoirs are, however, stratified and heterogeneous (see Sec. VI). Similar to every phenomenon discussed so far, two-phase flows in heterogeneous rocks have also been studied both experimentally and by numerical simulations. Let us first describe a few key experimental papers, and then review the theoretical studies.

Ogandzjanjanc (1960) was perhaps the first to study experimentally flow in a stratified porous medium. He used an unconsolidated porous medium and showed that there is significant crossflow between the strata. He observed that, initially the flow velocity is higher in the more permeable layer, and that flow in each layer was similar to a single-phase flow system. However, because of the crossflow the distance between the interfaces in the two layers stabilizes. Since this early work, there have been several other experimental studies, including those of Novosad *et al.* (1984), Sorbie *et al.* (1987), Ahmed *et al.* (1988), and Bertin *et al.* (1990). Bertin *et al.* (1990) studied waterflooding in a system of two strata, where one stratum was made of Aerolith-10, an artificial sintered porous medium, and the other was Berea sandstone. The two strata had the same thickness. The results indicated the strong effect of heterogeneities within each stratum and the contrast between them on the performance of the waterflood and the volume fraction of the recovered oil. Bertin *et al.* (1990) found that even small scale heterogeneities within the sandstone layer could strongly affect the waterflood process.

Most of the theoretical studies of two-phase flow in stratified porous media have two goals. The first is to examine the crossflow between the strata, its significance, and its variations with time as the displacement proceeds. The second goal is to determine its properties and those of the displacement process. For example, Douglass *et al.* (1959) studied imbibition in a layered system and used an averaged form of Darcy's law to describe the two-phase flow problem. Goddin *et al.* (1966) studied waterflood processes in stratified media and concluded that crossflows can be caused by both capillary and viscous forces, while Yokoyama and Lake (1981) undertook an extensive study of the effect of capillary forces on crossflows. Kyte and Berry (1975) used large scale numerical simulation to study immiscible displacements in stratified media, while Coats *et al.* (1971) used a hydrostatic distribution of various fluid phases in the vertical

direction to obtain large scale capillary pressure and relative permeability curves for their stratified medium. With this introduction, let us now describe two-phase flow in stratified and heterogeneous porous media more quantitatively.

Perhaps the simplest heterogeneous system to consider is a stratified medium of several layers with no crossflow between them. Each stratum is characterized by an effective permeability. Dykstra and Parsons (1950) considered two-phase flow in such a medium and, assuming that flow in each stratum was pistonlike (constant velocity), they derived an expression for the amount of recovered oil just at the breakthrough point, i.e., at the point where the interface in one of the strata reaches the outlet of the system. Reznik *et al.* (1984) generalized this model and derived expressions that can be used for calculating the amount of oil recovered at any stage of the process, and the RPs at that stage. If we do calculate these, we find that the shape of the resulting RP curves are not similar to those of macroscopically homogeneous media discussed above.

The literature on two-phase flow in stratified media with communicating layers is relatively extensive. Starting with Goddin *et al.* (1966), many authors (Coats *et al.*, 1967, 1971; Martin, 1968; Hearn, 1971; Jacks *et al.*, 1973; Kyte and Berry, 1975; Killough and Foster, 1979; Yokoyama and Lake, 1981; Kortekaas, 1983; Wright and Dawe, 1983; Ypma, 1983; Bertin *et al.*, 1990) have studied two-phase flows in stratified media using numerical simulations. To give the reader some idea about how such calculations are carried out, we consider a two-dimensional system with only two layers. Suppose that the two fluids are water and oil, and that the fluids and the rock are incompressible. If we write a material balance for the water phase, we obtain

$$\frac{\partial}{\partial x} \left[\frac{k_{xw}}{\eta_w} \left(\frac{\partial P_0}{\partial x} - \frac{\partial P_c}{\partial x} \right) \right] + \frac{\partial}{\partial y} \left[\frac{k_{yw}}{\eta_w} \left(\frac{\partial P_0}{\partial y} - \frac{\partial P_c}{\partial y} \right) \right] = \phi \frac{\partial S_w}{\partial t}, \quad (8.81)$$

where P_0 is the pressure in the oil phase, and k_{xw} , k_{yw} are the water phase permeabilities in the x and y directions, respectively (recall that a stratified medium is anisotropic). If functional forms for k_{xw} , k_{yw} and P_c are assumed, then Eq. (8.81) can be solved numerically for various boundary conditions at the interface between the two layers, and injection conditions. If the layers are homogeneous, then the results of the previous sections can be used for k_{xw} , k_{yw} , and P_c within each layer. The crossflows between various layers can be of various natures. One may have systems with only viscous crossflows, or with viscous and capillary crossflows, etc. If we rewrite Eq. (8.81) in a dimensionless form, then *direction-dependent* capillary numbers appear. The two capillary numbers Ca_x and Ca_y would be related to one another by

$$Ca_y = Ca_x R_L^2, \quad (8.82)$$

$$R_L^2 = \left(\frac{L}{H} \right)^2 \left(\frac{k_{yref}}{k_{xref}} \right)^{1/2}, \quad (8.83)$$

where L and H are the length and thickness of the medium, and k_{xref} and k_{yref} are the permeabilities to a reference phase (which can be taken to be either oil or water). In effect R_L is some kind of aspect ratio which has been corrected by the permeability anisotropy.

Normally, the results of such simulations are averaged over the vertical direction. If this is done, then one ends up with quantities that are referred to as *pseudofunctions* in the petroleum engineering literature. For example, one can use pseudofunctions for RPs and another pseudofunction for the capillary pressure. These pseudofunctions are in fact nothing but what Quintard and Whitaker (1988) refer to as *large-scale* RPs and capillary pressure, i.e., RPs and capillary pressure for a heterogeneous porous medium (which, in general, may or may not be anisotropic or stratified). Of course, from a scientific point of view, *large-scale functions* are much more appealing than pseudofunctions, since as Quintard and Whitaker (1988) pointed out, the prefix *pseudo* suggests that these functions are something less than what they purport to be, whereas an analysis such as that of Quintard and Whitaker (see below) shows that such functions can be deduced from a rigorous analysis for *any* heterogeneous medium.

Quintard and Whitaker (1988) developed a large-scale averaging technique for two-phase flow in heterogeneous rock. Starting from Eqs. (8.16)–(8.19) as the *locally averaged* equations, they developed large-scale averaged continuity and momentum equations for each fluid phase. In their equations, they allowed for the possibility that a portion of a fluid phase may be trapped by another phase (see our discussion of trapping phenomenon given above). The technique they used is along the same lines as those mentioned for dispersion in heterogeneous media in Sec. VI. In order to make the theory tractable, they assumed that the system is in local mechanical equilibrium, which means that the *local* fluid distribution is determined by capillary pressure-saturation relations, and is not limited by the solution of an evolutionary transport equation. In two later papers, the authors studied the effect of large scale spatial and temporal gradients (Quintard and Whitaker, 1990a), and investigated two-phase flow in a heterogeneous and stratified medium under quasistatic and dynamic conditions (Quintard and Whitaker, 1990b), using the theory developed in Quintard and Whitaker (1988). Quasistatic condition in the present context means that, the local capillary pressure, everywhere in the averaging volume, is set equal to the large-scale P_c evaluated at the centroid of the averaging volume, and that the large-scale P_c is given by the difference between the large-scale pressures in the two fluid phases. As such, the large-scale P_c is assumed to be independent of such complex factors as transient, gravitational and flow effects. If there is significant departure from the quasistatic conditions, then one is in the dynamic regime.

They found that even at relatively low flow rates, dynamic effects may be important. Bertin *et al.* (1990) used this theory and compared its predictions with their experimental data, and found only qualitative agreement.

L. Two-phase flow in fractured rocks

Although two-phase flow in fractured rocks is important to enhanced oil and gas recovery, isolation of radioactive waste, exploitation of geothermal fields for generating energy, and recovery of coal-bed methane, very little is known about the laws governing such flows. The conventional approach has been based on the assumption that Darcy's law is applicable to both fluid phases, and that the cross terms of Eqs. (8.16) and (8.18) can be neglected. Moreover, it is usually assumed that the RP to each phase is equal to its saturation. This assumption is supported to some extent by the experimental work of Romm (1966), in which oil and water were confined to different regions of a *smooth* fracture by controlling the wettability of the fracture surface. Pruess *et al.* (1983) analyzed some field data from geothermal reservoirs and provided further support for this work. However, theoretical analysis of Pruess and Tsang (1990) for *rough* fractures, and computer simulations of Mukhopadhyay and Sahimi (1992), who used a network of interconnected discrete fractures to study two-phase flow and heat transfer in a geothermal field, indicated that this assumption may be in serious error. In the petroleum engineering literature, the double-porosity model that was discussed in Sec. IV has been used for simulating two-phase flows in rocks with fractures and pores. This field of research remains largely undeveloped.

IX. ADVANCES IN COMPUTATIONAL METHODS

Simulation of multiphase, multicomponent flows in natural porous media, often called *reservoir simulation* in the petroleum industry, requires enormous amounts of supercomputer time. Even the three-dimensional percolation and network models described in Sec. VIII, which are relatively simple models of the actual phenomena, need a large amount of computer time. In fact, as already discussed, some of such models have not even been studied in three dimensions. The reservoir simulators that are normally used in the petroleum industry are usually one of two types. The first type are the so-called *black oil* simulators, in which it is assumed that the fluids (usually oil, gas, and water) are homogeneous. It is also assumed that gas can dissolve in the oil, or vice versa, in any proportion. This avoids the problem of computing the detailed phase diagrams of the system, which requires accurate equations of state. The second type of simulator is more complex; they are usually called *compositional simulators*. Such simulators represent the oil as a mixture of several hydrocarbons and perform detailed phase equilibria calculations in order to determine the distribution of components between the liquid and vapor phases in the reservoir.

In most reservoir simulators the preferred numerical method is a finite-difference approximation to the transport equations. The reservoir is divided into blocks, and the fluid flow is computed between the blocks. A five-point (in two dimensions) or seven-point (in three dimensions) finite-difference approximation is normally used. This has both advantages and disadvantages. The main advantage of using a finite-difference method is that it is straightforward to set up the discretized transport equations that are to be solved. The main disadvantage is that the method may not be accurate enough, especially if large blocks are used, and may lead to *numerical dispersion*, which can mimic *physical dispersion* discussed in Sec. VI. While this can be advantageous, if physical dispersion is actually present, it can also be a disadvantage, in the sense of producing solutions that do not actually mimic the true situation.

In any event, once the equations are set up, they are usually solved by iterative methods. Nonlinear equations are also linearized and solved using the Newton-Raphson method. Direct methods such as Gaussian elimination are *never* used (although, in principle, they are much more accurate than iterative methods), simply because the number of equations is so large that no computer memory can fit the enormous matrix of the coefficients, even though these matrices are usually sparse and banded. Solving these equations by iterative methods means that there has to be a tradeoff between the desired accuracy of the solution and the computer time that one has to consume in order to achieve that accuracy. Another problem with finite-difference methods is that they are not suitable for systems that have complex boundaries, unless the discretization is very refined there. But a very refined discretization also implies a much larger number of equations to be solved. Various finite-element methods are better suited for such computations, but the matrix of coefficients in finite-element methods is usually full and dense, not sparse and banded as in finite-difference methods.

For these reasons, devising efficient numerical methods for solving the transport equations has always been an active area of research. We do not intend to review the literature on the subject here, since it is very large and deserves a separate review paper by itself. The interested reader can consult Cheshire and Pollard (1988) and Christie (1988) for an updated review of the subject. However, we would like to discuss a new method of simulating flow in porous media based on cellular automata (CA), or lattice gases (LG), which we believe can dramatically change the way people think about simulation of flow in porous media and reservoir simulation. What follows is a review of the basic ideas about cellular automata and the recent advances that have been made.

A. Cellular automaton and lattice-gas simulation of fluid flow

Cellular automata (see Wolfram, 1986a; Doolen, 1991; Boon, 1992; for collections of reviews) are large lattices in

which each site can be in one of several discrete states. The state of each site at the next time step is determined completely by the present state of the neighboring sites. Thus both time and space are discrete, and connections are between neighbors only, ideal conditions for high-speed simulations on vector or parallel computers like a Cray. The CA approximation of the Navier-Stokes equation in two dimensions is based on particles of unit mass either resting on the site of a lattice or moving with unit velocity on one of the six bonds emanating from each lattice site. Frisch *et al.* (1986, 1987), using a model developed by Hardy *et al.* (1973, 1976), showed that in order that the discrete equations reduce to the usual Navier-Stokes equations, two-dimensional simulations have to be done on a triangular lattice.

Up to six particles may reside at any site on the triangular lattice. Figure 62 shows how the particles move on this lattice. If particles hit each other, they are scattered according to the laws of momentum conservation. For example, one particle hitting another one that is at rest may be scattered such that its direction changes by 60° , and that the previously resting particle moves in a direction inclined at -60° with respect to the direction of the incoming particle. Usually up to four particle collisions are employed (5 and 6 particle collisions almost never happen). If a particle hits a solid wall, it is reflected by 180° to simulate the no-slip boundary condition. The extension to three dimensions is more complex, since no regular three-dimensional lattice is isotropic, and thus in the continuum limit one has spurious terms, in addition to those in the Navier-Stokes equation, which are caused by the anisotropy of the lattice. However, there are now several methods of circumventing this difficulty. For example, one can use a three-dimensional topologically random lattice, such as the Voronoi lattice, which is macroscopically isotropic (Sahimi, 1989, unpublished). Alternatively, one can use (d'Humières *et al.*, 1986) a *four-dimensional* face-centered-hypercubic (FCHC) lattice. For this lattice, which has a coordination number of 24, all pairwise symmetric fourth-order tensors are isotropic, and therefore one can simulate the

Navier-Stokes equation on such a lattice. We may then make the observation that any solution of the four-dimensional equation that does not depend on the fourth dimension is a solution of the three-dimensional equation. This suggests the use of an FCHC lattice that wraps around periodically in the fourth direction. One actually uses a lattice that is only one lattice unit long in the fourth dimension and therefore has an effectively three-dimensional structure. The disadvantage of this method is that, although the fourth dimension is very thin, the discrete velocities still have components in *all* directions; therefore the model is bit intensive (24 or 25 bits per site as compared with 6 in two dimensions). A third approach (d'Humières *et al.*, 1986) is to use a three-dimensional cubic lattice in which the particles move with speeds zero, one, and $\sqrt{2}$ (instead of one and zero in two dimensions). This model uses only 19 bits per site. Despite the discrete nature of cellular automata in both two and three dimensions, these models are capable of exhibiting rich macroscopic complexity such as turbulence (d'Humières and Lallemand, 1986).

B. Cellular automata and lattice-gas simulation of single-phase flow in porous media

In order to simulate flow through porous media with the CA method, one distributes obstacles randomly or in a prescribed fashion in a two- or three-dimensional lattice. For example, Rothman (1988) used rectangular obstacles or a variation of them in his two-dimensional simulations, while Brosa and Stauffer (1989, 1991), Duarte and Brosa (1990), Kohring (1991a, 1991b, 1991c), and Sahimi and Stauffer (1991) used circular and overlapping or non-overlapping obstacles. One main advantage of using cellular automata is that any configuration of the pore space can be used. Thus even the exact digital image of a natural porous medium can be used in the CA simulations.

Once the desired pore-space configuration is generated, the simulation can be started. At the beginning of the simulation, one constructs a transition table that tells how one of the present states (determined by the velocity of the incoming particles) is transformed into the next state, determined by the outgoing velocities. The table contains all of the possible states (for example, in two dimensions, 2^8). One then starts the simulation using the two-, three- and four-body collisions at a site which conserve momentum and energy. The rules are such that no new particle is created, and in one time step all particles on the lattice first move to different lattice sites and then undergo transitions at the new sites. One iteration in the simulation consists of updating all lattice sites according to the transition table. The number of required iterations for reaching a steady-state solution depends on the porosity of the medium. If the system is far from the percolation threshold, about 10^3 iterations suffice. However, near the percolation threshold many more iterations may be required.

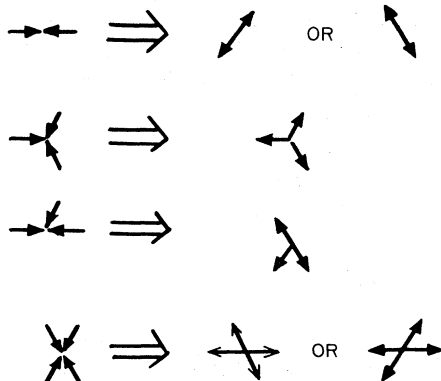


FIG. 62. Collision rules for particle movement on a triangular lattice during cellular automata simulations of fluid flow.

An issue of particular importance is the mean free path of the particles and its relation to the size of the obstacles. As Rothman (1988) showed, in order for the CA simulation results to approach the continuum limit, the mean size of the void area in the lattice must be at least twice the mean free path of the particles, which is about 9 lattice bonds. If this condition is not obeyed in the simulations, the result may not represent a macroscopic continuum. Thus simulations such as those of Balasubramanian *et al.* (1987), in which a fraction of the sites are blocked at random in order to create random obstacles, may not correspond to true flow in an actual porous medium, because their simulations do not obey the constraint imposed by the mean free path of the particles.

The cellular automata model that we have described has been used by various authors to investigate flow phenomena in porous media. Rothman (1988) used it to study single-phase flow in porous media. Succi *et al.* (1989) studied the same problem in three dimensions. Duarte *et al.* (1992) and Knackstedt *et al.* (1993) used the CA method to study the dynamic permeability of a porous medium. Brosa and Stauffer (1989, 1991), Kohring (1991a, 1991b, 1991c), and Sahimi and Stauffer (1991) looked at flow in two-dimensional porous media with various obstacle shapes and arrangements (random versus regular and periodic) and paid particular attention to the efficiency of the simulation. For example, Kohring (1991a) achieved a speed of 233 million site updates per second (233 MUPS) on a single processor of the Cray Y-MP/832, and 1690 MUPS when running multiprocessor batch mode. This is the fastest algorithm currently available. Vollman and Duarte (1992) studied flow through a porous membrane and investigated the effect of various boundary conditions. Many other hydrodynamical problems in nonporous systems have been treated with this method; see Wolfram (1986b), Kadanoff *et al.* (1989), Zanetti (1989), Doolen (1991), and Boon (1992).

Let us emphasize once again that, in order for a CA or LG model to represent a physical phenomenon, the lattice used in the simulation must have sufficient symmetry; mass, momentum, and energy must be conserved; and local equilibrium must exist and depend only upon the conserved quantities. However, CA and LG models are not yet free of drawbacks. For example, they suffer from statistical noise. This results in some physical phenomena that lead, among other things, to the divergence of viscosity in two dimensions. Moreover, they have a velocity-dependent pressure and are not usually Galilean invariant. Various schemes have been proposed to circumvent these difficulties (McNamara and Zanetti, 1988; Higuera *et al.*, 1989; Qian *et al.*, 1992). In particular, Qian *et al.* (1992) proposed a relaxation method such that, if n_i is the density of particle i and \mathbf{v}_i is its velocity, then

$$n_i(t+1, \mathbf{x} + \mathbf{v}_i) = (1 - \omega_r) n_i(t, \mathbf{x}) + \omega_r n_{ip}(t, \mathbf{x}), \quad (9.1)$$

where ω_r is a relaxation parameter and n_{ip} is the predict-

ed value of n_i at time t , given by

$$n_{ip}(t, \mathbf{x}) = e_p \rho \left[1 + \frac{\mathbf{v}_{i\alpha} \mathbf{v}_\alpha}{v_s^2} + \frac{\mathbf{v}_\alpha \mathbf{v}_\beta}{2v_s^2} \left(\frac{\mathbf{v}_{i\alpha} \mathbf{v}_{i\beta}}{v_s^2} - \delta_{\alpha\beta} \right) \right], \quad (9.2)$$

where α and β denote Cartesian coordinates (with implied summation for repeated indices), v_s is the speed of sound, \mathbf{v}_α is the fluid velocity in the α direction, the index p is the square modulus of the particle's velocity, and e_p is the corresponding equilibrium distribution for $\mathbf{v}=0$. The e_p 's are calculated so that the fourth-order velocity tensor is isotropic and the system is Galilean invariant. It can then be shown that the pressure is also independent of velocity.

C. Cellular automaton and lattice-gas simulation of two-phase flow in porous media

Rothman and Keller (1988), Rothman and Zaleski (1989), Somers and Rem (1989, 1991), and S. Chen *et al.* (Chen, Diemer *et al.*, 1991; Chen, Doolen, *et al.*, 1991; Chen, Doolen, and Matthaus, 1991) generalized the model to study the flow of two immiscible fluids in two-dimensional porous media. Rem and Somers (1989) also studied the same problem in three dimensions. Let us consider the method of Rothman and co-workers on a triangular lattice. We follow the description given by Rothman (1990). Two types of particles, say red and blue, reside on the lattice. The velocities at a given site are numbered from 0 to 6 with $v_0=0$ and $v_{j+1}=[\cos(2\pi j/6), \sin(2\pi j/6)]$. Two Boolean variables $r_i(\mathbf{x})$ and $b_i(\mathbf{x})$ are introduced that indicate the presence or absence of a red or blue particle with velocity v_i at lattice site \mathbf{x} . The system evolves in two steps. In the first step particles are propagated to the nearest-neighbor sites, where they may collide with other particles. The number of both red and blue particles is conserved. To simulate the surface tension between the two fluids, the configuration resulting from a collision depends on the configuration at the nearest-neighbor sites on the lattice. Those collisions which carry red particles in the direction where the neighbors contain a relative majority of red particles are favored, and likewise for blue particles.

Two vectors are now introduced. The first one is the *color flux*, given by

$$\mathbf{q} = \sum_i \mathbf{v}_i [r_i(\mathbf{x}) - b_i(\mathbf{x})], \quad (9.3)$$

while the second is the *color field*, defined by

$$\mathbf{f} = \sum_i \mathbf{v}_i \sum_j [r_j(\mathbf{x} + \mathbf{v}_i) - b_j(\mathbf{x} + \mathbf{v}_i)]. \quad (9.4)$$

The particle configuration that results from a collision is that configuration which maximizes $\mathbf{f} \cdot \mathbf{q}$, such that the number of red and blue particles, as well as the total number of particles, is conserved. This rule ensures that the fluxes of the red and blue particles in the direction of

their respective mass gradient is maximized. Rothman and Keller (1988) showed that Darcy's law is valid within the regions of the red and blue particles and that, when the particles are at rest, the pressure drop across the interface between the red and blue regions obeys the Young-Laplace equation, Eq. (8.6). To simulate the effect of wettability, the sites of the lattice that belong to the solid matrix and are at the interface between the solid and the fluid are colored red or blue, so that the vector \mathbf{f} calculated in the vicinity would be biased to point in the direction of the solid site. Thus red (blue) particles would preferentially spread on the red (blue) solid sites. If the "density" of coloring on the solid sites is varied, then various regimes of wettability discussed in Sec. VIII can be simulated. Chen *et al.* used somewhat different rules for simulating two-phase flows, which they claimed to be more realistic and also more efficient.

Rothman (1990) used this method to study flow in a two-dimensional model similar to the etched network of Lenormand *et al.* (1983). Good agreement between his simulations and Lenormand *et al.*'s data was found. We should mention that Appert and Zaleski (1990) proposed a CA model for the liquid-vapor phase transition of the same fluid species. Thus their model may be used to simulate two-phase flow of liquids and vapors in a porous medium, an important problem in thermal oil recovery processes. Gunstensen and Rothman (1991) extended the model further and developed a model for three-phase fluid flow problems (for example, oil-water-gas mixtures).

Finally, we should point out that because of the ease with which flow in complex geometries of a pore space can be simulated with the CA method, one can use this method to estimate the permeability of a three-dimensional porous medium with a given geometry and compare the results with various rigorous results and bounds for the permeability of the same system (see Sec. V). Cancelliére *et al.* (1990) undertook such a study for the Swiss cheese or randomly-distributed-penetrable-sphere model discussed in Secs. IV and V, and found that at high solid fractions the calculated permeability is within one order of magnitude of the most accurate upper bound due to Weissberg and Prager (1970) and Berryman and Milton (1985). Moreover, one can use the CA and random-walk methods to calculate the permeability k and the electrical conductivity σ of the same model pore space and thus test the validity of the relation between k and σ proposed by Katz and Thompson (1986) and Johnson *et al.* (1986). It is this author's opinion that cellular automata offer the most promising method for simulating complex problems of flow, dispersion, and displacement processes in natural porous media.

X. CONCLUSIONS

Many aspects of the morphology of rocks are now reasonably well understood. Although their origin is not yet completely understood, we now know that fractal concepts play a fundamental role in characterization of

rock properties. Aside from a few issues regarding the effect of small-scale heterogeneities on miscible and immiscible displacement processes, we can claim with confidence that flow, dispersion, and displacement processes are also reasonably well understood in microscopically disordered, macroscopically homogeneous porous media. However, how these phenomena behave in heterogeneous porous media, and especially in stratified and fractured rocks, is not as yet understood. As our discussion has indicated, even at the level of macroscopic and larger-scale heterogeneities, fractal concepts and long-range correlations play fundamental roles. Moreover, our discussion was restricted to Newtonian fluids, and much less is known about non-Newtonian and nonlinear flow phenomena in porous media (Sahimi, 1993a).

One goal of this review was to present and contrast two fundamental approaches to flow phenomena in reservoir rocks. One of them, favored by engineers, uses macroscopic continuum equations of transport. The other, which has mainly been advocated by physicists and allied scientists, employs discrete models and attempts to discover the universal features of flow phenomena in porous media. An engineer is interested in a method that is applicable over the entire range of the parameters of a given flow phenomenon, and does not usually pay much attention to the universal scaling laws, which are normally valid over a small range of the parameter space. On the other hand, in order to discover the universal features of a phenomenon, physicists have sometimes oversimplified a given flow phenomenon. It is clear that both approaches have their shortcomings and strengths, and the ideal model would take advantage of the strengths of the two in order to eliminate their shortcomings. This review has attempted to unify these two approaches. It was also written with the hope that the reader could get a reasonably clear picture of what is now understood and what remains to be done to resolve the remaining issues. Hopefully, by the time the next review is written, many of these issues will have been resolved.

ACKNOWLEDGMENTS

Many friends and colleagues have contributed to my understanding of the problems discussed in this review. First of all, I would like to express my appreciation and gratitude to Ted Davis and Skip Scriven, who in 1979 accepted me as their graduate student, introduced me to some of these problems, and taught me the fundamentals. Over the past decade Dietrich Stauffer has greatly contributed to my understanding of transport in disordered systems and critical phenomena. I am deeply grateful to him. I would like to thank Iraj Ershaghi, Joe Goddard, Adel Heiba, Barry Hughes, Mark Knackstedt, Michelle Robertson, Charlie Sammis, and Yanis Yortsos for their stimulating discussions and fruitful collaborations. My graduate students, Sepehr Arbabi, Abdussalam Imdakm, Valerie Jue, Sumit Mukhopadhyay, and Habib Siddiqui have helped me to gain a better understanding of the

problems we have worked on together. I would like to thank Gamward Chung and Karen Woo for cheerfully typing the first draft of this paper. In the past fourteen years my work at various stages has been supported by the Department of Energy, the National Science Foundation, the Petroleum Research Fund Administered by the American Chemical Society, the USC Center for Study of Fractured Reservoirs, supported by Shell Western, Texaco, Unocal, Oryx, Minerals Management Services, the U.S. Department of Interior, and the California State Lands Commission, and the Minnesota and San Diego Supercomputer Centers. Their support is gratefully acknowledged. Some portions of this paper were prepared in the Fall of 1991 while I was visiting the Department of Mathematics of the University of Melbourne, Australia. I would like to thank the Department for warm hospitality, and the Advanced Mineral Products Centre and the Department of Mathematics of the University of Melbourne for financial support. The final version of the paper was mostly prepared while I was visiting the HLRZ Supercomputer Center at KFA Jülich as an Alexander von Humboldt Foundation Research Fellow. I would like to thank the Center and Hans Herrmann for warm hospitality, and the Foundation for financial support.

REFERENCES

- Ababou, R., and L. W. Gelhar, 1990, in *Dynamics of Fluids in Hierarchical Porous Media*, edited by J. H. Cushman (Academic, San Diego), p. 394.
- Abbasi, M. H., J. W. Evans, and I. S. Abramson, 1983, AIChE J. **29**, 617.
- Abdassah, D., and I. Ershaghi, 1986, SPE Formation Evaluation J. **1**, 113.
- Abrams, A., 1975, Soc. Pet. Eng. J. **15**, 437.
- Adamson, A. W., 1990, *Physical Chemistry of Surfaces*, 5th edition (Wiley, New York).
- Adler, P. M., 1985a, Int. J. Multiphase Flow **11**, 91.
- Adler, P. M., 1985b, Int. J. Multiphase Flow **11**, 213.
- Adler, P. M., 1985c, Int. J. Multiphase Flow **11**, 241.
- Adler, P. M., 1985d, Int. J. Multiphase Flow **11**, 853.
- Adler, P. M., and H. Brenner, 1984a, Physicochem. Hydro. **5**, 245.
- Adler, P. M., and H. Brenner, 1984b, Physicochem. Hydro. **5**, 269.
- Adler, P. M., and H. Brenner, 1984c, Physicochem. Hydro. **5**, 287.
- Ahmed, G., and J. A. Blackman, 1979, J. Phys. C **12**, 837.
- Ahmed, G., L. M. Castanier, and W. E. Brigham, 1988, SPE Reservoir Eng. **3**, 45.
- Akanni, K. A., J. W. Evans, and I. S. Abramson, 1987, Chem. Eng. Sci. **42**, 1945.
- Aki, K., 1981, in *Earthquake Prediction: An Introductory Review*, edited by D. W. Simpson and P. G. Richards (American Geophysical Union, Washington, D.C.), p. 566.
- Alben, R., G. S. Cargill, III, and J. Wenzel, 1976, Phys. Rev. B **13**, 835.
- Alexander, S., and R. Orbach, 1982, J. Phys. (Paris) Lett. **43**, 625.
- Alexandroff, P., 1961, *Elementary Concepts of Topology* (Dover, New York).
- Alexandrowicz, Z., 1980, Phys. Lett. A **80**, 284.
- Amaefule, J. O., and L. L. Handy, 1982, Soc. Pet. Eng. J. **22**, 371.
- Ambegaokar, V., B. I. Halperin, and J. S. Langer, 1971, Phys. Rev. B **4**, 2612.
- Amott, E., 1959, Trans. AIME **216**, 156.
- Anderson, W. G., 1986, J. Pet. Tech. **38**, 1246.
- Anderson, W. G., 1987a, J. Pet. Tech. **39**, 1283.
- Anderson, W. G., 1987b, J. Pet. Tech. **39**, 1453.
- Andersson, J., and B. Dverstorp, 1987, Water Resour. Res. **23**, 1876.
- Andersson, T. B., and R. Jackson, 1967, Ind. Eng. Chem. Fundam. **6**, 527.
- Andrews, D. J. 1980, J. Geophys. Res. **85**, 3867.
- Androutsopoulos, G. P., and R. Mann, 1979, Chem. Eng. Sci. **34**, 1203.
- Appert, C., and S. Zaleski, 1990, Phys. Rev. Lett. **64**, 1.
- Araktingi, V. G., and F. M. Orr, Jr., 1988, paper SPE 18095, presented at the 63rd Annual Conference of the Society of Petroleum Engineers, Houston, Texas.
- Archie, G. E., 1942, Trans. AIME **146**, 54.
- Aris, R., 1956, Proc. R. Soc. London, Ser. A **235**, 67.
- Aris R., 1959, Chem. Eng. Sci. **11**, 194.
- Aronovitz, J. A., and D. R. Nelson, 1984, Phys. Rev. A **30**, 1948.
- Arriola, A., G. P. Wilhite, and D. W. Green, 1983, Soc. Pet. Eng. J. **23**, 99.
- Arya, A., T. A. Hewett, R. G. Larson, and L. W. Lake, 1988, SPE Reservoir Eng. **3**, 139.
- Auriault, J.-L., L. Borne, and R. Champon, 1985, J. Acoust. Soc. Am. **77**, 1641.
- Avellaneda, M., and S. Torquato, 1991, Phys. Fluids A **3**, 2529.
- Aviles, C. A., C. H. Scholz, and J. Boatwright, 1987, J. Geophys. Res. **92**, 331.
- Avnir, D., D. Farin, and P. Pfeifer, 1983, J. Chem. Phys. **79**, 3566.
- Avnir, D., D. Farin, and P. Pfeifer, 1985, J. Colloid Interface Sci. **103**, 112.
- Bachmat, Y., 1969, Water Resour. Res. **5**, 139.
- Bachmat, Y., 1972, Israel J. Tech. **10**, 391.
- Bacri, J.-C., C. Leygnac, and D. Salin, 1984, J. Phys. (Paris) Lett. **45**, L767.
- Bacri, J.-C., C. Leygnac, and D. Salin, 1985, J. Phys. (Paris) Lett. **46**, L467.
- Bacri, J.-C., N. Rakotomalala, and D. Salin, 1987, Phys. Rev. Lett. **58**, 2035.
- Bacri, J.-C., N. Rakotomalala, and D. Salin, 1990, Phys. Fluids A **2**, 674.
- Bacri, J.-C., M. Rosen, and D. Salin, 1990, Europhys. Lett. **11**, 127.
- Bacri, J.-C., D. Salin, and R. Wouméni, 1991, Phys. Rev. Lett. **67**, 2005.
- Bail, P. T., 1956, Producers Monthly **21**, 20.
- Baker, L. E., 1977, Soc. Pet. Eng. J. **17**, 219.
- Bakr, A. A., L. W. Gelhar, A. L. Gutjahr, and J. R. MacMillan, 1978, Water Resourc. Res. **14**, 263.
- Bakurov, V. G., V. I. Gusev, A. F. Izmailov, and A. R. Kessel, 1990, J. Phys. A **23**, 2507.
- Balasubramanian, K., F. Hayot, and W. F. Saam, 1987, Phys. Rev. A **36**, 2248.
- Balberg, I., and N. Bienbaum, 1983, Phys. Rev. B **28**, 3799.
- Balberg, I., and N. Bienbaum, 1985, Phys. Rev. A **31**, 1222.
- Balberg, I., N. Bienbaum, and C. H. Anderson, 1983, Phys.

- Rev. Lett. **51**, 1605.
- Balberg, I., N. Bienbaum, and N. Wagner, 1984, Phys. Rev. Lett. **52**, 1465.
- Bale, H. D., and P. W. Schmidt, 1984, Phys. Rev. Lett. **53**, 596.
- Banavar, J. R., M. Cieplak, and D. L. Johnson, 1988, Phys. Rev. B **37**, 7975.
- Banavar, J. R., and D. L. Johnson, 1987, Phys. Rev. B **35**, 7283.
- Banavar, J. R., M. Lipsicas, and J. F. Willemsen, 1985, Phys. Rev. B **32**, 6066.
- Banavar, J. R., and L. M. Schwartz, 1987, Phys. Rev. Lett. **58**, 1411.
- Barabási, A.-L., S. V. Buldyrev, S. Havlin, G. Huber, H. E. Stanley, and T. Vicsek, 1992, in *Growth Patterns in Physical Sciences*, Proceedings of the Les Houches Workshop, edited by R. Jullien, J. Kertész, P. Meakin, and D. E. Wolf (Nova Science, New York).
- Barenblatt, G. E., I. P. Zheltov, and I. N. Kochina, 1960, J. Appl. Math. Mech. (USSR) **24**, 1286.
- Barnsley, M. F., and S. Demko, 1985, Proc. R. Soc. London, Ser. A **399**, 243.
- Barret, L. K., and C. S. Yust, 1970, Metall (Berlin) **3**, 1.
- Barrett, E. P., L. G. Joyner, and P. P. Halenda, 1951, J. Am. Chem. Soc. **73**, 373.
- Bartell, F. E., and F. L. Miller, 1928, Ind. Eng. Chem. **20**, 738.
- Barton, C. C., and P. A. Hsieh, 1989, *Physical and Hydrological-Flow Properties of Fractures*, Guidebook T385 (American Geophysical Union, Las Vegas, Nevada).
- Barton, C. C., and E. Larsen, 1985, in *Proceedings of the International Symposium on Fundamentals of Rock Joints*, edited by O. Stephenson (Björkliden, Sweden), p. 77.
- Barton, C. C., T. A. Schutter, W. R. Page, and J. K. Samuel, 1987, Trans. Am. Geophys. Union **68**, 1295.
- Batchelor, G. K., and R. W. O'Brien, 1977, Proc. R. Soc. London, Ser. A **355**, 313.
- Batrouni, G., B. Kahng, and S. Redner, 1988, J. Phys. A **21**, L23.
- Batycky, J. P., F. G. McCaffery, P. K. Hodgins, and D. B. Fisher, 1981, Soc. Pet. Eng. J. **21**, 296.
- Bear, J., 1972, *Dynamics of Fluids in Porous Media* (Elsevier, New York).
- Ben-Jacob, E., R. Godby, N. D. Goldenfeld, J. Koplik, H. Levine, T. Mueller, and L. M. Sander, 1985, Phys. Rev. Lett. **55**, 1315.
- Ben-Jacob, E., G. Deutscher, P. Garik, N. D. Goldenfeld, and Y. Lareath, 1986, Phys. Rev. Lett. **57**, 1903.
- Benham, A. L., and R. W. Olson, 1963, Soc. Pet. Eng. J. **3**, 138.
- Benner, F. C., W. W. Riches, and F. E. Bartell, 1943, in *Fundamental Research on Occurrence and Recovery of Petroleum* (American Petroleum Institute, New York), p. 74.
- Bensimon, D., L. P. Kadanoff, S. Liang, B. I. Shraiman, and C. Tang, 1986, Rev. Mod. Phys. **58**, 977.
- Beran, M. J., 1968, *Statistical Continuum Theories* (Interscience, New York).
- Berman, D., B. G. Orr, H. M. Jaeger, and A. M. Goldman, 1986, Phys. Rev. B **33**, 4301.
- Bernal, J. D., 1960, Nature (London) **185**, 68.
- Bernal, J. D., I. A. Cherry, J. L. Finney, and K. R. Knight, 1970, J. Phys. E **3**, 388.
- Bernard, R. A., and R. H. Wilhelm, 1950, Chem. Eng. Prog. **46**, 233.
- Bernasconi, J., 1974, Phys. Rev. B **9**, 4575.
- Bernasconi, J., 1978, Phys. Rev. B **18**, 2185.
- Bernasconi, J., and H. J. Wiesmann, 1976, Phys. Rev. B **13**, 1131.
- Berryman, J. G., and S. C. Blair, 1986, J. Appl. Phys. **60**, 1430.
- Berryman, J. G., and G. W. Milton, 1985, J. Chem. Phys. **83**, 745.
- Bertin, H., M. Quintard, Ph. V. Corpel, and S. Whitaker, 1990, Transp. Porous Media **5**, 543.
- Bhattacharya, R. N., and V. K. Gupta, 1983, Water Resour. Res. **19**, 338.
- Bilardo, U., G. C. Borgia, V. Bortolotti, P. Fantazzini, and E. Mesim, 1991, J. Pet. Sci. Eng. **5**, 273.
- Billaux, D., J. P. Chiles, K. Hestir, and J. C. S. Long, 1989, Int. J. Rock Mech. Min. Sci. Geomech. Abstr. **26**, 281.
- Birovljev, A., L. Furberg, J. Feder, T. Jøssang, K. J. Måløy, and A. Aharony, 1991, Phys. Rev. Lett. **67**, 584.
- Bjerrum, N., and E. Manegold, 1927, Kolloid Z. **43**, 5.
- Blackman, J. A., 1976, J. Phys. C **9**, 2049.
- Blackwell, R. J., 1962, Soc. Pet. Eng. J. **2**, 1.
- Blackwell, R. J., J. R. Rayne, and W. M. Terry, 1959, Trans. AIME **216**, 1.
- Blatt, H., G. Middleton, and R. Murray, 1980, *Origin of Sedimentary Rocks* (Prentice-Hall, Englewood Cliffs, NJ), Chap. 14.
- Blumberg Selinger, R., J. Nittmann, and H. E. Stanley, 1989, Phys. Rev. A **40**, 2590.
- Blunt, M., and P. R. King, 1988, Phys. Rev. A **37**, 3935.
- Blunt, M., and P. R. King, 1990, Phys. Rev. A **42**, 4780.
- Blunt, M., and P. R. King, 1991, Transp. Porous Media **6**, 407.
- Bonnecaze, R. T., and J. F. Brady, 1990, Proc. R. Soc. London, Ser. A **430**, 285.
- Bonnet, J., and R. Lenormand, 1977, Rev. Inst. Fr. Pet. **42**, 477.
- Boon, J. P. 1992, Ed., *Proceedings of Advanced Research Workshop on Lattice Gas Automata Theory, Implementation, and Simulation*, J. Stat. Phys. **68**, No. 3/4.
- Bouchaud, J. P., A. George, J. Koplik, A. Provata, and S. Redner, 1990, Phys. Rev. Lett. **64**, 2503.
- Brace, W. F., and A. S. Orange, 1968, J. Geophys. Res. **73**, 5407.
- Brace, W. F., J. B. Walsh, and W. T. Frangos, 1968, J. Geophys. Res. **73**, 2225.
- Bracewell, R. N., O. Buneman, H. Hao, and J. Villasenor, 1986, Proc. IEEE **74**, 1282.
- Brandt, W. W., 1975, J. Chem. Phys. **63**, 5162.
- Brenner, H., 1962, Chem. Eng. Sci. **17**, 229.
- Brenner, H., 1980, Philos. Trans. R. Soc. London, Ser. A **297**, 81.
- Brenner, H., and P. M. Adler, 1982, Philos. Trans. R. Soc. London, Ser. A **307**, 149.
- Brigham, W. E., 1974, Soc. Pet. Eng. J. **14**, 91.
- Brigham, W. E., P. W. Reed, and J. N. Dew, 1961, Soc. Pet. Eng. J. **1**, 1.
- Broadbent, S. R., and J. M. Hammersley, 1957, Proc. Cambridge Philos. Soc. **53**, 629.
- Brosa, U., and D. Stauffer, 1989, J. Stat. Phys. **57**, 399.
- Brosa, U., and D. Stauffer, 1991, J. Stat. Phys. **63**, 405.
- Brown, S. R., and C. H. Scholz, 1985, J. Geophys. Res. **B90**, 12575.
- Brownstein, K. R., and C. E. Tarr, 1979, Phys. Rev. A **19**, 2446.
- Bruggeman, D. A. G., 1935, Ann. Phys. (Leipzig) **24**, 636.
- Bruinsma, R., and G. Aeppli, 1984, Phys. Rev. Lett. **52**, 1547.
- Bryant, S. L., P. R. King, and D. W. Mellor, 1990 (unpublished).
- Buckley, J. S., 1991, in *Interfacial Phenomena in Petroleum Recovery*, edited by N. R. Morrow (Marcel Dekker, New York), p. 157.
- Buka, A., J. Kertész, and T. Vicsek, 1986, Nature (London) **323**,

- 424.
- Buldyrev, S. V., A.-L. Barabási, F. Caserta, S. Havlin, H. E. Stanley, and T. Vicsek, 1992, Phys. Rev. A **45**, R8313.
- Bunde, A., A. Coniglio, D. C. Hong, and H. E. Stanley, 1985, J. Phys. A **18**, L137.
- Bunde, A., and S. Havlin, 1991, *Fractals and Disordered Systems* (Springer, Berlin).
- Bussian, A. E., 1983, Geophysics **48**, 1258.
- Butcher, P. N., 1975, J. Phys. C **8**, L324.
- Buyevich, Y. A., A. I. Lenov, and V. M. Safrai, 1969, J. Fluid Mech. **37**, 371.
- Caldwell, J. A., 1972, in *Proceedings of Symposium on Percolation Through Fissured Rocks* (International Society for Rock Mechanics and International Association of Engineering Geology, Stuttgart, Germany), p. 115.
- Carberry, J. J., and R. H. Bretton, 1958, AIChE J. **4**, 367.
- Cancellière, A., C. Chang, E. Foti, D. H. Rothman, and S. Succhi, 1990, Phys. Fluids A **2**, 2085.
- Carbonell, R. G., and S. Whitaker, 1983, Chem. Eng. Sci. **38**, 1795.
- Chan, D. Y. C., B. D. Hughes, and L. Paterson, 1986, Phys. Rev. A **34**, 4079.
- Chan, D. Y. C., B. D. Hughes, L. Paterson, and C. Sirakoff, 1988, Phys. Rev. A **38**, 4106.
- Chandler, R., J. Koplik, K. Lerman, and J. F. Willemsen, 1982, J. Fluid Mech. **119**, 249.
- Chang, S.-H., and J. C. Slattery, 1986, Transp. Porous Media **1**, 179.
- Chapman, A. M., and J. J. L. Higdon, 1992, Phys. Fluids A **4**, 2099.
- Charlaix, E., 1986, J. Phys. A **18**, L533.
- Charlaix, E., E. Guyon, and N. River, 1984, Solid State Commun. **50**, 999.
- Charlaix, E., E. Guyon, and S. Roux, 1987, Transp. Porous Media **2**, 31.
- Charlaix, E., J. P. Hulin, and T. J. Plona, 1987, Phys. Fluids **30**, 1690.
- Charlaix, E., J. P. Hulin, and J. P. Plona, 1988, J. Phys. D **21**, 1727.
- Charlaix, E., A. P. Kushnik, and J. P. Stokes, 1988, Phys. Rev. Lett. **61**, 1595.
- Chatenever, A., and J. C. Calhoun, 1952, Pet. Trans. AIME **195**, 149.
- Chatwin, P. C., 1977, J. Fluid Mech. **80**, 33.
- Chatzis, I., and F. A. L. Dullien, 1977, J. Can. Pet. Tech. **16**, 97.
- Chatzis, I., and F. A. L. Dullien, 1982, Rev. Inst. Fr. Pet. **37**, 183.
- Chatzis, I., and F. A. L. Dullien, 1985, Int. Chem. Eng. **25**, 47.
- Chatzis, I., and N. R. Morrow, 1984, Soc. Pet. Eng. J. **24**, 555.
- Chatzis, I., N. R. Morrow, and H. T. Lim, 1983, Soc. Pet. Eng. J. **23**, 311.
- Chaudhari, N. M., and A. E. Scheidegger, 1965, Can. J. Phys. **43**, 1776.
- Chayes, J. T., L. Chayes, and C. M. Newman, 1986, Commun. Math. Phys. **107**, 611.
- Chelidze, T., and Y. Gueguen, 1990, Int. J. Rock Mech. Min. Sci. Geomech. Abstr. **27**, 223.
- Chen, J.-D., and J. Koplik, 1985, J. Colloid Interface Sci. **108**, 304.
- Chen, J.-D., and N. Wada, 1986, Exp. Fluids **4**, 336.
- Chen, J.-D., and D. Wilkinson, 1985, Phys. Rev. Lett. **55**, 1892.
- Chen, S., K. Diemer, G. D. Doolen, K. Eggert, S. Gutman, and B. J. Travis, 1991, Physica D **47**, 72.
- Chen, S., G. D. Doolen, K. Eggert, D. G. Grunau, and E. Y. Loh, 1991, Phys. Rev. A **43**, 245.
- Chen, S., G. D. Doolen, and W. H. Matthaeus, 1991, J. Stat. Phys. **64**, 1133.
- Chen, Z.-X., 1989, Transp. Porous Media **4**, 147.
- Cheshire, I. M., and R. K. Pollard, 1988, in *Mathematics of Oil Production*, edited by S. F. Edwards and P. R. King (Clarendon, Oxford), p. 253.
- Chikhliwala, E. D., A. B. Huang, and Y. C. Yortsos, 1988, Transp. Porous Media **3**, 257.
- Chikhliwala, E. D., and Y. C. Yortsos, 1988, SPE Reservoir Eng. **3**, 1268.
- Childress, S., 1972, J. Chem. Phys. **56**, 2527.
- Chouke, R. L., P. van Meurs, and C. van der Poel, 1959, Trans. AIME **216**, 188.
- Christie, M. A., 1988, in *Mathematics of Oil Production*, edited by S. F. Edwards and P. R. King (Clarendon, Oxford), p. 269.
- Christie, M. A., and D. J. Bond, 1987, SPE Reservoir Eng. **2**, 514.
- Chu, C. F., and K. M. Ng, 1989, AIChE J. **35**, 148.
- Cieplak, M., and M. O. Robbins, 1988, Phys. Rev. Lett. **60**, 2042.
- Cieplak, M., and M. O. Robbins, 1990, Phys. Rev. B **41**, 11508.
- Clément, E., C. Baudet, E. Guyon, and J. P. Hulin, 1987, J. Phys. D **20**, 608.
- Closmann, P. J., 1975, Soc. Pet. Eng. J. **15**, 385.
- Cloud, W. F., 1941, Oil Weekly **103**, 26.
- Coats, K. H., J. R. Dempsey, and J. H. Henderson, 1971, Soc. Pet. Eng. J. **11**, 63.
- Coats, K. H., R. L. Nielson, M. H. Terhune, and A. G. Weber, 1967, Soc. Pet. Eng. J. **7**, 377.
- Coats, K. H., and B. D. Smith, 1964, Soc. Pet. Eng. J. **4**, 73.
- Cohen, M. H., 1987, in *Physics and Chemistry of Porous Media*, edited by J. R. Banavar, J. Koplik, and K. W. Winkler (AIP, New York).
- Cohen, M. H., and K. S. Mendelson, 1982, J. Appl. Phys. **53**, 1127.
- Collins, R. E., 1961, *Flow of Fluids Through Porous Media* (Pennwell, Tulsa), p. 196.
- Conner, Wm. C., J. Horowitz, and A. M. Lane, 1988, AIChE Symp. Series **88** (No. 266), 29.
- Conner, Wm. C., and A. M. Lane, 1984, J. Catal. **84**, 217.
- Conner, Wm. C., A. M. Lane, and A. J. Hoffman, 1984, J. Colloid Interface Sci. **600**, 185.
- Constantinides, G. N., and A. C. Payatakes, 1989, Chem. Eng. Commun. **81**, 55.
- Constantinides, G. N., and A. C. Payatakes, 1991, J. Colloid Interface Sci. **141**, 486.
- Cox, R. G., 1985, J. Fluid Mech. **168**, 169.
- Craig, F. F., 1971, *The Reservoir Engineering Aspects of Waterflooding* (Society of Petroleum Engineers, Richardson, Texas), p. 12.
- Crossley, P. A., L. M. Schwartz, and J. R. Banavar, 1991, Appl. Phys. Lett. **59**, 3553.
- Cuiec, L., 1984, paper SPE 13211, presented at the 59th Annual Meeting of the Society of Petroleum Engineers, Houston, Texas.
- Cushman, J. H., 1984, Water Resour. Res. **20**, 1668.
- Daccord, G., J. Nittmann, and H. E. Stanley, 1986, Phys. Rev. Lett. **56**, 336.
- Dagan, G., 1981, Water Resour. Res. **17**, 107.
- Dagan, G., 1982a, Water Resour. Res. **18**, 813.
- Dagan, G., 1982b, Water Resour. Res. **18**, 1571.
- Dagan, G., 1986, Water Resour. Res. **22**, 1205.
- Dagan, G., 1987, Annu. Rev. Fluid Mech. **19**, 183.

- David, C., Y. Gueguen, and G. Pampoukis, 1990, J. Geophys. Res. **95**, 6993.
- Davis, H. T., 1989, Europhys. Lett. **8**, 629.
- Davis, H. T., R. A. Novy, L. E. Scriven, and P. G. Toledo, 1990, J. Phys. Condens. Matter **2**, SA457.
- Davis, H. T., L. R. Valencourt, and C. E. Johnson, 1975, J. Am. Ceram. Soc. **58**, 446.
- Davis, J. A., and S. C. Jones, 1968, J. Pet. Tech. **20**, 1415.
- Day, P. R., 1956, Trans. Am. Geophys. Union **37**, 595.
- Dean, R. H., and L. L. Lo, 1988, SPE Reservoir Eng. **2**, 638.
- Deans, H. A., 1963, Soc. Pet. Eng. J. **3**, 49.
- de Arcangelis, L., J. Koplik, S. Redner, and D. Wilkinson, 1986, Phys. Rev. Lett. **57**, 996.
- de Arcangelis, L., S. Redner, and A. Coniglio, 1986, Phys. Rev. B **34**, 4656.
- Debye, P., H. R. Anderson, Jr., and H. Brumberger, 1957, J. Appl. Phys. **28**, 679.
- de Gennes, P. G., 1976, La Recherche **7**, 919.
- de Gennes, P. G., 1982, C. R. Acad. Sci. **295**, 1061.
- de Gennes, P. G., 1983a, J. Fluid Mech. **136**, 189.
- de Gennes, P. G., 1983b, Phys. Chem. Hydro. **4**, 175.
- de Gennes, P. G., 1985, in *Physics of Disordered Materials*, edited by M. Daoud (Plenum, London), p. 227.
- de Gennes, P. G., 1988, Europhys. Lett. **5**, 689.
- de Gennes, P. G., and E. Guyon, 1978, J. Mech. **17**, 403.
- DeGregoria, A. J., 1985, Phys. Fluids **28**, 2933.
- DeGregoria, A. J., 1986, Phys. Fluids **29**, 3557.
- de Josselin de Jong, G., 1958, Trans. Am. Geophys. Union **39**, 67.
- Delshad, M., D. J. MacAllister, G. A. Pope, and B. A. Rouse, 1985, Soc. Pet. Eng. J. **25**, 476.
- Derrida, B., and J. Vannimenus, 1982, J. Phys. A **15**, L557.
- d'Humières, D., and P. Lallemand, 1986, Physica A **140**, 326.
- d'Humières, D., P. Lallemand, and U. Frisch, 1986, Europhys. Lett. **2**, 291.
- Dias, M. M., and A. C. Payatakes, 1986a, J. Fluid Mech. **164**, 305.
- Dias, M. M., and A. C. Payatakes, 1986b, J. Fluid Mech. **164**, 337.
- Dias, M. M., and D. Wilkinson, 1986, J. Phys. A **19**, 3131.
- Diaz, C. E., I. Chatzis, and F. A. L. Dullien, 1987, Transp. Porous Media **2**, 215.
- Dienes, J. K., 1980, Los Alamos Scientific Laboratory Report LA-8553-PR, p. 19.
- Dodd, C. G., and O. G. Keil, 1959, J. Phys. Chem. **63**, 299.
- Donaldson, E. C., P. B. Lorenz, and R. D. Thomas, 1966, paper SPE 1562, presented at the 41st Annual Conference of the Society of Petroleum Engineers, Dallas, Texas.
- Donaldson, E. C., R. D. Thomas, and P. B. Lorenz, 1969, Soc. Pet. Eng. J. **9**, 13.
- Doolen, G., 1991, ed., *Proceedings of NATO Advanced Research Workshop on Lattice Gas Methods for PDE's: Theory, Application and Hardware*, Physica D **47**.
- Dougherty, E. L., 1963, Soc. Pet. Eng. J. **3**, 155.
- Douglas, J., D. W. Peaceman, and H. H. Rachford, 1959, Trans. AIME **216**, 297.
- Doyen, P. M., 1988, J. Geophys. Res. **93**, 7729.
- Duarte, J. A. M. S., and U. Brosa, J. Stat. Phys. **59**, 501.
- Duarte, J. A. M. S., M. Sahimi, and J. de Carvalho, 1992, J. Phys. (Paris) II **2**, 1.
- Dullien, F. A. L., 1975, AIChE J. **21**, 299.
- Dullien, F. A. L., 1979, *Porous Media: Fluid Transport and Pore Structure* (Academic, New York).
- Dullien, F. A. L., and G. K. Dhawan, 1975, J. Colloid Interface Sci. **52**, 129.
- Dullien, F. A. L., F. S. Y. Lai, and I. F. MacDonald, 1986, J. Colloid Interface Sci. **109**, 201.
- Dussan V., E. B., 1979, Annu. Rev. Fluid Mech. **11**, 371.
- Dussan V., E. B., and S. H. Davis, 1974, J. Fluid Mech. **65**, 71.
- Dverstorp, B., and J. Andersson, 1989, Water Resour. Res. **25**, 540.
- Dykstra, H., and R. L. Parsons, 1950, in *Secondary Recovery of Oil in the United States*, 2nd ed. (American Petroleum Institute, New York), p. 160.
- Egbogah, E. O., and R. A. Dawe, 1980, Bull. Can. Pet. Tech. **28**, 200.
- Ehrlich, R., P. J. Brown, J. M. Yarus, and D. T. Eppler, 1980, in *Advanced Particulate Morphology*, edited by J. K. Beddow and T. P. Meloy (CRC Press, Boca Raton, Florida), p. 101.
- Eidsath, A., R. G. Carbonell, S. Whitaker, and L. R. Herrmann, 1983, Chem. Eng. Sci. **38**, 1803.
- Elam, W. T., A. R. Kerstein, and J. J. Rehr, 1984, Phys. Rev. Lett. **52**, 1516.
- Emanuel, A. S., G. K. Alameda, R. A. Behrens, and T. A. Hewett, 1989, SPE Reservoir Eng. **3**, 311.
- Endo, H. K., J. C. S. Long, C. R. Wilson, and P. A. Witherpoon, 1984, Water Resour. Res **20**, 1390.
- Englman, R., Y. Gur, and Z. Jaeger, 1983, J. Appl. Mech. **50**, 707.
- Erdös, P., and S. B. Haley, 1976, Phys. Rev. B **13**, 1720.
- Evans, J. W., M. H. Abbasi, and A. Sarin, 1980, J. Chem. Phys. **72**, 2967.
- Everett, D. H., 1954, Trans. Faraday Soc. **50**, 1077.
- Everett, D. H., 1967, in *The Solid-Gas Interface*, Vol. II, edited by E. Elison Flood (Marcel Dekker, New York), p. 1055.
- Family, F., 1984, in *Random Walks and Their Applications in the Physical and Biological Sciences*, edited by M. F. Shlesinger and B. J. West (AIP, New York), p. 33.
- Family, F., and T. Vicsek, 1985, J. Phys. A **18**, L75.
- Family, F., and T. Vicsek, 1991, Eds., *Dynamics of Fractal Surfaces* (World Scientific, Singapore).
- Fara, H. D., and A. E. Scheidegger, 1961, J. Geophys. Res. **66**, 3279.
- Fatt, I., 1956, Trans. AIME **207**, 144.
- Fatt, I., 1960, Science **131**, 158.
- Fayers, F. J., 1988, SPE Reservoir Eng. **3**, 542.
- Feder, J., 1988, *Fractals* (Plenum, New York).
- Feeney, R., S. L. Schmidt, P. Strickholm, J. Chadam, and P. Ortoleva, 1983, J. Chem. Phys. **78**, 1293.
- Feng, S., B. I. Halperin, and P. N. Sen, 1987, Phys. Rev. B **35**, 197.
- Ferer, M., R. A. Geisbrecht, W. N. Sams, and D. H. Smith, 1992, Phys. Rev. A **45**, R6973.
- Fernández, J. F., R. Rangel, and J. Rivero, 1991, Phys. Rev. Lett. **67**, 2958.
- Finney, J., 1968, Ph.D. thesis (University of London).
- Firoozabadi, A., and J. Hauge, 1990, J. Pet. Tech. **42**, 784.
- Firoozabadi, A., K. Ishimoto, and B. Dindoruk, 1991, paper SPE 21798 presented at the Western Regional Meeting of the Society of Petroleum Engineers, Long Beach, California.
- Fisher, M. E., 1971, in *Critical Phenomena: Enrico Fermi Summer School*, edited by M. S. Green (Academic, New York), p. 1.
- Fisher, M. E., and J. W. Essam, 1961, J. Math. Phys. **2**, 609.
- Fisher, R. L., and P. D. Lark, 1979, J. Colloid Interface Sci. **69**, 486.
- Flory, P. J., 1943, J. Am. Chem. Soc. **63**, 3083.
- Fowler, A. D., H. E. Stanley, and G. Daccord, 1989, Nature

- (London) **341**, 134.
- Frette, V., K. J. Måløy, F. Boger, J. Feder, T. Jøssang, and P. Meakin, 1990, Phys. Rev. A **42**, 3432.
- Fried, J. J., and M. A. Combarnous, 1971, Adv. Hydrosci. **7**, 169.
- Frisch, U., B. Hasslacher, and Y. Pomeau, 1986, Phys. Rev. Lett. **56**, 1505.
- Frisch, U., D. d'Humières, B. Hasslacher, P. Lallemand, Y. Pomeau, and J.-P. Rivet, 1987, Complex Syst. **1**, 648.
- Furuberg, L., J. Feder, A. Aharony, and T. Jøssang, 1988, Phys. Rev. Lett. **61**, 2117.
- Gardner, J. W., and J. G. J. Ypma, 1982, paper SPE 10686, presented at the 57th Annual Conference of the Society of Petroleum Engineers, New Orleans, Louisiana.
- Gawlinski, E. T., and S. Redner, 1983, J. Phys. A **16**, 1063.
- Gawlinski, E. T., and H. E. Stanley, 1981, J. Phys. A **14**, L291.
- Gefen, Y., A. Aharony, and S. Alexander, 1983, Phys. Rev. Lett. **50**, 77.
- Geffen, T. M., W. W. Owens, D. R. Parrish, and R. A. Morse, 1951, Trans. AIME **192**, 99.
- Gelhar, L. W., and C. L. Axness, 1983, Water Resour. Res. **19**, 161.
- Gelhar, L. W., A. L. Gutjahr, and R. J. Naff, 1979, Water Resour. Res. **15**, 1387.
- Gilman, J., and H. Kazemi, 1983, Soc. Pet. Eng. J. **23**, 675.
- Gingold, D. B., and C. J. Lobb, 1990, Phys. Rev. B **42**, 8220.
- Giordano, R. M., and S. J. Salter, 1984, paper SPE 13165, presented at the 59th Annual Conference of the Society of Petroleum Engineers, Houston, Texas.
- Giordano, R. M., S. J. Salter, and K. K. Mohanty, 1985, paper SPE 14365, presented at the 60th Annual Conference of the Society of Petroleum Engineers, Las Vegas, Nevada.
- Gist, G. A., A. H. Thompson, A. J. Katz, and R. L. Higgins, 1990, Phys. Fluids A **2**, 1533.
- Goddin, C. S., F. F. Craig, J. O. Wilkes, and M. R. Tek, 1966, J. Pet. Tech. **18**, 765.
- Golden, J. M., 1980, Water Resour. Res. **16**, 201.
- Goode, P. A., and T. S. Ramakrishnan, 1993, AIChE J. **39**, 1124.
- Gouyet, J. F., M. Rosso, and B. Sapoval, 1988, Phys. Rev. B **37**, 1832.
- Gray, W. G., 1975, Chem. Eng. Sci. **30**, 229.
- Gray, W. G., and K. O'Neil, 1976, Water Resour. Res. **12**, 148.
- Greenberg, R. J., and W. F. Brace, 1969, J. Geophys. Res. **74**, 2099.
- Greenkorn, R. A., C. R. Johnson, and R. E. Haring, 1965, J. Pet. Tech. **5**, 329.
- Griffiths, A., 1911, Proc. R. Soc. London **23**, 190.
- Grisak, G. E., and J. F. Pickens, 1980, Water Resour. Res. **16**, 719.
- Gueguen, Y., and J. K. Dienes, 1989, Math. Geol. **21**, 1.
- Gunn, D. J., and C. Pryce, 1969, Trans. Inst. Chem. Eng. **47**, T341.
- Gunstensen, A., and D. H. Rothman, 1991, Physica D **47**, 47.
- Gutjahr, A. L., and L. W. Gelhar, 1981, Water Resour. Res. **19**, 161.
- Gutjahr, A. L., L. W. Gelhar, A. A. Bakr, and J. R. MacMillan, 1978, Water Resour. Res. **14**, 953.
- Güven, O., R. W. Falta, F. J. Molz, and J. G. Melville, 1985, Water Resour. Res. **21**, 676.
- Güven, O., F. J. Molz, and J. G. Melville, 1984, Water Resour. Res. **20**, 1337.
- Guyer, R. A., 1985, Phys. Rev. A **32**, 2324.
- Guyon, E., L. Oger, and T. J. Plona, 1987, J. Phys. D **20**, 1637.
- Haan, S. W., and R. Zwanzig, 1977, J. Phys. A **10**, 1547.
- Habermann, B., 1960, Trans. AIME **219**, 264.
- Hagiwara, T., 1984, paper SPE 13100, presented at the 59th Annual Meeting of the Society of Petroleum Engineers, Houston, Texas.
- Hagoort, J., 1974, Soc. Pet. Eng. J. **14**, 63.
- Haji-Sheikh, A., and E. M. Sparrow, 1966, SIAM J. Appl. Math. **14**, 370.
- Haldorsen, H. H., P. J. Brand, and C. J. MacDonald, 1988, in *Mathematics in Oil Production*, edited by S. F. Edwards, P. R. King (Clarendon, Oxford), p. 109.
- Haldorsen, H. H., and E. Damsleth, 1990, J. Pet. Tech. **42**, 404.
- Haldorsen, H. H., and L. W. Lake, 1984, Soc. Pet. Eng. J. **24**, 447.
- Hall, P. L., D. F. R. Mildner, and R. L. Brost, 1986, J. Geophys. Res. B **91**, 2183.
- Halperin, B. I., S. Feng, and P. N. Sen, 1985, Phys. Rev. Lett. **54**, 2891.
- Hammond, P. S., 1983, J. Fluid Mech. **137**, 363.
- Han, N.-W., J. Bhakta, and R. G. Carbonell, 1985, AIChE J. **31**, 277.
- Hansen, J. P., and A. T. Skjeltorp, 1988, Phys. Rev. B **38**, 2635.
- Happel, J., and H. Brenner, 1983, *Low Reynolds Number Hydrodynamics* (Nijhoff, San Diego).
- Hardy, J., O. de Pazzis, and Y. Pomeau, 1976, Phys. Rev. A **13**, 1949.
- Hardy, J., Y. Pomeau, and O. de Pazzis, 1973, J. Math. Phys. **14**, 1746.
- Haring, R. E., and R. A. Greenkorn, 1970, AIChE J. **16**, 477.
- Harleman, D. R. F., and R. R. Rumer, 1963, J. Fluid Mech. **16**, 385.
- Harris, A. B., and A. Aharony, 1987, Europhys. Lett. **4**, 1355.
- Harris, C. K., 1990, Transp. Porous Media **5**, 517.
- Hasimoto, H., 1959, J. Fluid Mech. **5**, 317.
- Hatzivramidis, D. T., 1988, SPE Reservoir Eng. **3**, 631.
- Haus, J. W., and K. W. Kehr, 1987, Phys. Rep. **150**, 263.
- Havlin, S., and D. Ben-Avraham, 1987, Adv. Phys. **36**, 695.
- Havlin, S., S. V. Buldyrev, H. E. Stanley, and G. H. Weiss, 1991, J. Phys. A **24**, L925.
- Hayes, J. B., 1979, *The Society of Paleontologists and Mineralogists Special Publication No. 26*, p. 127.
- Hearn, C. L., 1971, J. Pet. Tech. **23**, 805.
- Heaviside, J., 1991, in *Interfacial Phenomena in Petroleum Recovery*, edited by N. R. Morrow (Marcel Dekker, New York), p. 377.
- Heiba, A. A., 1985, Ph.D. thesis (University of Minnesota, Minneapolis).
- Heiba, A. A., H. T. Davis, and L. E. Scriven, 1983, paper SPE 12172, presented at the 58th Annual Meeting of the Society of Petroleum Engineers, San Francisco, California.
- Heiba, A. A., H. T. Davis, and L. E. Scriven, 1984, paper SPE 12690, presented at the SPE/DOE Fourth Symposium on Enhanced Oil Recovery, Tulsa, Oklahoma.
- Heiba, A. A., M. Sahimi, L. E. Scriven, and H. T. Davis, 1982, paper SPE 11015, presented at the 57th Annual Meeting of the Society of Petroleum Engineers, New Orleans, Louisiana.
- Heiba, A. A., M. Sahimi, L. E. Scriven, and H. T. Davis, 1992, SPE Reservoir Eng. **7**, 123.
- Hele-Shaw, H. J. S., 1898, Nature (London) **58**, 34.
- Heller, J. P., 1966, J. Appl. Phys. **37**, 1566.
- Heller, J. P., 1972, in *Proceedings of the Second International Conference on Fundamentals of Transport Phenomena in Porous Media*, edited by D. E. Elrick (International Association of Hydraulic Research, Guelph, Canada), p. 1.

- Hentschel, H. G. E., and F. Family, 1991, Phys. Rev. Lett. **66**, 1982.
- Hestir, K., and J. C. S. Long, 1990, J. Geophys. Res. **95**, 21565.
- Hewett, T. A., 1986, paper SPE 15386, presented at the 61st Annual Technical Conference of the Society of Petroleum Engineers, New Orleans, Louisiana.
- Hewett, T. A., and R. A. Behrens, 1990, SPE Formation Evaluation **5**, 217.
- Hickernell, F. J., and Y. C. Yortsos, 1986, Stud. Appl. Math. **74**, 93.
- Higuera, F., S. Succi, and R. Benzi, 1989, Europhys. Lett. **9**, 663.
- Hilfer, R., 1991a, Phys. Rev. B **44**, 628.
- Hilfer, R., 1991b, Phys. Rev. **44**, 60.
- Hill, S., 1952, Chem. Eng. Sci. **1**, 247.
- Hinch, E. J., 1977, J. Fluid Mech. **83**, 695.
- Hoffman, R. L., 1975, J. Colloid Interface Sci. **50**, 228.
- Homsy, G. M., 1987, Annu. Rev. Fluid Mech. **19**, 271.
- Hori, M., and F. Yonezawa, 1977, J. Phys. C **10**, 229.
- Horn, F. J. M., 1971, AIChE J. **17**, 613.
- Horváth, V. K., F. Family, and T. Vicsek, 1990, Phys. Rev. Lett. **65**, 1388.
- Horváth, V. K., F. Family, and T. Vicsek, 1991a, J. Phys. A **24**, L25.
- Horváth, V. K., F. Family, and T. Vicsek, 1991b, Phys. Rev. Lett. **67**, 3207.
- Horváth, V. K., J. Kertész, and T. Vicsek, 1987a, Europhys. Lett. **4**, 1133.
- Horváth, V. K., T. Vicsek, and J. Kertész, 1987b, Phys. Rev. A **35**, 2353.
- Hoshen, J., and R. Kopelman, 1976, Phys. Rev. B **24**, 3438.
- Hough, S. E., 1989, Geophys. Res. Lett. **16**, 673.
- Howells, I. D., 1974, J. Fluid Mech. **64**, 449.
- Howison, S. D., 1986, SIAM J. Appl. Math. **46**, 20.
- Huang, A. B., E. D. Chikhlialava, and Y. C. Yortsos, 1984, paper SPE 13163, presented at the 59th Annual Conference of the Society of Petroleum Engineers, Houston, Texas.
- Huang, J., and D. L. Turcotte, 1989, J. Geophys. Res. B **94**, 7491.
- Hughes, B. D., 1993, *Random Environments and Random Walks* (Oxford University Press, London).
- Hughes, B. D., and M. Sahimi, 1982, J. Stat. Phys. **29**, 781.
- Hughes, B. D., and M. Sahimi, 1993, Phys. Rev. Lett. **70**, 2581.
- Huh, C., and L. E. Scriven, 1971, J. Colloid Interface Sci. **35**, 85.
- Hulin, J. P., E. Charlaix, T. J. Plona, L. Oger, and E. Guyon, 1988, AIChE J. **34**, 610.
- Hulin, J. P., E. Clément, C. Baudet, J. F. Gouyet, and M. Rosso, 1988, Phys. Rev. Lett. **61**, 333.
- Hurst, H.E., R. P. Black, and Y. M. Simaika, 1965, *Long Term Storage; An Experimental Study* (Constable, London).
- Imdakm, A. O., and M. Sahimi, 1991, Chem. Eng. Sci. **46**, 1977.
- Ingle, J. C., Pacific Section, 1981, *Society of Economic Paleontologists and Mineralogists Special Publication No. 159*.
- Isaacs, C. M., 1984, paper SPE 12733, presented at the 1984 California Regional Meeting of the Society of Petroleum Engineers, Long Beach, California.
- Jacks, H. H., O. J. E. Smith, and C.C. Mattax, 1973, Soc. Pet. Eng. J. **13**, 175.
- Jacquin, C., 1985, C. R. Acad. Sci. B **300**, 721.
- Jerauld, G. R., H. T. Davis, and L. E. Scriven, 1984, paper SPE 13164, presented at the 59th Annual Conference of the Society of Petroleum Engineers, Houston, Texas.
- Jerauld, G. R., J. C. Hatfield, L. E. Scriven, and H. T. Davis, 1984, J. Phys. C **17**, 1519.
- Jerauld, G. R., L. C. Nitsche, G. F. Teletzke, H. T. Davis, and L. E. Scriven, 1984, paper SPE 12691, presented at the SPE/DOE Joint Symposium on Enhanced Oil Recovery, Tulsa, Oklahoma.
- Jerauld, G. R., and S. J. Salter, 1990, Trans. Porous Media **5**, 103.
- Jerauld, G. R., L. E. Scriven, and H. T. Davis, 1984, J. Phys. C **16**, 3429.
- Joanny, J. F., and P. G. de Gennes, 1984, J. Chem. Phys. **81**, 552.
- Joanny, J. F., and M. O. Robbins, 1990, J. Chem. Phys. **92**, 3206.
- Johnson, D. L., 1989, Phys. Rev. Lett. **63**, 580.
- Johnson, D. L., J. Koplik, and L. M. Schwartz, 1986, Phys. Rev. Lett. **57**, 2564.
- Johnson, D. L., J. Koplik, and R. Dashen, 1987, J. Fluid Mech. **176**, 379.
- Johnson, E. F., D. P. Gassler, and V. D. Naumann, 1959, Trans. AIME **216**, 270.
- Joy, T., and W. Strieder, 1978, J. Phys. C **11**, L867.
- Joy, T., and W. Strieder, 1979, J. Phys. C **12**, L279.
- Kadanoff, L. P., 1985, J. Stat. Phys. **39**, 267.
- Kadanoff, L., G. McNamara, and G. Zanetti, 1989, Phys. Rev. A **40**, 4527.
- Kalaydjian, F., and B. Legait, 1987, C. R. Acad. Sci. **304**, 1035.
- Kantzas, A., and I. Chatzis, 1988, Chem. Eng. Commun. **69**, 191.
- Kardar, K., G. Parisi, and Y.-C. Zhang, 1986, Phys. Rev. Lett. **56**, 889.
- Katz, A. J., and A. H. Thompson, 1985, Phys. Rev. Lett. **54**, 1325.
- Katz, A. J., and A. H. Thompson, 1986, Phys. Rev. B **34**, 8179.
- Katz, A. J., and A. H. Thompson, 1987, J. Geophys. Res. B **92**, 599.
- Katz, A. J., A. H. Thompson, and R. A. Rashke, 1988, Phys. Rev. A **38**, 4901.
- Katz, A. J., and S. A. Trugman, 1988, J. Colloid Interface Sci. **123**, 8.
- Kazemi, H., 1969, Soc. Pet. Eng. J. **9**, 451.
- Kazemi, H., L. S. Merrill, K. L. Porterfield, and P. R. Zoman, 1976, Soc. Pet. Eng. J. **16**, 317.
- Keller, J. B., 1980, in *Nonlinear P.D.E. in Engineering and Applied Sciences*, edited by R. L. Sternberg, A.J. Kalinowski, and J. S. Papadakis (Marcel Dekker, New York), p. 263.
- Kenyon, W. E., P. I. Day, C. Straley, and J. F. Willemse, 1988, SPE Formation Evaluation **3**, 622.
- Kerstein, A. R., 1983, J. Phys. A **16**, 3071.
- Kertész, J., and T. Vicsek, 1986, J. Phys. A **19**, L257.
- Kessler, D., J. Koplik, and L. Levine, 1988, Adv. Phys. **37**, 255.
- Kessler, D., and H. Levine, 1986, Phys. Rev. A **33**, 2634.
- Kessler, D., H. Levine, and Y. Tu, 1991, Phys. Rev. A **43**, 4551.
- Killough, J. E., and H. P. Foster, 1979, Soc. Pet. Eng. J. **19**, 279.
- Killins, C. R., R. F. Nielsen, and J. C. Calhoun, 1953, Production Monthly **18**, 30.
- Kim, I. C., and S. Torquato, 1990, J. Appl. Phys. **68**, 3892.
- Kim, I. C., and S. Torquato, 1991, J. Appl. Phys. **69**, 2280.
- Kim, J. M., and J. M. Kosterlitz, 1989, Phys. Rev. Lett. **62**, 2289.
- Kim, S., and W. B. Russel, 1985, J. Fluid Mech. **154**, 269.
- King, G. C. P., 1984, Pure Appl. Geophys. **121**, 761.
- King, M. J., W. B. Lindquist, and L. Reyna, 1984, paper SPE 13953, presented at the 59th Annual Conference of the Society of Petroleum Engineers, Houston, Texas.
- King, M. J., and H. Scher, 1987, Phys. Rev. A **35**, 929.

- King, M. J., and H. Scher, 1990, Phys. Rev. A **41**, 874.
- King, P. R., 1987a, J. Phys. A **20**, 3935.
- King, P. R., 1987b, J. Phys. A **20**, L529.
- King, P. R., 1989, Transp. Porous Media **4**, 37.
- Kiriakidis, D. G., E. Mitsoulis, and G. H. Neale, 1991, Can. J. Chem. Eng. **60**, 557.
- Kirkpatrick, S., 1971, Phys. Rev. Lett. **27**, 1722.
- Kirkpatrick, S., 1973, Rev. Mod. Phys. **45**, 574.
- Kirkpatrick, S., 1979, in *Ill-Condensed Matter*, edited by R. Balian, R. Maynard, and G. Toulouse (North-Holland, Amsterdam), p. 323.
- Kirkpatrick, S., C. D. Gelatt, and M. P. Vecchi, 1983, Science **220**, 671.
- Klafter, J., G. Zumofen, and A. Blumen, 1991, J. Phys. A **24**, 4835.
- Knackstedt, M. A., M. Sahimi, and D. Y. C. Chan, 1993, Phys. Rev. E **47**, 2593.
- Koch, D. L., and J. F. Brady, 1985, J. Fluid Mech. **154**, 399.
- Koch, D. L., and J. F. Brady, 1987, Chem. Eng. Sci. **42**, 1377.
- Koch, D. L., and J. F. Brady, 1988, Phys. Fluids **31**, 965.
- Koch, D. L., R. G. Cox, H. Brenner, and J. F. Brady, 1989, J. Fluid Mech. **200**, 173.
- Kohring, G. A., 1991a, Int. J. Mod. Phys. C **2**, 755.
- Kohring, G. A. 1991b, J. Phys. (Paris) II **1**, 593.
- Kohring, G. A., 1991c, J. Stat. Phys. **63**, 411.
- Koonce, T. K., and R. J. Blackwell, 1965, Soc. Pet. Eng. J. **5**, 318.
- Koplik, J., 1981, J. Phys. C **14**, 4821.
- Koplik, J., 1982, J. Fluid Mech. **119**, 219.
- Koplik, J., J. R. Banavar, and J. F. Willemse, 1988, Phys. Rev. Lett. **60**, 1282.
- Koplik, J., and T. J. Lasseter, 1984, Chem. Eng. Commun. **26**, 285.
- Koplik, J., and T. J. Lasseter, 1985, Soc. Pet. Eng. J. **25**, 89.
- Koplik, J., and H. Levine, 1985, Phys. Rev. B **32**, 280.
- Koplik, J., C. Lin, and M. Vermette, 1984, J. Appl. Phys **56**, 3127.
- Koplik, J., S. Redner, and D. Wilkinson, 1988, Phys. Rev. A **37**, 2619.
- Kortekaas, T. F. M., 1983, paper SPE 12112, presented at the 58th Annual Conference of the Society of Petroleum Engineers, San Francisco, California.
- Kostek, S., L. M. Schwartz, and D. L. Johnson, 1992, Phys. Rev. B **45**, 186.
- Koval, E. J., 1963, Soc. Pet. Eng. J. **3**, 145.
- Kreyszig, E., 1959, *Differential Geometry* (University of Toronto, Toronto).
- Krohn, C. E., 1988a, J. Geophys. Res. B **93**, 3286.
- Krohn, C. E., 1988b, J. Geophys. Res. B **93**, 3297.
- Krohn, C. E., and A. H. Thompson, 1986, Phys. Rev. B **33**, 6366.
- Krug, J., 1991, Phys. Rev. A **44**, R801.
- Ksenzhek, O. S., 1963, J. Phys. Chem. **37**, 691.
- Kwiecien, M. J., I. F. Macdonald, and F. A. L. Dullien, 1989, J. Microsc. **159**, 343.
- Kyle, C. R., and R. L. Perrine, 1965, Soc. Pet. Eng. J. **5**, 189.
- Kyte, J. R., and D. W. Berry, 1975, Soc. Pet. Eng. J. **15**, 269.
- Lahbabi, A., and H.-C. Chang, 1985, Chem. Eng. Sci. **40**, 435.
- Laidlaw, W. G., G. R. Hamilton, R. B. Fleweiling, and W. G. Wilson, 1988, J. Stat. Phys. **53**, 713.
- Lake, L. W., and H. B. Carroll, Jr., 1986, Eds., *Reservoir Characterization* (Academic, New York).
- Lake, L. W., and G. J. Hirasaki, 1981, Soc. Pet. Eng. J. **21**, 459.
- Landauer, R., 1952, J. Appl. Phys. **23**, 779.
- Landauer, R., 1978, in *Electrical Transport and Optical Properties of Inhomogeneous Media*, edited by J. C. Garland and D. B. Tanner, AIP Conference Proceedings **40** (AIP, New York), p. 2.
- Lane, A. M., N. Shah, and Wm. C. Conner, 1986, J. Colloid Interface Sci. **109**, 235.
- Larson, R. E., and J. J. L. Higdon, 1987, J. Fluid Mech. **178**, 119.
- Larson, R. E., and J. J. L. Higdon, 1989, Phys. Fluids A **1**, 38.
- Larson, R. G., 1977, M. S. thesis (University of Minnesota, Minneapolis).
- Larson, R. G., 1981, Ind. Eng. Chem. Fund. **20**, 132.
- Larson, R. G., H. T. Davis, and L. E. Scriven, 1981a, Chem. Eng. Sci. **36**, 75.
- Larson, R. G., and N. R. Morrow, 1981, Powder Tech. **30**, 123.
- Larson, R. G., L. E. Scriven, and H. T. Davis, 1977, Nature **268**, 409.
- Larson, R. G., L. E. Scriven, and H. T. Davis, 1981b, Chem. Eng. Sci. **36**, 57.
- Latour, L. L., R. L. Kleinberg, and A. Sezginer, 1992, J. Colloid Interface Sci. **150**, 535.
- Leath, P. L., 1976, Phys. Rev. B **14**, 5046.
- Le Doussal, P., 1989, Phys. Rev. B **39**, 4816.
- Leclerc, D. F., and G. H. Neale, 1988, J. Phys. A **21**, 2979.
- Lee, J., A. Coniglio, and H. E. Stanley, 1990, Phys. Rev. A **41**, 4589.
- Le Febvre du Prey, E. J., 1973, Soc. Pet. Eng. J. **13**, 39.
- Legait, B., and C. Jacquin, 1982, C. R. Acad. Sci. **294**, 487.
- Legaski, M. W., and D. L. Katz, 1967, Soc. Pet. Eng. J. **7**, 43.
- Lenormand, R., 1989, Proc. R. Soc. London, Ser. A **423**, 159.
- Lenormand, R., 1990, in *Hydrodynamics of Dispersed Media*, edited by J. P. Hulin, A. M. Cazabat, E. Guyon, and F. Carmona (North-Holland, Amsterdam), p. 287.
- Lenormand, R., and S. Bories, 1980, C. R. Acad. Sci. B **291**, 279.
- Lenormand, R., F. Kalaydjian, M.-T. Bieber, and J.-M. Lombard, 1990, paper SPE 20475, presented at the 65th Annual Technical Conference of the Society of Petroleum Engineers, New Orleans, Louisiana.
- Lenormand, R., E. Toubol, and C. Zarcone, 1988, J. Fluid Mech. **189**, 165.
- Lenormand, R., and C. Zarcone, 1984, in *Kinetics of Aggregation and Gelation*, edited by F. Family and D. P. Landau (Elsevier, Amsterdam), p. 177.
- Lenormand, R., and C. Zarcone, 1985a, Phys. Rev. Lett. **54**, 2226.
- Lenormand, R., and C. Zarcone, 1985b, Physicochem. Hydro. **6**, 497.
- Lenormand, R., C. Zarcone, and A. Sarr, 1983, J. Fluid Mech. **135**, 337.
- Leverett, M. C., 1939, Trans. AIME **132**, 149.
- Leverett, M. C., 1941, Trans. AIME **142**, 159.
- Levine, S., and D. L. Cuthill, 1986, J. Can. Pet. Tech. **25**, 74.
- Levinstein, M., M. S. Shur, and E. L. Efros, 1976, Sov. Phys. JETP **42**, 1120.
- Li, Y., and N. C. Wardlaw, 1986a, J. Colloid Interface Sci. **109**, 461.
- Li, Y., and N. C. Wardlaw, 1986b, J. Colloid Interface Sci. **109**, 473.
- Li, Y., W. G. Laidlaw, and N. C. Wardlaw, 1986, Adv. Colloid Interface Sci. **26**, 1.
- Liang, S., 1986, Phys. Rev. A **33**, 2663.
- Liao, K. H., and A. E. Scheidegger, 1969, Bull. Int. Assoc. Sci. Hydrol. **12**, 137.

- Lichtner, P. C., E. H. Oelkers, and H. C. Helgeson, 1986, J. Geophys. Res. **91**, 7531.
- Lin, C., and M. H. Cohen, 1982, J. Appl. Phys. **53**, 4152.
- Lin, C., and J. Hamasaki, 1983, J. Sediment. Pet. **53**, 670.
- Lin, C., G. Pirei, and M. Vermette, 1986, J. Geophys. Res. **91**, 2173.
- Lin, C.-Y., and J. C. Slattery, 1982, AIChE J. **28**, 311.
- Lipsicas, M., J. R. Banavar, and J. Willemsen, 1986, Appl. Phys. Lett. **48**, 1544.
- Long, J. C. S., and D. Billaux, 1987, Water Resour. Res. **23**, 1201.
- Long, J. C. S., P. Gilmour, and P. A. Witherspoon, 1985, Water Resour. Res. **21**, 1105.
- Long, J. C. S., K. Karasaki, A. Davey, J. Peterson, M. Landsfeld, J. Kemeny, and S. Martel, 1991, Int. J. Rock Mech. Min. Sci. Geomech. Abstr. **28**, 121.
- Long, J. C. S., J. S. Remer, C. R. Wilson, and P. A. Witherspoon, 1982, Water Resour. Res. **18**, 645.
- Long, J. C. S., and P. A. Witherspoon, 1985, J. Geophys. Res. **90**, 3087.
- Lowell, R. P., 1989, Water Resour. Res. **25**, 774.
- Lucido, G., R. Triolo, and E. Caponetti, 1988, Phys. Rev. B **38**, 9031.
- Lumley, J. L., and H. A. Panofsky, 1974, *The Structure of Atmospheric Turbulence* (Wiley, New York).
- Madden, T. R., 1976, Geophysics **41**, 1104.
- Madden, T. R., 1983, J. Geophys. Res. **88**, 585.
- Mahaffey, J. L., W. M. Rutherford, and C. S. Mathews, 1966, Soc. Pet. Eng. J. **6**, 73.
- Maier, R., and W. G. Laidlaw, 1990, Transp. Porous Media **5**, 421.
- Maier, R., and W. G. Laidlaw, 1991a, J. Stat. Phys. **62**, 269.
- Maier, R., and W. G. Laidlaw, 1991b, Math. Geol. **23**, 87.
- Måløy, K. J., F. Boger, J. Feder, T. Jøssang, and P. Meakin, 1987, Phys. Rev. A **36**, 318.
- Måløy, K. J., F. Boger, J. Feder, and T. Jøssang, 1985, Phys. Rev. Lett. **55**, 2688.
- Mandelbrot, B. B., 1983, *The Fractal Geometry of Nature* (Freeman, San Francisco).
- Mandelbrot, B. B., 1985, Phys. Scr. **32**, 257.
- Mandelbrot, B. B., and J. W. van Ness, 1968, SIAM Rev. **10**, 422.
- Marle, C. M., 1967, Rev. Inst. Fr. Pet. **22**, 1471.
- Marle, C. M., 1981, *Multiphase Flow in Porous Media* (Gulf Publishing Co., Houston, Texas).
- Marle, C. M., P. Simandoux, J. Pacsirsky, and C. Gaulier, 1967, Rev. Inst. Fr. Pet. **22**, 272.
- Martin, J. C., 1968, Soc. Pet. Eng. J. **8**, 370.
- Martys, N., M. Cieplak, and M. O. Robbins, 1991, Phys. Rev. Lett. **66**, 1058.
- Mason, G., 1982, J. Colloid Interface Sci. **88**, 36.
- Mason, G., 1983, Proc. R. Soc. London, Ser. A **390**, 47.
- Mason, G., 1988, Proc. R. Soc. London, Ser. A **415**, 453.
- Matheron, G., 1967, Rev. Inst. Fr. Pet. **22**, 443.
- Matheron, G., and G. de Marsily, 1980, Water Resour. Res. **16**, 901.
- Mathews, J. L., A. S. Emanuel, and K. A. Edwards, 1989, J. Pet. Tech. **41**, 1136.
- Mattax, C. C., and J. R. Kyte, 1961, Oil Gas J. **59**, 115.
- Maxwell-Garnett, J. C., 1904, Philos. Trans. R. Soc. London **203**, 385.
- McCaffery, F. G., 1972, J. Can. Pet. Tech. **11**, 26.
- McCaffery, F. G., and D. W. Bennion, 1974, J. Can. Pet. Tech. **13**, 42.
- McCall, K. R., D. L. Johnson, and R. A. Guyer, 1991, Phys. Rev. B **44**, 7344.
- McLachlan, D. S., M. B. Button, S. R. Adams, V. M. Gorringe, J. D. Keen, J. Muoe, and E. Wedepohl, 1987, Geophysics **52**, 194.
- McNamara, G., and G. Zanetti, 1988, Phys. Rev. Lett. **61**, 2332.
- Meakin, P., 1986, Phys. Rev. A **33**, 4199.
- Meakin, P., 1987, Phys. Rev. A **36**, 2833.
- Meakin, P., 1988, in *Phase Transitions and Critical Phenomena*, Vol. 12, edited by C. Domb and J. L. Lebowitz (Academic, London), p. 335.
- Meakin, P., 1991, Physica A **173**, 305.
- Meakin, P., F. Family, and T. Vicsek, 1987, J. Colloid Interface Sci. **117**, 394.
- Meakin, P., M. Murat, A. Aharony, J. Feder, and T. Jøssang, 1989, Physica A **155**, 1.
- Melrose, J. C., 1965, Soc. Pet. Eng. J. **5**, 259.
- Melrose, J. C., 1968, Ind. Eng. Chem. **60**, 53.
- Melrose, J. C., 1982, paper SPE 10971, presented at the 57th Annual Conference of the Society of Petroleum Engineers, New Orleans, Louisiana.
- Melrose, J. C., 1988, paper SPE 18331, presented at the 63rd Annual Conference of the Society of Petroleum Engineers, Houston, Texas.
- Melrose, J. C., and C. F. Brandner, 1974, Can. J. Pet. Tech. **13**, 54.
- Mendelson, K. S., 1982, J. Appl. Phys. **53**, 6465.
- Mendelson, K. S., 1986, Phys. Rev. B **34**, 6503.
- Mendelson, K. S., and M. H. Cohen, 1982, Geophysics **47**, 257.
- Meneveau, C., and K. R. Sreenivasan, 1987, Phys. Rev. Lett. **59**, 1424.
- Mercado, A., 1967, International Association Sci. Hydrol. Publication 72 (Int. Assoc. Hydrol. Sci., Gentbrugge, Belgium), p. 23.
- Meyer, H. I., 1953, J. Appl. Phys. **24**, 510.
- Mildner, D. F. R., R. Rezvani, P. L. Hall, and R. L. Brost, 1986, Appl. Phys. Lett. **48**, 1314.
- Miller, A., and E. Abrahams, 1960, Phys. Rev. **120**, 745.
- Milton, G. W., 1984, in *Physics and Chemistry of Porous Media*, edited by D. L. Johnson and P. N. Sen, AIP Conference Proceedings 107 (AIP, New York), p. 66.
- Mitescu, C. D., and J. Roussenq, 1976, C. R. Acad. Sci. **283**, 999.
- Mizell, S. A., A. L. Gutjahr, and L. W. Gelhar, 1982, Water Resour. Res. **18**, 1053.
- Mohanty, K. K., 1981, Ph.D. thesis (University of Minnesota, Minneapolis).
- Mohanty, K. K., H. T. Davis, and L. E. Scriven, 1980, paper SPE 9406, presented at the 55th Annual Conference of the Society of Petroleum Engineers, Dallas, Texas.
- Mohanty, K. K., H. T. Davis, and L. E. Scriven, 1987, SPE Reservoir Eng. **2**, 113.
- Mohanty, K. K., and S. J. Salter, 1982, paper SPE 11018, presented at the 57th Annual Conference of the Society of Petroleum Engineers, New Orleans, Louisiana.
- Molz, F. J., O. Güven, and J. G. Melville, 1983, Ground Water **21**, 715.
- Morgan, J. T., and D. T. Gordon, 1970, J. Pet. Tech. **22**, 1194.
- Morrow, N. R., 1970, Ind. Eng. Chem. **62**, 32.
- Morrow, N. R., 1976, J. Can. Pet. Tech. **15**, 49.
- Morrow, N. R., 1991, in *Interfacial Phenomena in Petroleum Recovery*, edited by N. R. Morrow (Marcell Dekker, New York), p. 1.
- Morrow, N. R., and F. G. McCaffery, 1978, in *Wetting, Spread-*

- ing, and Adhesion*, edited by G. F. Padday (Academic, New York), p. 289.
- Mukhopadhyay, S., and M. Sahimi, 1992, paper SPE 24043, presented at the California Regional Meeting of the Society of Petroleum Engineers, April 1–3, Bakersfield, California.
- Mungan, N., 1966, Soc. Pet. Eng. J. **6**, 247.
- Murat, M., and A. Aharonov, 1986, Phys. Rev. Lett. **57**, 1875.
- Naar, J., G. R. Wygal, and J. H. Henderson, 1962, Soc. Pet. Eng. J. **2**, 13.
- Nakamo, Y., and J. W. Evans, 1983, J. Chem. Phys. **78**, 2568.
- Neimark, A. V., 1984a, Colloid J. (USSR) **46**, 727.
- Neimark, A. V., 1984b, Colloid J. (USSR) **46**, 1158.
- Neretnitsk, I., 1980, J. Geophys. Res. B **85**, 4379.
- Neumann, S. P., 1977, Acta Mech. **25**, 153.
- Neumann, S. P., 1990, Water Resour. Res. **26**, 887.
- Ng, K. M., and A. C. Payatakes, 1980, AIChE J. **26**, 419.
- Nicholson, D., 1968, Trans. Faraday Soc. **64**, 3416.
- Nicholson, D., and J. H. Petropoulos, 1971, J. Phys. D **4**, 181.
- Nicholson, D., and J. H. Petropoulos, 1975, J. Phys. D **8**, 1430.
- Nicholson, D., and J. H. Petropoulos, 1977, J. Phys. D **10**, 2423.
- Nickel, B., and D. Wilkinson, 1983, Phys. Rev. Lett. **51**, 71.
- Niemeyer, L., L. Pietronero, and H. J. Weismann, 1984, Phys. Rev. Lett. **52**, 1033.
- Nimmo, J. R., and K. C. Akstin, 1988, Solid Sci. Soc. Am. J. **52**, 303.
- Nitsche, L. C., and H. Brenner, 1989, Arch. Ration. Mech. Anal. **107**, 225.
- Nittmann, J., G. Daccord, and H. E. Stanley, 1985, Nature **314**, 141.
- Nobles, M. A., and H. B. Janzen, 1958, Pet. Trans. AIME **213**, 356.
- Nolen-Hoeksema, R. C., and R. B. Gordon, 1987, Int. J. Rock Mech. Min. Sci. Geomech. Abstr. **24**, 135.
- Nolte, D. D., L. J. Pyrak-Nolte, and N. G. W. Cook, 1989, Pure Appl. Geophys. **131**, 111.
- Noorishad, J., and M. Mehran, 1982, Water Resour. Res. **18**, 588.
- Novak, C. F., R. S. Schechter, and L. W. Lake, 1989, AIChE J. **35**, 1057.
- Novosad, J., E. Inescu-Forniciov, and K. Mannhardt, 1984, paper CIM 843542, presented at the 35th Annual Conference of the Society of CIM, Calgary.
- Novy, R. A., P. G. Toledo, H. T. Davis, and L. E. Scriven, 1989, Chem. Eng. Sci. **44**, 1785.
- Nyame, B. K., and J. M. Ilbston, 1980, in 7th International Symposium on the Chemistry of Cement Paste, Paris, Vol. 3: VI, p. 181.
- Odagaki, T., and M. Lax, 1981, Phys. Rev. B **24**, 5284.
- Odeh, A. S., 1959, Trans. AIME **216**, 346.
- Odeh, A. S., 1965, Soc. Pet. Eng. J. **5**, 60.
- Oger, L., J. P. Troadec, D. Bideau, J. A. Dodds, and M. Powell, 1986, Powder Tech. **46**, 121.
- Ogandzhanjanc, V. G., 1960, Izv. Akad. Nauk USSR **20**, 129.
- Okubo, P. G., and K. Aki, 1987, J. Geophys. Res. B **92**, 345.
- Orford, J. D., and W. B. Whalley, 1983, Sedimentology **30**, 655.
- O'Shaughnessy, B., and I. Procaccia, 1985, Phys. Rev. Lett. **54**, 455.
- Outmans, H. D., 1962, Soc. Pet. Eng. J. **2**, 165.
- Owen, J. E., 1952, Trans. AIME **195**, 169.
- Owens, W. W., and D. L. Archer, 1971, J. Pet. Tech. **23**, 873.
- Oxaal, U., 1991, Phys. Rev. A **44**, 5038.
- Pakula, R. J., and R. A. Greenkorn, 1971, AIChE J. **19**, 1265.
- Palciauskas, V. V., and P. A. Domenico, 1976, Geol. Soc. Am. Bull. **87**, 207.
- Pandey, R. B., D. Stauffer, A. Margolina, and J. G. Zabolitzky, 1984, J. Stat. Phys. **34**, 427.
- Park, C.-W., S. Gorrell, and G. M. Homsy, 1984, J. Fluid Mech. **141**, 257.
- Parlar, M., and Y. C. Yortsos, 1988, J. Colloid Interface Sci. **124**, 162.
- Parlar, M., and Y. C. Yortsos, 1989, J. Colloid Interface Sci. **132**, 425.
- Parsons, R. W., 1966, Soc. Pet. Eng. J. **6**, 126.
- Passioura, J. B., 1971, Soil Sci. **111**, 339.
- Paterson, L., 1981, J. Fluid Mech. **113**, 513.
- Paterson, L., 1983, Int. J. Hydrogen Energy **8**, 53.
- Paterson, L., 1984, Phys. Rev. Lett. **52**, 1621.
- Paterson, L., 1985, Phys. Fluids **28**, 26.
- Paterson, L., V. Hornof, and G. H. Neale, 1982, Powder Technol. **33**, 265.
- Paterson, L., V. Hornof, and G. H. Neale, 1984a, Rev. Inst. Fr. Pet. **39**, 517.
- Paterson, L., V. Hornof, and G. H. Neale, 1984b, Soc. Pet. Eng. J. **24**, 325.
- Pathak, P., H. T. Davis, and L. E. Scriven, 1982, paper SPE 11016, presented at the 57th Annual Conference of the Society of Petroleum Engineers, New Orleans, Louisiana.
- Patsoules, M. G., and J. C. Cripps, 1983, Energy Sources **7**, 15.
- Payandeh, B., 1980, Riv. Nuovo Cimento **3**, 1.
- Payatakes, A. C., 1982, Annu. Rev. Fluid Mech. **14**, 365.
- Payatakes, A. C., and M. M. Dias, 1984, Rev. Chem. Eng. **2**, 85.
- Payatakes, A. C., K. M. Ng, and R. W. Flumerfelt, 1980, AIChE J. **26**, 430.
- Peaceman, D. W., and H. H. Rachford, Jr., 1962, Soc. Pet. Eng. J. **2**, 327.
- Perkins, T. K., and O. C. Johnston, 1963, Soc. Pet. Eng. J. **3**, 70.
- Perkins, T. K., and O. C. Johnston, 1969, Soc. Pet. Eng. J. **9**, 39.
- Perkins, T. K., O. C. Johnston, and R. N. Hoffman, 1965, Soc. Pet. Eng. J. **5**, 301.
- Perrine, R. L., 1961, Soc. Pet. Eng. J. **1**, 17.
- Perrine, R. L., 1963, Soc. Pet. Eng. J. **3**, 205.
- Peters, E. J., and D. L. Flock, 1981, Soc. Pet. Eng. J. **21**, 249.
- Peters, E. J., W. H. Broman, and J. A. Broman, 1984, paper SPE 13167, presented at the 59th Annual Conference of the Society of Petroleum Engineers, Houston, Texas.
- Pfeifer, P., and D. Avnir, 1983, J. Chem. Phys. **79**, 3558.
- Pfeifer, P., D. Avnir, and D. Farin, 1984, J. Stat. Phys. **36**, 699.
- Philip, J. R., 1957, Solid Science **83**, 345.
- Philip, J. R., 1986, Transp. Porous Media **1**, 319.
- Pickell, J. J., B. F. Swanson, and W. B. Hickman, 1966, Soc. Pet. Eng. J. **6**, 55.
- Pickens, J. F., and G. E. Grisak, 1981, Water Resour. Res. **17**, 1191.
- Piggott, A. R., and D. Elsworth, 1989, Water Resour. Res. **25**, 457.
- Pike, G. E., and C. H. Seager, 1974, Phys. Rev. B **10**, 1421.
- Pis'men, L. M., 1972, Dokl. Akad. Nauk SSSR **207**, 657.
- Pittmann, E. D., 1984, in *Physics and Chemistry of Porous Media*, edited by D. L. Johnson and P. N. Sen (AIP, New York), p. 1.
- Plumb, O. A., and S. Whitaker, 1988a, Water Resour. Res. **24**, 913.
- Plumb, O. A., and S. Whitaker, 1988b, Water Resour. Res. **24**, 927.
- Pokorny, M., C. M. Newman, and D. Meiron, 1990, J. Phys. A **23**, 1431.
- Pollard, D. D., 1976, Geophys. Res. Lett. **3**, 513.
- Pomeau, Y., and J. Vannimenus, 1985, J. Colloid Interface Sci.

- 104**, 447.
- Porod, G., 1951, *Kolloidn. Zh.* **124**, 83.
- Poulton, M. M., N. Mojtabai, and I. W. Farmer, 1990, *Int. J. Rock Mech. Min. Sci. Geomech. Abstr.* **27**, 219.
- Prager, S., 1961, *Phys. Fluids* **4**, 1477.
- Press, W. H., B. P. Flannery, S. A. Teukolsky, and W. T. Vetterling, 1986, *Numerical Recipes* (Cambridge University Press, Cambridge).
- Pruess, K., G. S. Bodvarsson, and V. Stefansson, 1983, in *Proceedings of Sixteenth Stanford Geothermal Workshop*, Stanford University (Stanford University Press, Stanford, CA).
- Pruess, K., and Y. V. Tsang, 1990, *Water Resour. Res.* **26**, 1915.
- Qian, Y. H., D. d'Humières, and P. Lallemand, 1992, *Europhys. Lett.* **17**, 479.
- Quintard, M., and S. Whitaker, 1988, *Transp. Porous Media* **3**, 357.
- Quintard, M., and S. Whitaker, 1990a, *Transp. Porous Media* **5**, 341.
- Quintard, M., and S. Whitaker, 1990b, *Transp. Porous Media* **5**, 429.
- Raats, P. A. C., and A. Klute, 1968, *Soil Sci. Soc. Am. J.* **32**, 452.
- Rachford, H. H., 1964, *Soc. Pet. Eng. J.* **4**, 249.
- Raimondi, P., and M. A. Torcaso, 1964, *Soc. Pet. Eng. J.* **4**, 49.
- Ramakrishnan, T. S., and D. T. Wasan, 1984, paper SPE 12693, presented at the 4th SPE/DOE Symposium on Enhanced Oil Recovery, Tulsa, Oklahoma.
- Ramakrishnan, T. S., and D. T. Wasan, 1986, *Int. J. Multiphase Flow* **12**, 357.
- Rao, P. S. C., D. E. Ralston, R. E. Jessup, and J. M. Davidson, 1980, *Soil Sci. Soc. Am. J.* **44**, 1139.
- Raphael, E., and P. G. de Gennes, 1989, *J. Chem. Phys.* **90**, 7577.
- Reed, R. L., and R. J. Healy, 1977, in *Improved Oil Recovery by Surfactant and Polymer Flooding*, edited by D. O. Shah and R. S. Schechter (Academic, New York).
- Rem, P., and J. Somers, 1989, in *Discrete Kinetic Theory, Lattice-Gas Dynamics, and Foundations of Hydrodynamics*, edited by R. Monaco (World Scientific, Singapore), p. 268.
- Reynolds, P. J., H. E. Stanley, and W. Klein, 1980, *Phys. Rev. B* **21**, 1223.
- Reznik, A. A., R. M. Enick, and S. B. Panuelker, 1984, *Soc. Pet. Eng. J.* **24**, 643.
- Richardson, J. G., J. G. Kerver, J. A. Hafford, and J. Osoba, 1952, *Trans. AIME* **195**, 187.
- Rillaerts, E., and P. Joos, 1980, *Chem. Eng. Sci.* **35**, 883.
- Rink, M., and J. R. Schopper, 1968, *Geophys. Prospect.* **16**, 277.
- Ritter, H. L., and L. C. Drake, 1945, *Ind. Eng. Chem.* **17**, 782.
- Robbins, M. O., and J. F. Joanny, 1987, *Europhys. Lett.* **3**, 729.
- Roberts, J. N., and L. M. Schwartz, 1985, *Phys. Rev. B* **31**, 5990.
- Robinson, P. C., 1984a, Ph.D. thesis (St. Catherine's College, Oxford University).
- Robinson, P. C., 1984b, *J. Phys. A* **17**, 2823.
- Roman, H. E., 1990, *J. Stat. Phys.* **58**, 375.
- Romm, E. S., 1966, *Fluid Flow in Fractured Rocks* (in Russian) (Nedra Publishing House, Moscow; English Translation, W. R. Blake, Bartlesville, OK, 1972).
- Roof, J. G., 1970, *Soc. Pet. Eng. J.* **10**, 85.
- Rose, H. E., 1945, *Proc. Inst. Mech. Eng. Appl. Mech.* **153**, 141.
- Rose, W. D., 1957, *Illinois State Geol. Surv. Circ.* **237**.
- Rose, W. D., 1972, in *Proceedings of the Second International Conference on Fundamentals of Transport Phenomena in Porous Media*, edited by D. E. Erlick (International Association of Hydraulic Research, Guelph, Canada), p. 158.
- Rose, W. D., and W. A. Bruce, 1949, *Trans. AIME* **186**, 127.
- Rose, W. D., and P. A. Witherspoon, 1956, *Illinois State Geol. Surv. Circ.* **224**.
- Ross, B., 1986, *Water Resour. Res.* **22**, 823.
- Rothman, D. H., 1988, *Geophysics* **53**, 509.
- Rothman, D. H., 1990, *J. Geophys. Res.* **95**, 8663.
- Rothman, D. H., and J. M. Keller, 1988, *J. Stat. Phys.* **52**, 1119.
- Rothman, D. H., and S. Zaleski, 1989, *J. Phys. (Paris)* **50**, 2161.
- Roux, J.-N., and D. Wilkinson, 1988, *Phys. Rev. A* **37**, 3921.
- Roux, S., and E. Guyon, 1989, *J. Phys. A* **22**, 3693.
- Roux, S., C. Mitescu, E. Charlaix, and C. Baudet, 1986, *J. Phys. A* **19**, L687.
- Rubinstein, J., and S. Torquato, 1989, *J. Fluid Mech.* **206**, 25.
- Rubio, M. A., C. A. Edwards, A. Dougherty, and J. P. Gollub, 1989, *Phys. Rev. Lett.* **63**, 1685.
- Ryan, D., R. G. Carbonell, and S. Whitaker, 1980, *Chem. Eng. Sci.* **35**, 10.
- Saeger, R. B., L. E. Scriven, and H. T. Davis, 1991, *Phys. Rev. A* **44**, 5087.
- Saffman, P. G., 1959, *J. Fluid Mech.* **6**, 321.
- Saffman, P. G., 1960, *J. Fluid Mech.* **7**, 194.
- Saffman, P. G., 1986, *J. Fluid Mech.* **173**, 73.
- Saffman, P. G., and G. I. Taylor, 1958, *Proc. R. Soc. London, Ser. A* **245**, 312.
- Sahimi, M., 1984, *J. Phys. C* **17**, 3957.
- Sahimi, M., 1985, *Phys. Rev. Lett.* **55**, 1698.
- Sahimi, M., 1987, *J. Phys. A* **20**, L1293.
- Sahimi, M., 1988a, *Chem. Eng. Commun.* **64**, 177.
- Sahimi, M., 1988b, *Chem. Eng. Sci.* **43**, 2981.
- Sahimi, M., 1991, *Phys. Rev. A* **43**, 5367.
- Sahimi, M., 1993a, *AICHE J.* **39**, 369.
- Sahimi, M., 1993b, *Applications of Percolation Theory* (Taylor and Francis, London).
- Sahimi, M., and S. Arbabi, 1991, *J. Stat. Phys.* **62**, 453.
- Sahimi, M., H. T. Davis, and L. E. Scriven, 1983, *Chem. Eng. Comm.* **23**, 329.
- Sahimi, M., H. T. Davis, and L. E. Scriven, 1985, *Soc. Pet. Eng. J.* **25**, 235.
- Sahimi, M., G. R. Gavalas, and T. T. Tsotsis, 1990, *Chem. Eng. Sci.* **45**, 1443.
- Sahimi, M., and J. D. Goddard, 1986, *Phys. Rev. B* **33**, 7848.
- Sahimi, M., A. A. Heiba, B. D. Hughes, H. T. Davis, and L. E. Scriven, 1982, paper SPE 10969, presented at the 57th Annual Meeting of the Society of Petroleum Engineers, New Orleans, Louisiana.
- Sahimi, M., A. A. Heiba, H. T. Davis, and L. E. Scriven, 1986, *Chem. Eng. Sci.* **41**, 2123.
- Sahimi, M., and B. D. Hughes, 1993, *Water Resour. Res.* (to be published).
- Sahimi, M., B. D. Hughes, L. E. Scriven, and H. T. Davis, 1983a, *Phys. Rev. B* **28**, 307.
- Sahimi, M., B. D. Hughes, L. E. Scriven, and H. T. Davis, 1983b, *J. Chem. Phys.* **78**, 6849.
- Sahimi, M., B. D. Hughes, L. E. Scriven, and H. T. Davis, 1986, *Chem. Eng. Sci.* **41**, 2103.
- Sahimi, M., and A. O. Imdadm, 1988, *J. Phys. A* **21**, 3833.
- Sahimi, M., and A. O. Imdadm, 1991, *Phys. Rev. Lett.* **66**, 1169.
- Sahimi, M., and V. L. Jue, 1989, *Phys. Rev. Lett.* **62**, 629.
- Sahimi, M., and M. A. Knackstedt, 1993, *J. Phys. A* (to be published).
- Sahimi, M., M. C. Robertson, and C. G. Sammis, 1993, *Phys. Rev. Lett.* **70**, 2186.

- Sahimi, M., L. E. Scriven, and H. T. Davis, 1984, *J. Phys. C* **17**, 1941.
- Sahimi, M., and H. Siddiqui, 1987, *J. Phys. A* **20**, L89.
- Sahimi, M., and D. Stauffer, 1991, *Chem. Eng. Sci.* **46**, 2225.
- Sahimi, M., and B. N. Taylor, 1991, *J. Chem. Phys.* **95**, 6749.
- Sahimi, M., and T. T. Tsotsis, 1985, *J. Catal.* **96**, 552.
- Sahimi, M., and Y. C. Yortsos, 1985, *Phys. Rev. A* **32**, 3762.
- Salathiel, R. A., 1973, *J. Pet. Tech.* **25**, 1216.
- Salter, S. J., and K. K. Mohanty, 1982, paper SPE 11017, presented at the 57th Annual Fall Meeting of the Society of Petroleum Engineers, New Orleans, Louisiana.
- Sammis, C. G., G. C. P. King, and R. Beigel, 1985, *Pure Appl. Geophys.* **125**, 777.
- Sangani, A. S., and A. Acrivos, 1982a, *Int. J. Multiphase Flow* **8**, 193.
- Sangani, A. S., and A. Acrivos, 1982b, *Int. J. Multiphase Flow* **8**, 343.
- Sapoval, B., M. Rosso, and J. F. Gouyet, 1985, *J. Phys. (Paris) Lett.* **46**, L149.
- Sarkar, S. K., 1985, *Phys. Rev. A* **31**, 3468.
- Sarkar, S. K., and M. H. Jensen, 1987, *Phys. Rev. A* **35**, 1877.
- Schaefer, D. W., J. E. Martin, P. Wiltzuis, and D. S. Cannell, 1984, *Phys. Rev. Lett.* **52**, 2371.
- Scheidegger, A. E., 1954, *J. Appl. Phys.* **25**, 994.
- Scheidegger, A. E., 1965, *Bull. Int. Assoc. Sci. Hydrol.* **10**, 38.
- Scheidegger, A. E., 1974, *The Physics of Flow Through Porous Media*, 3rd ed. (University of Toronto, Toronto).
- Scheidegger, A. E., and E. F. Johnson, 1961, *Can. J. Phys.* **39**, 326.
- Scher, H., and R. Zallen, 1970, *J. Chem. Phys.* **53**, 3759.
- Schmidt, E. J., K. K. Velasco, and A. M. Nur, 1986, *J. Appl. Phys.* **59**, 2788.
- Schmidt, V., and D. A. McDonald, 1979, *Society of Economic Paleontologists and Mineralogists Special Publication No. 26*, p. 209.
- Scholz, C. H., and B. B. Mandelbrot, 1989, Eds., *Fractals in Geophysics* (Birkhäuser, Basel).
- Schowalter, W. R., 1965, *AIChE J.* **11**, 99.
- Schwartz, F. W., 1977, *Water Resour. Res.* **13**, 743.
- Schwartz, F. W., L. Smith, and A. S. Crowe, 1983, *Water Resour. Res.* **19**, 1253.
- Schwartz, L. M., and J. R. Banavar, 1989, *Phys. Rev. B* **39**, 11965.
- Schwartz, L. M., J. R. Banavar, and B. I. Halperin, 1989, *Phys. Rev. B* **40**, 9155.
- Schwartz, L. M., and S. Kimminau, 1987, *Geophysics* **52**, 1402.
- Schwartz, L. M., P. N. Sen, and D. L. Johnson, 1989, *Phys. Rev. B* **40**, 2450.
- Seaton, N. A., 1991, *Chem. Eng. Sci.* **46**, 1895.
- Seeburger, D. A., and A. Nur, 1984, *J. Geophys. Res.* **89**, 527.
- Sen, A. K., and S. Torquato, 1988, *J. Chem. Phys.* **89**, 3799.
- Sen, P. N., 1981, *Appl. Phys. Lett.* **39**, 667.
- Sen, P. N., 1984, *Geophysics* **49**, 586.
- Sen, P. N., C. Scala, and M. H. Cohen, 1981, *Geophysics* **46**, 781.
- Sevik, E. M., P. A. Monson, and J. M. Ottino, 1988, *J. Chem. Phys.* **88**, 1198.
- Shankland, T. J., and H. S. Waff, 1974, *J. Geophys. Res.* **79**, 4863.
- Shante, V. K. S., 1977, *Phys. Rev. B* **16**, 2597.
- Shante, V. K. S., and S. Kirkpatrick, 1971, *Adv. Phys.* **20**, 325.
- Shaw, T. M., 1987, *Phys. Rev. Lett.* **59**, 1671.
- Sheffield, R. E., and A. B. Metzner, 1976, *AIChE J.* **22**, 736.
- Sheng, P., 1980, *Phys. Rev. B* **22**, 6364.
- Sheng, P., 1990, *Phys. Rev. B* **41**, 4507.
- Sheng, P., and M.-Y. Zhou, 1988, *Phys. Rev. Lett.* **61**, 1591.
- Sherwood, J. D., 1986, *J. Phys. A* **19**, L195.
- Sherwood, J. D., and J. Nittmann, 1986, *J. Phys. (Paris)* **47**, 15.
- Shraiman, B. I., and D. Bensimon, 1984, *Phys. Rev. A* **30**, 2840.
- Siddiqui, H., and M. Sahimi, 1990a, *Chem. Eng. Sci.* **45**, 163.
- Siddiqui, H., and M. Sahimi, 1990b, *J. Phys. A* **23**, L497.
- Siddiqui, H., and M. Sahimi, 1983, *Water Resour. Res.* (to be published).
- Simon, R., and F. J. Kelsey, 1971, *Soc. Pet. Eng. J.* **11**, 99.
- Simon, R., and F. J. Kelsey, 1972, *Soc. Pet. Eng. J.* **12**, 345.
- Sing, K. S. W., D. H. Everett, R. A. W. Haul, L. Moscou, R. A. Pierotti, J. Rouquerol, and T. Siemieniwska, 1985, *Pure Appl. Chem.* **57**, 603.
- Singhal, A. K., and W. H. Somerton, 1977, *J. Inst. Fr. Pet.* **32**, 897.
- Sinha, S. K., T. Freloft, and J. Kjems, 1984, in *Kinetics of Aggregation and Gelation*, edited by F. Family and D. P. Landau (Elsevier, New York), p. 87.
- Slattery, J. C., 1967, *AIChE J.* **13**, 1066.
- Slattery, J. C., 1969, *AIChE J.* **15**, 866.
- Slobod, R. L., and R. A. Thomas, 1963, *Soc. Pet. Eng. J.* **3**, 9.
- Smith, D. M., and D. G. Huizenga, 1984, in *Proceedings of the 10th IASTED Symposium in Applied Modelling and Simulation* (Acta Press, Calgary, Canada), p. 13.
- Smith, L., and R. A. Freeze, 1979, *Water Resour. Res.* **15**, 1543.
- Smith, L., and F. W. Schwartz, 1980, *Water Resour. Res.* **16**, 303.
- Smith, L., and F. W. Schwartz, 1981a, *Water Resour. Res.* **17**, 351.
- Smith, L., and F. W. Schwartz, 1981b, *Water Resour. Res.* **17**, 1463.
- Smith, L., and F. W. Schwartz, 1984, *Water Resour. Res.* **20**, 1241.
- Snow, D. T., 1969, *Water Resour. Res.* **5**, 1273.
- Somers, J. A., and P. C. Rem, 1989, in *Discrete Kinematic Theory, Lattice Gas Dynamics, and Foundation of Hydrodynamics*, edited by R. Monaco (World Scientific, Singapore), p. 268.
- Sorbie, K. S., R. M. Swat, and T. C. Rowe, 1987, *Trans. AIME, SPE 16706*.
- Stalkup, F. I., 1984, *Miscible Displacement* (Society of Petroleum Engineers, Dallas).
- Stanley, H. E., and P. Meakin, 1988, *Nature* **335**, 405.
- Stanley, H. E., P. J. Reynolds, S. Redner, and F. Family, 1982, in *Real-Space Renormalization*, edited by T. W. Burkhardt and J. M. J. van Leeuwen (Springer, Berlin), p. 169.
- Stauffer, D., and A. Aharony, 1992, *Introduction to Percolation Theory*, 2nd edition (Taylor and Francis, London).
- Stauffer, D., A. Coniglio, and M. Adam, 1982, *Adv. Polymer Sci.* **44**, 103.
- Stinchcombe, R. B., 1974, *J. Phys. C* **7**, 201.
- Stinchcombe, R. B., and B. P. Watson, 1976, *J. Phys. C* **9**, 3221.
- Stockmayer, W. H., 1943, *J. Chem. Phys.* **11**, 45.
- Stockton, A. D., R. P. Thomas, R. H. Chapman, and H. Dykstra, 1984, *J. Pet. Tech.* **36**, 2137.
- Stokes, J. P., M. J. Higgins, A. P. Kushnik, S. Bhattacharya, and M. O. Robbins, 1990, *Phys. Rev. Lett.* **65**, 1885.
- Stokes, J. P., A. P. Kushnik, and M. O. Robbins, 1988, *Phys. Rev. Lett.* **60**, 1386.
- Stokes, J. P., D. A. Weitz, J. P. Gollub, A. Dougherty, M. O. Robbins, P. M. Chaikin, and H. M. Lindsay, 1986, *Phys. Rev. Lett.* **57**, 1718.
- Straley, C., A. Mateson, S. Feng, L. M. Schwartz, W. E. Kenyon, and J. R. Banavar, 1987, *Appl. Phys. Lett.* **51**, 1146.

- Straley, J. P., 1977a, *J. Phys. C* **10**, 1903.
- Straley, J. P., 1977b, *J. Phys. C* **10**, 3009.
- Stroud, D., 1975, *Phys. Rev. B* **12**, 3368.
- Succi, S., E. Foti, and F. Higuera, 1989, *Europhys. Lett.* **10**, 433.
- Sudicky, E. A., and J. A. Cherry, 1979, *Water Pollut. Res. Can.* **14**, 1.
- Sudicky, E. A., J. A. Cherry, and E. O. Frind, 1985, *Water Resour. Res.* **21**, 1035.
- Sudicky, E. A., and E. O. Frind, 1982, *Water Resour. Res.* **18**, 1634.
- Swanson, B. F., 1981, *J. Pet. Tech.* **33**, 2498.
- Szep, J., J. Cresti, and J. Kertész, 1985, *J. Phys. A* **18**, L413.
- Tabeling, P., and A. Libchaber, 1986, *Phys. Rev. A* **33**, 794.
- Taber, J. J., 1969, *Soc. Pet. Eng. J.* **9**, 3.
- Talash, A. W., 1976, paper SPE 5810, presented at the Improved Recovery Symposium of the Society of Petroleum Engineers, Tulsa, Oklahoma.
- Tan, C.-T., and G. M. Homsy, 1986, *Phys. Fluids* **29**, 3549.
- Tan, C.-T., and G. M. Homsy, 1987, *Phys. Fluids* **30**, 1239.
- Tan, C.-T., and G. M. Homsy, 1992, *Phys. Fluids A* **4**, 1099.
- Tang, C., 1985, *Phys. Rev. A* **31**, 1977.
- Tang, D. H., E. O. Frind, and E. A. Sudicky, 1981, *Water Resour. Res.* **17**, 555.
- Tang, D. H., F. W. Schwartz, and L. Smith, 1982, *Water Resour. Res.* **18**, 231.
- Tang, L.-H., and H. Leschhorn, 1992, *Phys. Rev. A* **45**, R8309.
- Tao, R., M. A. Novotny, and K. Kaski, 1988, *Phys. Rev. A* **8**, 1019.
- Tartar, L., 1980, Appendix 2 of *Nonhomogeneous Media and Vibration Theory*, Lecture Notes in Physics **127** (Springer, Berlin).
- Taylor, G. I., 1953, *Proc. R. Soc. London, Ser. A* **219**, 186.
- Tchalenko, J. S., 1970, *Geol. Soc. Am. Bull.* **81**, 1625.
- Thomas, L. D., T. N. Dixon, and R. G. Pierson, 1983, *Soc. Pet. Eng. J.* **23**, 42.
- Thompson, A. H., 1991, *Annu. Rev. Earth Planet. Sci.* **19**, 237.
- Thompson, A. H., A. J. Katz, and C. E. Krohn, 1987, *Adv. Phys.* **36**, 652.
- Thompson, A. H., A. J. Katz, and R. A. Rashke, 1987, *Phys. Rev. Lett.* **58**, 29.
- Thompson, A. H., S. W. Sinton, S. L. Huff, A. J. Katz, R. A. Raschke, and G. A. Gist, 1989, *J. Appl. Phys.* **65**, 3259.
- Thorpe, M. F., and P. N. Sen, 1985, *J. Acoust. Soc. Am.* **77**, 1674.
- Tilton, J. N., and A. C. Payatakes, 1984, *AIChE J.* **30**, 1016.
- Timur, A., 1968, *Log Anal.* **9**, 8.
- Timur, A., 1969, *J. Pet. Tech.* **21**, 775.
- Todd, M. R., and W. J. Longstaff, 1972, *Soc. Pet. Eng. J.* **12**, 874.
- Todorovic, P. N., 1970, *Water Resour. Res.* **6**, 211.
- Todorovic, P. N., 1971, in *Proceedings of the International Symposium on Stochastic Hydrology* (International Association of Scientific Hydrology, Pittsburgh, Pennsylvania), p. 632.
- Todorovic, P. N., 1975, *Water Resour. Res.* **11**, 348.
- Todorovic, P. N., 1982, *Adv. Water Resour.* **5**, 42.
- Toledo, P. G., R. A. Novy, H. T. Davis, and L. E. Scriven, 1990, *Soil Sci. Soc. Am. J.* **54**, 673.
- Tompson, A. F. B., and W. G. Gray, 1986, *Water Resour. Res.* **22**, 591.
- Topp, G. C., 1971, *Solid Sci. Soc. Am. Proc.* **35**, 219.
- Torquato, S., 1990, *Phys. Rev. Lett.* **64**, 2644.
- Torquato, S., 1991, *Appl. Mech. Rev.* **44**, 37.
- Torquato, S., and J. D. Beasley, 1987, *Phys. Fluids* **30**, 633.
- Torquato, S., J. D. Beasley, and Y. C. Chiew, 1988, *J. Chem. Phys.* **88**, 6540.
- Torquato, S., and B. Lu, 1990, *Phys. Fluids A* **2**, 487.
- Torelli, L., 1972, *Pure Appl. Geophys.* **96**, 75.
- Torelli, L., and A. E. Scheidegger, 1972, *J. Hydrol.* **15**, 23.
- Triber, L. E., D. L. Archer, and W. W. Owens, 1972, *Soc. Pet. Eng. J.* **12**, 531.
- Trugman, S. A., 1983, *Phys. Rev. B* **27**, 7539.
- Tryggvason, G., and A. Aref, 1985, *J. Fluid Mech.* **154**, 287.
- Tsakiroglou, C. D., and A. C. Payatakes, 1990, *J. Colloid Interface Sci.* **137**, 315.
- Tsallis, C., A. Coniglio, and S. Redner, 1983, *J. Phys. C* **16**, 4339.
- Tsang, Y. W., and P. A. Witherspoon, 1981, *J. Geophys. Res.* **86**, 9287.
- Turban, L., 1978, *J. Phys. C* **11**, 449.
- Turcotte, D. L., 1986, *J. Geophys. Res. B* **91**, 1921.
- Turner, G. A., 1959, *Chem. Eng. Sci.* **10**, 14.
- Underwood, E. E., 1970, *Quantitative Stereology* (Addison Wesley, New York).
- Van Brakel, J., 1975, *Powder Tech.* **11**, 205.
- Van Damme, H., C. Laroche, and L. Gatineau, 1987a, *Revue. Phys. Appl.* **22**, 241.
- Van Damme, H., C. Laroche, L. Gatineau, and P. Levitz, 1987b, *J. Physique* **48**, 1121.
- Van den Broeck, C., 1982, *Physica A* **112**, 343.
- Van den Broeck, C., and R. M. Mazo, 1983, *Phys. Rev. Lett.* **51**, 1309.
- Van den Broeck, C., and R. M. Mazo, 1984, *J. Chem. Phys.* **81**, 3624.
- van Meurs, P., 1957, *Trans. AIME* **210**, 295.
- Viani, B. E., P. F. Low, and C. B. Roth, 1983, *J. Colloid Interface Sci.* **96**, 229.
- Vicsek, T., 1984, *Phys. Rev. Lett.* **53**, 2281.
- Vicsek, T., 1985, *Phys. Rev. A* **32**, 3084.
- Vollmar, S., and J. A. M. S. Darte, 1992, *J. Phys. (Paris) II* **2**, 1565.
- Vonk, C. G., 1976, *J. Appl. Crystallogr.* **9**, 433.
- Voss, R. F., 1985, in *Fundamental Algorithms for Computer Graphics*, edited by R. A. Earnshaw, NATO ASI Series, Vol. F17 (Springer, Berlin), p. 805.
- Wagner, O. R., and R. O. Leach, 1959, *J. Pet. Tech.* **1**, 65.
- Wall, G. C., and R. J. C. Brown, 1981, *J. Colloid Interface Sci.* **82**, 141.
- Walsh, M. P., S. L. Bryant, R. S. Schechter, and L. W. Lake, 1984, *AIChE J.* **30**, 317.
- Ward, J. S., and N. R. Morrow, 1987, *SPE Formation Evaluation* **2**, 345.
- Wardlaw, N. C., 1976, *AAPG Bull.* **60**, 245.
- Wardlaw, N. C., 1982, *J. Can. Pet. Tech.* **21**, 21.
- Wardlaw, N. C., and J. P. Cassan, 1978, *Bull. Can. Pet. Geol.* **27**, 117.
- Wardlaw, N. C., Y. Li, and D. Forbes, 1987, *Transp. Porous Media* **2**, 597.
- Warren, J. E., and H. S. Price, 1961, *Soc. Pet. Eng. J.* **1**, 153.
- Warren, J. E., and P. J. Root, 1963, *Soc. Pet. Eng. J.* **3**, 245.
- Warren, J. E., and F. F. Skiba, 1964, *Soc. Pet. Eng. J.* **4**, 215.
- Washburn, E. W., 1921, *Proc. Nat. Acad. Sci. USA* **7**, 115.
- Watson, B. P., and P. L. Leath, 1974, *Phys. Rev. B* **9**, 4893.
- Webman, I., 1981, *Phys. Rev. Lett.* **47**, 1496.
- Weinbrandt, R. M., and I. Fatt, 1969, *J. Pet. Technol.* **21**, 543.
- Weissberg, H. L., and S. Prager, 1962, *Phys. Fluids* **5**, 1390.
- Weissberg, H. L., and S. Prager, 1970, *Phys. Fluids* **13**, 2958.
- Weitz, D. A., J. P. Stokes, R. C. Ball, and A. P. Kushnik, 1987,

- Phys. Rev. Lett. **59**, 2967.
- Wheatcraft, S. W., and S. W. Tyler, 1988, Water Resour. Res. **24**, 566.
- Whitaker, S., 1967, AIChE J. **13**, 420.
- Whitaker, S., 1986a, Transp. Porous Media **1**, 3.
- Whitaker, S., 1986b, Transp. Porous Media **1**, 105.
- White, I., P. M. Calumbera, and J. R. Philip, 1976, Soil Sci. Soc. Am. J. **41**, 483.
- Wilke, S., E. Guyon, and G. de Marsily, 1985, Math. Geol. **17**, 17.
- Wilkinson, D., 1984, Phys. Rev. A **30**, 520.
- Wilkinson, D., 1986, Phys. Rev. A **34**, 1380.
- Wilkinson, D., and M. Barsony, 1984, J. Phys. A **17**, L129.
- Wilkinson, D., and J. F. Willemsen, 1983, J. Phys. A **16**, 3365.
- Willemsen, J. F., 1984, Phys. Rev. Lett. **52**, 2197.
- Willemsen, J. F., 1985, Phys. Rev. A **31**, 432.
- Williams, C. E., and B. M. Fung, 1982, J. Magn. Res. **50**, 71.
- Wilson, S. D. R., 1975, J. Colloid Interface Sci. **51**, 532.
- Winterfeld, P. H., L. E. Scriven, and H. T. Davis, 1981, J. Phys. C **14**, 2361.
- Witten, T. A., and L. M. Sander, 1981, Phys. Rev. Lett. **47**, 1400.
- Witten, T. A., and Sander, L. M., 1983, Phys. Rev. B **27**, 5686.
- Wolfram, S., 1986a, *Theory and Applications of Cellular Automata* (World Scientific, Singapore).
- Wolfram, S., 1986b, J. Stat. Phys. **45**, 471.
- Wong, P.-Z., J. Howard, and J.-S. Lin, 1986, Phys. Rev. Lett. **57**, 637.
- Wong, P.-Z., J. Koplik, and J. P. Tomanic, 1984, Phys. Rev. B **30**, 6606.
- Wood, J. R., and T. A. Hewett, 1982, Geochim. Cosmochim. Acta **46**, 1707.
- Wood, J. R., and R. C. Surdam, 1979, *The Society of Economic Paleontologists and Mineralogists Special Publication No. 26*, p. 243.
- Wooding, R. A., 1962, Z. Angew. Math. Phys. **13**, 255.
- Wooding, R. A., 1969, J. Fluid Mech. **39**, 477.
- Wooding, R. A., and H. J. Morel-Seytoux, 1976, Annu. Rev. Fluid Mech. **8**, 233.
- Wright, R.-J., and R. A. Dawe, 1983, Rev. Inst. Fr. Pet. **38**, 455.
- Wyllie, M. R. J., and W. D. Rose, 1950, Pet. Trans. AIME **189**, 105.
- Xia, W., and M. F. Thorpe, 1988, Phys. Rev. B **38**, 2650.
- Yadav, G. D., F. A. L. Dullien, I. Chatzis, and I. F. MacDonald, 1987, SPE Reservoir Eng. **2**, 137.
- Yanuka, M., F. A. L. Dullien, and D. E. Elrick, 1984, J. Microscopy **135**, 159.
- Yokoyama, Y., and L. W. Lake, 1981, paper SPE 10109, presented at the 56th Annual Conference of the Society of Petroleum Engineers, San Antonio, Texas.
- Yonezawa, F., and M. H. Cohen, 1983, J. Appl. Phys. **54**, 2895.
- Yortsos, Y. C., 1987a, AIChE J. **33**, 1912.
- Yortsos, Y. C., 1987b, Phys. Fluids **30**, 2928.
- Yortsos, Y. C., 1990 (unpublished notes).
- Yortsos, Y. C., and F. J. Hickernell, 1989, SIAM J. Appl. Math. **49**, 730.
- Yortsos, Y. C., and A. B. Huang, 1986, SPE Reservoir Eng. **1**, 378.
- Yortsos, Y. C., and M. Zeybek, 1988, Phys. Fluids **31**, 3511.
- Young, A. P., and R. B. Stinchcombe, 1975, J. Phys. C **8**, L535.
- Ypma, J. G. J., 1983, paper SPE 12158, presented at the 58th Annual Conference of the Society of Petroleum Engineers, San Francisco, California.
- Zanetti, G., 1989, Phys. Rev. A **40**, 1539.
- Zhdanov, V. P., V. B. Fenelonov, and D. K. Efremov, 1987, J. Colloid Interface Sci. **120**, 218.
- Zhang, Y.-C., 1990a, J. Phys. (Paris) **51**, 2113.
- Zhang, Y.-C., 1990b, Physica A **170**, 1.
- Zheng, L. H., and Y. C. Chiew, 1989, J. Chem. Phys. **90**, 322.
- Zhou, M.-Y., and P. Sheng, 1989, Phys. Rev. B **39**, 12027.
- Zick, A. A., and G. M. Homsy, 1982, J. Fluid Mech. **115**, 13.
- Ziman, J. M., 1982, *Models of Disorder* (Cambridge University Press, Cambridge), p. 154.
- Zimmerman, W. B., and G. M. Homsy, 1991, Phys. Fluids A **3**, 1859.

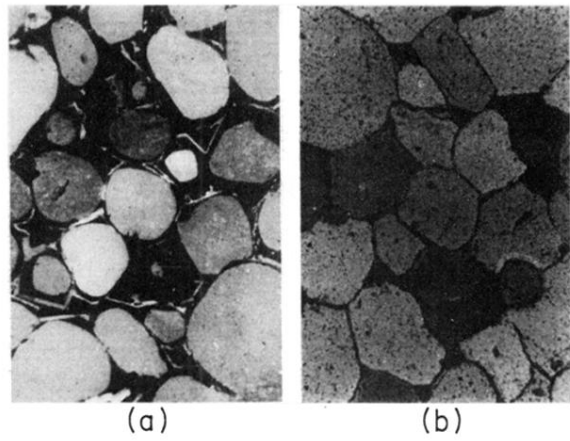


FIG. 3. Heavily cemented Devonian sandstone from Illinois observed (a) with cathodoluminescence to show the original round sand grains, and (b) with ordinary light to show the angular forms of the grains after cementing, for which the grain-consolidation model of Fig. 2 is intended (from Roberts and Schwartz, 1985).

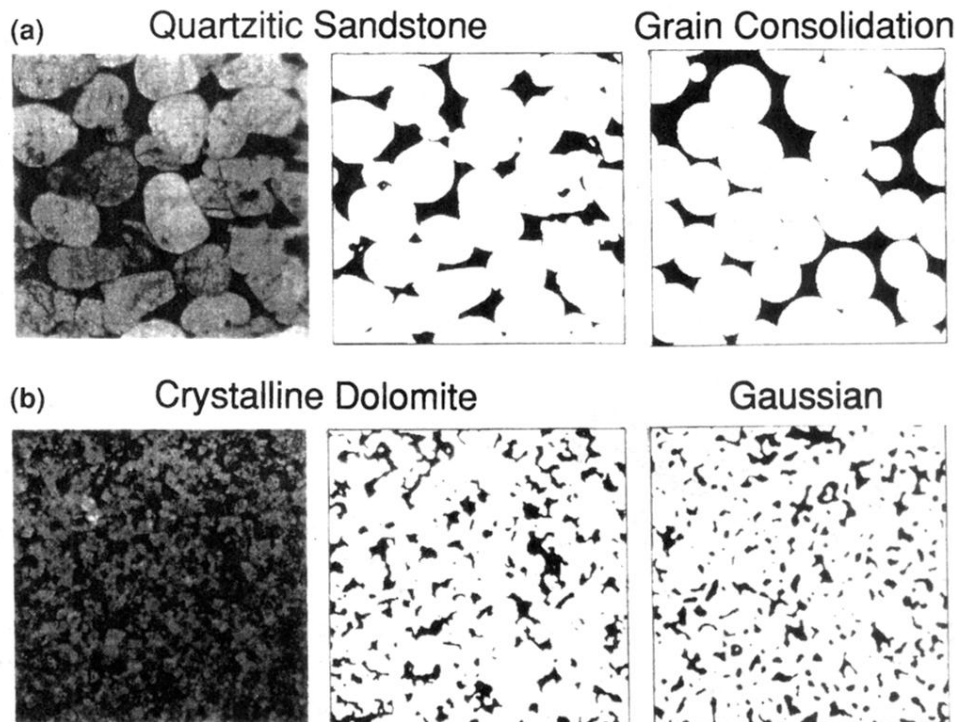


FIG. 4. Comparison of the models and the actual porous media. (a) Left-hand and middle panel show a thin-section optical photo and the corresponding binary (pore=black, grain=white) representation. Right-hand panel shows a section based on the consolidation of densely packed spherical grains. The model porosity has been adjusted to equal that of the sandstone. (b) Left-hand and middle panels are the same as those in (a), except that they are for a crystalline dolomite. Right-hand panel shows a single plane from a Gaussian smoothed 3d model. The model porosity has been adjusted to equal that of the dolomite section (from Crossley *et al.*, 1991).

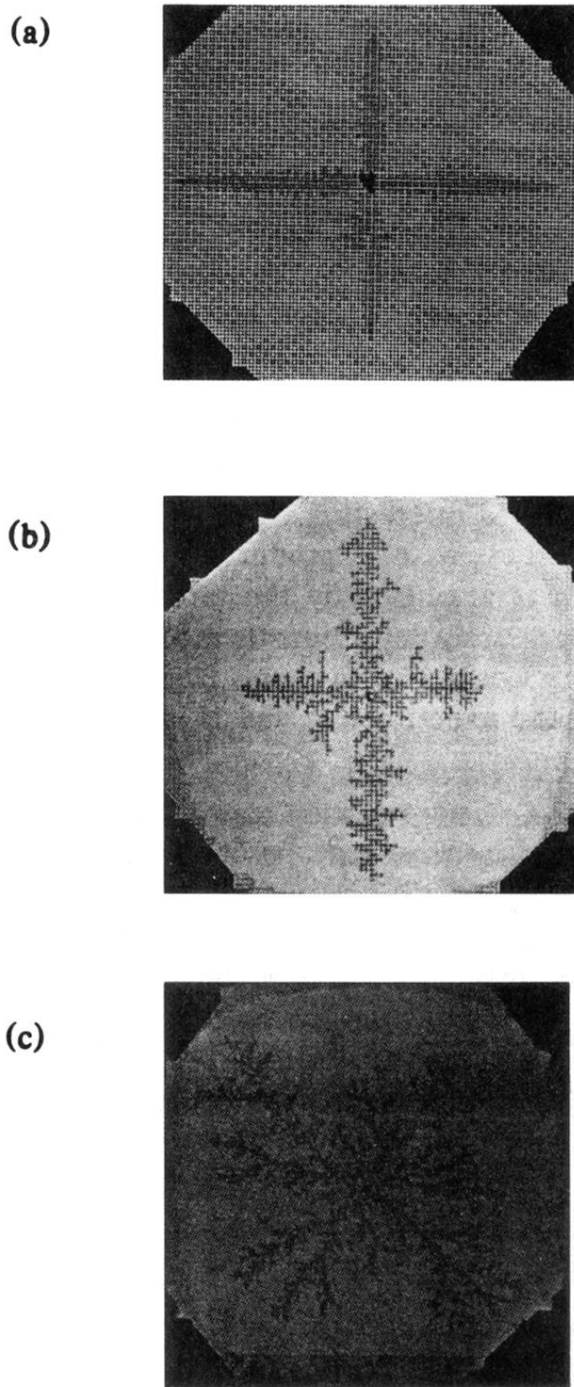


FIG. 44. Patterns of viscous fingers in an etched-glass network. In (a) all pores have the same radius, while in (c) the network is completely disordered (from Chen and Wilkinson, 1985).